Side Friction for Superelevation on Horizontal Curves

Final Technical Report
Volume II

C. C. MacAdam
P. S. Fancher
L. Segel

Contract Number: DTFH61-82-C-00019

August 1985

UMTRI The University of Michigan
Transportation Research Institute

NOTICE

This document is disseminated under the sponsorship of the Department of Transportation in the interest of information exchange. The United States Government assumes no liability for its contents or use thereof.

The contents of this report reflect the view of the contractor, who is responsible for the accuracy of the data presented herein. The contents do not necessarily reflect the official policy of the Department of Transportation.

This report does not constitute a standard, specification, or regulation.

The United States Government does not endorse products or manufacturers. Trade or manufacturers' names appear herein only because they are considered essential to the object of this document.

Technical Report Documentation Page

1. Report No.	2. Government Accession No.	3. Recipient's Catalog No.

4. Title and Subtitle	5. Report Date
SIDE FRICTION FOR SUPERELEVATION ON HORIZONTAL CURVES Vol. II - Technical Report	August 1985
	6. Performing Organization Code
7. Author(s) C.C. MacAdam, P.S. Fancher, L. Segel	8. Performing Organization Report No. UMTRI-85-18/2
9. Performing Organization Name and Address The University of Michigan Transportation Research Institute 2901 Baxter Road Ann Arbor, Michigan 48109	10. Work Unit No.
	11. Contract or Grant No. DTFH61-82-C-00019
	13. Type of Report and Period Covered Final 6/82 - 7/85
12. Sponsoring Agency Name and Address Federal Highway Administration U.S. Department of Transportation Washington, D.C. 20590	14. Sponsoring Agency Code

15. Supplementary Notes

COTR - Mr. Lawrence McCarthy
FCP Project 1S, "Design and Corrective Geometries"

16. Abstract

The basic objective of this study has been to address the issue of how adequate point-mass representations are in predicting friction requirements for actual vehicles operating along superelevated curves. The project focused on this and related questions by combining computer analysis and full-scale vehicle testing. Simple-to-use models for predicting the friction factor requirements at individual wheel locations were first developed and applied to the steady-turning condition. An existing comprehensive computer model used for predicting transient or nonsteady maneuvering situations was also employed to analyze friction demand while maneuvering along superelevated curves. Highway tests were then performed for two passenger cars and a five-axle tractor-semitrailer to collect representative test data and assist in validing the predictions of the computer models. Finally, a sensitivity analysis was performed to illustrate the relative importance and interactions of various vehicle parameters and highway geometrics in influencing side friction requirements.

17. Key Words	18. Distribution Statement
friction factor, highway design, superelevated curves, computer models, vehicle tests, steady turning, obstacle avoidance	No restrictions. This document is available to the public through the National Technical Information Service, Springfield, Virginia 22161

19. Security Classif. (of this report)	20. Security Classif. (of this page)	21. No. of Pages	22. Price
Unclassified	Unclassified		

CONTENTS

CONTENTS (Continued)

LIST OF FIGURES

LIST OF FIGURES (Continued)

Figure

LIST OF FIGURES (Continued)

LIST OF FIGURES (Continued)

Figure

LIST OF FIGURES (Continued)

Figure

LIST OF TABLES

Chapter 1

INTRODUCTION

This document is the final report for the Federal Highway Administration project entitled, "Side Friction for Superelevation on Horizontal Curves," performed under Contract Number DTFH61-82-C-00019. The basic objective of this project has been to address the issue of how adequate point-mass representations are in predicting friction requirements for actual vehicles operating along superelevated curves. Since current design practice characterizes the vehicle under conditions of steady turning motion as a simple point-mass, legitimate questions concerning the friction requirements at individual wheel locations and how they relate to the point-mass representation are examined.

The project focused on this and related questions by combining computer analysis and full scale vehicle testing. Simple-to-use models for predicting the friction factor requirements at individual wheel locations were first developed and applied to the steady turning condition. An existing comprehensive computer model (UMTRI "Phase 4", [5]) used for predicting transient or nonsteady maneuvering situations was also employed to analyze friction demand while maneuvering along superelevated curves. Highway tests were then performed for two passenger cars and a five-axle tractor-semitrailer to collect representative test data and assist in validating the predictions of the computer models. Finally, a sensitivity analysis was performed to illustrate the relative importance and interactions of various vehicle parameters and highway geometrics in influencing side friction requirements.

Because the principal concern of this study was to evaluate frictional requirements of vehicles during negotiation of horizontal curves, portions of this report contain results which illustrate how changes in vehicle properties as well as changes in curve geometry affect the eventual answers. Consequently, the interaction between vehicle and highway will frequently rely upon, or be illustrated in terms of, selected vehicle responses. In certain cases, this is desirable in order to demonstrate, for example, that although

certain vehicle properties may change, the side friction requirements may not. Thus, the modification of certain vehicle properties would be illustrated by changes in vehicle responses, while simultaneously showing that the friction factors remain unaffected.

In addition to the Executive Summary (volume I), the main report is organized into eight chapters and a set of six appendices. Volume II contains the main body of the technical report. Volume III contains the appendices A to G which provide detailed information relating to the computer models / predictions and experimental test data.

Chapter 2 of this volume presents an overview of the project and its organization. The basic technical questions are first introduced, followed by a general description of the tasks employed in accomplishing the project goals. Chapter 3 describes the models developed and used during the project work. Use and interpretation of the model predictions are also discussed. Chapter 4 covers the vehicle testing phase of the project. Test vehicles, curve sites, and test maneuvers are first described. Example results are then shown for each vehicle and briefly discussed. A comparison of vehicle test results and model predictions are presented in chapter 5. Steady turning, obstacle avoidance, and braking / accelerating maneuvers performed along superelevated curves are used as representative maneuvers for challenging the validity of the various models. Chapter 6 presents findings of the sensitivity analysis which studied the influence of various vehicle and highway geometric parameters on friction demand. In addition, several special studies were conducted to examine 1) low friction conditions during steady turning and obstacle avoidance, 2) the sensitivity of friction factor estimates to measurement errors, and 3) contributions of driver steering activity and vehicle characteristics to friction demand levels beyond that predicted by the point-mass value. Certain recommendations from previous studies for modifying current design policy are also examined. Chapter 7 relates the basic research findings to current AASHTO design policy and also to recent studies performed by other investigators. Lastly, chapter 8 presents conclusions and recommendations on the work performed within this project.

Chapter 2

PROJECT OVERVIEW

This chapter provides a general overview of the work performed within this project and introduces the technical issues which motivate the reasons for it. Greater detail and in-depth discussions of the material presented in this chapter can be found in subsequent chapters and the accompanying appendices. The chapter begins with material which explains the technical reasons motivating the work while also illustrating basic concepts and terminology used throughout the report. The remaining sections of this chapter provide a short summary of the project work.

2.1 Comparison of Point-Mass and Individual Wheel Friction Factors

This section illustrates how friction factor values can become distributed on actual vehicles by presenting three simple models, starting from the simplest "point-mass" model and increasing in realism to a four-wheel representation of a passenger car. As the realism of each model is increased, a level is reached which requires differences in individual friction factors to occur and differ from the simple point-mass model. The first model considered is that in which the total vehicle mass is assumed concentrated at one location. This is followed by a "bicycle" model in which the vehicle is represented as having front and rear tires but no width. The third case is a four-wheel model which adds width, or side-to-side properties, and an elevated mass center to the "bicycle" model.

2.1.1 Point-Mass Model

Figure 1 introduces the concept of the point-mass model for representing steady turning motion along a superelevated curve of constant radius, R. If the vehicle is represented, not by a distributed mass system, but rather as an object with its mass concentrated at a single point, figure 1 may be used to derive and illustrate the required friction force. In figure 1 the point-mass, m, moves on a circular path of radius, R, at a speed, V. The surface (road) on which it moves is superelevated an amount, e. In order for the

Force Equilibrium

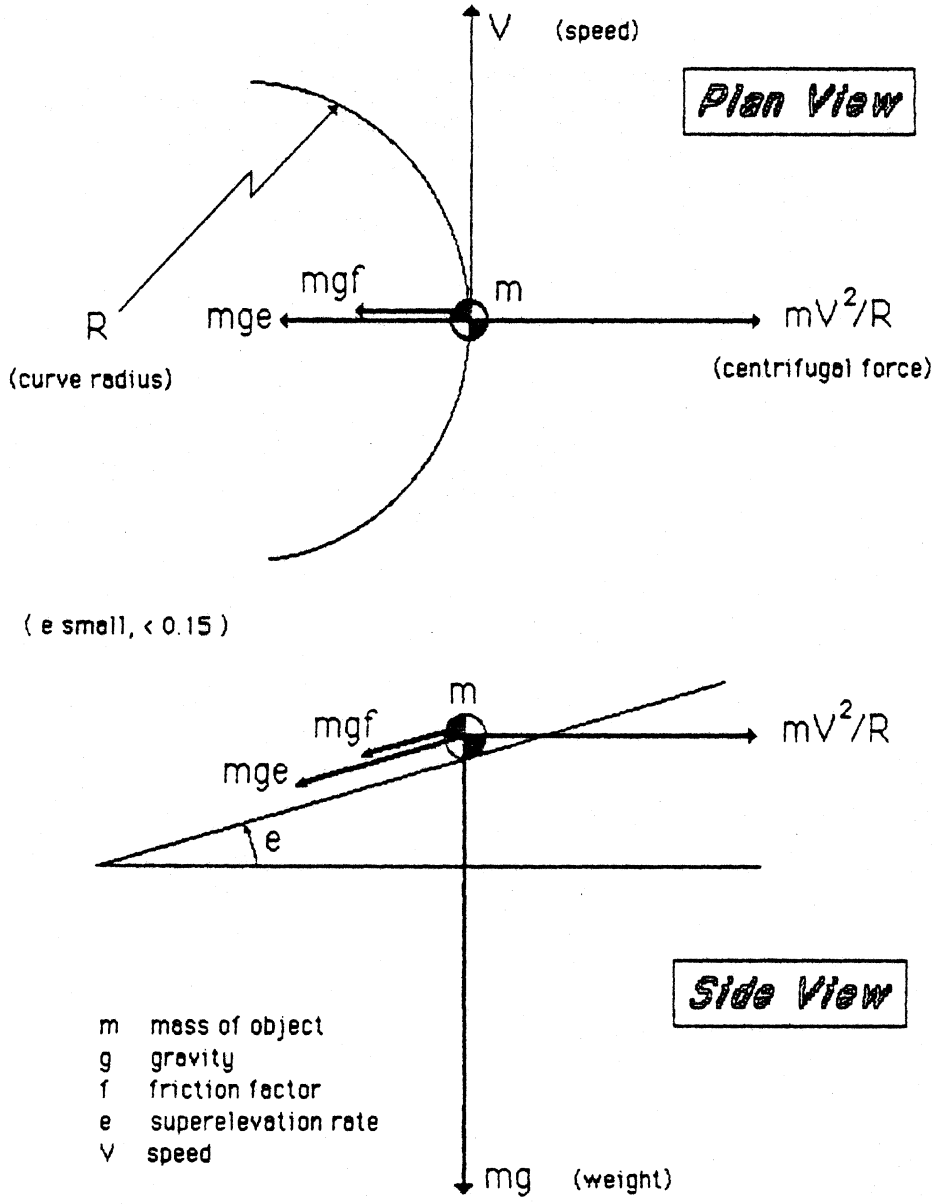

Figure 1. Force equilibrium.

point-mass to move in this circular manner the forces acting on the object must balance, or be in equilibrium, in a radial direction. Figure 1 shows three forces acting on the mass in the radial direction: 1) the centrifugal force, mV^2/R, acting outward from the center of the turn, 2) the weight component of the object acting inward (down the slope), mge, due to the superelevation of the surface, and 3) the remaining friction force, mgf, required to balance the sum of forces acting on the object. Expressing this required force equilibrium as an equation

$$mge + mgf = mV^2/R \qquad (1)$$

results in a "model" for the point-mass which permits the calculation of the required friction force. Since m, V, e, and R are assumed known, the friction force required for steady turning is simply

$$mgf = mV^2/R - mge \qquad (2)$$

or, dividing each term by the object weight, mg, results in the standard point-mass design equation for the "friction factor," f,

$$f = V^2/(R\,g) - e \qquad (3)$$

Figure 2 illustrates the point-mass model in this form with "normalized" forces (accelerations) replacing the forces appearing in figure 1 .

2.1.2 Bicycle Model

If the point-mass model is now extended to include one front and one rear tire located at distances a and b, respectively, from the mass center, m, the point-mass model becomes a "bicycle" model. Figure 3 shows a diagram analogous to that used for the point-mass model. Introduction of front and rear tires now requires two individual wheel friction factors (front and rear), f_1 and f_2 , to be determined. What exactly is meant by the term "individual wheel friction factors" is illustrated in figure 4. The friction factor simply represents the normalized lateral tire force, or ratio of lateral tire force to vertical tire force at each wheel location.

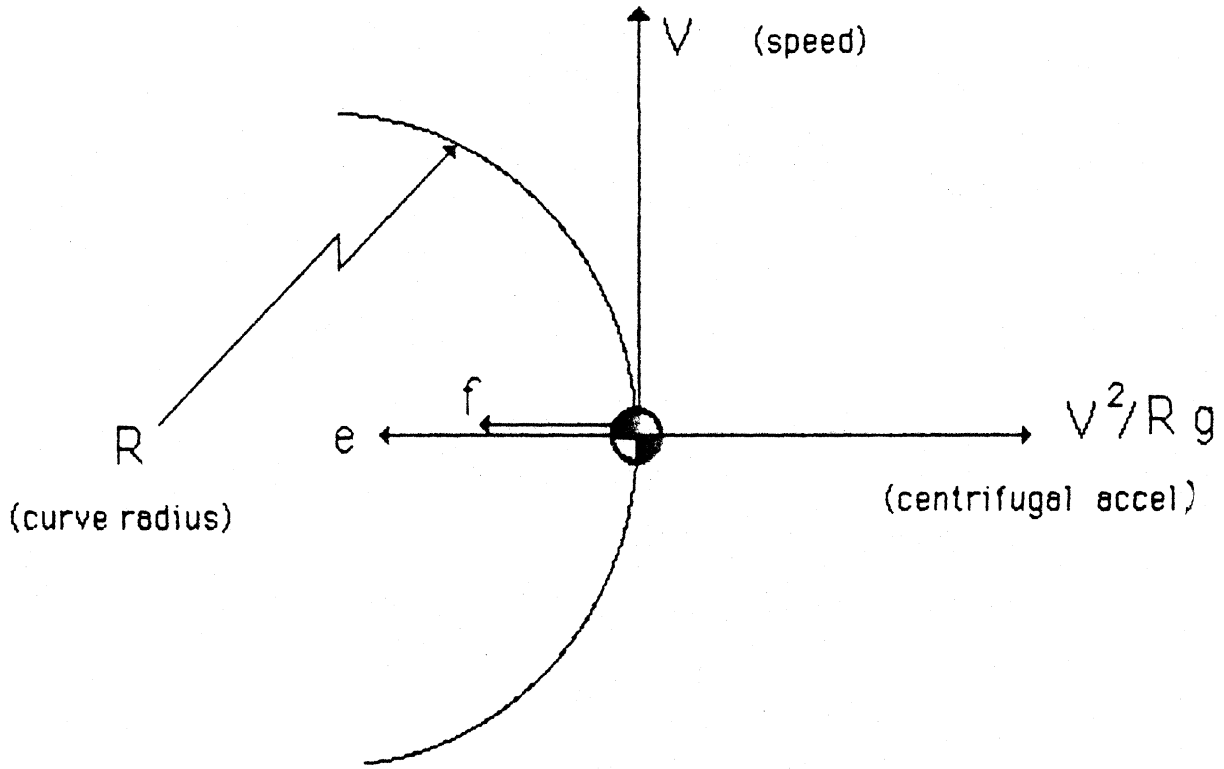

$$e + f = V^2 / R g$$

superelevation: e

friction factor: f

Figure 2. Point-mass model

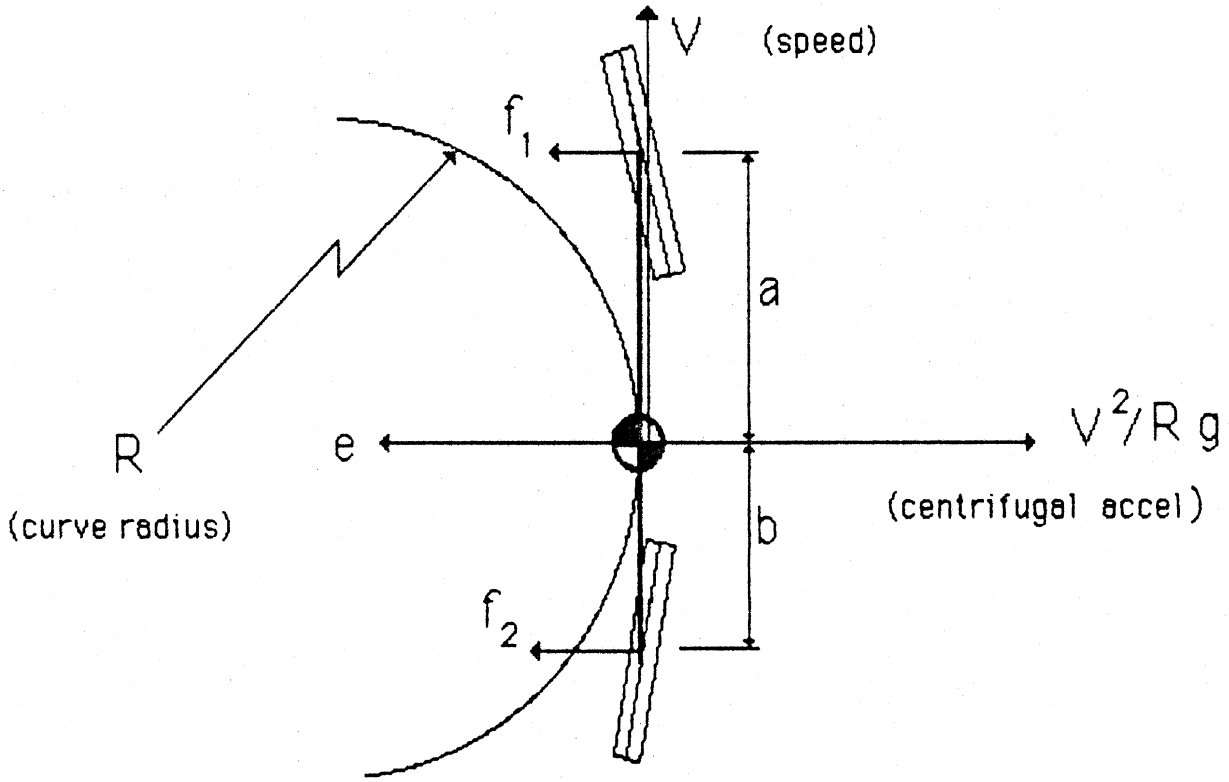

$$f_1 = f_2 = V^2/R\,g - e$$

superelevation: e

friction factors: f_1, f_2

Figure 3. Bicycle model

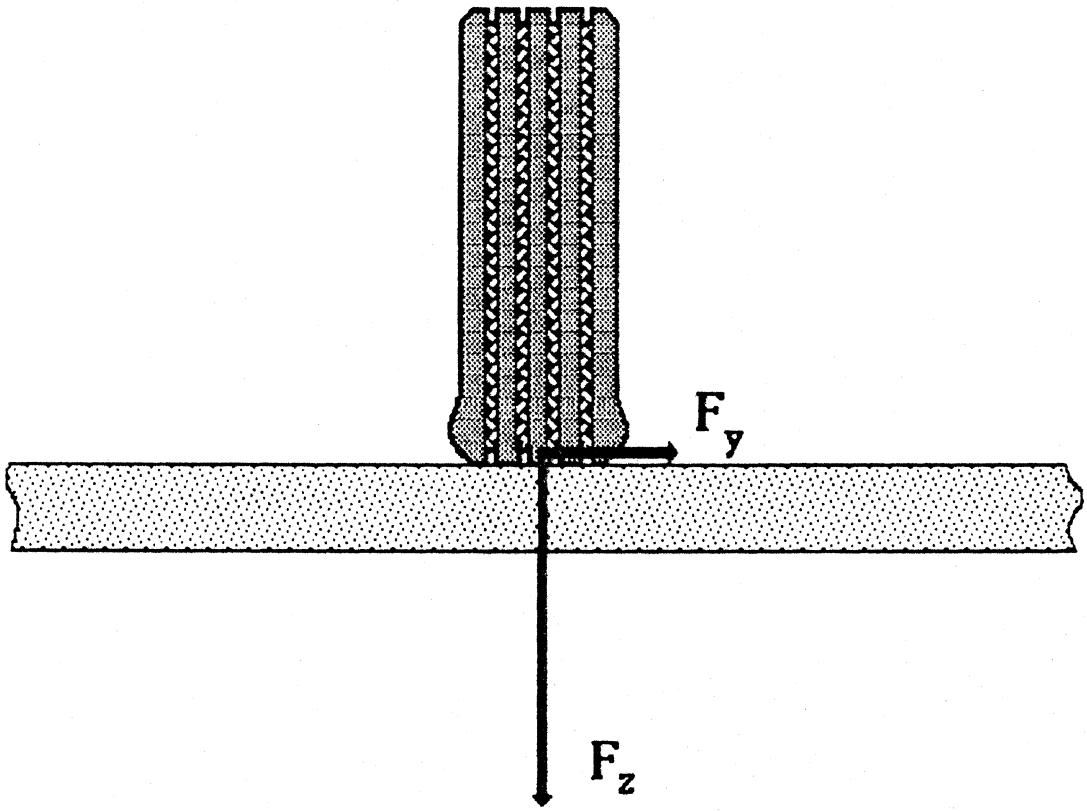

$$f = F_y / F_z$$

f : "friction factor"

F_y : Lateral Tire Force

F_z : Vertical Tire Force

Figure 4. Tire forces defining the individual wheel "friction factor"

Because the road-plane forces acting on the mass in figure 3 are not concentrated at one point, a moment balance as well as a force balance must exist about the mass center in order for a steady turning condition to prevail. The additional moment balance condition provides a second equation to permit identification of the additional friction force in this model. Hence, the two equations defining the "bicycle" model are given by:

$$mgf_1 b/(a+b) + mgf_2 a/(a+b) + emg = mV^2/R \qquad (4)$$

and

$$mgf_1 ab/(a+b) - mgf_2 ab/(a+b) = 0 \qquad (5)$$

Equation (4) represents the radial force balance condition while equation (5) expresses the moment balance requirement. Solving these two equations for the two unknown friction factors, f_1 and f_2 , shows them to be equal to the point-mass result:

$$f_1 = f_2 = V^2/Rg - e \qquad (6)$$

Therefore, distributing the friction forces in a simple fore/aft manner as shown here with the bicycle model indicates that the individual friction factor requirements are identical to the point-mass value.

2.1.3 Two-Axle Model

Figure 5 represents the next step toward realism by adding width to the bicycle model in the form of left and right side tires and a mass center elevated some distance above ground. As a result, two additional unknown friction factors, f_3 and f_4, are introduced due to the side-to-side tire force distribution. If this model is presumed to permit vertical load transfer from side to side as occurs in actual vehicles because of an elevated mass center, roll equlibrium must also exist. The roll equilibrium condition provides an additional equation to help determine the additional unknown frictional side forces. Without presenting the mathematical details, it is not difficult to see that the two-axle case is very similar to the bicycle model, except for differing vertical tire loads across each axle. Since the lateral tire forces

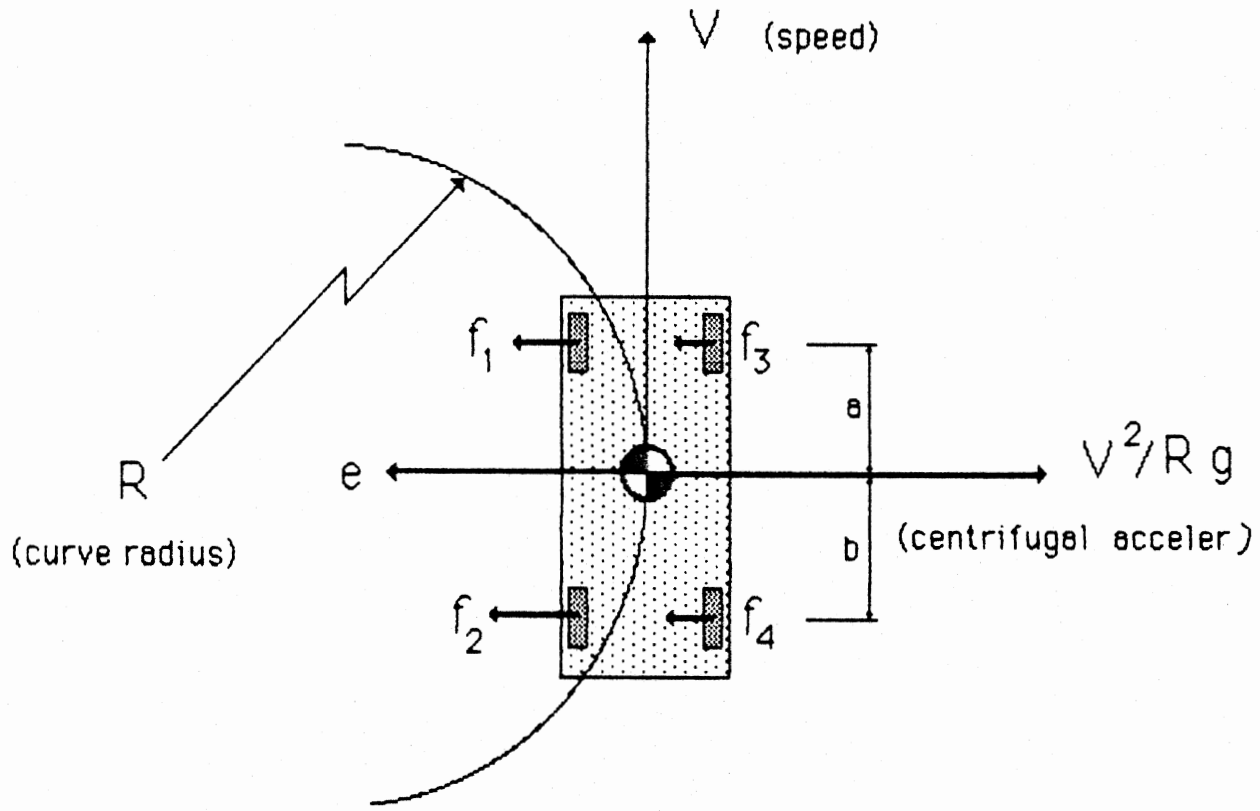

$$f_1 \neq f_2 \neq f_3 \neq f_4 \neq [V^2/R\,g - e]$$

superelevation: e

friction factors: f_1, f_2, f_3, f_4

Figure 5. Two-axle model

are nominally the same at each wheel location of the same axle (unless they are strongly dependent upon vertical load, which is not normally the case), the variation in individual wheel friction factors across an axle is primarily determined by side-to-side differences in vertical tire load. Figure 6 helps to further illustrate this point.

As a result, the friction factor values observed in the two-axle case will not normally be equal to the point-mass value. In general, the inside or more lightly loaded tires will exhibit friction factor values greater than the point-mass value, while the outside or more heavily loaded tires will exhibit friction factor values less than the point-mass value. Key questions that then arise are: How much variation in friction factor values can be expected to occur at different wheel locations? How do different vehicles influence the amount of variation? And lastly: Is the level of friction factor variation significant in the sense that horizontal curve design policy should be modified to account for it?

2.2 Special Factors That Exaggerate Friction Factor Dispersion

In addition to the matter of different side-to-side vertical tire loads contributing to the variation in individual wheel friction factors, other vehicle related factors can also influence and contribute to this phenomena. Several of these factors are discussed briefly in the following section.

2.2.1 Tandem Axle Effects

When vehicles equipped with tandem axles are considered, whether they are heavy duty commercial vehicles or utility trailers pulled by passenger cars, the presence of a tandem axle set (or additional axles) causes the degree of friction factor variation to increase further. The additional dispersion is a direct result of the load leveling mechanism in most tandem suspensions coupled with the requirement that the tires on each of the tandem axles produce different lateral tire forces due to their fore/aft locations. Hence, the same-side tires of a tandem suspension carry about the same load (vertical tire force), but differ significantly in lateral tire force production. The net result is increased variation in the friction factors at the tandem axles

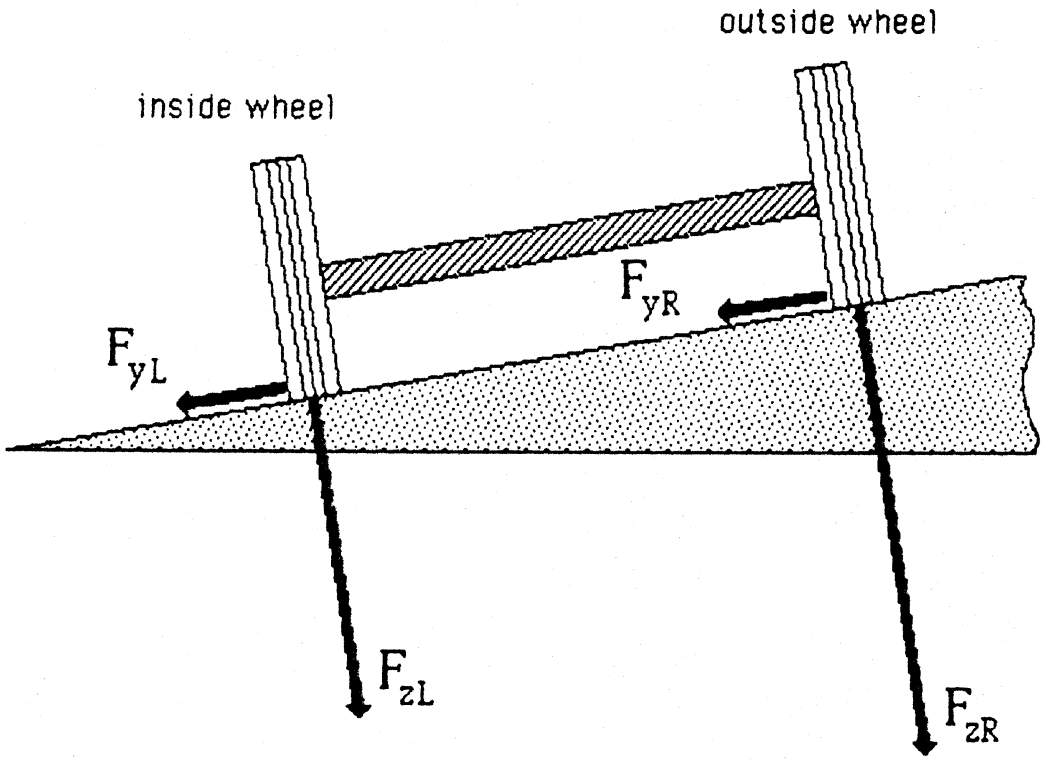

$$f_L = F_{yL} / F_{zL} \qquad \text{(left side friction factor)}$$

$$f_R = F_{yR} / F_{zR} \qquad \text{(right side friction factor)}$$

$$F_{yL} \cong F_{yR} \qquad F_{zL} < F_{zR}$$

$$f_L > f_R$$

Figure 6. Side-to-side variation in friction factors due to differences in vertical tire loads

due to variations in same-side lateral tire forces. Note that this is in direct contrast to the effect discussed in the previous section, which depended upon differences occuring in side-to-side vertical tire forces while the lateral tire forces remained the same.

2.2.2 Tire Load Sensitivity Properties

The manner in which tires produce lateral (or side) force in response to changes in the vertical load that they carry also plays an important role in the degree to which friction factors will vary. Since the friction factor is simply the ratio of lateral to vertical tire force, the sensitivity of a tire's lateral force to changes in vertical tire force is important. For small tire sideslip angles and constant loads, typical of most highway operating conditions, the pneumatic tire is generally observed to produce lateral tire force in direct proportion to its sideslip angle. This relationship is usually expressed as

$$F_y = C_a(F_z)\ B \qquad (7)$$

where F_y is the lateral tire force, B is the tire sideslip angle, and C_a is the tire cornering stiffness which depends upon vertical load, F_z. For typical highway operating conditions, knowledge about a tire's cornering stiffness dependence upon vertical load will reveal the principal friction factor sensitivity to vertical load changes.

Figure 7 shows typical cornering stiffness dependencies upon vertical load for a passenger car tire and a heavy truck tire. Since the typical passenger car tire is designed to operate at a tire load which places it near the peak of its cornering stiffness plot and because its range of operating load is typically small, the passenger car tire is seen to have a nearly constant cornering stiffness. Thus, side-to-side load variations across an axle do not measurably affect a passenger car tire's cornering stiffness and consequently its lateral tire force production. The result is that friction factor values, which are the ratio of this nonvarying lateral force to a varying vertical force, are significantly affected by the side-to-side load transfer across an axle.

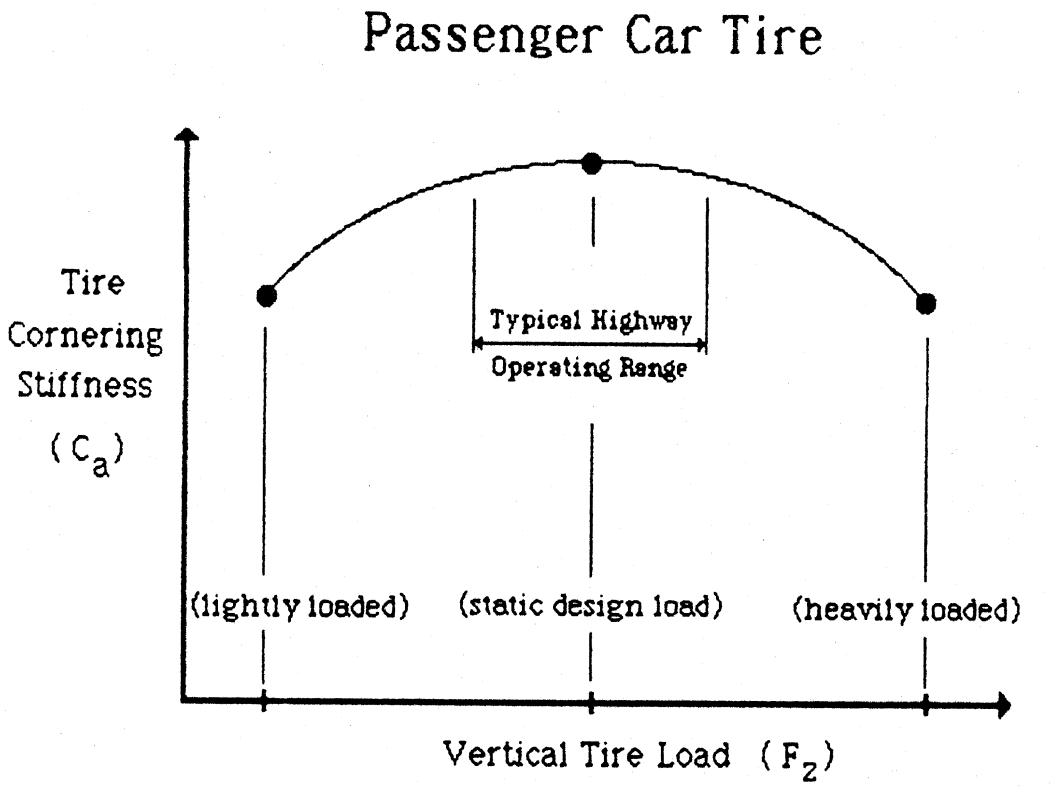

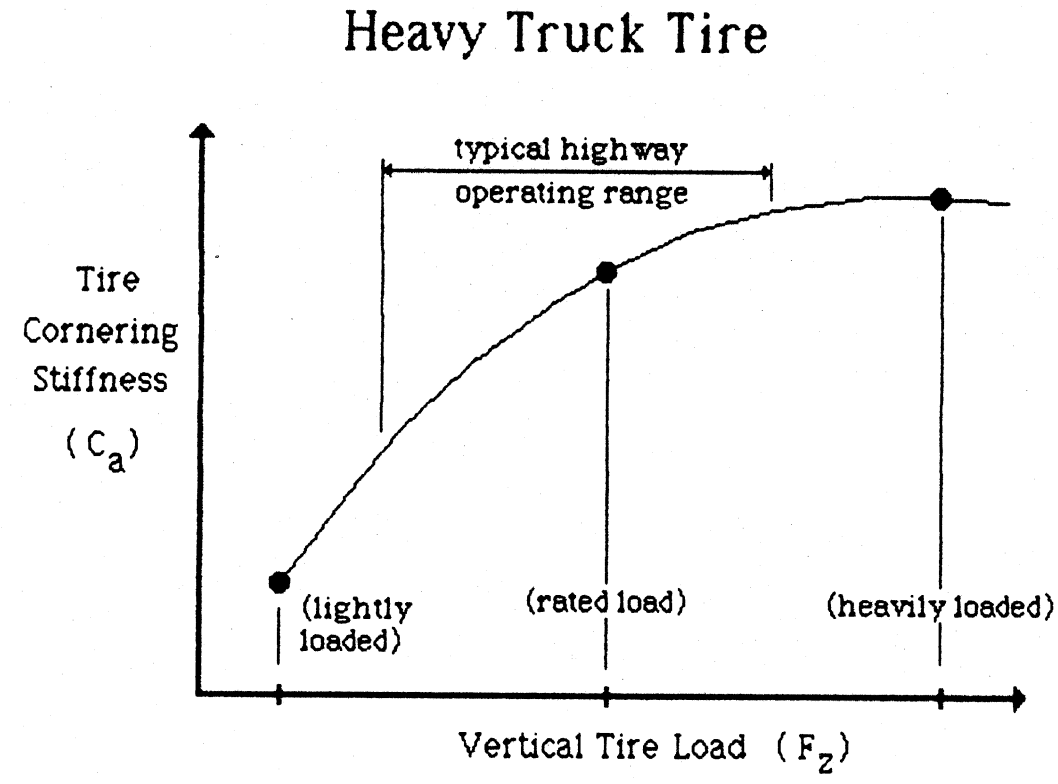

Figure 7. Passenger car tire vs truck tire

In direct contrast to the passenger car tire is the heavy truck tire, also seen in Figure 7. The cornering stiffness plot for the heavy truck shows that the typical operating range causes it to vary nearly in proportion to the vertical load. That is, as vertical tire load increases, so does the cornering stiffness and consequently the lateral tire force. Since the typical truck tire behaves in this manner, its friction factor sensitivity to vertical load changes is less than that of a typical passenger car tire. (If the cornering stiffness increased and decreased at the same rate as the vertical load, the tire would exhibit no change in its friction factor in response to the accompanying load changes.) As a result, the mechanical properties of the truck tire play an influential role in lessening its susceptibility to friction factor variations deriving from vertical load changes. Unfortunately, the typical heavy truck, unlike the passenger car, is saddled with a number of other features which contribute adversely to friction factor dispersion, thereby offsetting this one advantage.

2.2.3 Elevated Mass Center

Vehicles characterized by high centers of gravity, most typically the commercial vehicle, also suffer disproportionately in terms of friction factor variation, the reason being that high center-of-gravity (c.g.) vehicles transfer more load side-to-side in a given turn than do vehicles having lower mass centers. Fortunately, for many of these vehicles the reduced load sensitivity of their tire properties, as discussed in the previous section, prevent them from having significantly higher friction factor variations. Nevertheless, the normal load transfer in commercial vehicles can be considerable and does contribute adversely to additional dispersion in friction factor values.

For other special-case vehicles falling in an intermediate class, such as light trucks carrying a high c.g. payload, and which are equipped with tires behaving similarly to passenger car tires, the propensity for differing friction factors is significantly increased. However, the type of vehicle most likely to exhibit significant friction factor dispersion and still be representative of a portion of the vehicle population would be one having

multiple axles and an elevated center of gravity (e.g., a cement mixer equipped with a tandem or tri-axle rear suspension).

2.3 Methodology

In order to address the technical issues raised in the preceding sections from a firm foothold, computer-based analysis and vehicle testing were combined to predict and measure the degree of friction factor variations or dispersion likely to be exhibited by typical passenger cars and commercial vehicles. Simple-to-use computer models for predicting steady turning performance were first developed and tailored to the specific technical issues being addressed. Typical data input required for these models are curve radius, superelevation rate, travel speed, and various vehicle characteristics (tire and suspension properties, geometry, and weights). The output consists of individual wheel friction factors, the point-mass friction factor value, and additional vehicle response variables such as required steering angle, roll angle, and drive thrust. The model output therefore predicts what friction factors and vehicle responses are required in order to achieve the turning conditions specified as input to the program. The programs were developed to run on typical microcomputers and operate in an interactive and simple manner, thereby increasing their general availability and encouraging their likely use by potential users.

The second major phase of the project plan consisted of testing several vehicles along selected highway curve sites. A front wheel drive and rear wheel drive passenger car, as well as a five-axle tractor-semitrailer, were each tested under similar conditions along the same highway curves. The vehicles selected were considered representative of average vehicles operating on the highway system. Data collected from this activity were then used to document typical vehicle responses operating along superelevated curves and to validate predictions from the computer models. In cases where significant discrepancies were apparent between test results and model predictions, the test data would be used to correct identifiable errors or deficiencies in the models.

Following the vehicle testing and model validation activity, a sensitivity analysis was conducted to determine what vehicle parameters, highway geometric features, and operating conditions have the greatest influence in modifying friction factor demand. If, for example, a particular vehicle parameter variation was accompanied by significant variation in individual wheel friction factors, the highway design engineer may wish to anticipate the likelihood of this occurring in the vehicle population and thereby modify current design practice which ignores its influence. In addition to examining the influence of typical parameter variations, several special studies were performed to consider the impact of low friction conditions during steady turning and obstacle avoidance maneuvers. Finally, an informal error analysis was performed to help determine to what extent nominal errors in test measurements may contribute to errors in estimates of friction factors based on these measurements.

2.4 Overview of Model Development

The model development work performed during the project was comprised of two basic parts. The first part was directed at the development of two microcomputer-based models used to predict the steady turning performance of (1) single-unit vehicles (passenger cars, multiple-axle straight trucks, etc.) and (2) articulated vehicles (tractor-semitrailers, car-trailers, etc.). These models are intended for studying low level lateral acceleration conditions as typically encountered during steady turning on most highway curves. (Chapter 3 and appendices A and B describe and document these models in greater detail.) The primary advantage of these models over more complex models which are capable of providing similar information, is their simplicity. Furthermore, the parametric input and model outputs are specifically tailored to the analysis of side friction requirements used in highway curve design.

The second part of the model development work involved modification of an existing vehicle dynamics simulation (UMTRI "Phase 4" [5], normally used to model heavy trucks and commercial vehicles) to better represent passenger car behavior. This model was then subsequently used to model transient and nonlinear dynamic maneuvers performed by automobiles and tractor-semitrailers

along superelevated curves. Typical usage would include simulation of obstacle avoidance maneuvers in which drivers move from one lane to another, or, braking during curve negotiation. The use of this type of model, in contrast to the steady-turning microcomputer models, allows one to identify peak friction demands during transient or dynamic maneuvering as well as representation of nonlinear operating conditions (e.g., low friction conditions in which tire forces saturate).

2.5 Overview of Vehicle Testing

The three vehicles used in the highway curve testing are shown in the photographs of figures 13 through 15 (Chapter 4). Vehicle A (figure 13) is a compact front-wheel-drive passenger car weighing 3,200 lb (1,452 kg) in its test condition. Vehicle B (figure 14) is a midsize rear-wheel-drive passenger car weighing 3,500 lb (1589 kg) in its test condition. Vehicle C (figure 15) is a five-axle tractor-semitrailer having a gross vehicle weight of approximately 76,000 lb (34,504 kg) when tested. Each vehicle carried two passengers (including the driver), an instrumentation package, and an onboard electrical generator during the highway tests. During each test various vehicle reponses were measured and stored on tape for subsequent data analysis.

Three types of maneuvers were performed for each vehicle at the selected curve sites. The first maneuver was simple steady turning in which the test driver drove the superelevated curve at a fixed speed in one lane. The second highway test was an obstacle avoidance maneuver in which the driver, starting from a steady turn condition in the outside travel lane, steered to the inside travel lane and back again, similar to a passing maneuver. The third maneuver was braking / accelerating in a turn and duplicated the steady turning maneuver except that the brakes were applied to a moderate level while in the curve causing the vehicle to slow down. This was then followed immediately by a period of acceleration in which the vehicle was brought back up to its initial speed. Each of these highway maneuvers represent reasonable scenarios for vehicles operating along superelevated highway curves and, as such, were selected as the basis of the experimental measurements.

The vehicle tests were performed at three highway curve sites. Each site was a conventional connector-type ramp containing two traffic lanes in the direction of travel. Each curve had a 1273 ft (388 m) radius and was superelevated to either 6.7 percent or 7.0 percent. The posted speed limit was 55 mph (88 km/h) for all curves. Some additional data was collected at an exit ramp site having a radius of 230 ft (70 m) and superelevation of 7 percent. The advisory speed limit for the ramp was 25 mph (40 km/h). The ramp data provided a good alternative benchmark to the other curves, in terms of speed and radius, to further check and validate the computer models.

2.6 Sensitivity Analysis Overview

Following the vehicle testing and model validation efforts, a sensitivity analysis was conducted to evaluate typical variations of vehicle and highway geometric parameters as influences for affecting friction factor levels or their wheel-to-wheel distribution on a vehicle. A passenger car and a five-axle tractor-semitrailer were used as baseline vehicles for this study. If a particular vehicle parameter, such as tire cornering stiffness, was shown to strongly affect friction factor values and their distribution about a typical vehicle, the highway design engineer may need to consider its influence in the present design policy. On the other hand, if typical variations of vehicle parameters are seen to have little affect upon altering the friction factor values of a vehicle, the highway engineer can feel confident that nominal differences in vehicle characteristics normally occurring in the vehicle population will not significantly affect a highway curve design based upon a representative vehicle.

In addition to examining parameter variation influences, sensitivity analyses were also conducted for low friction conditions involving steady turning and obstacle avoidance maneuvers. The nonlinear model was used to study minimal surface friction requirements for performing the indicated maneuvers with a passenger car and five-axle tractor-semitrailer. The primary purpose was to help determine and compare friction factor variations required for steady turning maneuvers with those required in performing modest and representative highway obstacle avoidance maneuevers. Contributions to friction factor demand beyond that predicted by the point-mass model deriving

from vehicle characteristics and driver steering behavior were also considered in the analysis. Finally, a simplified analysis aimed at determining relationships between friction factor values and vehicle response variables is discussed from the viewpoint of how measurement errors can influence estimates of friction factor values.

Chapter 3

MODEL DEVELOPMENT

3.1 Introduction to the Different Models and Their Uses

Three basic model development activities occurred during this project. Two of these models were developed to predict steady turning performance of passenger cars and commercial vehicles and can be implemented on microcomputers. The microcomputer models are intended to study simple steady turning motion of vehicles at low levels of lateral acceleration normally encountered along superelevated highway curves. The remaining model development activity was concerned with modifying an existing large-scale computer model [5] to better represent passenger car suspension properties. The large-scale model is far more comprehensive but less convenient to use and is primarily intended for simulating transient or nonlinear vehicle maneuvers, such as obstacle avoidance or braking in a turn. The principal advantage of both types of models over a point-mass formulation lies in their more realistic representation of vehicle-highway interactions, which in turn provides more detailed information about vehicle responses and required tire forces.

If such models become too cumbersome and their advantages are negated by complicated rules of usage, their utility can be severely diminished. The microcomputer models developed during this project hopefully strike a balance between model realism and simplicity of use. In any event, the mathematical details underlying the microcomputer models developed here have been thoroughly documented (appendices A and B) such that future enhancements or translation to specific machines are easily accomplished.

The remaining sections of this chapter describe the specific models and present sample results of their usage. Interpretation of their predictions and recommended restrictions concerning their intended use conclude the chapter.

3.2 Single-Unit Steady Turning Model

3.2.1 Model Description

The "single-unit" model is used to represent passenger cars, straight trucks, and full trailers undergoing steady turning motion along superelevated highway curves of constant radius. One vehicle body element (sprung mass) and as many as six axles (unsprung masses) are permitted. Input to the model is in the form of parametric data which describes the vehicle and the highway geometry. Given a set of vehicle characteristics (weights and geometric information), a speed of travel, and the specified highway geometry (curve radius, superelevation, and grade), the model calculates the set of tire forces and steer angle required to negotiate the specified curve at the specified speed with that vehicle. Basic model output includes the orientation of the vehicle relative to the road, the required steer angle, drive thrust, tire forces, individual wheel friction factors, and the corresponding point-mass friction factor value.

Figures 8 through 10 illstrate the basic features of the single-unit model. The vehicle body or sprung mass element, m_s , is allowed to move vertically and to rotate in roll, pitch, and yaw. The suspension or unsprung masses, m_f and m_r, are fixed in height relative to the road plane. The vehicle has a body-axis coordinate system (x,y,z) whose origin is located at (x_0,y_0,z_0) and which translates and rotates with the vehicle body. The x-axis points forward, the y-axis to the right, and the z-axis downward. The inertial coordinate system (X,Y,Z) is fixed in space with the Z-axis aligned in the direction of the gravity vector. All body motions (translation and rotation) are expressed as relative motion between the body-axis system (x,y,z) and the inertial coordinate system (X,Y,Z). The origins and axes of the two coordinate systems coincide exactly if the vehicle is traveling in a straight line on a purely horizontal road plane (normal to the gravity vector). This condition can therfore be viewed as the "reference condition" with which to compare the model calculations for travel along a curve containing superelevation and/or grade.

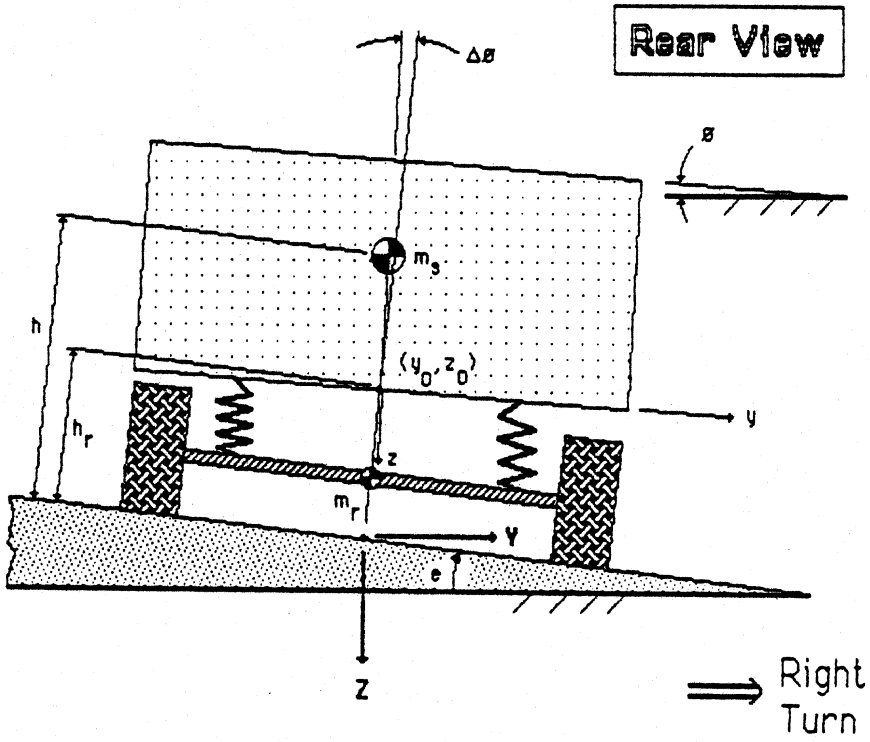

Figure 8. Single-unit model; rear view.

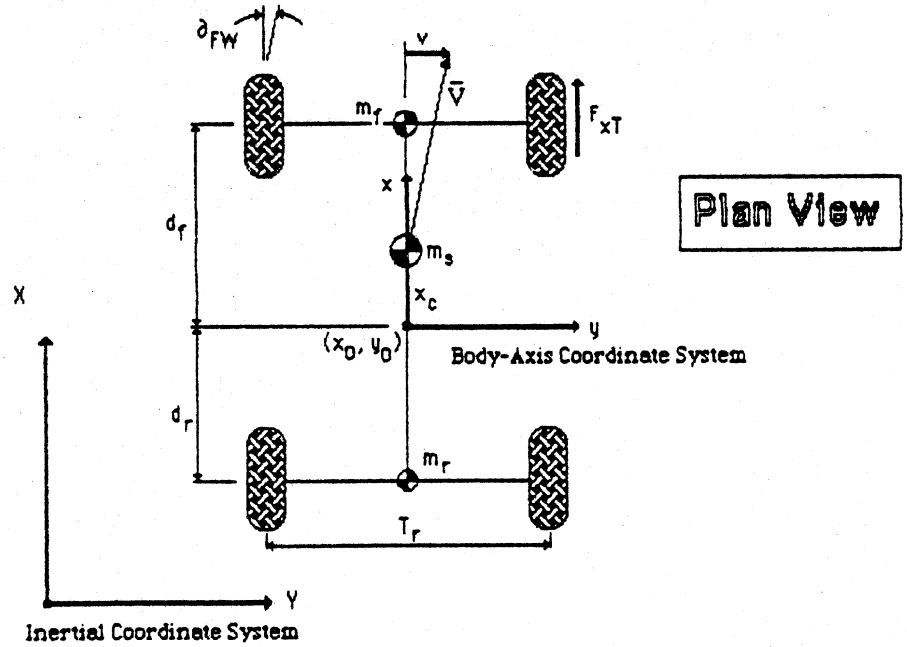

Figure 9. Single-unit model; plan view.

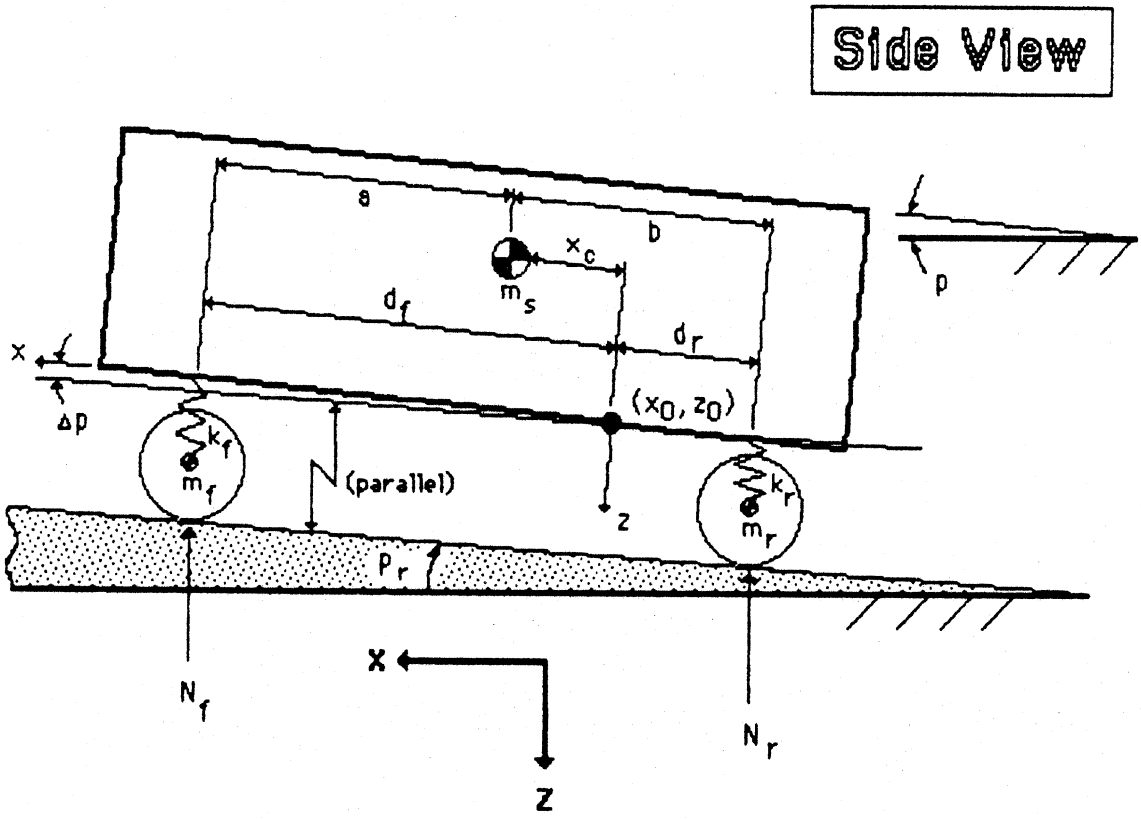

Figure 10. Single-unit model: side view

For example, figure 8 (Rear View) shows the road surface superelevated an amount, e, for the vehicle turning to the right. The body of the vehicle is seen as having rolled an amount $\Delta\phi$ relative to the superelvated road surface, or an amount ϕ relative to the horizontal plane (normal to the gravity vector). By the aforementioned convention, the model calculates the angle ϕ which is the angle between the body-fixed coordinate system y-axis and the inertial coordinate system Y-axis. The quantity $\Delta\phi$ is simply the difference between ϕ and e. (Thus, if ϕ is zero, $\Delta\phi$ is equal to -e.)

Sign conventions for displacements and rotations follow normal SAE practice [7].

1. A positive z-displacement of the body (bounce motion) is down and toward the road surface.
2. Positive roll motion of the body is clockwise when viewed from the rear as in figure 8.
3. Positive pitch motion of the body is defined as "nose up" as shown in figure 10.
4. Positive superelevation is defined as a road surface sloping downward to the right as seen in figure 8.
5. Positive grade, p_r, is a road surface sloping upward as seen in figure 10.

The single-unit model calculates for the specified steady turning condition the following basic quantities, also seen in figures 8 through 10:

F_{XT} the required tire drive thrust (front or rear drive)

p the pitch angle of the body (relative to the reference condition)

v the lateral sideslip velocity of the vehicle sprung mass center

z the vertical bounce motion of the body (relative to the reference condition)

d_{FW} the required steer angle

and

ϕ the roll angle of the body (relative to the reference condition)

From this information the necessary lateral and vertical tire forces are then calculated. Values for the individual wheel friction factors and the equivalent point-mass value friction factor conclude the set of model calculations. Additional details on the single-unit model calculations can be found in appendix A.

3.2.2 Parametric Input Data

In order to perform the calculations identified in the previous section, certain parametric input data describing the vehicle and the highway geometry are needed. The following parameters are required as input by the single-unit model and over which the model user has direct control for studying and analyzing various types of highway-vehicle interactions. The listing of the parameters is in the same order as required by the microcomputer model (appendix D):

n_f number of axles on the front suspension (1 to 5)

n_r number of axles on the rear suspension (1 to $6-n_f$)

C_{af} front tire cornering stiffness

C_{ar} rear tire cornering stiffness

K_f front suspension stiffness

K_r rear suspension stiffness

WB vehicle wheelbase

e highway superelevation

p_r highway grade

V vehicle speed

R highway curve radius

N_f front static axle load(s)

N_r rear static axle load(s)

z_f height above ground of front suspension roll center

z_r height above ground of rear suspension roll center

h height above ground of sprung mass c.g.

T_F front suspension spread

T_R rear suspension spread

TT_f front tire track

TT_r rear tire track

W_f weight of front unsprung mass

W_r weight of rear unsprung mass

C_r rolling resistance percentage

The following aerodynamic parameters are optional:

h_A height above ground of the aerodynamic center of pressure

x_A distance of aerodynamic center of pressure ahead of the body mass center

AF Frontal cross-sectional area of vehicle

C_D aerodynamic drag coefficient

C_{LO} aerodynamic lift coefficient at trim pitch angle ($p = p_r$)

s_L slope of aerodynamic lift coefficient with respect to pitch

s_Y slope of aerodynamic side force with respect to relative (wind) yaw angle

Normally, in a computer implementation, the model user has the option of reading most of these parameters from prestored data files which would contain default values based upon vehicle size or weight categories. The remaining few data items associated with highway geometry and vehicle speed, and likely to be regularly altered, would be entered from the keyboard in an interactive fashion. Appendix D contains an informal user's manual for operating the Apple II+ microcomputer implementation of the single-unit model described here.

Numerous examples of the single-unit model calculations appear throughout this report, particularly in chapters 5 and 6 and also in appendix D.

3.3 Tractor-Semitrailer Steady Turning Model

3.3.1 Model Description

The tractor-semitrailer steady turning model is very similar in concept and purpose to the single-unit model described in the previous section. The tractor-semitrailer model of course contains an additional axle and sprung mass element (tractor) in addition to an articulation joint which connects the tractor to the semitrailer. Hence, the model calculates the steady turning orientation of two sprung mass elements (tractor and semitrailer), the required articulation angle between the two units, the tractor front wheel steer angle, and all of the tire forces and associated friction factor values. The tractor-semitrailer model permits only one axle on the tractor front suspension but allows the tractor rear suspension and semitrailer suspension to distribute as many as six axles in any manner.

Figure 11 shows a plan view of the tractor-semitrailer model. The very same rules concerning variable definitions discussed for the single-unit model apply equally to the tractor-semitrailer model. In figure 11 the articulation angle (angle between the x-axes of the tractor and semitrailer), Ω, and the tractor front axle steer angle, δ_{FW}, are defined. Also seen are the sideslip velocities, v_1 and v_2, of the tractor and semitrailer units. The model treats the tractor roll angle as equal to that of the semitrailer.

The single-unit model calculates for the specified steady turning condition the following basic quantities, identical in definition to those seen in figures 8 through 10 for the single unit model, and in figure 11 for the tractor-semitrailer model:

F_{xT} the required tractor rear tire drive thrust

p_1 the pitch angle of the tractor body (relative to the reference condition)

p_2 the pitch angle of the semitrailer body (relative to the reference condition)

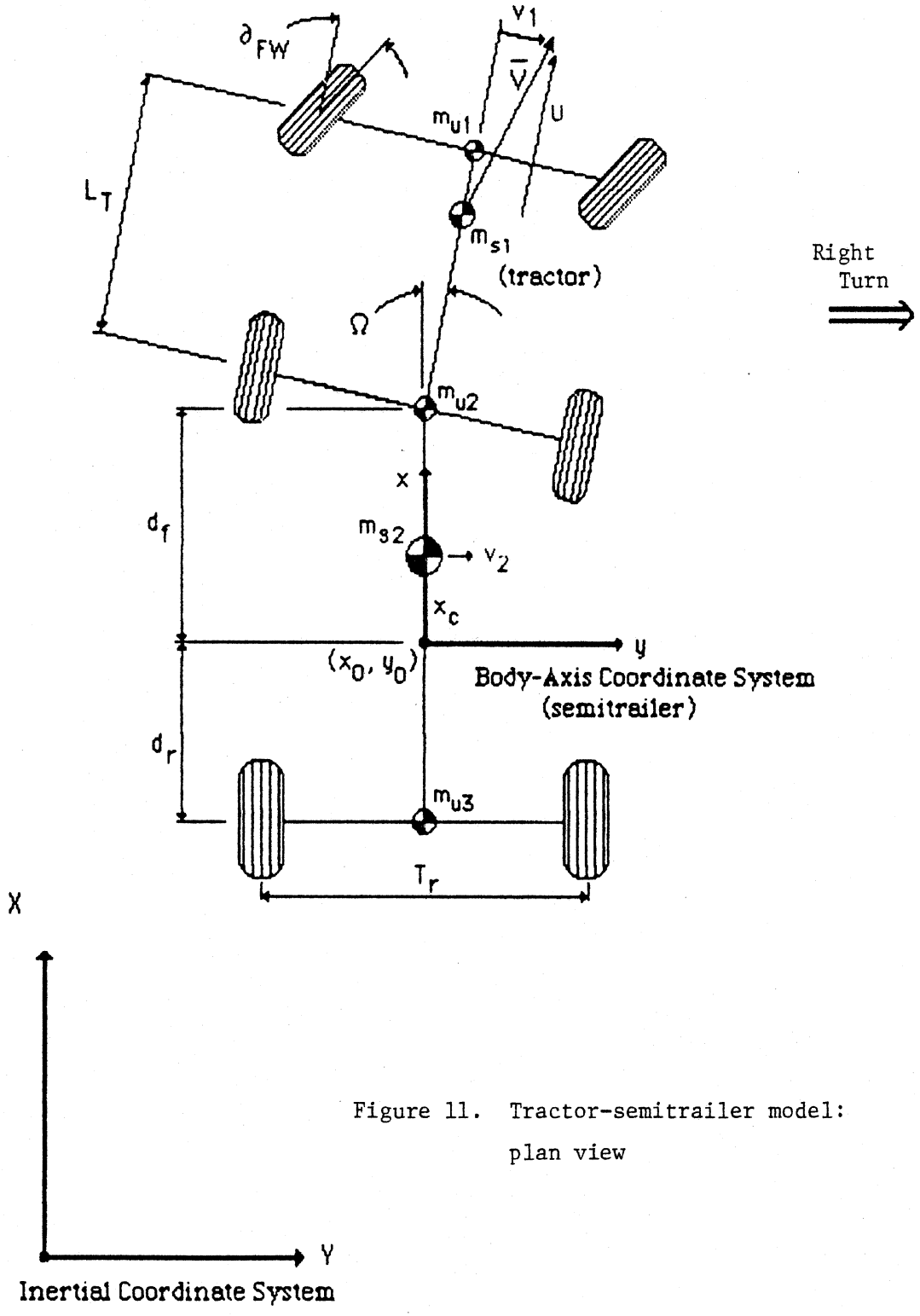

Figure 11. Tractor-semitrailer model: plan view

v_1 the lateral sideslip velocity of the tractor mass center

v_2 the lateral sideslip velocity of the semitrailer mass center

z_1 the vertical bounce motion of the tractor body (relative to the reference condition)

z_2 the vertical bounce motion of the semitrailer body (relative to the reference condition)

δ_{FW} the required tractor front axle steer angle

ϕ the roll angle of the tractor and the semitrailer bodies (relative to the reference condition)

Ω the required articulation angle between the tractor and semitrailer

As in the case of the single-unit model, the necessary lateral and vertical tire forces are then determined from this information. Values for the individual wheel friction factors and the equivalent point-mass friction factor value conclude the set of model calculations. Additional details on the tractor-semitrailer model calculations are contained in appendix B.

3.3.2 Parametric Input Data

The following list of parameters, similar to those seen in the single-unit model, are required as input to the tractor-semitrailer model. The listing of the parameters is in the same order as required by the microcomputer model (appendix D):

n_1	number of tractor rear axles
n_2	number of semitrailer rear axles
C_{a1}	tractor front tire cornering stiffness
C_{a2}	tractor rear tire cornering stiffness
C_{a3}	semitrailer rear cornering stiffness
K_1	tractor front suspension stiffness
K_2	tractor rear suspension stiffnesses
K_3	semitrailer suspension stiffnesses
dA1	fore/aft tandem axle spread on tractor
dA2	fore/aft tandem axle spread on semitrailer
WB_T	tractor wheelbase
WB	semitrailer wheelbase
e	highway superelevation
p_r	highway grade
V	vehicle speed
R	highway curve radius
N_s	tractor and semitrailer static axle loads
W_1	weight of tractor body
z_1	height above ground of tractor front suspension roll center
z_2	height above ground of tractor rear suspension roll center
z_3	height above ground of semitrailer suspension roll center
h_1	height above ground of tractor body mass center
h_2	height above ground of semitrailer sprung mass c.g.
h_5	Fifth wheel height above ground
h_F	Tractor frame height above ground
T	tractor and semitrailer suspension spreads
TT	tractor and semitrailer tire track widths
W_u	weight of axles
C_r	rolling resistance percentage

The following aerodynamic parameters are optional:

h_A	height above ground of the aerodynamic center of pressure
x_A	distance of semitrailer aerodynamic center of pressure ahead of the semitrailer mass center
AF	frontal cross-sectional area of vehicle
CD	aerodynamic drag coefficient of the combination vehicle
CL0	aerodynamic lift coefficient at trim pitch angle (p = pr)
s_L	slope of aerodynamic lift coefficient with respect to pitch
s_Y	slope of aerodynamic side force with respect to relative (wind) yaw angle

The additional number of parameters required for the tractor - semitrailer model are of course due to the increased number of units and possible axles. As in the case of the single-unit model, any computer implemenation of the tractor-semitrailer model would presumably store standard sets of these numerical values in data files associated with different vehicle types. Only those parameters routinely changed as part of some study or analysis would then be required as keyboard entry items. Appendix D contains instructions for operating the Apple II+ microcomputer implementation of the tractor-semitrailer model developed under this project. It is similar in concept and description to that outlined above.

3.4 Modifications to the Comprehensive Braking and Steering Model

As part of the model development activity, an existing large-scale computer simulation [5] primarily used for modeling commercial vehicles was modified to include independent wheel suspensions. This additional feature was added to this model so that improved simulation of passenger car behavior could be conducted within the project work. Frequently referred to as the "Phase 4" model, it was primarily intended for use in this project for simulating obstacle avoidance maneuvers along superelvated curves wherein a driver model steers the vehicle from one lane to another along a prescribed path. The other type of maneuver for which the Phase 4 model was employed was in simulating braking / accelerating maneuvers also along superelevated curves. The principal difference between the Phase 4 model and those

described in the previous two sections is that the Phase 4 model is a dynamic model capable of representing time-varying and/or nonlinear vehicle/driver responses. The steady turning models are static, fixed steer, constant velocity models intended for low level lateral acceleration operating conditions. The Phase 4 model of course can be used to simulate the same steady turning performance under low acceleration conditions. However, unless some special nonlinearity or other feature for which the steady turning models are not applicable is needed, the steady turning models will provide much the same information as the Phase 4 model, but at a considerably lower level of user effort and computer hardware.

The primary reference for the Phase 4 model is its user's manual [5]. The material contained here and in appendix C supplement the Phase 4 user's manual by documenting the independent suspension option added during the course of this project. Reference to figure 12 shows a sketch of the basic kinematics comprising the independent suspension model added during this project. The overall layout of the suspension resembles a McPherson strut assembly. The main strut, of rest length L_s, contains a linear spring and a viscous damping element. The strut is allowed to vary in length while pivoting about its end points in response to vehicle sprung mass motions or tire deflections. The lateral link, of length "a", locates the lower pivot point of the strut. The wheel axle assembly is assumed by the model to remain parallel to the road surface in response to suspension motion. Tire camber and steer motions resulting from suspension motion is accommodated by camber-bounce and steer-bounce coefficients specified by the program user.

By defining the geometric parameters b, c, and R_T shown in figure 12, the model user effectively determines the kinematic relationships required by the model to calculate the linkage motions. Specification of linear steer-bounce and camber-bounce coefficients permit simulation of additional tire-suspension motion dependencies. The independent wheel suspension model can be employed at any wheel location of a simulated vehicle. Further details concerning the model and associated modifications to the Phase 4 program can be found in appendix C.

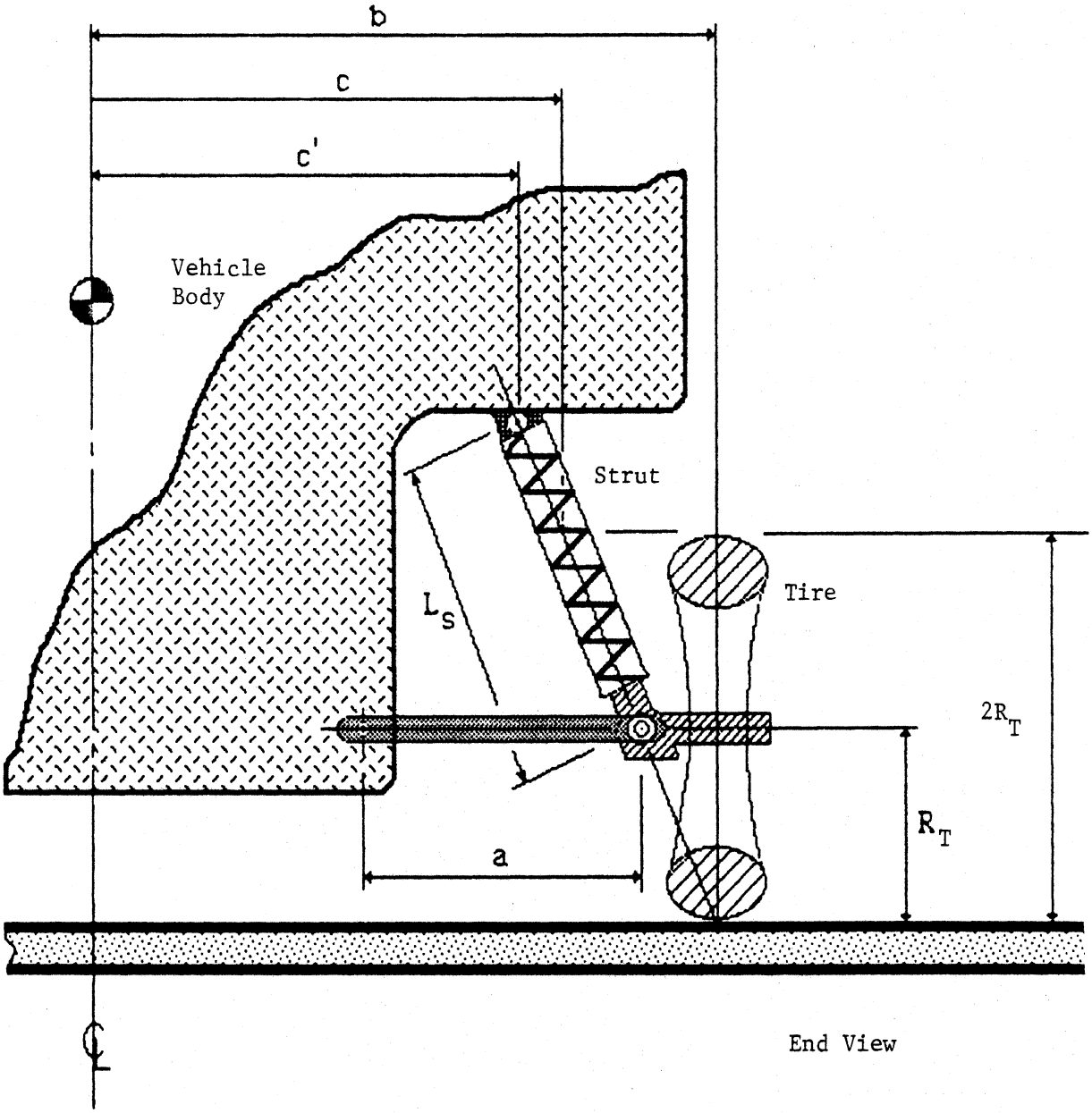

Input Parameters:

b tire track dimension
c spacing of upper strut pivot
R_T static tire radius

steer-bounce coefficient
camber-bounce coefficient

Figure 12. Independent suspension model (Phase 4)

The suspension model described here was used to simulate the independent suspension characteristics for passenger car vehicles tested and analyzed within the project. The addition of this suspension feature permitted the analysis of both passenger cars and commercial vehicles within the context of one vehicle dynamics program. Frequently when two different vehicle models are employed to compare results about similar vehicle dynamics problems, small differences in the models themselves can interfere with the interpretation of results, particularly when the differences in results might happen to be relatively small. Furthermore, switching from one vehicle type to another during a simulation exercise is more convenient and less prone to error with one model since the protocol regarding parameter modifications is more standardized.

3.5 Model Applications and Recommended Usage

Computer models are often developed for specific purposes and as such are earmarked for some restricted range of operating conditions or set of applicable rules of usage. In some cases these restrictions are implicit and not clearly defined. The material in this section is intended to help guide a potential user of the models and computer programs developed under this project to better estimate the range of applicability of the different models.

3.5.1 Single-Unit Steady Turning Model Applicability

The following list of operating conditions should be satisfied when using the simplified single-unit model to study passenger cars or similar vehicles.

* Constant velocity, constant radius, fixed steer turning maneuvers
* Superelevation rates less than 15 percent
* Grades less than 15 percent
* Vehicle speeds greater than 10 mph (16 km/h)
* Friction factor values less than 0.30
* Moderate or high tire/road surface friction levels (peak friction > 0.40)
* Presumption of simple linear vehicle characteristics

Noncompliance with these recommended operating conditions can result in model predictions that are less reliable and in some cases meaningless.

Use of the single-unit model to study commercial vehicles such as straight trucks or full trailers should follow the recommendations pertaining to the tractor-semitrailer model in the following section.

3.5.2 Tractor-Semitrailer Steady Turning Model Applicability

The simplified tractor-semitrailer model should observe the same usage restrictions as the single-unit model noted above, except for the maximum friction factor recommendation. Since the friction factor represents the road-plane lateral acceleration demand required of the vehicle, it also reflects, in more or less direct proportion, the amount of side-to-side load transfer occurring across the vehicle suspensions. As noted in section 2.2.2, significant vertical load changes in truck tires cannot be treated in quite the same manner as passenger car tires. That is, unless the friction factor values are less than about 0.10, the assumption that tire cornering stiffnesses are nearly constant begins to lose validity. Since most commercial vehicles can have a wide range of mass center heights which, together with lateral acceleration, are the principal determinants of side-to-side load transfer, the model user should restrict the range of friction factor applicability when studying commercial vehicles with elevated mass centers. In general, if a fully loaded commercial vehicle is being studied, the maximum friction factor should probably not exceed 0.20 to 0.25 depending upon the c.g. height. Most empty commercial vehicles can be studied up to maximum friction factor values of 0.30.

The tractor-semitrailer model contains an option for representing tire cornering stiffness as a function of vertical load for cases in which accurate tire load sensitivity is important. Normally this should be employed for commercial vehicles experiencing friction factor values above 0.15 . Constant cornering stiffness values for commercial vehicles can of course be used, but if so, the individual wheel friction factor values predicted by the model will

display slightly greater dispersion than should normally occur, due to the aforementioned cornering stiffness properties of typical truck tires.

3.5.3 Phase 4 Model Applicability

The Phase 4 model is far less restricted in its range of operating conditions than the steady turning models. The primary limitations for this model are noted below:

* Vehicle roll angles less than 15 degrees (0.25 rad)
* Vehicle pitch angles less than 15 degrees (0.25 rad)
* Vehicle speeds greater than 3 mph (5 km/h)

The principal reasons for the roll and pitch angle restrictions are due to "small angle" assumptions in the Phase 4 model for these motion variables. In general, this also implies restrictions for highway superelevation and grade equal to those identified for the steady turning models (< 15 percent). The low speed restriction does not apply to braking maneuvers so much as it does for very low speed turning maneuvers. At very low speed, the lateral tire force calculations are altered to avoid low speed computational difficulties and thereby become less accurate in this speed range.

Finally, it should be noted that following the development of the steady-turning models, several different comparisons under identical operating conditions were performed between the steady-turning models and the Phase 4 model. In all cases, the predicted vehicle responses of both models agreed within differences of less than 1 percent. Comparisons were made for superelevated and nonsuperelevated curves, as well as for straight superelevated tangents (infinite radius case for the simplified models). A passenger car and a three-axle tractor-semitrailer were used as comparison vehicles in this exercise. In short, the steady turning models developed during this project are viewed as accurate predictors of steady state vehicle turning performance when used within the intended range of applications cited earlier.

Chapter 4

VEHICLE TESTING

This chapter presents a description of the full scale vehicle testing which took part during the project. Two standard 1984 passenger cars and a five-axle tractor-semitrailer were used in the test program. The majority of tests were conducted along AASHTO horizontal curves at speeds near the posted limit. Data collected from the testing were used to validate the computer models developed during the course of the project research. The data collected also serve as a useful resource for current and future research programs.

The chapter begins with a description of the test vehicles, the curve sites, and vehicle test maneuvers performed. A description of the test measurements and the data acquistion system follows. Example test results are then presented for each vehicle. A general discussion of the test results concludes the chapter.

4.1 Test Vehicle Descriptions

Figures 13 through 15 show photographs of the three test vehicles labelled here as vehicles A, B, and C, respectively. Vehicle A is a standard 1984 front wheel drive four-door passenger car, and vehicle B is a 1984 two door rear wheel drive passenger car. Vehicle C is a five-axle tractor - semitrailer consisting of a 142 inch (3.6 m) wheelbase COE tractor and a 45 ft (13.7 m) van semitrailer. Table 1 lists basic parameters and features describing each of the three test vehicles.

Figure 13. Test vehicle A

Figure 14. Test vehicle B

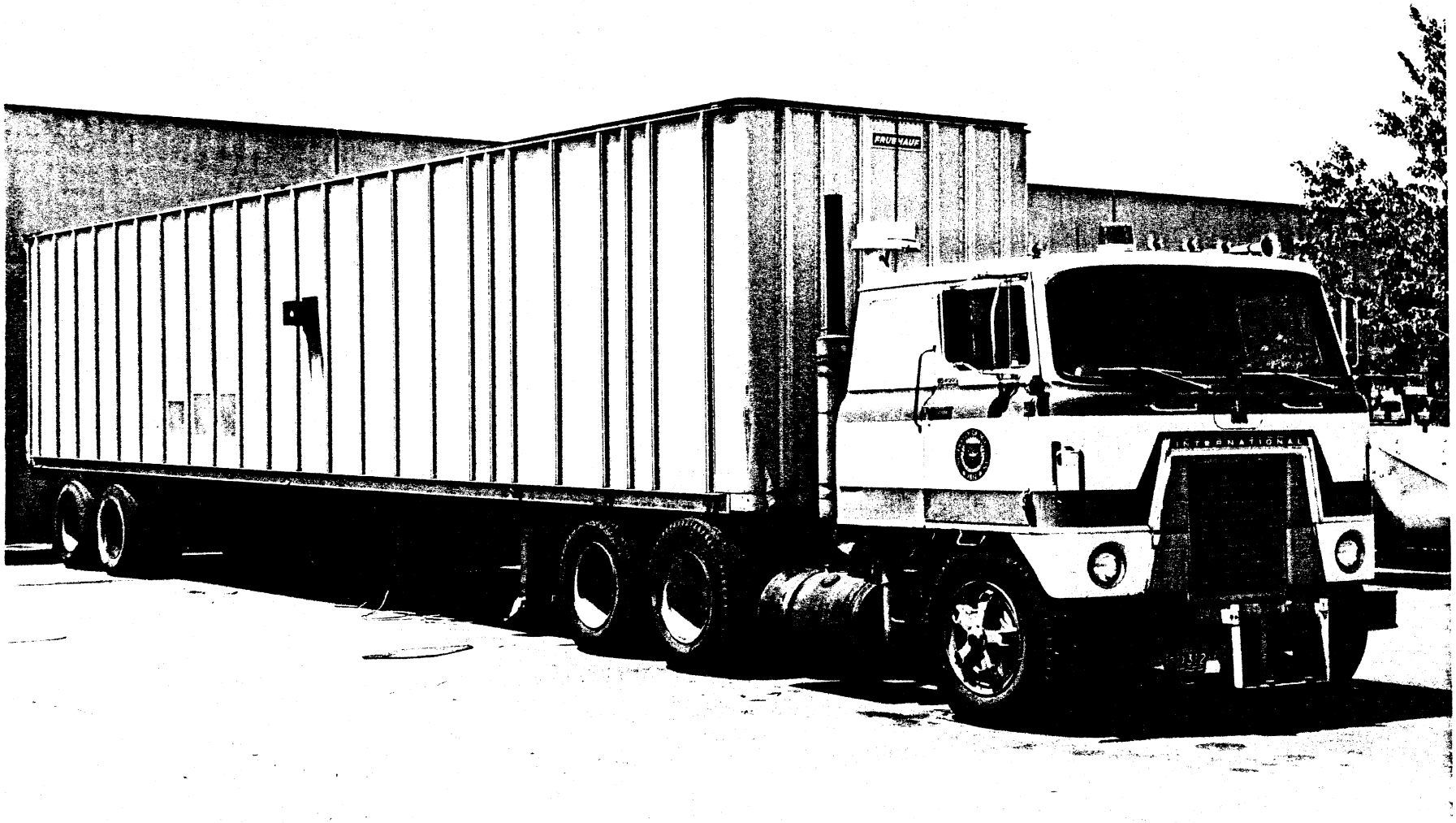

Figure 15. Test vehicle C

Table 1. Test vehicle descriptions

Passenger Car A:	
Wheelbase	100.3 "
Front axle load (2 passengers & instrumentation)	1800 lb
Rear axle load	1400 lb
Estimated c.g. height above ground	25 "
Front tire track	57 "
Rear tire track	57 "
Front wheel drive	
Passenger Car B:	
Wheelbase	105.6 "
Front axle load (2 passengers & instrumentation)	1925 lb
Rear axle load	1675 lb
Estimated c.g. height above ground	25 "
Front tire track	57 "
Rear tire track	57 "
Rear wheel drive	
5-Axle Tractor-Semitrailer C:	
Tractor wheelbase	142 "
Semitrailer wheelbase	410 "
Tractor front axle load	10,300 lb
Tractor rear axle loads (each)	15,700 lb
Semitrailer axle loads (each)	16,900 lb
Tractor c.g. height above ground	44 "
Semitrailer c.g. height above ground (body + payload)	70 "
Tractor front tire track	81 "
Tractor rear tire track	73 "
Semitrailer rear tire track	73 "

1 inch = 25.4 mm

1 pound = 0.454 kg

4.2 Horizontal Curve Site Descriptions

Three horizontal curves in the vicinity of Ann Arbor, Michigan were selected as sites at which to perform the vehicle measurements. Each of these sites was a conventional connector-type ramp having two traffic lanes in the direction of travel and a posted speed limit of 55 mph (88 km/h). Figures 16 and 17 illustrate each of the curves labeled as 1, 2, and 3, respectively. Table 2 lists the geometric data describing each curve and is based upon topographic survey maps obtained from the Michigan Department of Transportation.

In addition to the three curve sites 1 to 3, data was also collected on a standard clover-leaf exit ramp having a radius of 230 ft (70 m) and superelevation rate of 6 percent to 7 percent. (Field measurements performed by the Michigan Department of Transportation during the test program determined that the exit ramp superelevation rate was mildly variable in this range and primarily attributable to several resurfacing efforts since its initial construction.) The exit ramp, labeled as site 4, was primarily used to provide an alternative set of speed and radius conditions to further check and validate the computer models. Its basic geometric data are also shown in table 2 . A sketch of the ramp is shown in figure 17.

Table 2. Summary of curve site geometry

Curve Site #	Radius (ft)	Curvature (deg)	Superelevation (%)	Length (ft)	Grade (%)
1	1273	4 30'	6.7	1273	+0.5 to -1.2
2	1273	4 30'	7.0	1785	+0.3 to -1.9
3	1273	4 30'	6.7	1826	+1.0 to -1.2
4 (ramp)	230.7	24 50'	6.0 to 7.0	1087	0.0 to -2.0

1 ft = 0.305 m

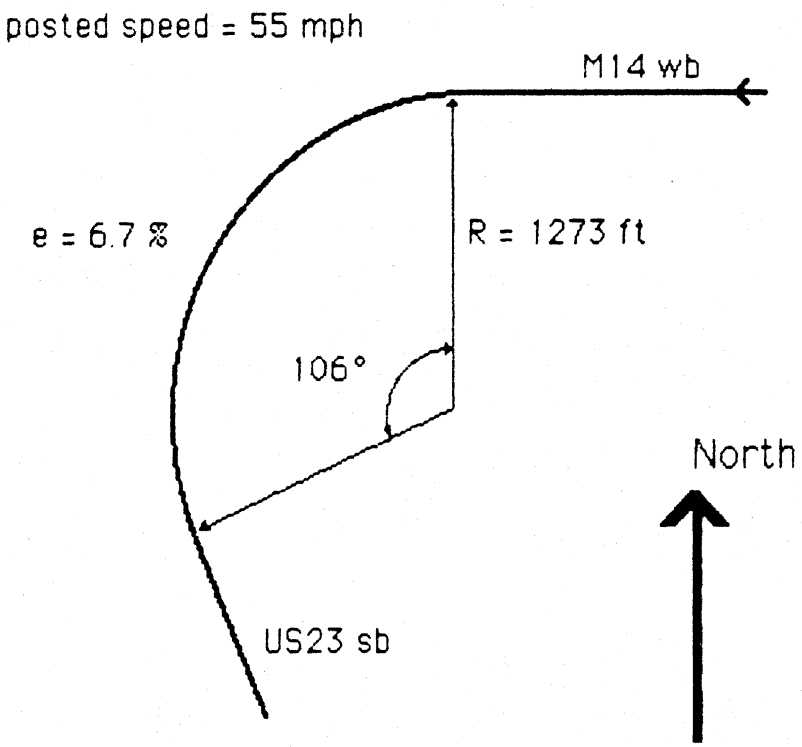

Curve site 1.

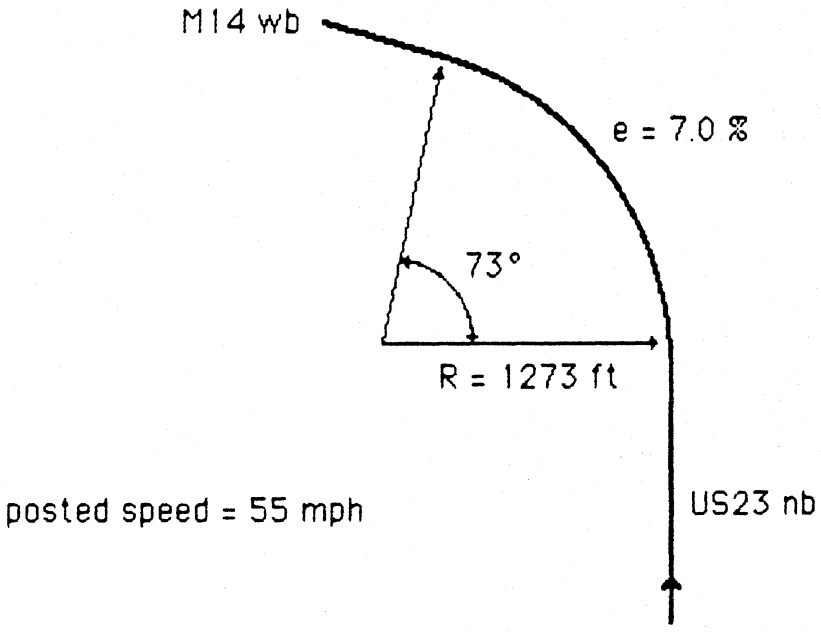

Curve site 2.

Figure 16. Curve site descriptions.

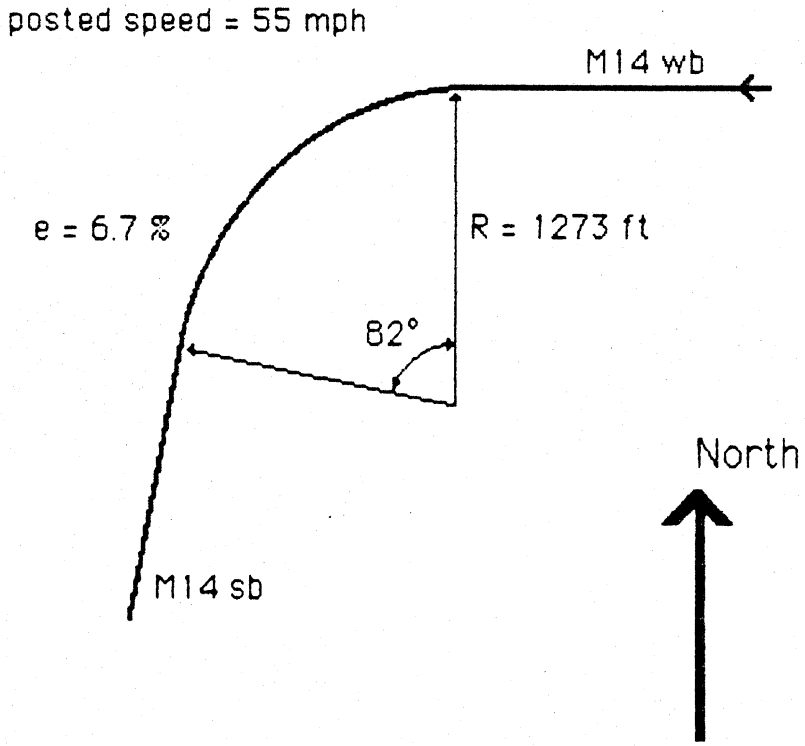

Curve site 3.

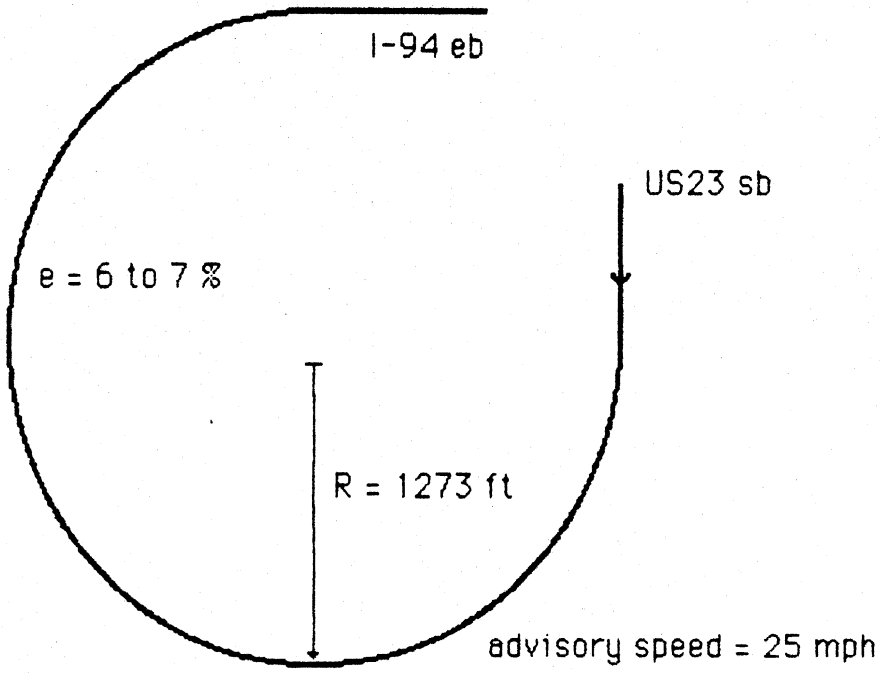

Curve site 4 (ramp).

Figure 17. Curve site descriptions.

4.3 Test Measurements and Data Acquisition

Sixteen channels of data were collected for the tractor-semitrailer test vehicle and ten channels of data for each of the passenger cars. Tables 3 and 4 list the type of data measured for each vehicle.

Table 3. Tractor-semitrailer measurements

Channel #	Measurement	Units	Symbol
1	Time	seconds	t
2	Vehicle Speed	mph	V
3	Trailer Lateral Accel	g's	ay2
4	Trailer Long Accel	g's	ax2
5	Trailer Yaw Rate	deg/sec	r2
6	Trailer Roll Angle	degrees	$\phi 2$
7	Trailer Pitch Angle	degrees	θ
8	Steering Wheel Angle	degrees	dsw
9	Left Front Steer Angle	degrees	dfwl
10	Right Front Steer Angle	degrees	dfwr
11	Articulation Angle	degrees	Gam
12	Wheel Rotation	degrees	---
13	Wheel Load A	pounds	A
14	Wheel Load B	pounds	B
15	Trolley Angle	degrees	Trolley
16	Tractor Yaw Rate	deg/sec	r

Table 4. Passenger car measurements

Channel #	Measurement	Units	Symbol
1	Time	seconds	t or T
2	Vehicle Speed	mph	V
3	Lateral Acceleration	g's	Ay
4	Longitud Acceleration	g's	Ax
5	Yaw Rate	deg/sec	r
6	Roll Angle	degrees	ϕ
7	Pitch Angle	degrees	θ
8	Steering Wheel Angle	degrees	dsw
9	Left Front Wheel Angle	degrees	dfw
10	Trolley Angle	degrees	Trolley

Data channels 3 to 7 were part of a stable platform measurement system which was located at the approximate center of gravity of the semitrailer and each passenger car. A conventional fifth wheel, as seen in figure 18, was used for the measurement of vehicle speed (channel 2). Linear potentiometers were used for all front wheel angle measurements; a rotary potentiometer was used for the measurement of steering wheel angle. A "string" potentiometer was used for measuring tractor-semitrailer articulation angle. Channels 12-14 for the tractor-semitrailer were measurements from the FHWA (Maritime Dynamics) Wheel Load Transducer [9] located at the right and rearmost wheel position of the semitrailer. Trolley Angle measurements for vehicle sideslip were made with the FHWA (MIRA) sideslip / roll trolley [8]. See figure 18. Tractor yaw rate, supplementing the trailer yaw rate measurement, was measured using a rate gyro mounted on the tractor frame rails. The yaw rate and vehicle speed measurements were used to estimate path curvature during steady turning conditions. The complete digital data acquisition system was located in the tractor cab and rear seats of each passeneger car during the tests. Other instrumentation is seen in figure 19.

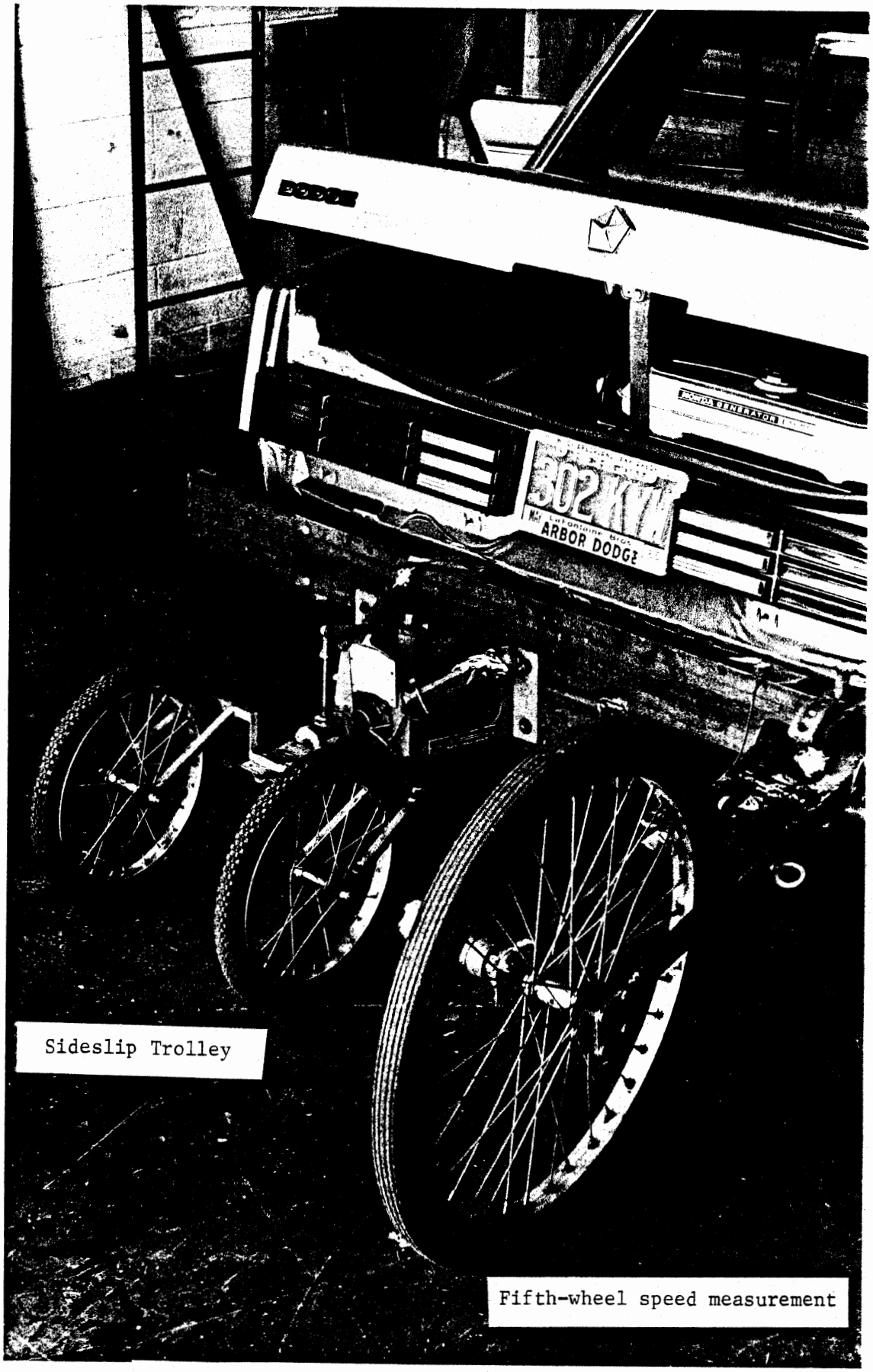

Figure 18. Trolley and fifth-wheel instrumentation.

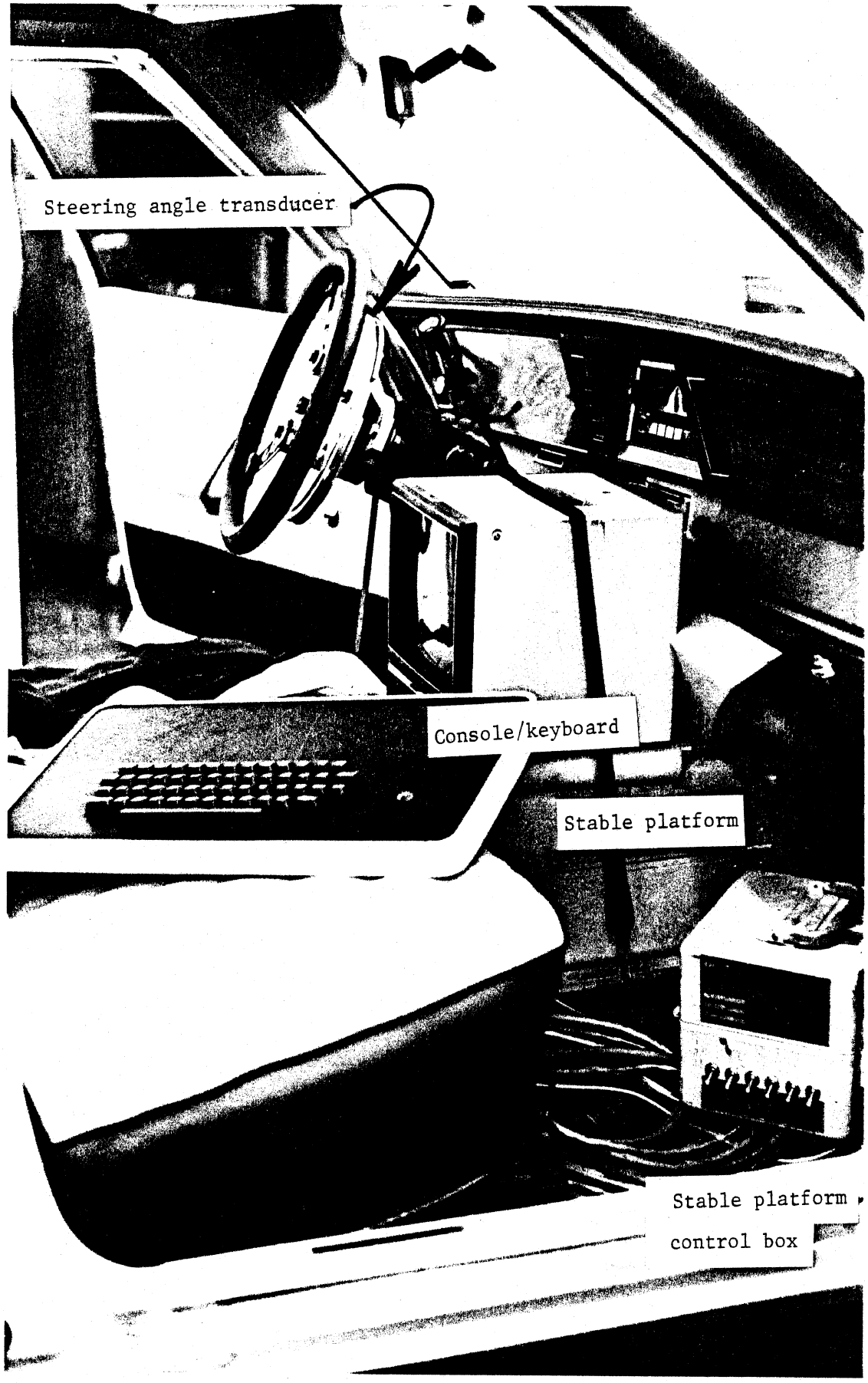

Figure 19. Instrumentation and data acquisition console.

The measured values of roll angle or predicted values from the models seen throughout this report are all relative to the true vertical (gravity vector). Also lateral acceleration values measured and predicted are those occurring in the horizontal plane. Hence, point-mass friction factors are obtained by subtracting the roadway superelevation from the lateral acceleration value (expressed in g's).

In addition to these vehicle-based measurements which occurred during highway testing, laboratory measurements of tire characteristics were also conducted. A sample tire from each suspension of each test vehicle (four passenger car tires; three truck tires) was selected for testing to measure lateral tire force properties as a function of tire slip angle and vertical load. These data were later used in the computer models during the model validation activity. The laboratory tire tests were performed on the UMTRI flat bed tire test machine. Each tire was tested at slip angles of -1, 0, +1, +2, and +4 degrees. Vertical tire loads above, below, and equal to the expected operating load during highway testing were used in the laboratory measurements. Tire cornering stiffness values used by the steady turning models were calculated from the average of the +1 and -1 degree lateral tire force measurements. Appendix E contains the complete set of laboratory tire measurements.

Steering system tests were also conducted on the tractor test vehicle. Since commercial vehicle steering system properties are often less well behaved than passenger car systems and frequently contain significant levels of hysteresis, laboratory tests were performed on this vehicle to gather basic information on steering gain and hysteresis. The steering wheel - front wheel measurements were collected to supplement front wheel measurements in the event transducer problems occurred during the vehicle tests. The steering system tests were conducted with the axle loaded normally and also with no load applied. The measurements, seen in appendix E, show that typical levels of hysteresis (40 degrees of dead zone at the steering wheel) did exist in the steering system of the tractor. The net result is that measurements of driver steering wheel movements during highway tests will usually be more active than, and less well correlated with, the corresponding front wheel angle measurements.

Lastly, the vehicle measurement time histories presented within the report are in an "as is" state. That is, except for simple averaging calculations and removal of signal offsets, no attempt was made to "massage" the data. In general, most of the vehicle measurement data collected during the test program are of good quality. Weaknesses exist here and there due to slight gain and offset errors, but overall, the measurements are viewed as reliable and worth preserving for future reference.

4.4 Vehicle Test Maneuvers

Three types of vehicle tests were conducted for each vehicle at the three superelevated highway curve sites. The first test was simple steady turning in which the test driver was asked to follow the curve in a normal and smooth fashion. Data collection was initiated just prior to entering the curve, usually on a straight tangent having small and somewhat variable cross-slope. Data collection was completed 25 to 40 seconds later, depending on the curve and test vehicle (tractor-semitrailer maximum times were limited to 25 seconds because of the additional number of data channels being recorded). Normally, straight-running "zero calibration" data was also collected 1 to 2 miles (1.6 to 3.2 km) prior to and/or after each curve site in order to help identify transducer zero offset readings for use in the subsequent data processing. The stable platform erection system was also disabled prior to each test to prevent centripetal acceleration during turning from influencing the erection system estimate of the true vertical.

The second vehicle test maneuver was an obstacle avoidance, or "double lane change" maneuver, also performed along each curve. The driver first entered the curve and reached a steady turning condition. After several seconds, the vehicle was steered into the adjoining lane and then back into the initial travel lane. The intent was to simulate movement around an obstacle resting in the initial travel lane. The rapidity of movement from one lane to another was casual to moderate. Emergency or panic-like movements were not performed. The obstacle avoidance maneuevers were performed starting from the outside travel lane as well as from the inside travel lane.

The last vehicle test was braking / accelerating in a turn. Again, the test driver entered the curve and reached a steady turning condition. Braking was then applied to decelerate the vehicle down to a speed of about 20 to 30 mph (32 to 48 km/h) (braking to a complete rest was not possible for reasons of safety and traffic interruption). The vehicle was then accelerated back up to normal speed. The level of braking was usually light to moderate and typically in the vicinity of 0.3 g's of deceleration.

4.5 Example Steady Turning Test Results

Figure 20 shows a set of steady turning response measurements collected during a typical test. The data seen in figure 20 correspond to passenger car A and curve site 1. The time histories seen here include each of the measurements listed in table 4. During a test, each measurement was digitized at a rate of 40 Hz and stored on a high density cartridge tape for subsequent data processing and plotting. The time histories seen here are 8-Hz (subsampled) plots of the digitized data and have had zero offsets removed based on straight running "zero calibration" data. The numerical values shown on the right hand side of some of these plots are average values of the time history variables for the 15-second interval starting at the 10-second mark. The average value readings were typically used to define and compare the test data with predictions from the steady turning models. Similar sets of data for this vehicle and the other two test vehicles are contained in appendix E. Summary plots of the steady turning data are presented in chapter 5 where comparisons between the measurements and model predictions are presented.

In addition to the standard set of vehicle response measurements performed during these tests, measurement of vertical load at a single wheel location on the semitrailer test vehicle was also attempted as part of the steady turning tests. Figure 21 shows two sample vertical load measurements processed from the FHWA wheel load cell. Figure 21 represents time history playbacks of the peak values of the load cell channel B signal (following forward and inverse Fourier transformation to increase the time domain resolution and accuracy of the peak values). The degree of load transfer seen in the charts of figure 21 is slightly inflated because of load cell cross-talk between vertical and lateral load. Using the load cell manufacturer's

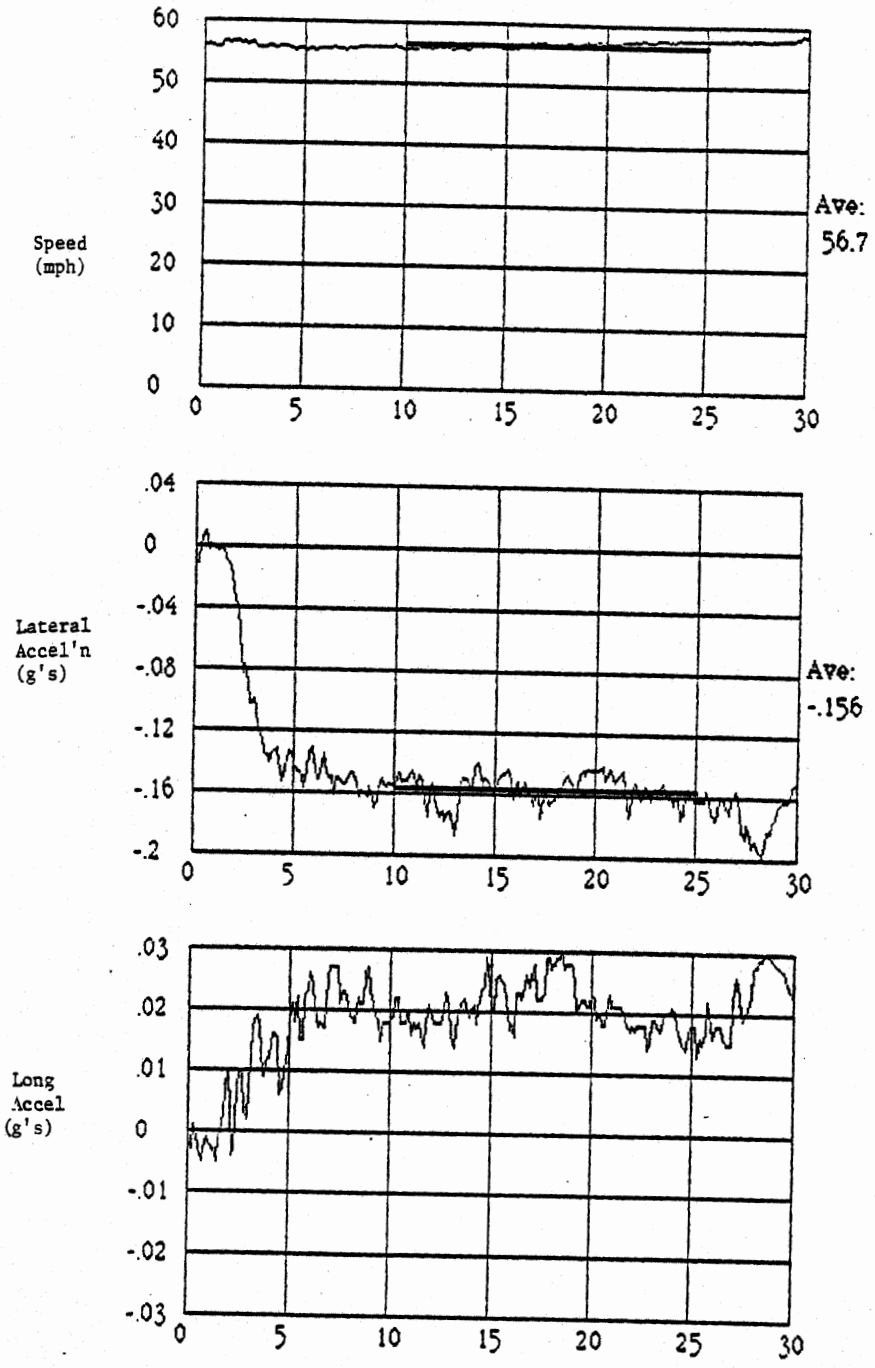

Figure 20. Example steady turning test result; vehicle A.

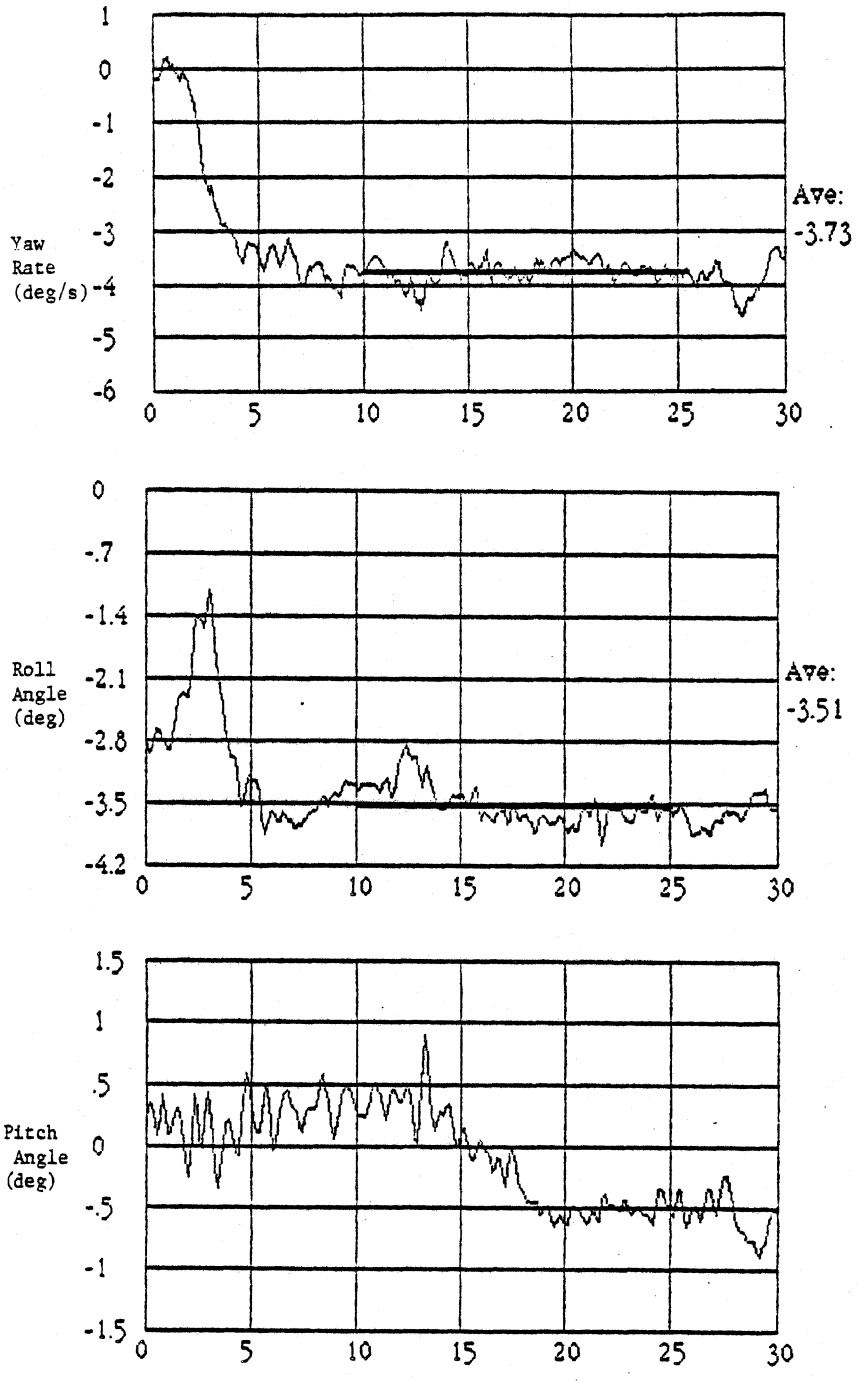

Figure 20 (cont)

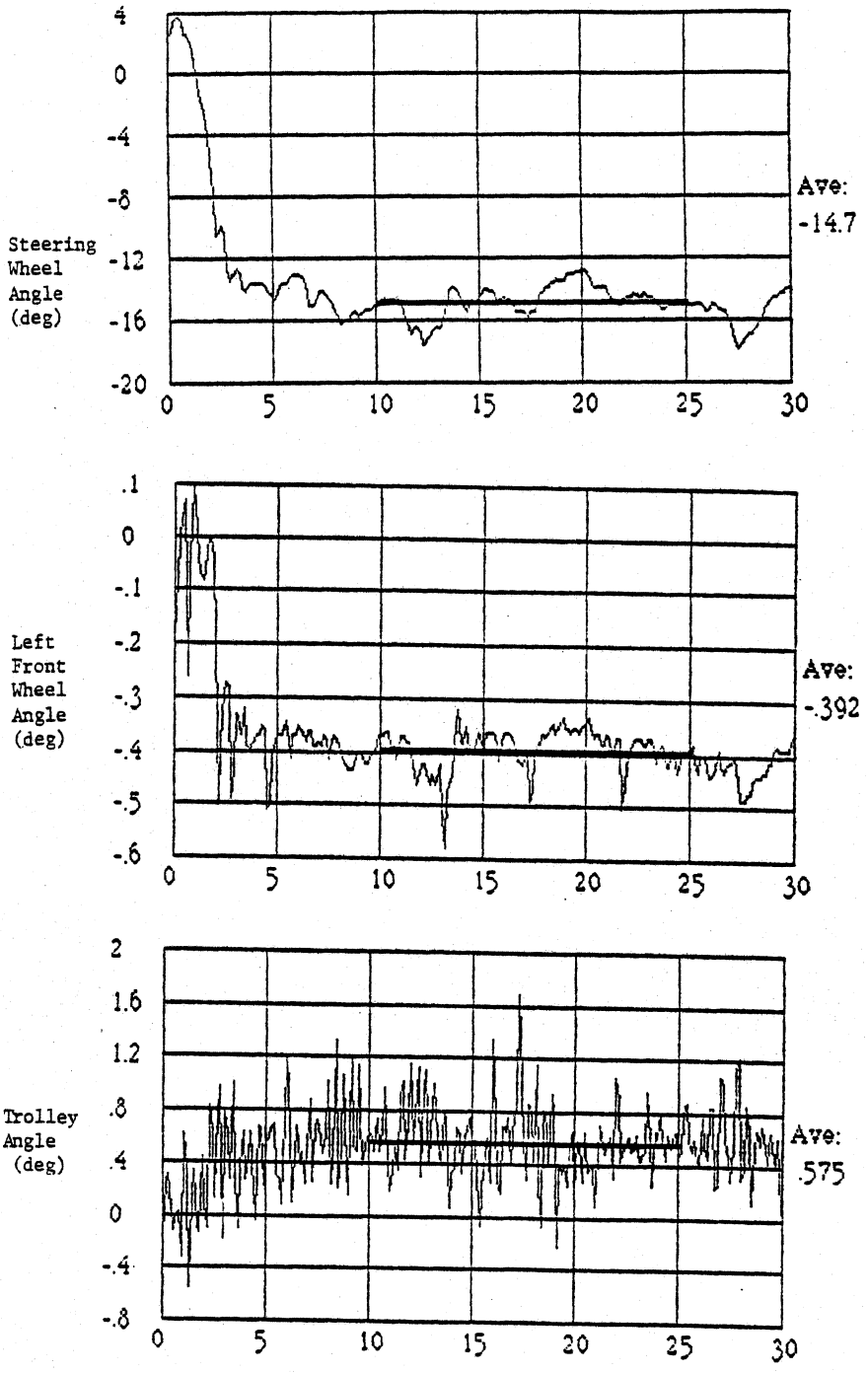

Figure 20 (cont)

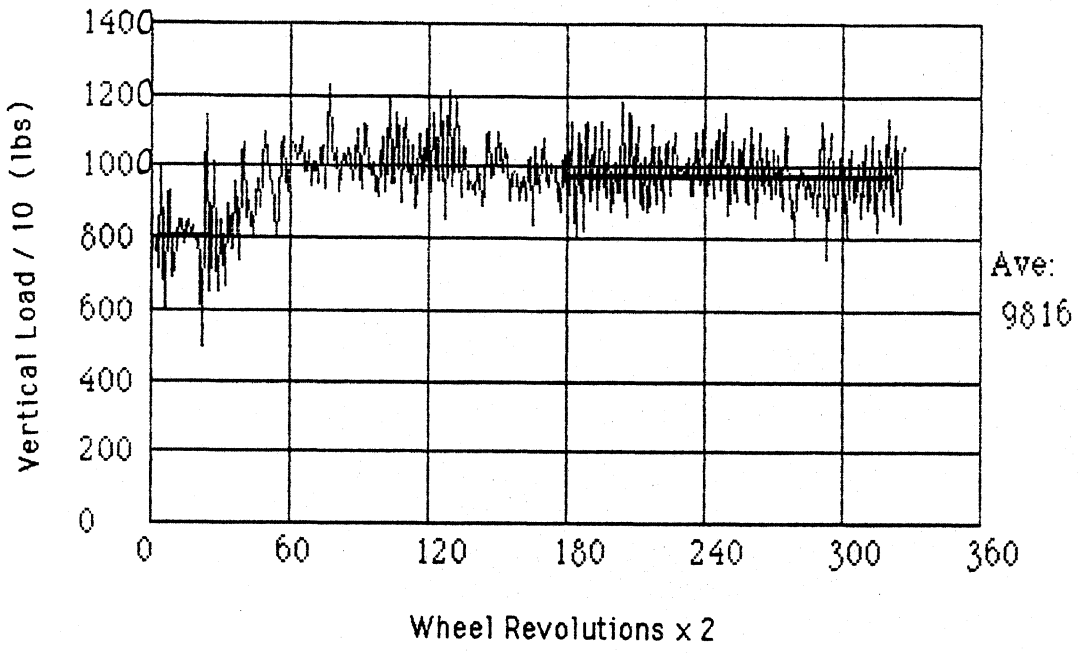

Vertical Wheel Load Measurement (prior to load cell cross-talk correction)
Semitrailer Rearmost Outside Wheel-Set
Curve #1 / Repeat 2 / 45.5 mph

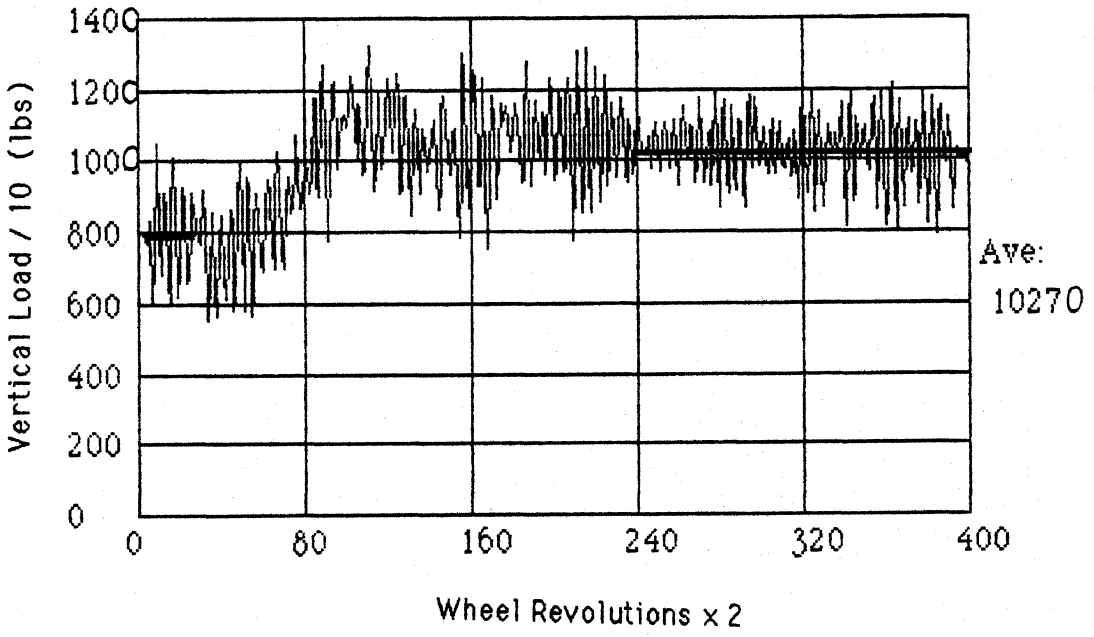

Vertical Wheel Load Measurement (prior to load cell cross-talk correction)
Semitrailer Rearmost Outside Wheel-Set
Curve #3 / Repeat 1 / 57.5 mph

Figure 21. Sample vertical load measurements

recommended crosstalk correction to the vertical load results in 3 percent to 6 percent lower readings in these data during normal cornering.

Figure 22 presents the completely processed vertical load measurements seen in Figure 21 along with corresponding model predictions in a ratioed form. The y-axis is simply the ratio of the measured (or predicted) wheel load when operating in the curve to an initial (or static) load measurement prior to entering the curve. Measurements for two different initial load values are shown in each case. The first case, identified as Initial Load 1, was obtained from the load cell reading just prior to entering each curve on the superelevated tangents. The second case, identified as Initial Load 2, was obtained from a straight line running condition (10 seconds in length) approximately 2 miles (3.2 km) prior to each curve. Mild drifting in load cell readings, apparently due to temperature sensitivities, have been observed in several of the processed wheel load data. These variations contributed to approximately 5 percent variations in the total load cell reading. The charts presented in Figure 22 portray similar variations in the measured wheel load data seen here. As such, the wheel load cell did not appear to offer a highly accurate means for measuring vertical wheel loads unless, possibly, "Initial Load 1" types of calculations are performed - closely spaced in time to account for gain drifting. (A more direct solution would be to substantially lower the temperature sensitivity of the load cell itself.)

Notwithstanding these accuracy concerns, the load cell measurements were still useful in the sense that they did provide "ballpark" estimates of vertical tire load time-histories that could be compared, in a qualitative manner, with similar predictions from the Phase 4 model to help identify and resolve any noteworthy differences. When several such comparisons were subsequently made with the model predictions, no unusual differences in the general nature of these time histories were observed.

4.6 Example Obstacle Avoidance Test Result

Figure 23 shows an example test result for the obstacle avoidance maneuever performed by the tractor-semitrailer test vehicle. The set of time histories seen in figure 23 represent a maneuver which begins as a steady

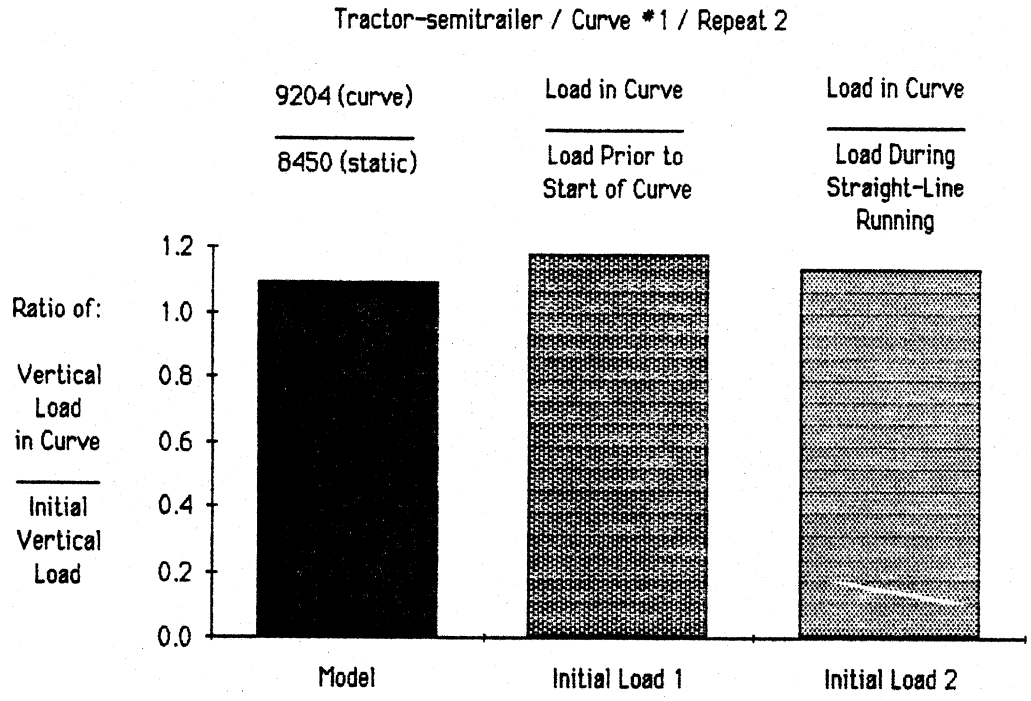

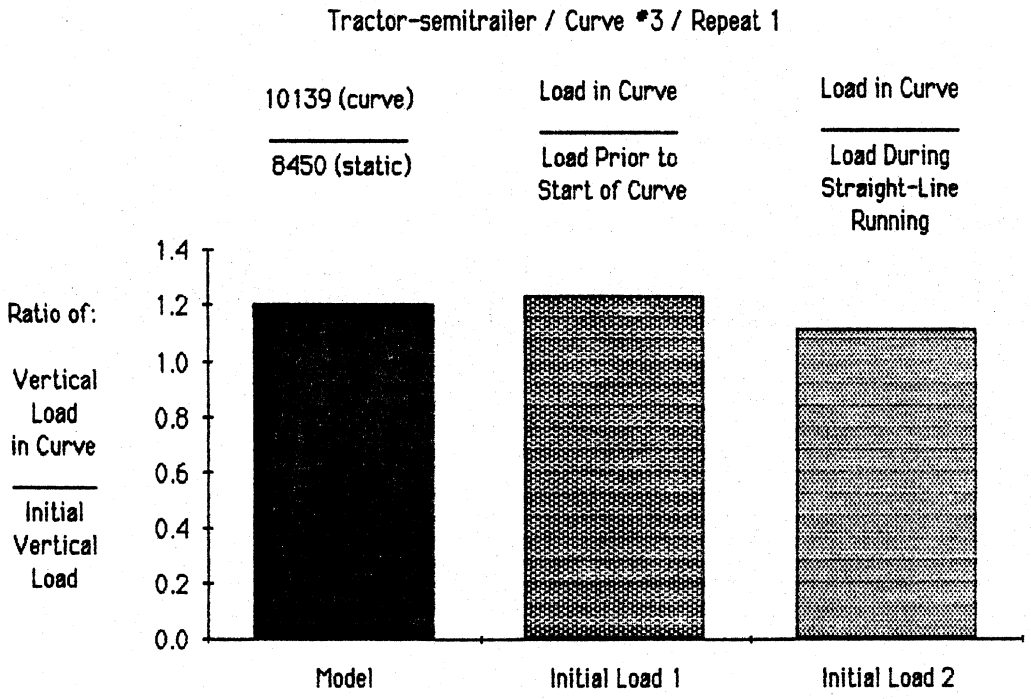

Figure 22. Normalized vertical tire load comparisons

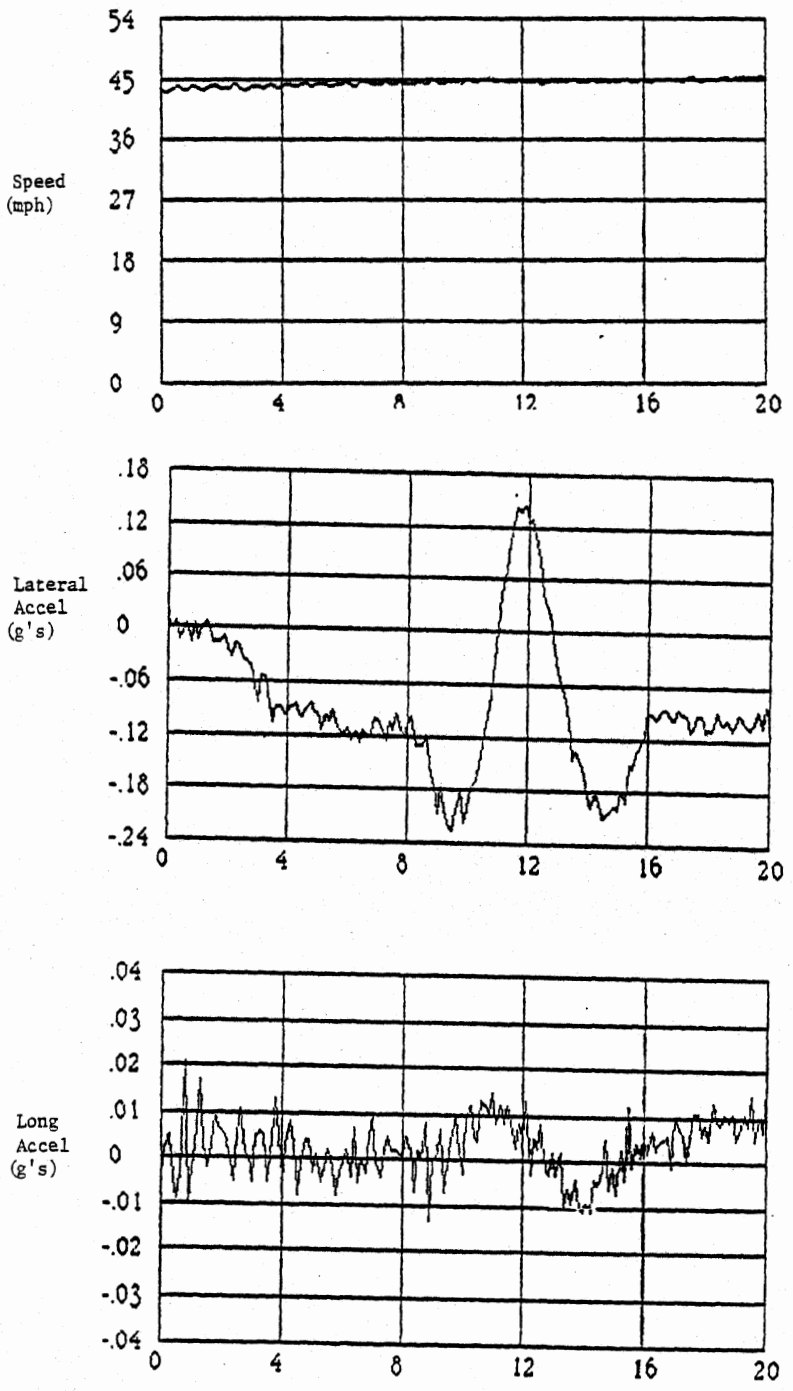

Figure 23. Obstacle avoidance test result example; vehicle C.

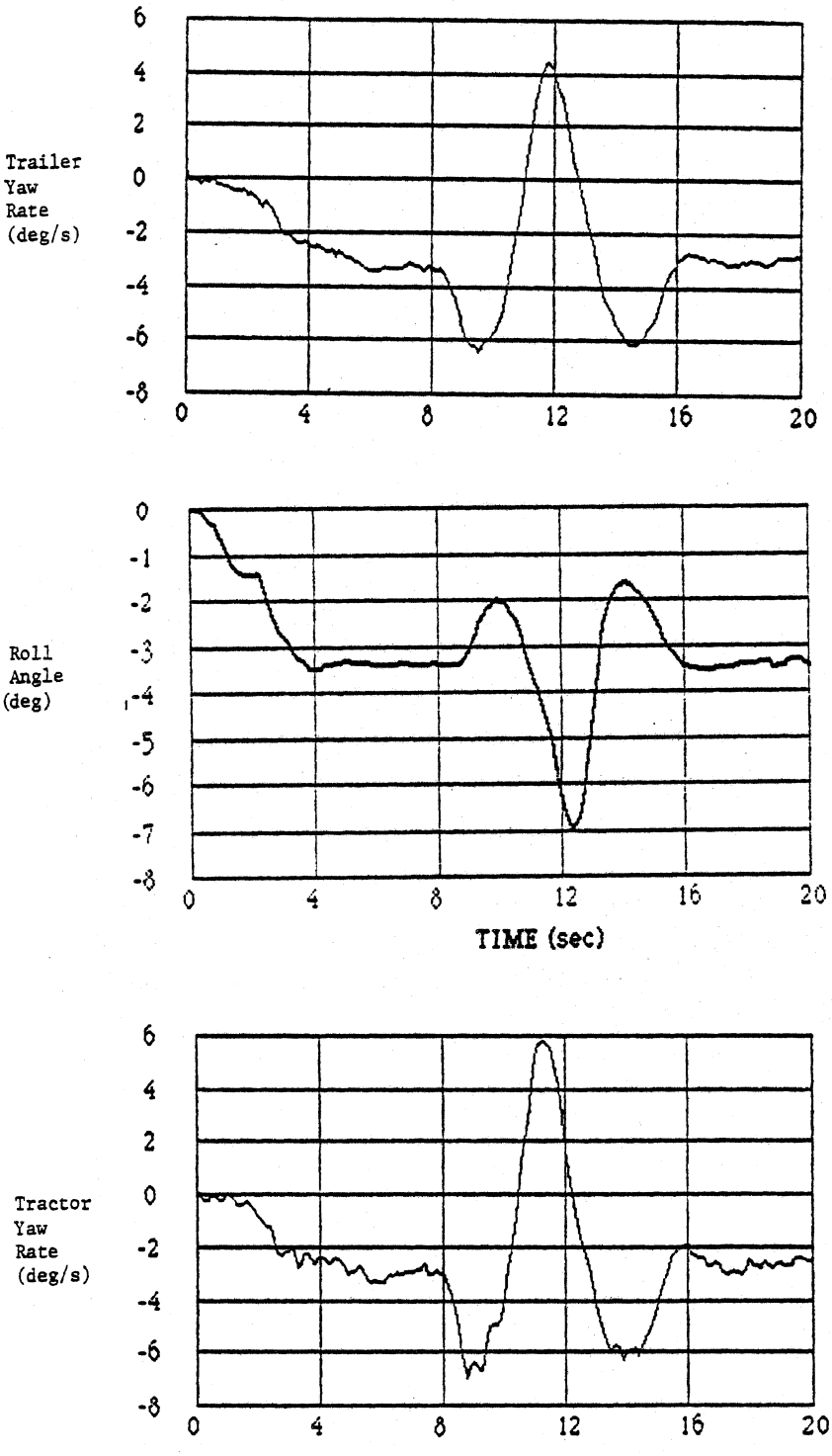

Figure 23 (cont)

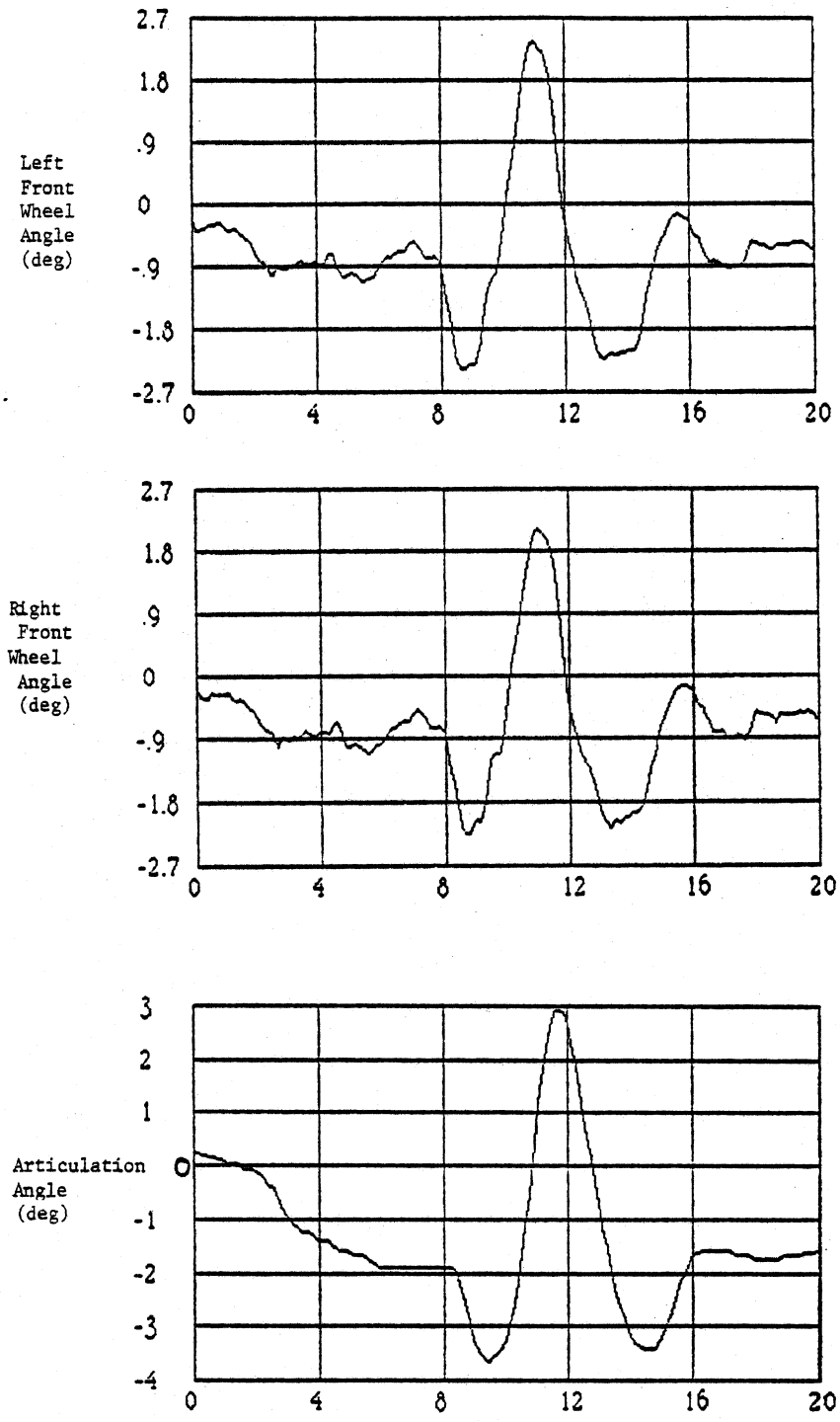

Figure 23 (cont)

turning maneuver in the outside travel lane. At approximately 8 seconds (in this figure), the vehicle is steered to the inside lane and then back to the outside lane, completing the maneuver at about the 16-second mark. Time histories such as these were used to evaluate peak friction demands of vehicles performing modest obstacle avoidance maneuvers, as well as to validate predictions of similar maneuvers performed with the Phase 4 model. Examples of obstacle avoidance maneuvers for the passenger cars and comparisons with Phase 4 model predictions are included in the next chapter.

4.7 Example Braking / Accelerating Test Result

Example test results for a braking / accelerating maneuver are presented in figure 24 for passenger car B at curve site 1. The time histories represent a maneuver which begins as a steady turning maneuver. At approximately the 13-second mark in this figure, the brakes are applied resulting in a longitudinal deceleration of 0.24 g's. At the 18-second mark the brakes are released and the vehicle accelerated (+0.10 g) back toward its initial speed. During this type of test the driver always kept the vehicle in the same lane throughout the maneuver. Braking / accelerating tests such as these were primarily used to further validate predictions for similar maneuevers performed with the Phase 4 model. Examples of braking / accelerating maneuvers for the tractor-semitrailer and passenger car test vehicles are also seen in chapter 5 where comparisons with the Phase 4 model are presented.

4.8 Observations and Conclusions Concerning the Test Results

The principal observations regarding the vehicle testing activity itself are noted below. Additional observations and conclusions related to the test measurements appear in the next chapter when comparisons between the experimental measurements and computer model predictions are presented and discussed. In regard to the vehicle test measurements themselves:

* Measurement of vehicle sideslip under conditions of steady turning, through use of the trolley device, was found to be surprisingly accurate and repeatable. Since the trolley device used in the test

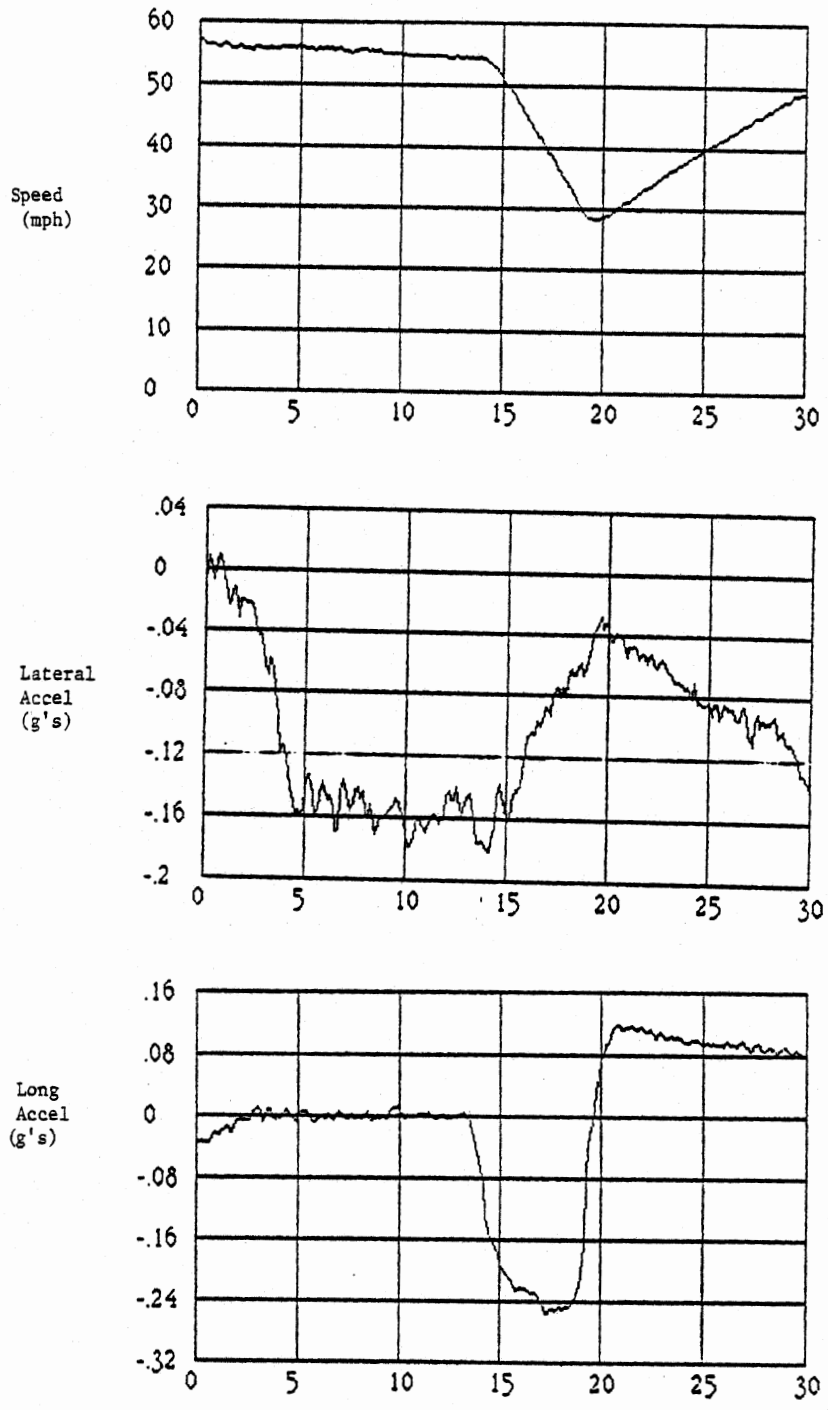

Figure 24. Braking/accelerating test result example; passenger car B.

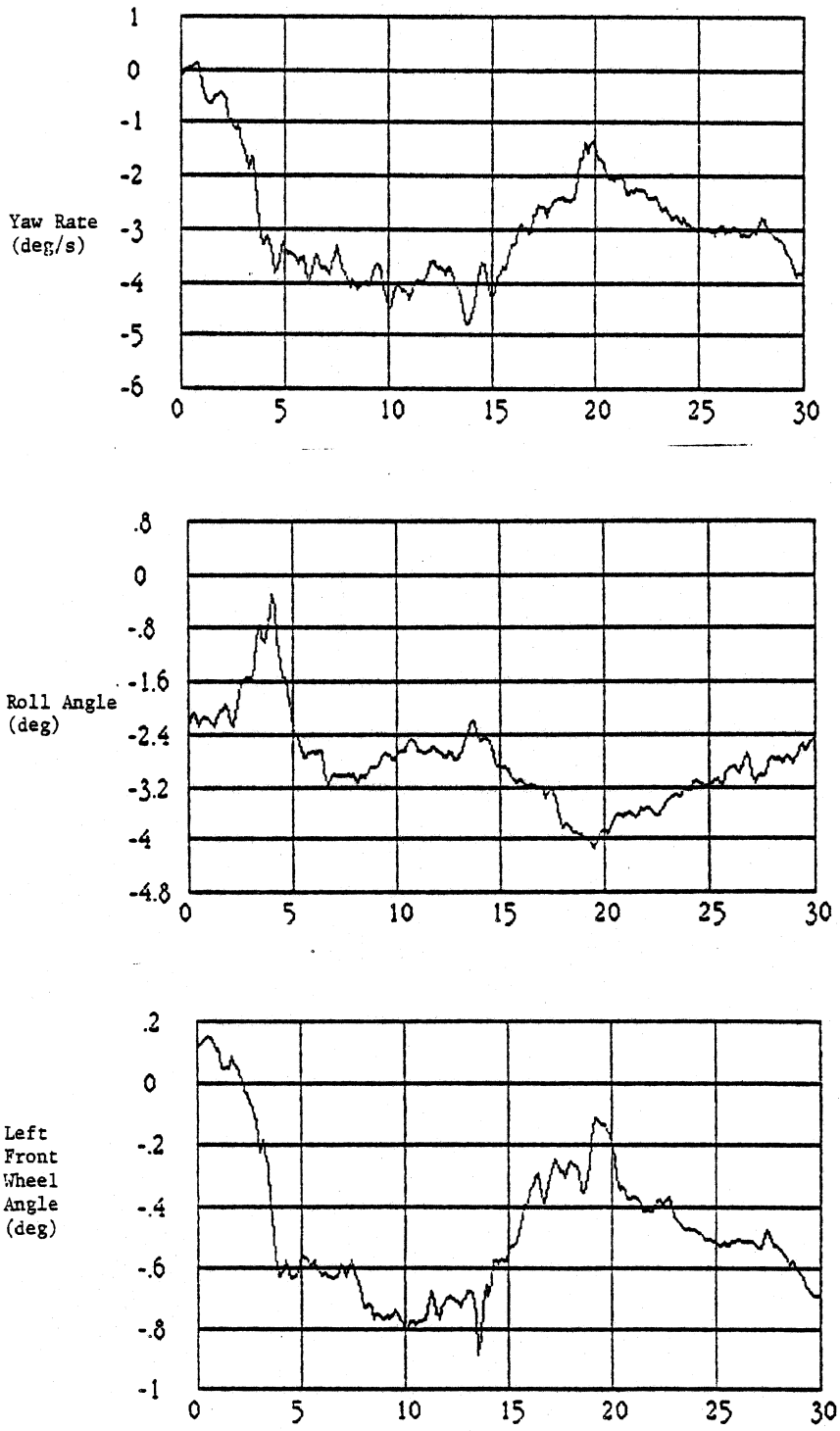

Figure 24 (cont)

series is primarily intended for use on smooth test pad surfaces, some reservations were held at the beginning of the testing on its performance in a more normal and noisy road environment. Although the durability and dynamic performance of the trolley device can be improved significantly by certain simple design changes, its use in future vehicle test programs requiring the measurement of vehicle sideslip during steady turning conditions appears useful. Among the design changes required for the sideslip trolley to improve its accurracy are: 1) use of more rugged wheel assemblies and low inflation pressure tires to better handle roughness levels encountered in normal highway environments, and 2) significant increase in its length, primarily the yaw-pivot to wheel dimension, in order to mimimize angular disturbances deriving from normal roadway disturbances.

* Measurement of vehicle roll angle using the stabilized platform proved to be highly variable and less accurate than originally anticipated. The primary cause of the roll inaccuracies lies with the servo control mechanism used in maintaining the platform in a horizontal position. Simple mercury switches are used to drive the platform back and forth about a horizontal position when disturbed, for example, by small external forces. The dead zone range (+- 0.4 degrees) is apparently large enough that significant offset errors are achieved in roll angle when the erection system was disabled during a test. The stable platform alignment errors did not affect lateral acceleration measurements since zero values of lateral acceleration were defined by the initial condition of every test and any lateral acceleration offsets deriving from platform alignment errors were therefore removed. Fortunately, the roll angle errors encountered here only affected the estimation of friction factors from side to side across an axle, and further, only to a small degree. Since good estimates of lateral load transfer can be made on the basis of lateral acceleration and fore/aft suspension distributions alone, the variability in roll angle measurements was not extremely critical to the overall research results. (Normally, for high lateral acceleration tests performed on a skid pad in which

large roll angles and accurate transient responses are required, the stable platform system is a proper choice for roll angle measurement. However, for more normal driving conditions of long duration, a ground-based potentiometer measurement system, similar to the FHWA trolley, appears more attractive as a method for roll angle measurement, particularly when roadway superelevation information is also known.)

* The modest degree of drifting observed in the processed load cell readings, apparently due to temperature sensitivities, prevented the use of this signal as an accurate measurement of prevailing vertical wheel load at the single tractor-semitrailer wheel location. However, its use did allow for qualitative evaluations of how vertical wheel loads vary on heavy vehicles when entering and traversing superelevated curves.

* Although the principal project motivation for performing the described vehicle tests was to assist in validating the developed computer models, a large body of useful test data was generated during this project and could be used as a source of representative driver/vehicle behavior on superevated curves for future projects or studies.

Chapter 5

COMPARISONS OF MODEL PREDICTIONS AND TEST RESULTS

Development of the steady turning model within this project and related questions concerning friction factor values at individual wheel locations focused most of the model validation efforts on the steady turning condition. Accordingly, the majority of data and model calculations presented in this chapter are associated with the steady turning maneuver. All model predictions seen in section 5.1 refer to the steady turning models developed during the project. Comparisons between Phase 4 model predictions and test results for the obstacle avoidance and braking / accelerating maneuvers are seen in sections 5.2 and 5.3 .

5.1 Steady Turning Comparisons

The comparisons between test results and model predictions seen here and in appendix F are presented in a bar-graph format for ease of reading. The experimental data, however, are also contained in appendix E in their raw time history format. Model predictions corresponding to the test data seen here (and appendix E) are contained in appendix D. Referral to appendix E is useful for a more detailed understanding of the nature of the data and its noise level. Also, although these experimental data are referred to as "steady turning," they are approximations to ideal steady turning motion because of external disturbances and normal driver steering behavior. Average value calculations were performed for most of the variables seen in appendix E over an eight-second or greater time span during each test. These average values are printed on the right portion of the plots contained in appendix E and are the same test result values presented in this section in a bar-graph format.

In most cases, zero values were defined for yaw rate, lateral acceleration, and pitch angle measurements taken on approach tangents prior to entering the curves. Other variables (steering wheel angle, front wheel

angle, roll angle, and trolley angle) used zero calibration runs prior to or following the curve site.

Referring to figure 25, seven charts corresponding to seven different variables are seen. Each chart contains three sets of bar-graphs which compare test results with predictions from the steady turning model. Each bar-graph set represents a test repeat at curve site 1. Speed, lateral acceleration, steer (average of right and left front wheel angles), roll angle, and articulation angle measurements are obtained directly from the average values seen in appendix E. The path radius graph is calculated from the ratio of the vehicle speed measurement, V (mph), and trailer yaw rate, r2 (deg/s), [i.e. Radius (ft) = (V)(88)(57.3) / (60)(r2)], with adjustments for the measurement units listed in Tables 3 and 4. The sideslip angle chart values in degrees (vehicle sideslip at the trailer mass center / car mass center) are obtained from the following equation:

$$\text{sideslip angle} = [(c)(r2)(60) / (88\ V)] - \text{trolley angle}$$

where: c is the rearward distance from the semitrailer c.g. (or car) to the trolley wheel (ft), and 60/88 is the unit correction factor for mph to ft/s.

A positive trolley angle corresponds to the angle between the tow vehicle and the trolley when the trolley is located at the rear of the vehicle during turning motion to the right. (The trolley measurements seen in appendix E contain a sign error per the above definition.)

It should also be noted that the bar-chart summaries seen here contain mostly positive values and therefore imply right hand turns by convention. Data for curves 1, 2, and 3 seen in appendix A (left turns) have had their signs changed in this section to provide consistency in the summary chart presentations.

5.1.1 Tractor-semitrailer Comparisons

The comparisons between test results and model predictions shown in Figure 25 for the tractor-semitrailer generally indicate very good agreement.

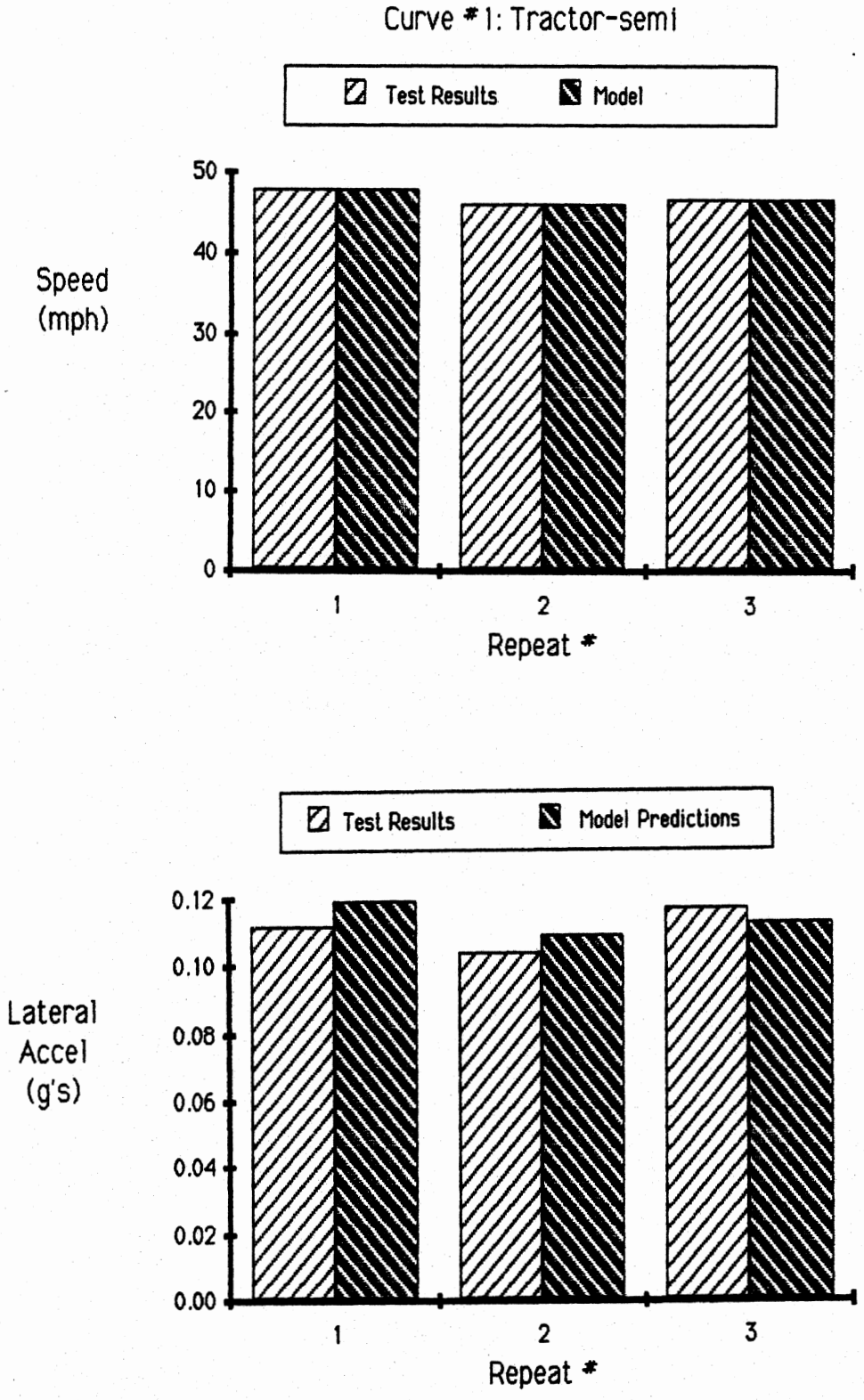

Figure 25. Model/test comparisons; vehicle C.

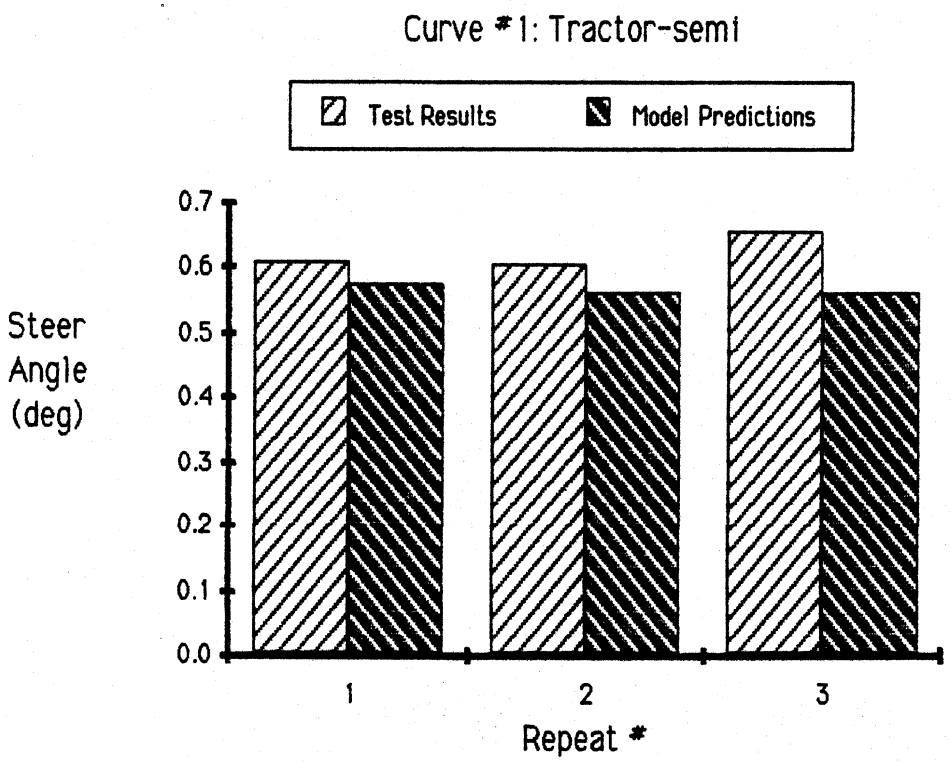

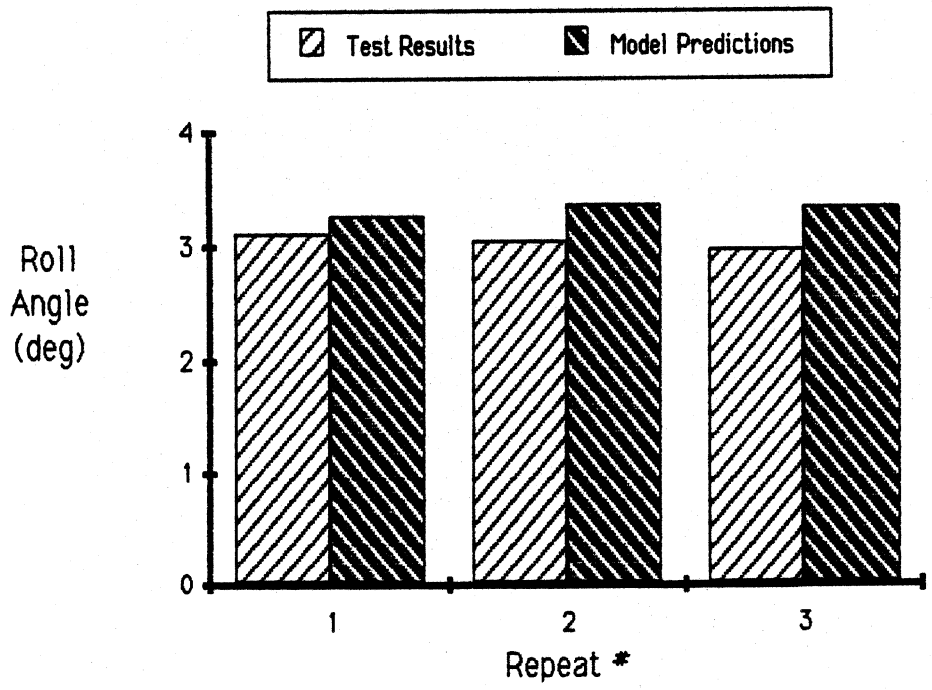

Figure 25 (cont)

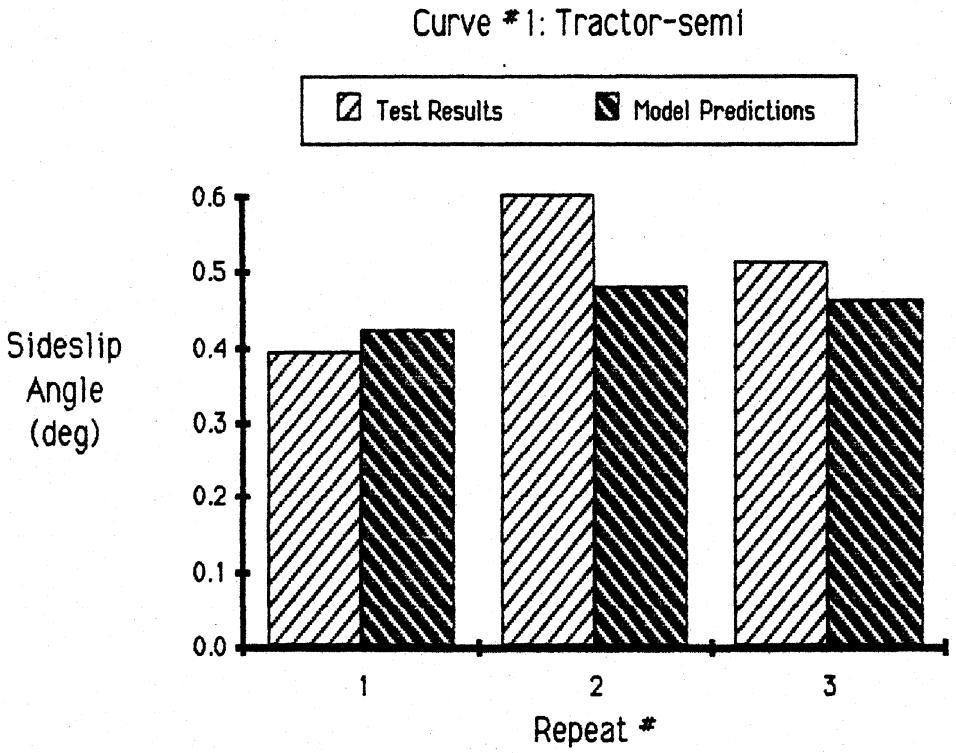

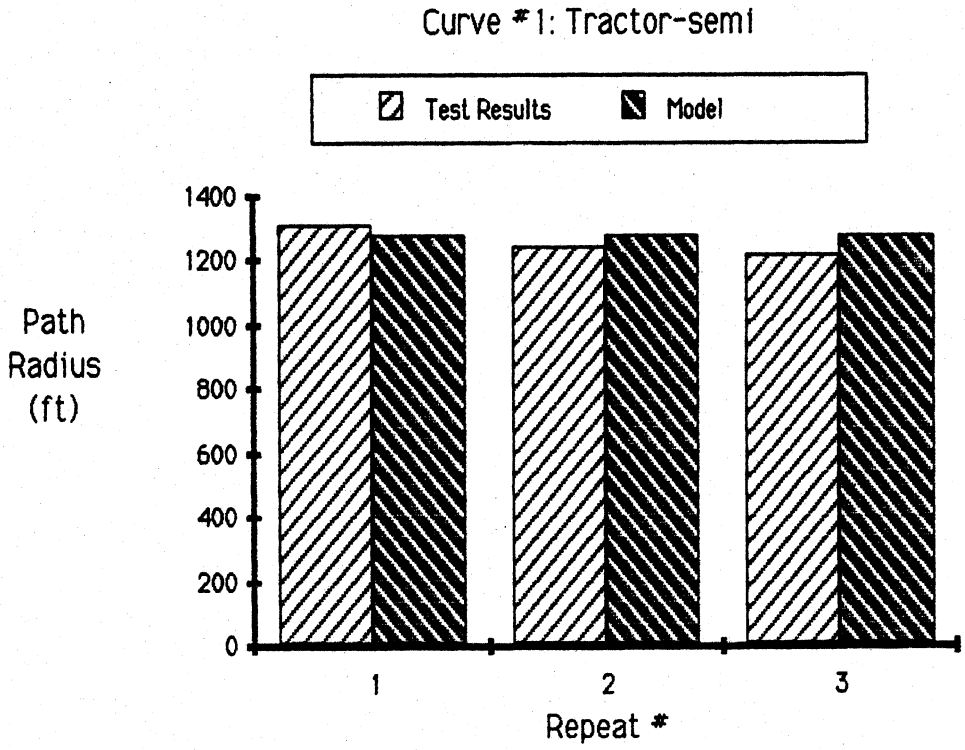

Figure 25 (cont)

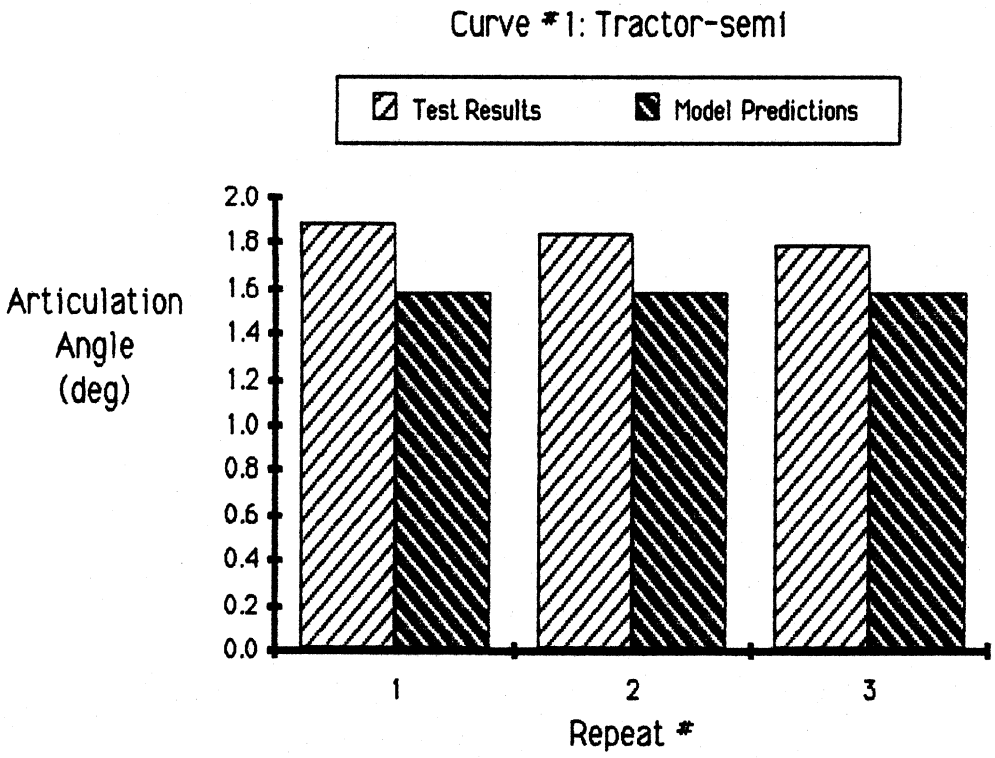

Figure 25 (cont)

Since the model (chapter 3 & appendix B) uses vehicle speed as an input value, the comparisons seen in the speed charts will always be identical and are included here primarily to indicate speed changes from test to test. The low power capacity of the tractor used in the test program and a modest uphill approach grade prevented operating speeds at curve site 1 much above 45 mph (72 km/h). At the speeds seen in figure 25 the tractor-semitrailer experiences about 0.11 g's of lateral acceleration in the horizontal plane, or approximately 0.04 g's (0.11 - 0.067) in terms of a point-mass friction factor in the road plane. The remaining variables seen in figure 25, with perhaps the exception of articulation angle, generally exhibit margins of agreement within 5 to 10% . The articulation angle measurements seen throughout the report show readings which are approximately 7% too high. An error in the value used to calibrate the articulation angle transducer was found subsequent to the data processing. The impact of this error on the overall research results is small and if corrected in the displayed graphs would act to further improve the level of agreement already observed.

Figure F-1 of appendix F shows similar results from curve sites 2 and 3. Again, most of the charts reflect general agreement. The roll angle measurement for curve 3 contains a modest error due to the stable platform roll corrections applied by the servo system. However, as indicated earlier, a result like this can be traced directly to an inaccurate zero reference value for roll angle. The sideslip discrepancy seen for curve 3 is attributable to an offset zero data value for this particular run. Ordinarily, the average values of sideslip (trolley) measurements are well within 0.1 to 0.2 degrees of ideal values. At first glance, observation of the noise level on the trolley signal, particularly for the tractor-semitrailer data (appendix E), would not suggest accuracies anywhere near the level achieved. However, averaging over periods of 10 seconds or so was shown to produce very repeatable and accurate trolley measurements in most cases.

Figure F-2 of appendix F shows similar comparisons for two repeats at the ramp site 4. The noteworthy item here is the increased level of lateral acceleration and reduced speed in contrast to the other three sites. The data seen here are for runs performed about 7 mph (11 km/h) above the advisory speed for the ramp. The elevated level of lateral acceleration for these test

results is beginning to exceed the legitimate range of application of the linear model --particularly for a loaded tractor-semitrailer vehicle. However, these results illustrate that even at these levels of lateral acceleration, the simplified steady turning models do a very reasonable job of predicting the steady turning response of a tractor-semitrailer vehicle. In general, the roll angle values measured at the ramp site were more erratic than those measured at the other curve sites. This was due, in part, to the noted variations in superelevation at the ramp site, as well as more variable driver steering and speed control which contributed to additional roll motions. The net effect of these additional roll motions at the ramp site was to introduce small, and largely inconsequential, variations in the estimates of vertical load transfer across each axle.

Figures 26 through 31 compare friction factor values derived strictly from the test measurements (as described in appendix E, section 4) with those predicted by the steady turning model. Greater scatter is seen in these sets of test results than in the previous vehicle response figures simply because each friction factor value depends on four or more vehicle measurements (speed, yaw rate, trolley angle, roll angle, articulation angle, and front wheel steer angle). As noted in chapter 4, modest noise or offsets in any one of the measurements will contribute to error in the friction factor estimate. The sensitivities to small cumulative errors are illustrated by comparing the friction factor test results seen in figures 26 through 28 (curve 1, repeats 1 to 3) with the level of test result scatter observed in figure 25. The friction factor differences seen in figure 26 are all on the tractor (axles 1 to 3) and are produced primarily by the 0.3 degree articulation angle discrepancy previously seen in figure 25. Superior estimates of friction factors at the semitrailer wheel locations (axles 5 and 6) are due to their dependence on fewer measurements (V, r2, trolley angle, and roll angle). In contrast, tractor front wheel friction factors depend on the greatest number of measurements (V, r2, trolley angle, roll angle, articulation angle, and front wheel steer angle).

Measurement errors can often be identified by the degree of discrepancies in estimated friction factors and where they occur on the vehicle. For example, since the semitrailer friction factor values depend primarily on

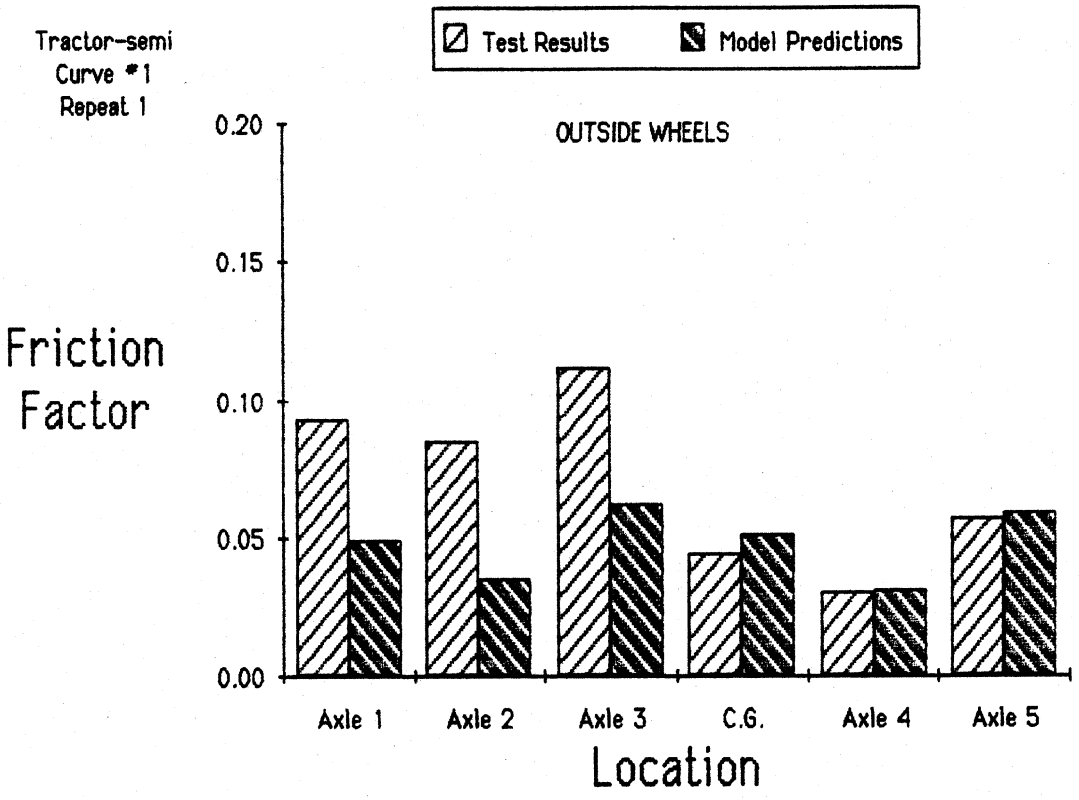

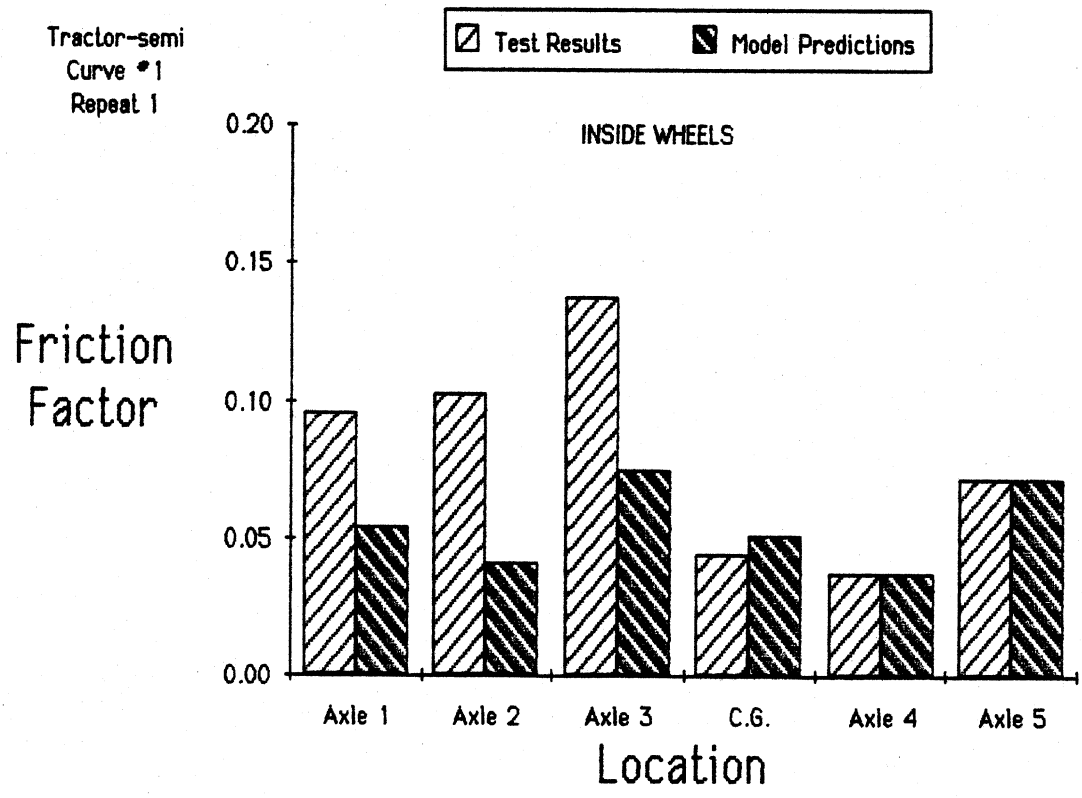

Figure 26. Friction factor comparisons; vehicle C

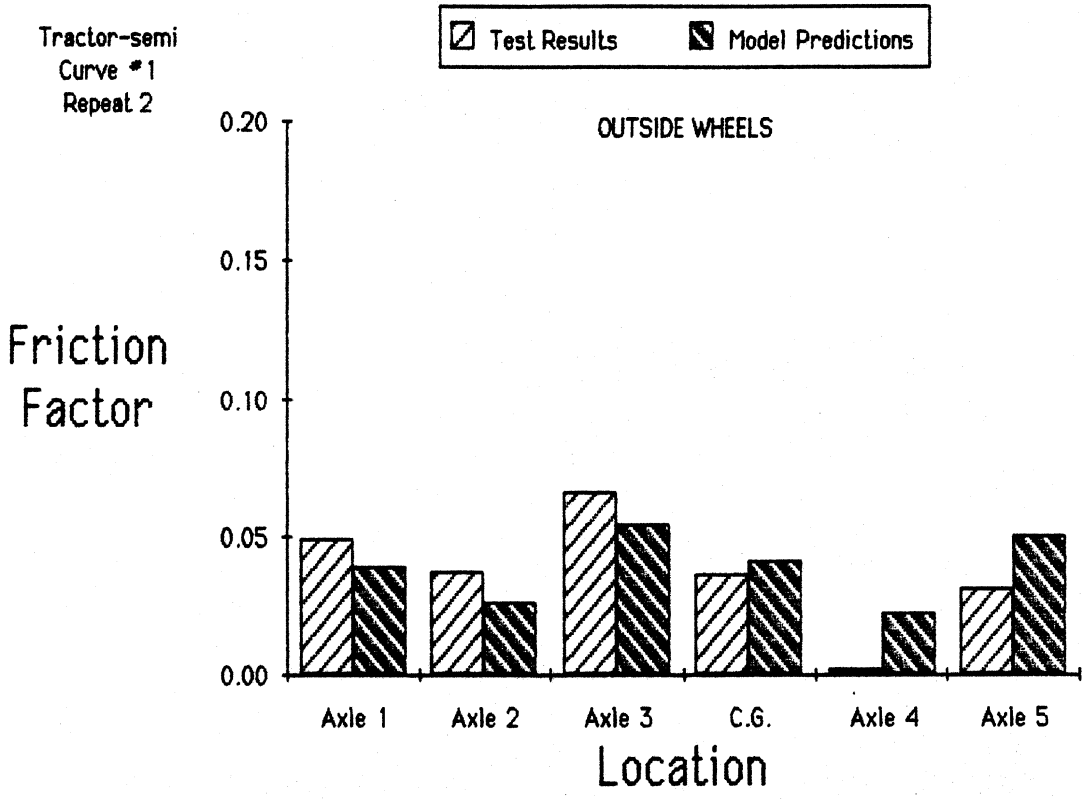

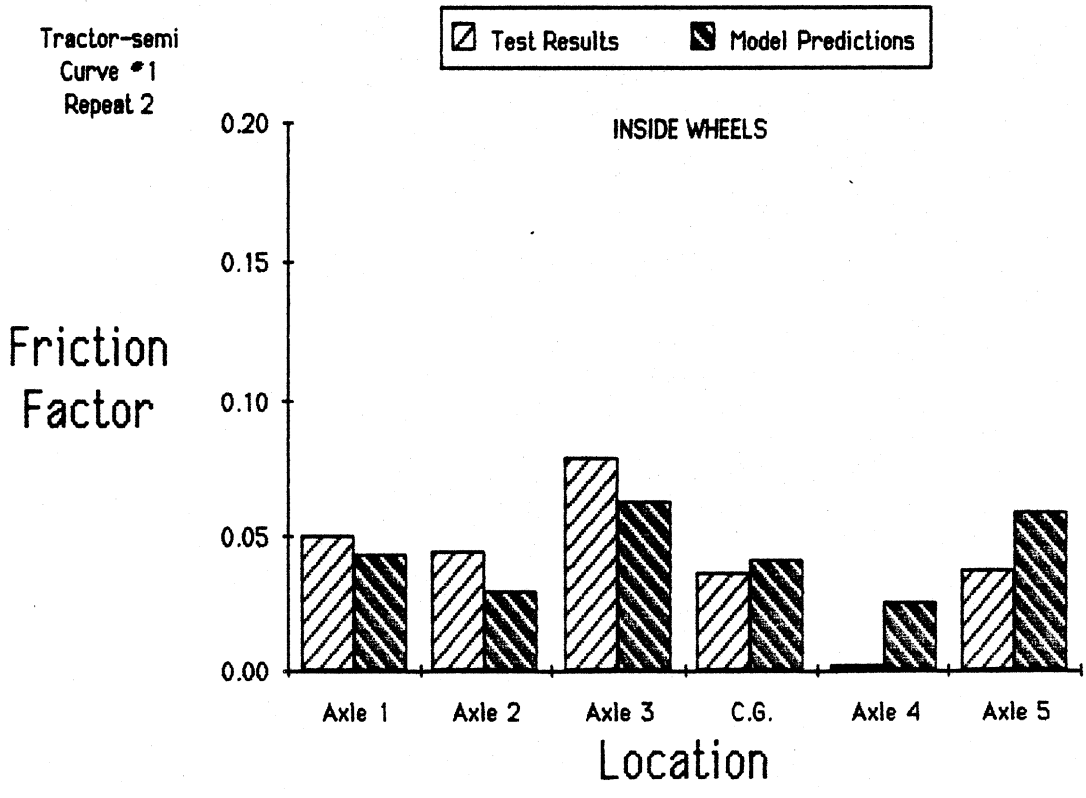

Figure 27. Friction factor comparisons; vehicle C

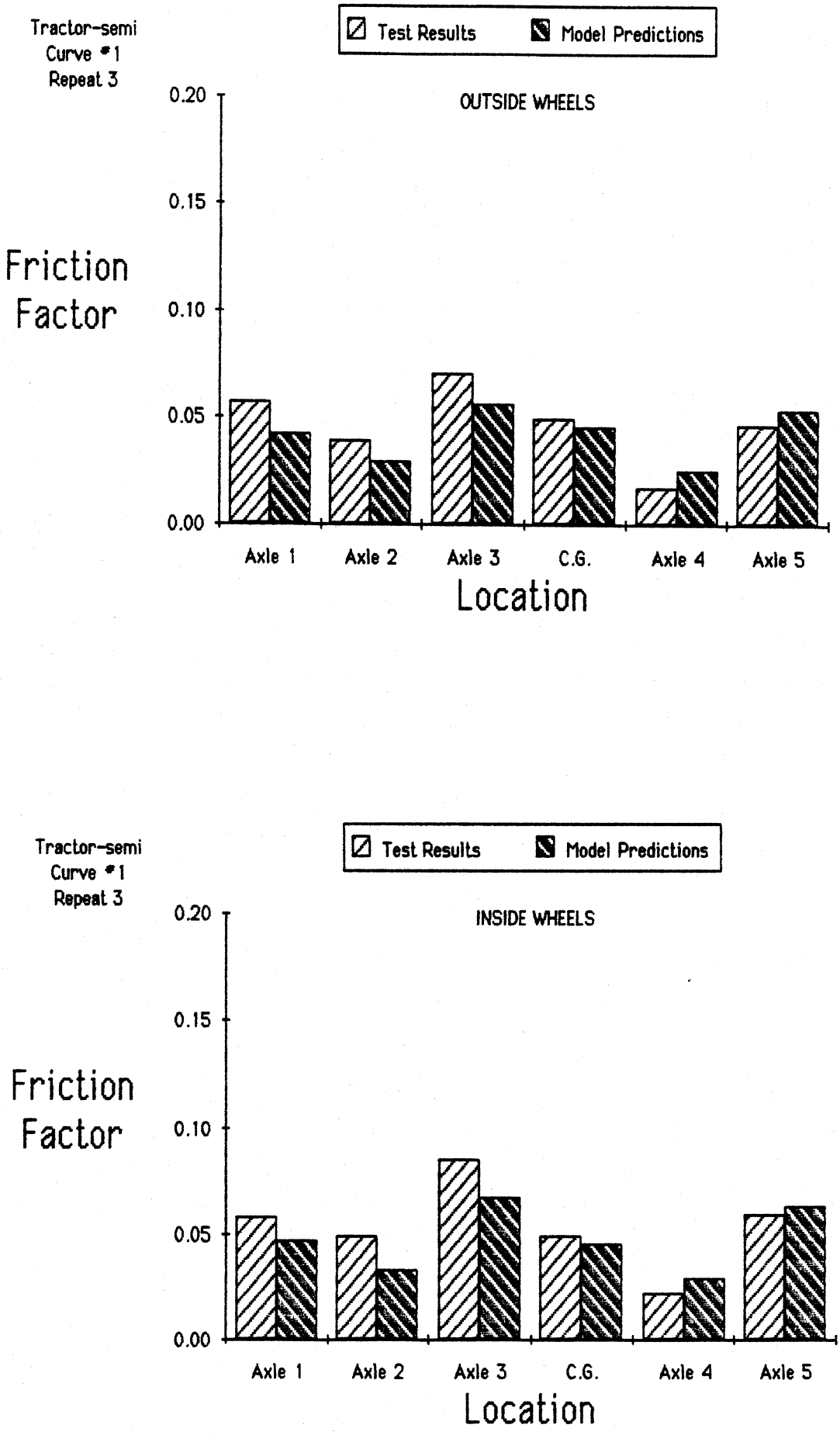

Figure 28. Friction factor comparisons; vehicle C

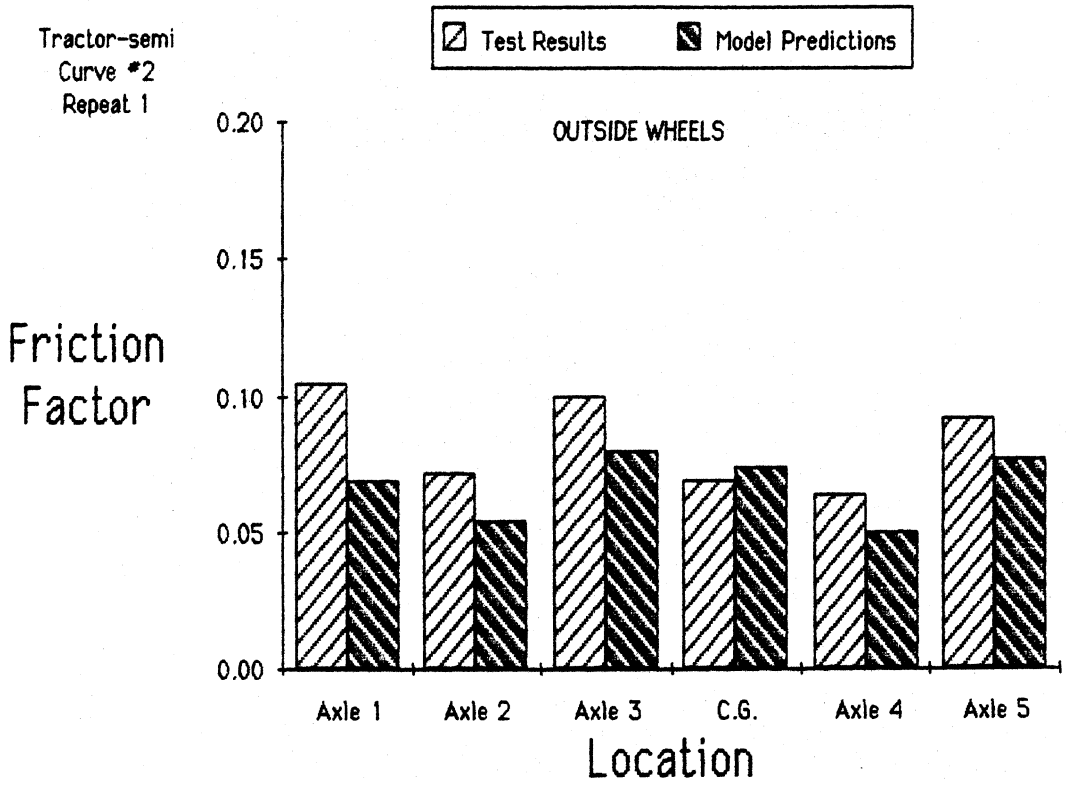

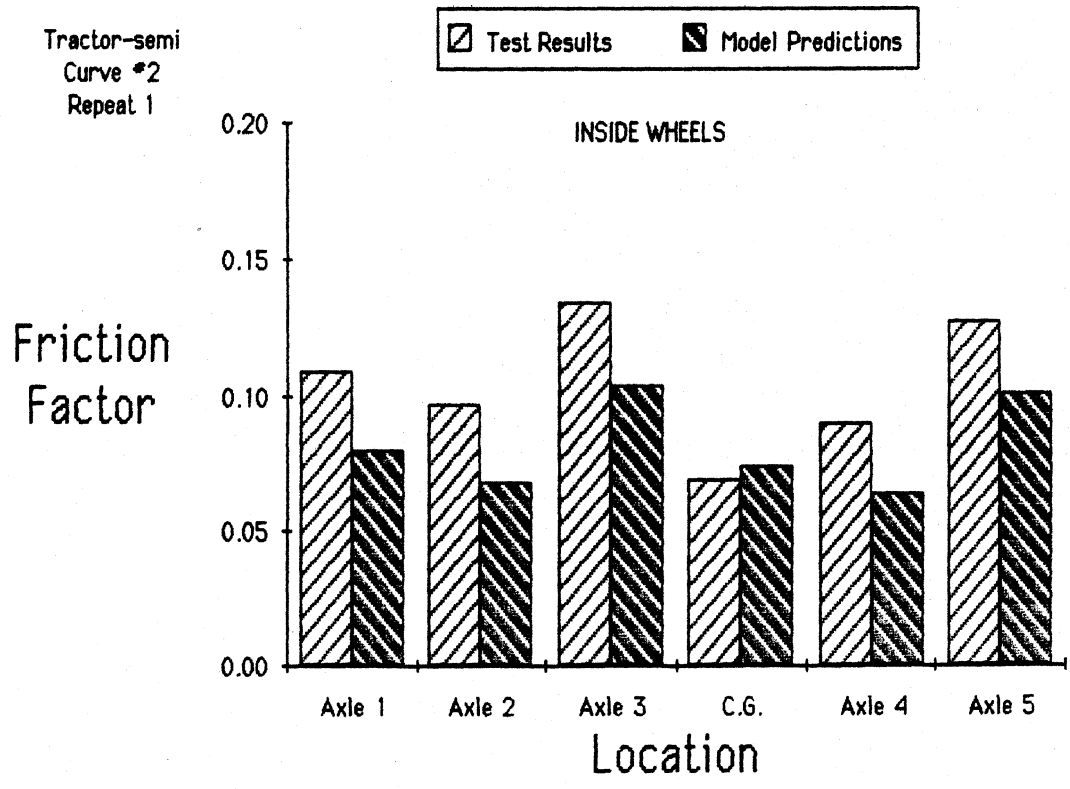

Figure 29. Friction factor comparisons; vehicle C

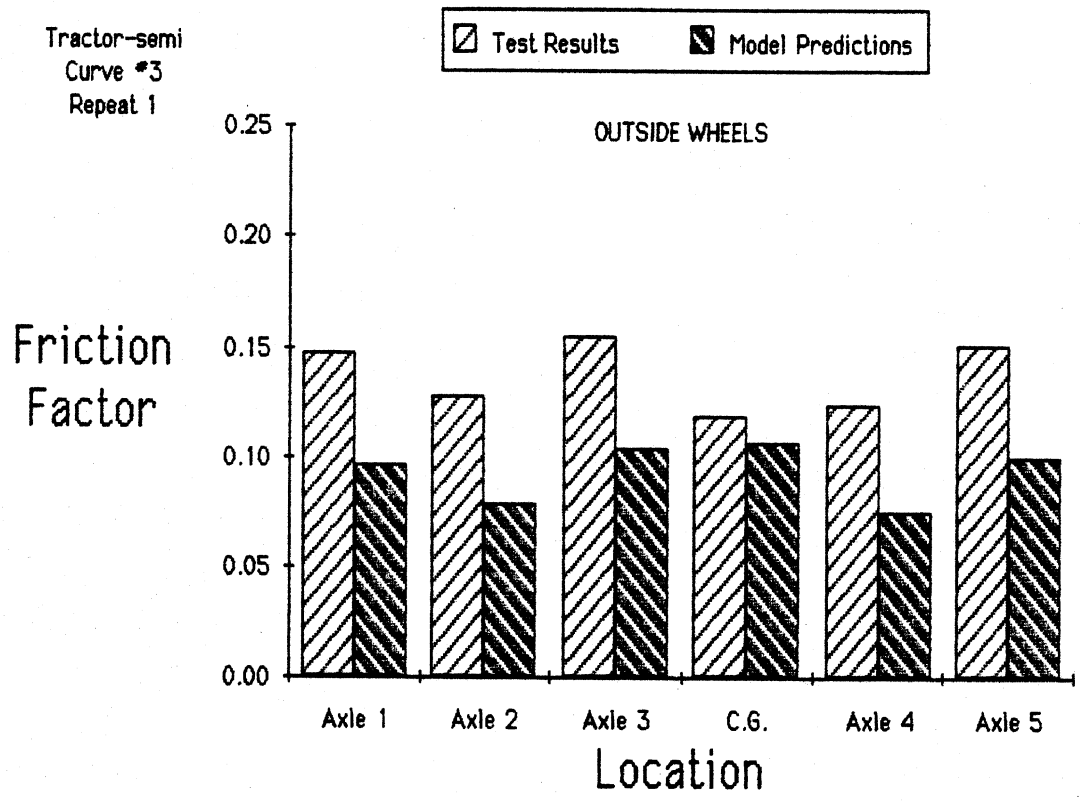

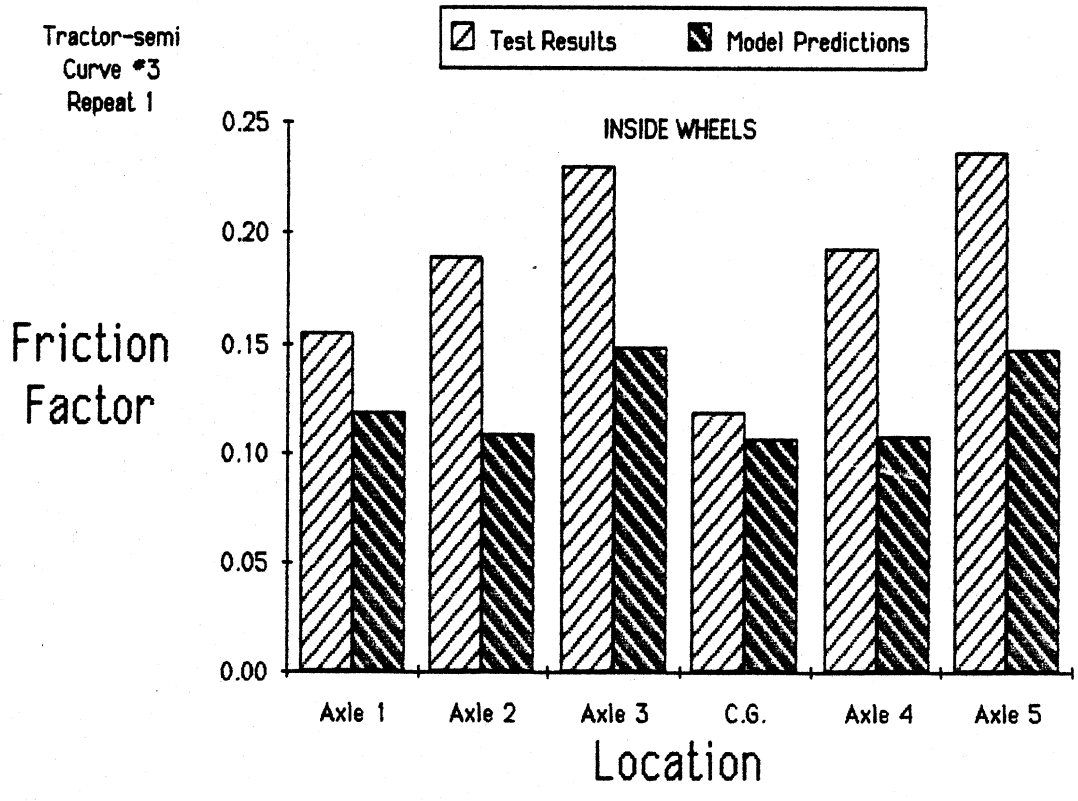

Figure 30. Friction factor comparisons; vehicle C

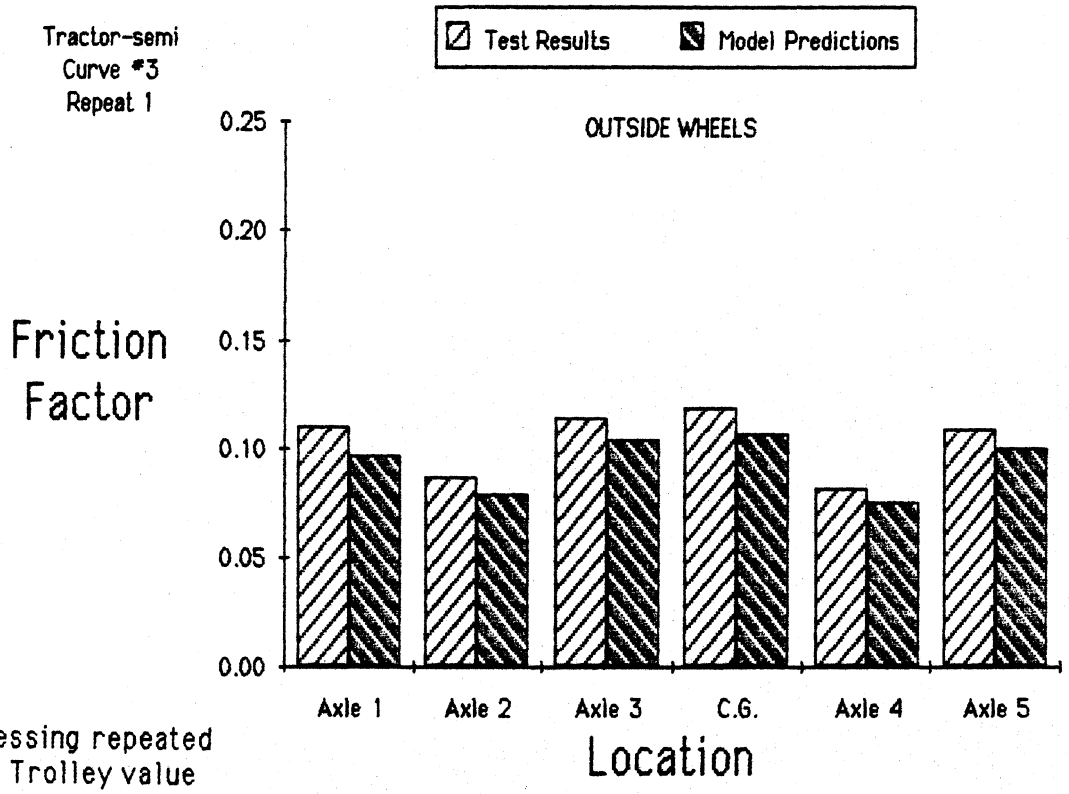

Processing repeated using Trolley value of -0.5 degrees (approx value measured in similar curves) in place of -0.2 degrees (value measured here & having apparent offset)

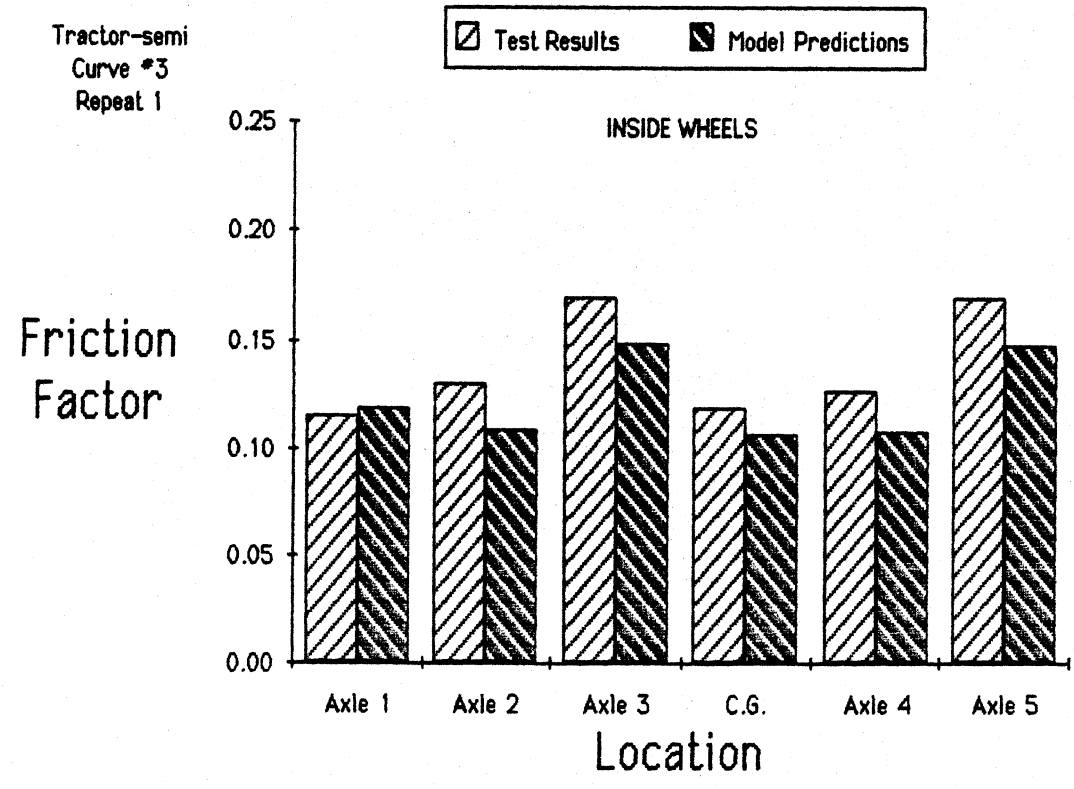

Figure 31. Friction factor comparisons; vehicle C

trolley measurements (V and r2 are usually quite accurate), a significant friction factor error at that location would imply an error in the trolley measurement. Similarly, large discrepancies only at the front tractor steering axle would suggest erroneous steering angle measurements, since only that axle depends upon steering wheel angle measurements in estimating friction factor values. (More modest discrepancies at the front axle location can also be attributed to vehicle roll - tire camber suspension properties. This is discussed further under the data presented for passenger car B.)

Figures 27 through 29 indicate that the individual wheel friction factors derived from the test data are comparable to the values predicted by the steady turning models and vary from wheel to wheel location in a very similar manner. The largest variations away from the point-mass (c.g.) value occur on the inside wheels, and usually at the tractor and semitrailer rearmost axle.

Finally, Figures 30 and 31 illustrate the effect that a 0.3 degree change in trolley angle measurement can have on the friction factor estimates for the entire tractor-semitrailer. Figure 30 shows experimentally determined friction factor values which appear consistently larger than the values predicted by the model. This is a direct consequence of the erroneous sideslip (trolley) measurement noted earlier in Figure F-1 of appendix F for curve 3. Figure 31 corresponds to the very same set of measurements used in figure 30, except for an altered value of trolley angle measurement. Significant improvement in each of the friction factor estimates occurs as a result of replacing the trolley measurement with a more accurate value.

5.1.2 Pasenger Car A Comparisons

The steady turning comparisons for the front wheel drive test vehicle presented in figures 32 to 35 (and similar figures F-3 and F-4 of appendix F) are generally quite good. The most noticeable discrepancy in these comparisons appears for steering angle where the test results consistently fall below the model predictions. The apparent cause of this appears to be a small instrumentation gain error in the front wheel steer measurement. The roll angle measurements showed improved consistency in the passenger car A data. The trolley again performed very well in the vehicle A series of tests

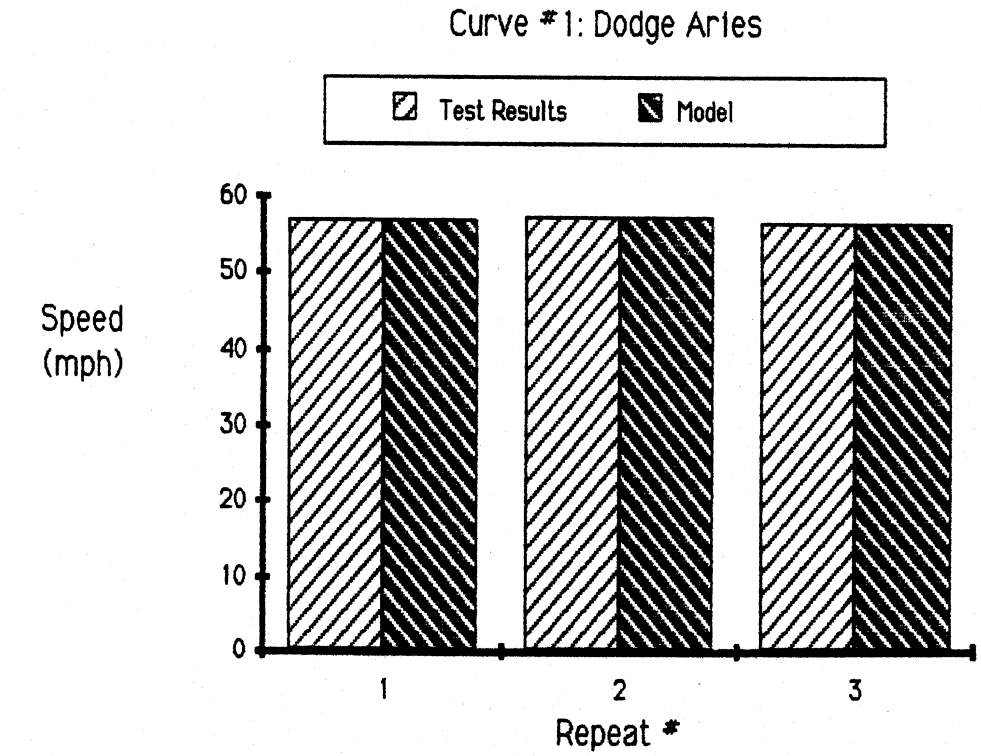

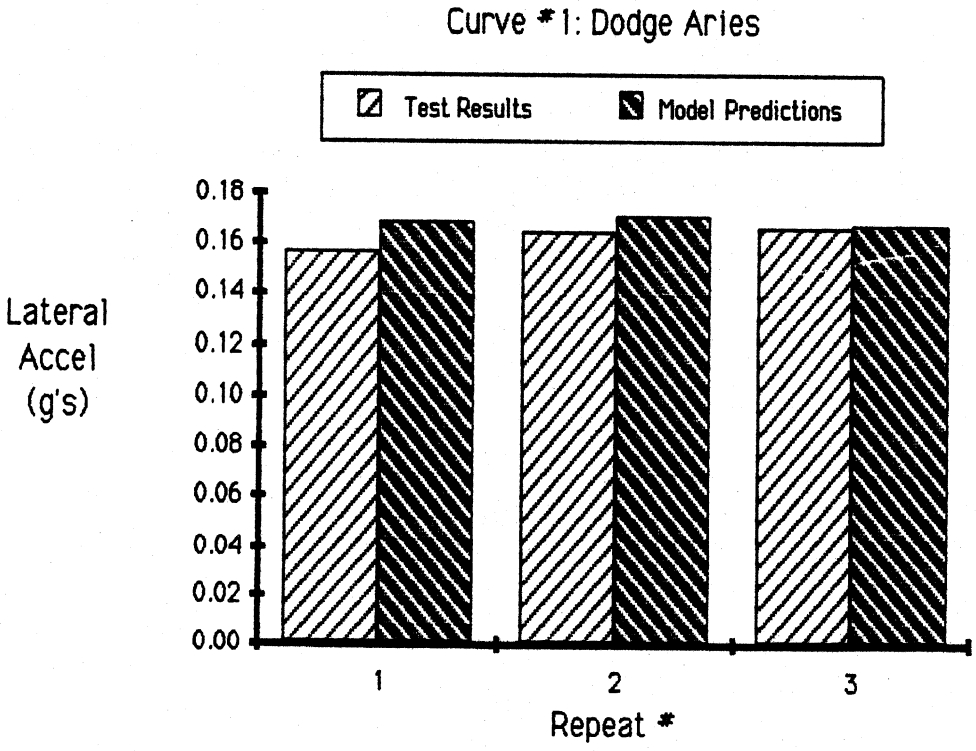

Figure 32. Model/test comparisons; vehicle A

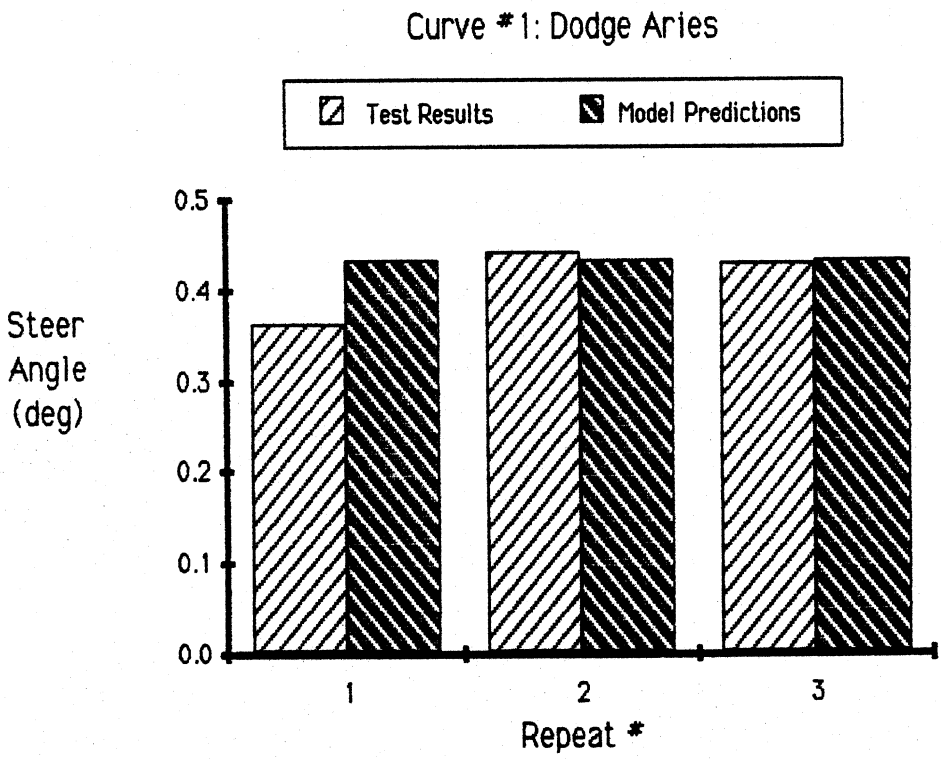

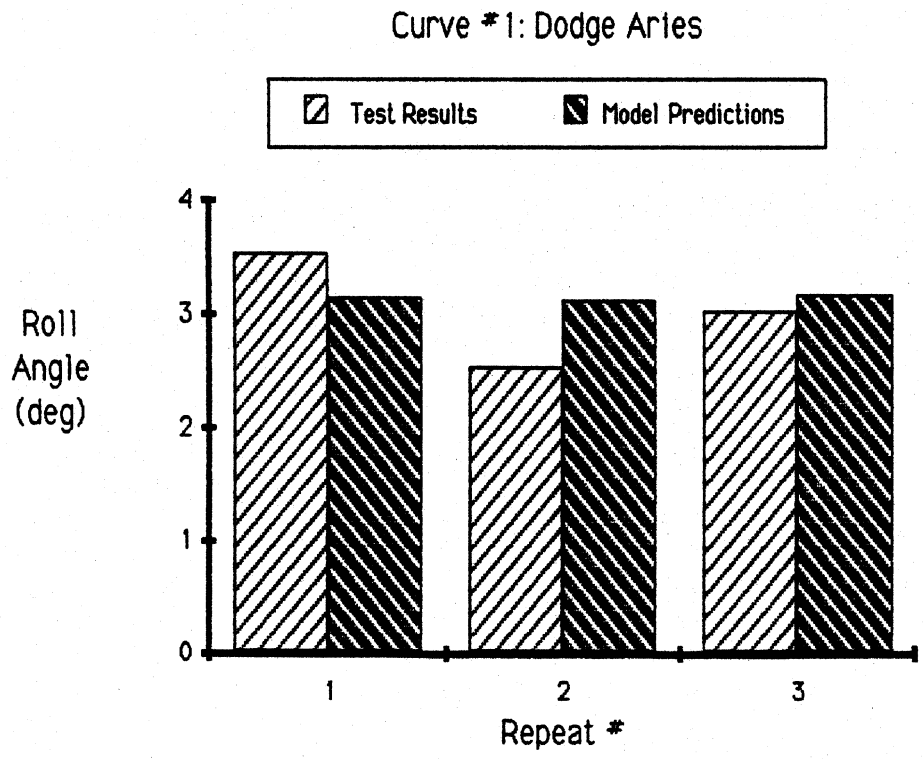

Figure 32 (cont)

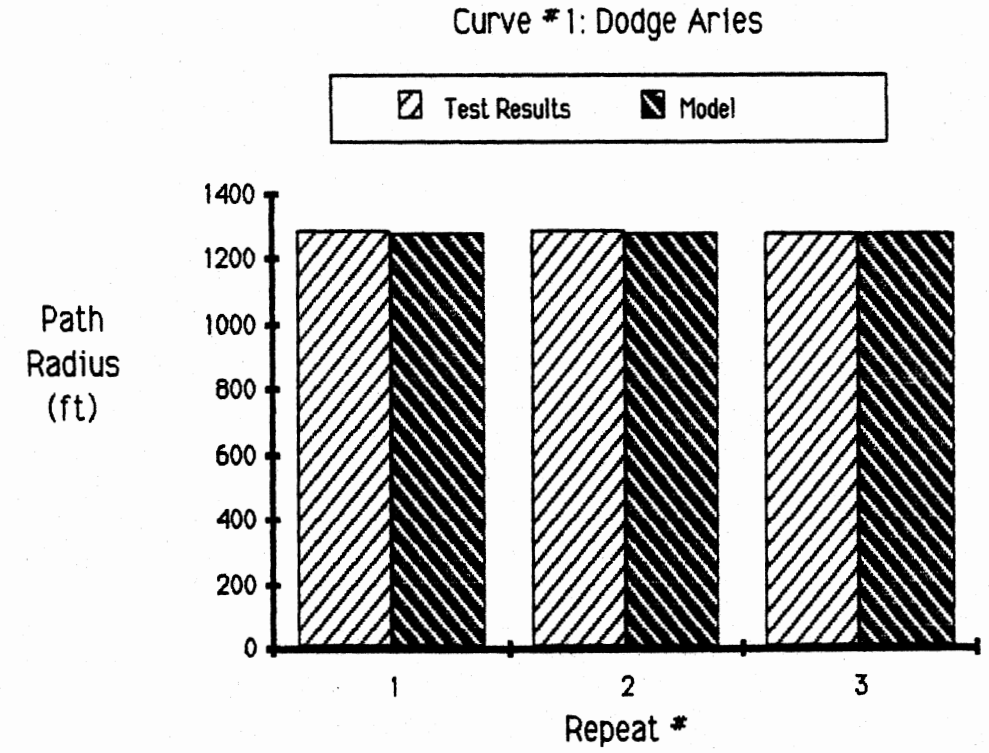

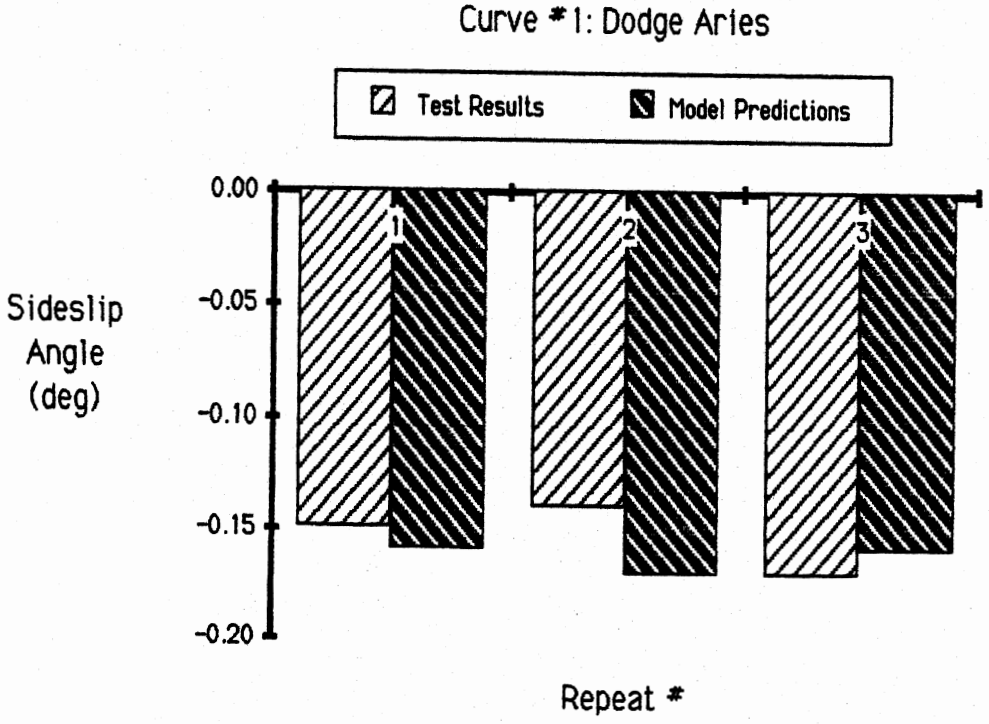

Figure 32 (cont)

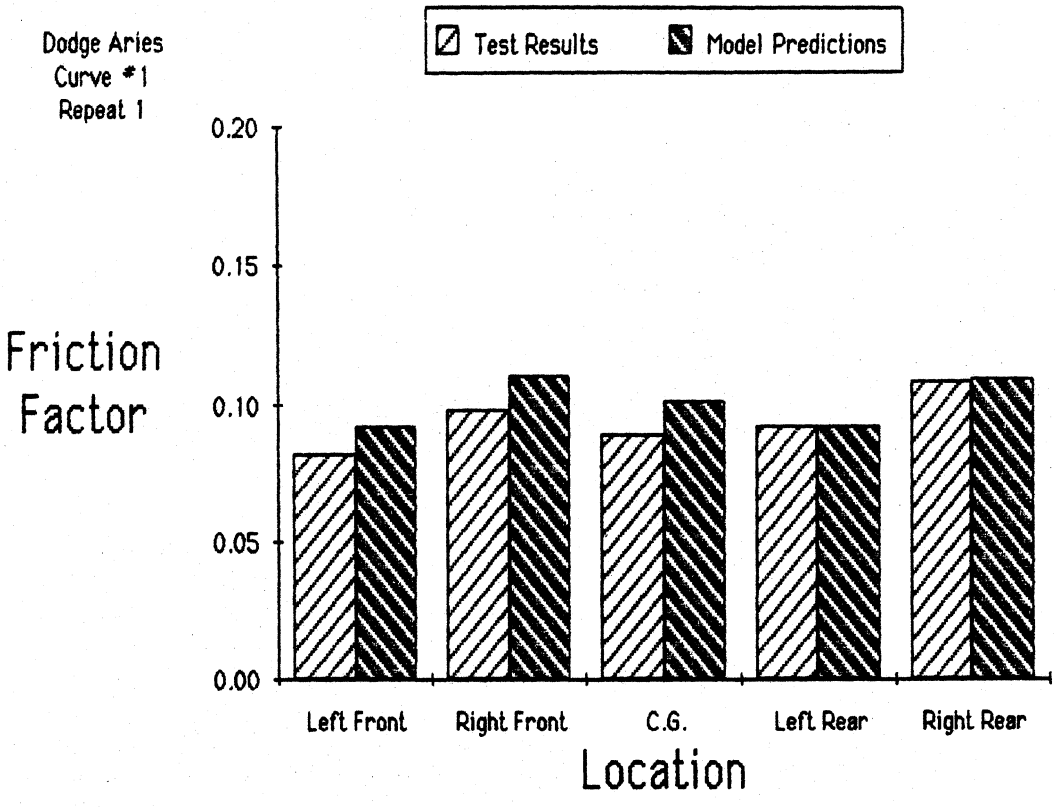

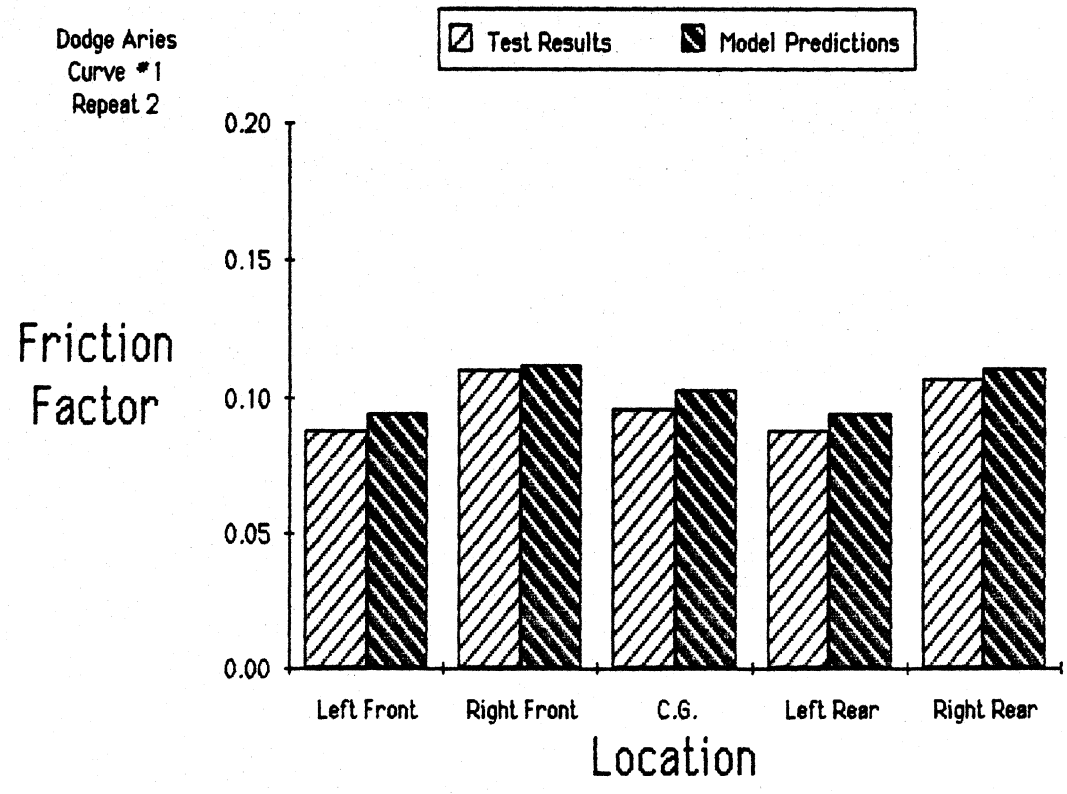

Figure 33. Friction factor comparisons; vehicle A

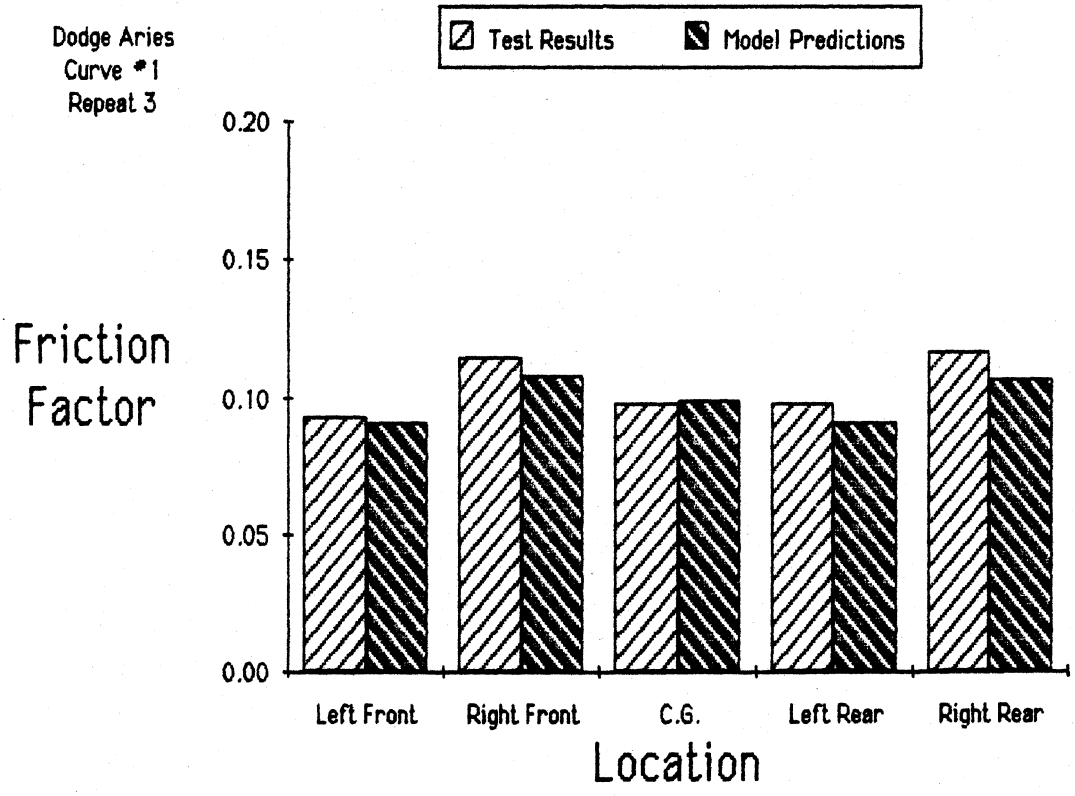

Figure 33 (cont)

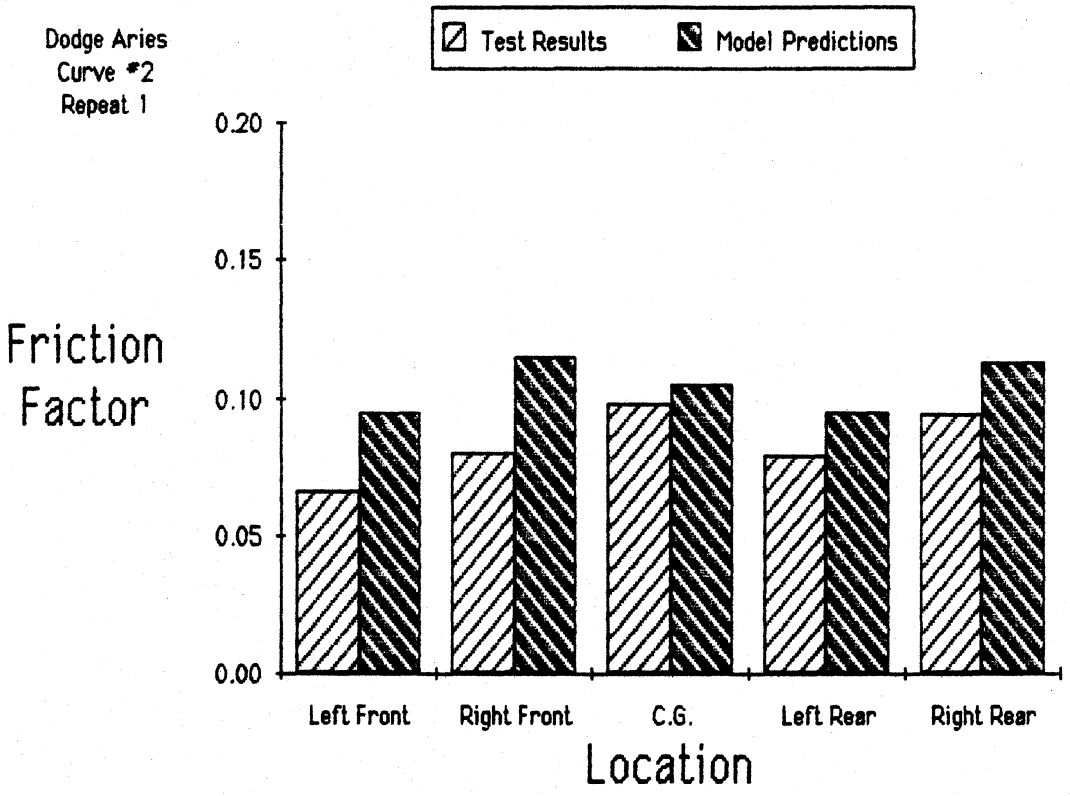

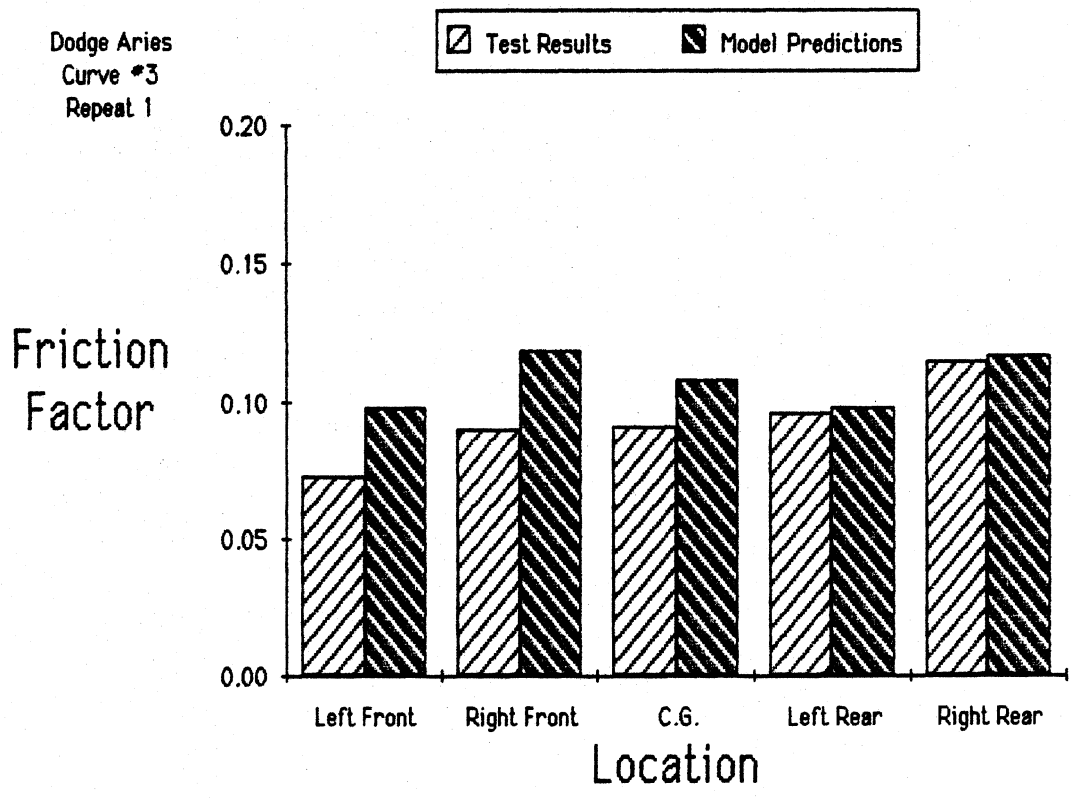

Figure 34. Friction factor comparisons; vehicle A

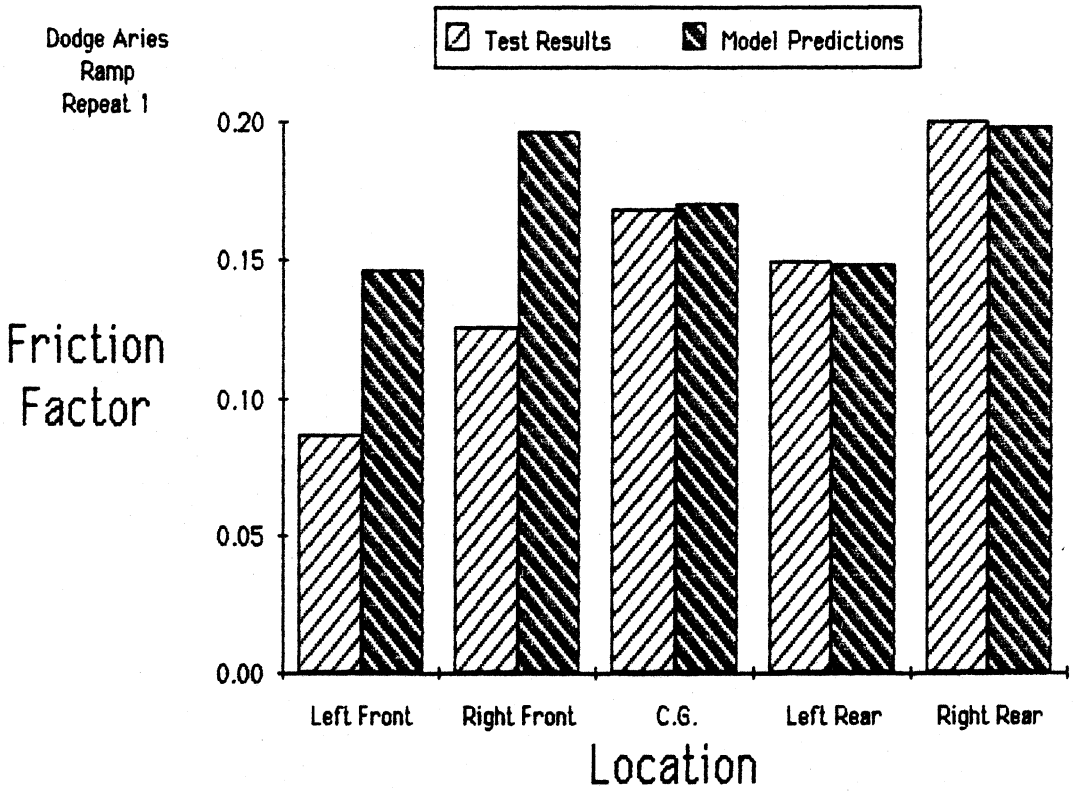

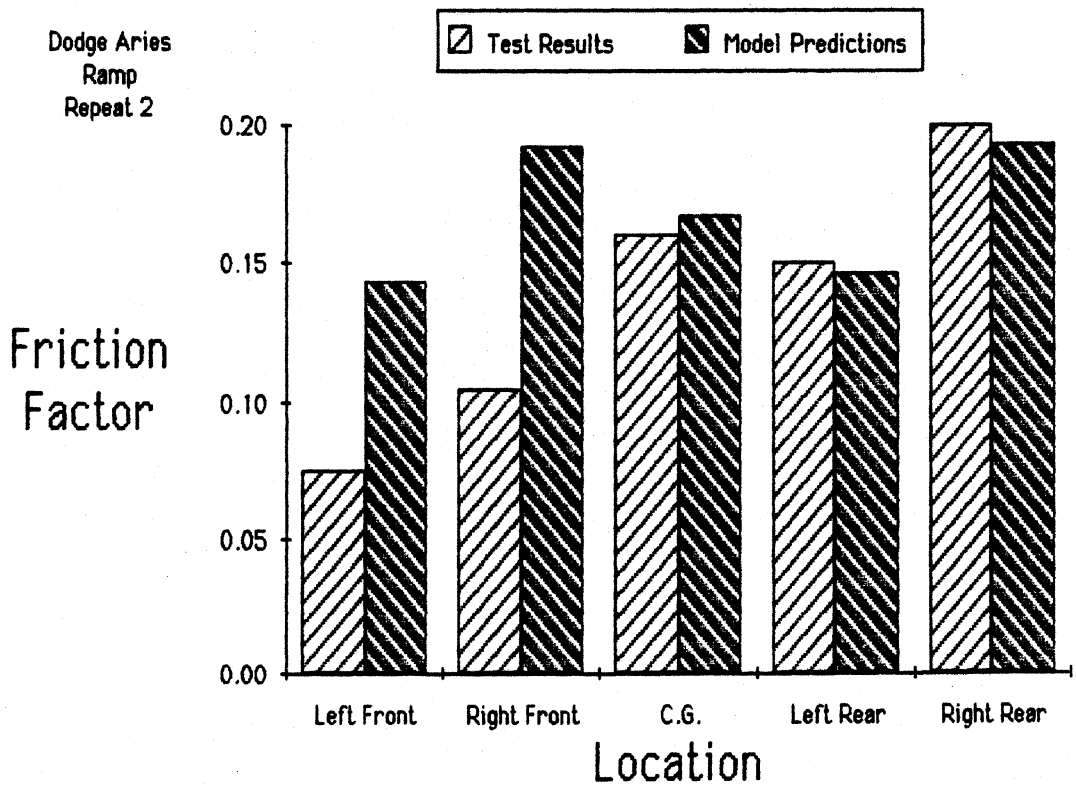

Figure 35. Friction factor comparisons; vehicle A

benefitting especially from a much smoother ride from the passenger car. The overall level of noise in the trolley time histories (appendix E) is greatly reduced from that seen in the tractor-semitrailer tests.

The friction factor comparisons seen in figure 33 for curve 1 and vehicle A are generally quite good and exhibit levels of variation expected from experimental measurements performed under these operating conditions. The friction factor comparisons seen in figure 34 for curves 2 and 3 exhibit greater discrepancies at the front wheel locations primarily because of the steering wheel differences seen in figure F-3 of appendix F. Eventhough the curve geometry and speeds were nearly identical for all these curve measurements, the steering wheel angle measurements for curves 2 and 3 are unexplainably lower than those observed in curve 1. Frequently, these differences are attributable to variations in zero data values obtained from different sections of roadway.

Finally, figure 35 compares friction factor values at the ramp site, curve 4, under conditions of lower speed and reduced curve radius. Although the front wheel locations show differences which are due to errors in front wheel angle measurement, the rear wheel values and point-mass value (c.g.) exhibit very good agreement. This particular figure underscores the point made earlier in the tractor-semitrailer data, that unless all vehicle response measurements that contribute to friction factor estimates are accurate, modest errors in certain measurements can significantly affect the accuracy of the friction factor estimates. In this case, the rear wheel friction factor estimates depend upon four measurements (yaw rate, speed, trolley angle, and roll angle), whereas the front wheel values depend upon the same measurements but steer angle as well. Consequently, only the front wheel friction factor estimates are affected in this particular case.

5.1.3 Passenger Car B Comparisons

The rear wheel drive passenger car comparisons seen in figures 36 and 37 (and figures F-5 and F-6 of appendix F) also indicate general agreement with the results predicted by the model. The primary discrepancy for vehicle B appears in the comparisons of front wheel steer angle. No explanation has

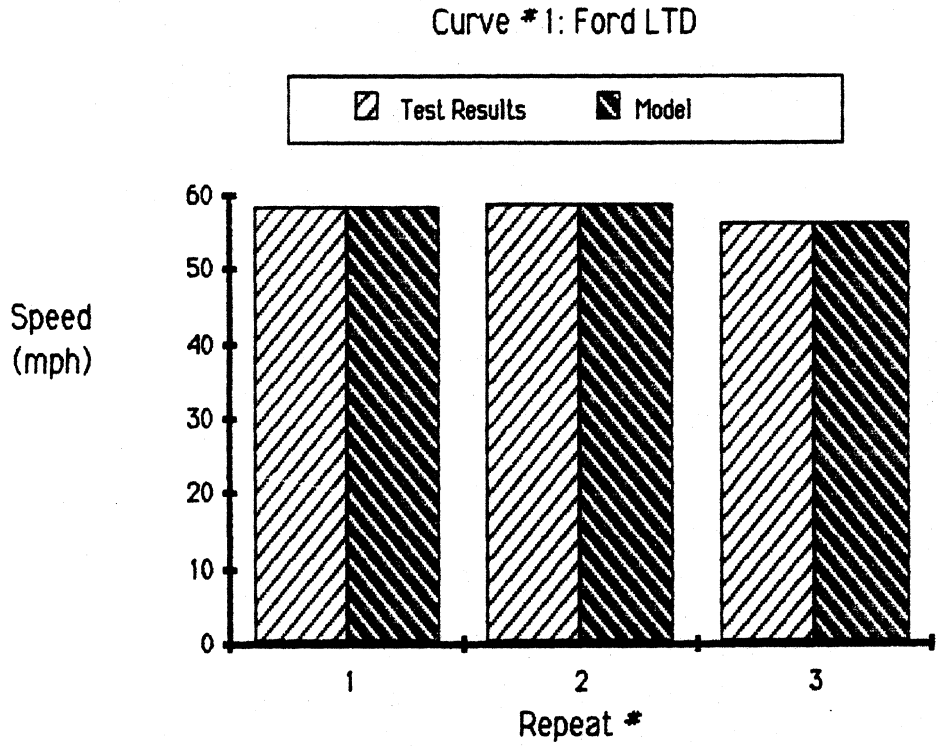

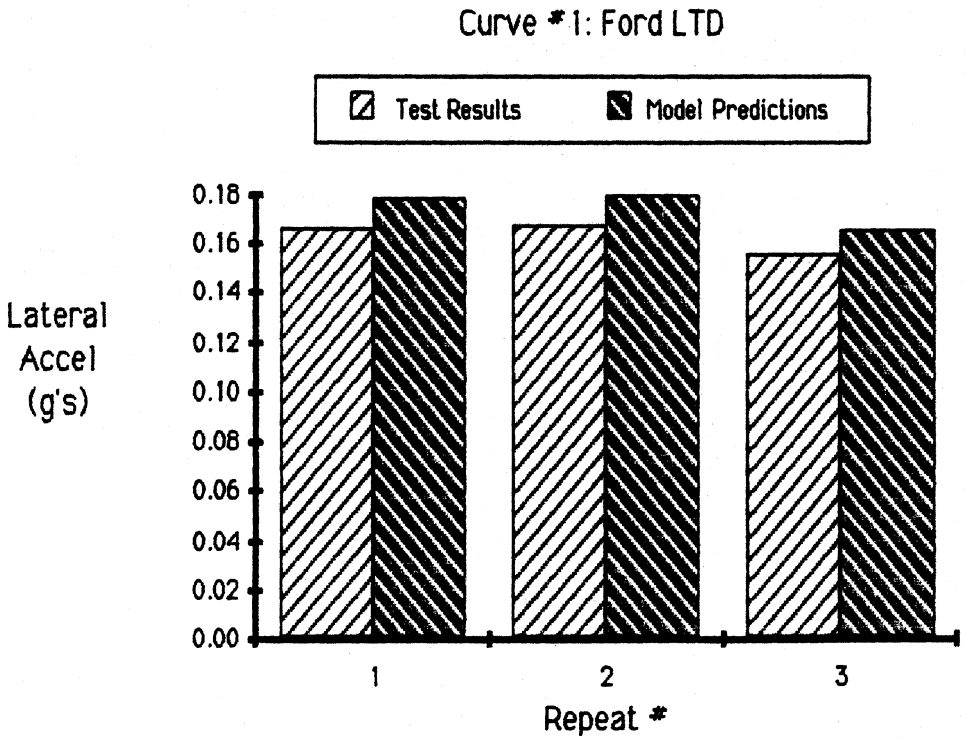

Figure 36. Model/test comparisons; vehicle B

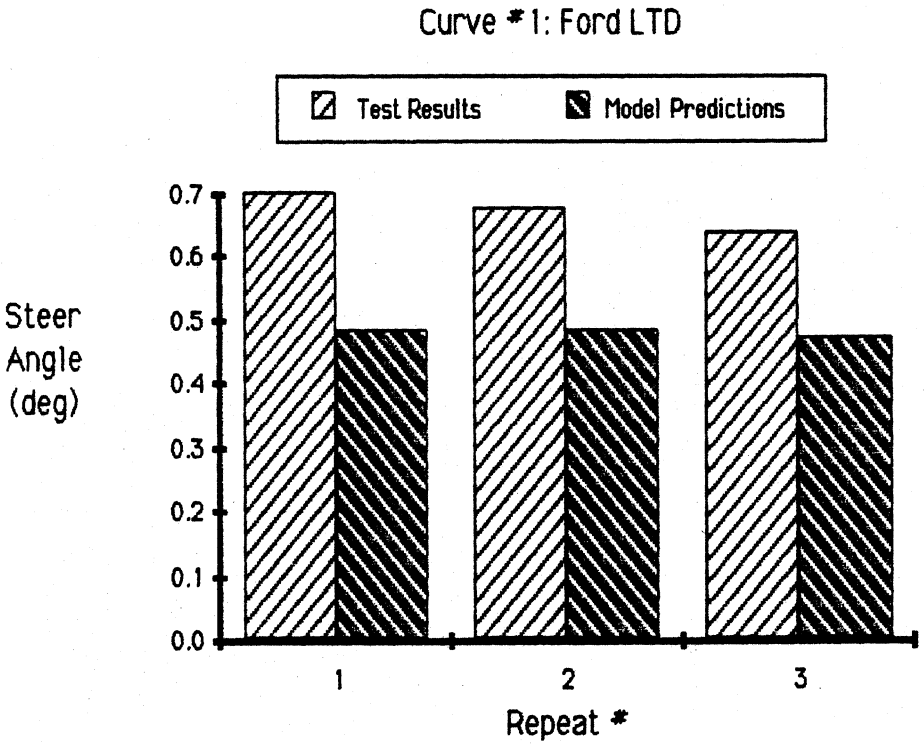

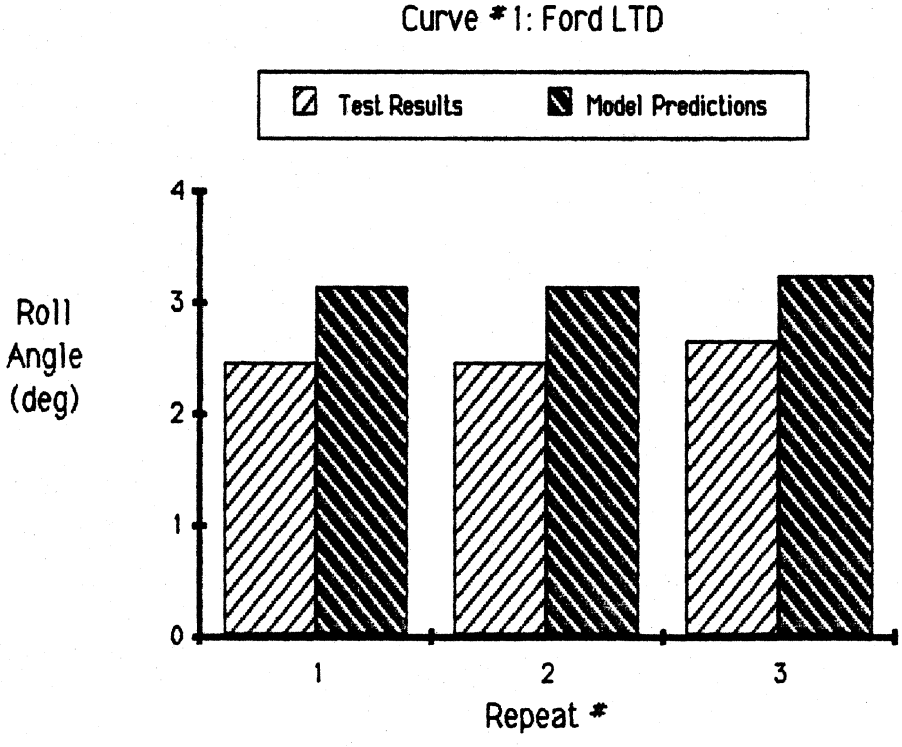

Figure 36 (cont)

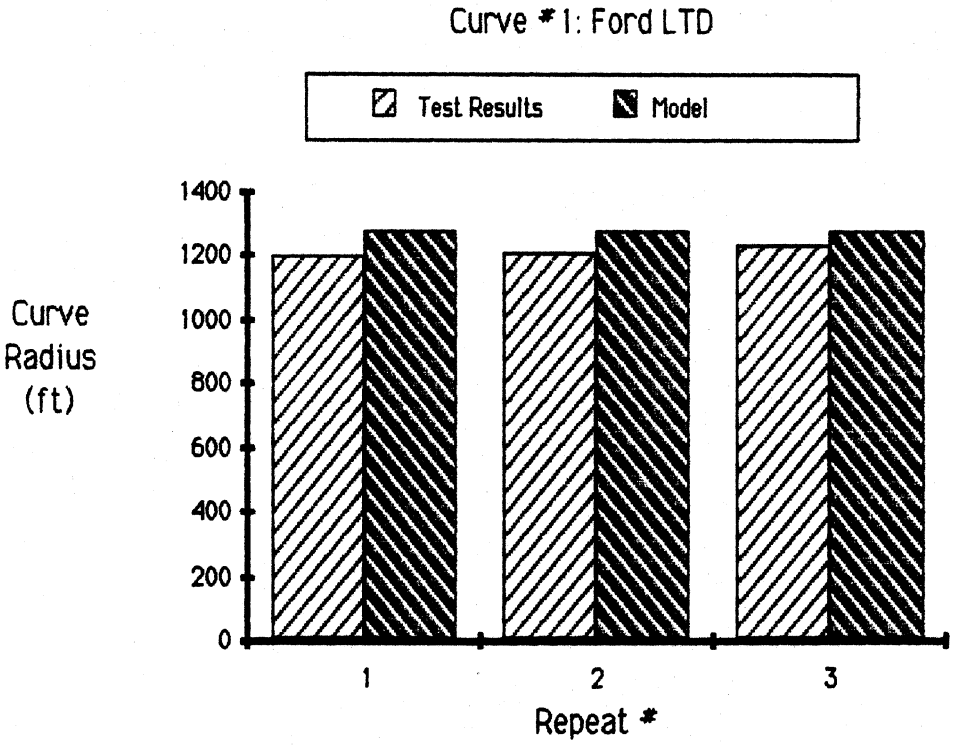

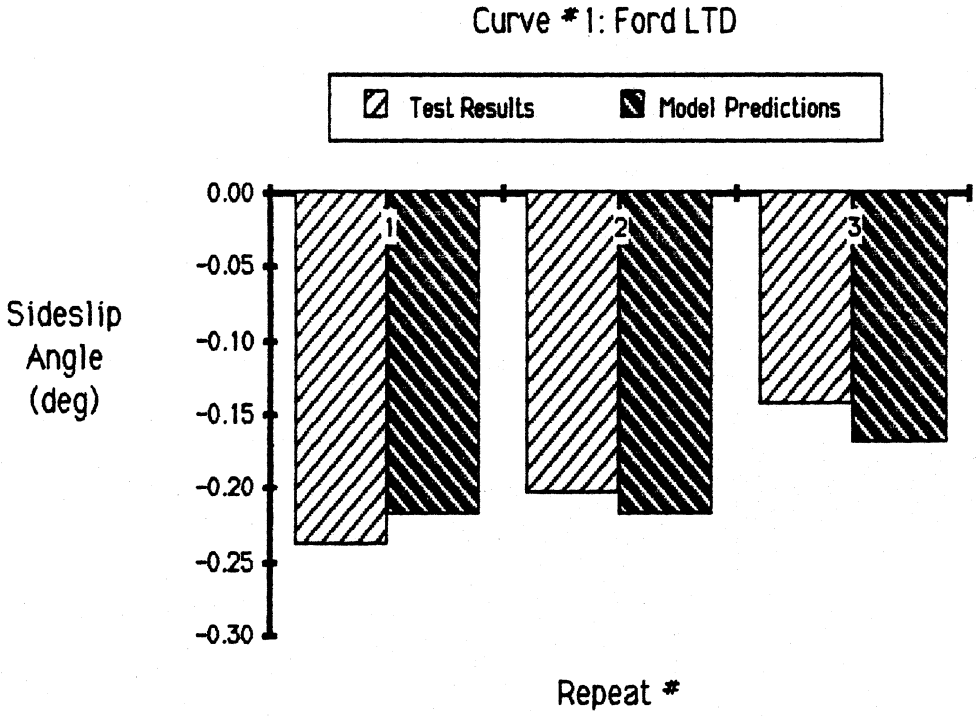

Figure 36 (cont)

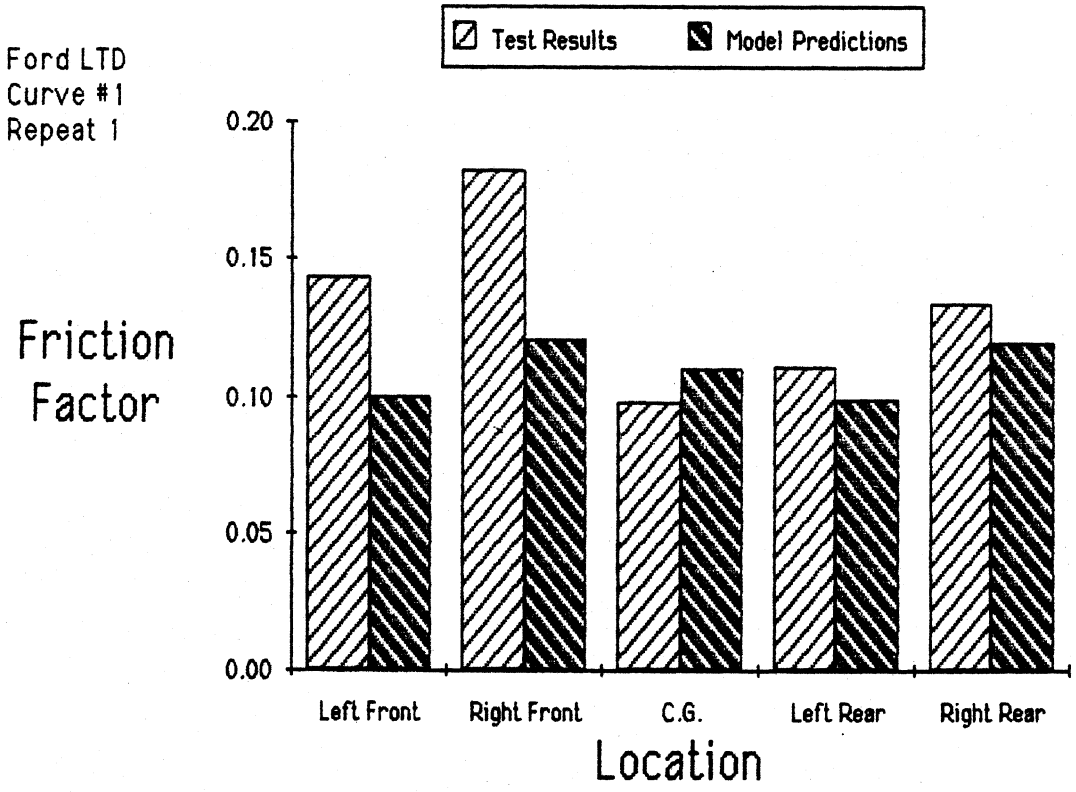

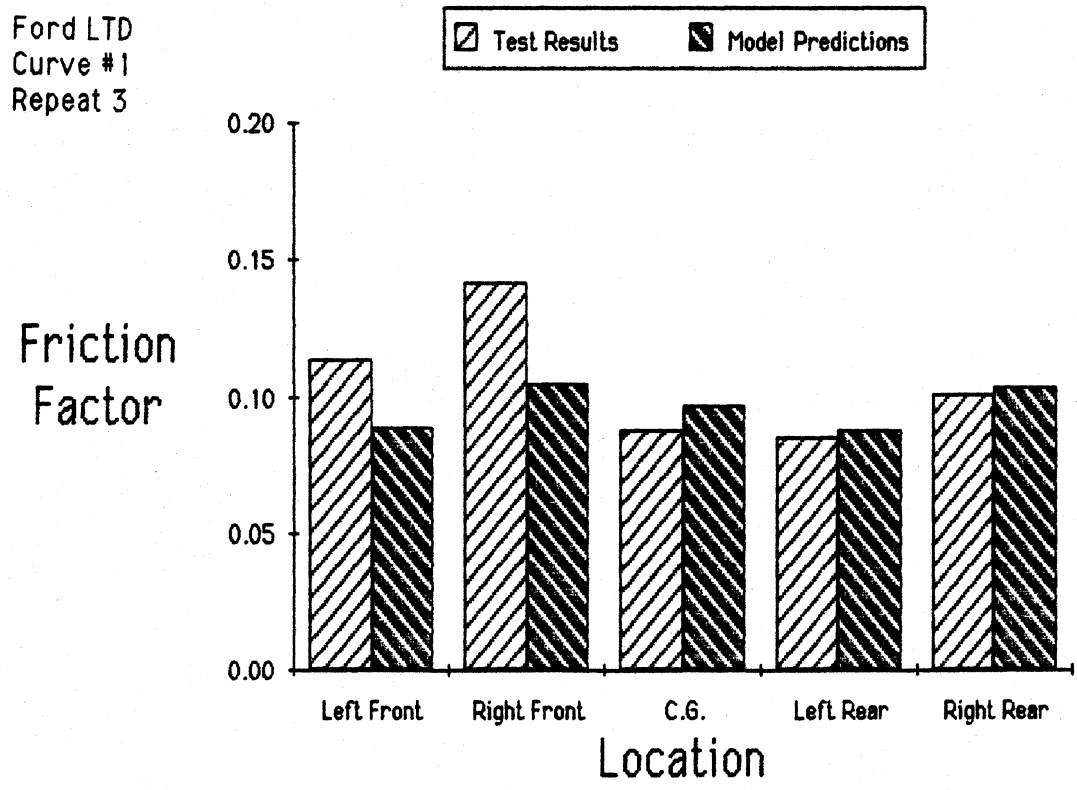

Figure 37. Friction factor comparisons; vehicle B

been specifically identified for the steer angle discrepancies, although an instrumentaion gain, automatically set by the data acquistion system, appears to be the probable cause. It is known that the front wheel steer angle measurements seen here are too high because many of the measurements suggest steering gear ratios (steering wheel angle / front wheel angle) that are too low. For example, the ramp data for vehicle B (appendix E) which includes the effects of steering system compliance, suggests steering gear ratios in the vicinity of 17 (a more reasonable value would be 25 or 30). Since the known gear ratio is 20 (and perhaps as low as 19.5 due to its variable steering gear properties), no explanation other than a transducer/instrumentation gain error is likely.

Aside from these matters, the remaining vehicle response measurements compare very favorably with the predictions from the steady turning models. Vehicle sideslip measurements for curve 1 show differences of less than 0.03 degrees for each of the three repeats. The sideslip measurements for the remaining three curve sites shown in this set of figures contain errors of less than 0.15 degrees. The curve radius and lateral acceleration measurements are normally within 5 percent of the actual or predicted values.

The friction factor results seen in figures 37 through 41 for the front wheels are of course greatly influenced by the front steer angle measurements. To indicate how the friction factor estimates are altered by more accurate estimates of front steer angle, several of these figures (38, 40, and 41) contain duplicate test result estimates - one using the measured front steer angle, the other using front steer angle predicted by the model. In each of these duplicate figures, the only measured quantity altered was front steer angle. The degree of improvement seen in the front wheel friction factor plots, resulting from a more accurate value of steer angle, again emphasizes the sensitivity of estimating friction factor values when modest errors in one measurement are present.

5.2 Obstacle Avoidance Comparisons

The model predictions presented in this and the next section make use of the nonlinear Phase 4 model. The comparisons seen here are presented in a

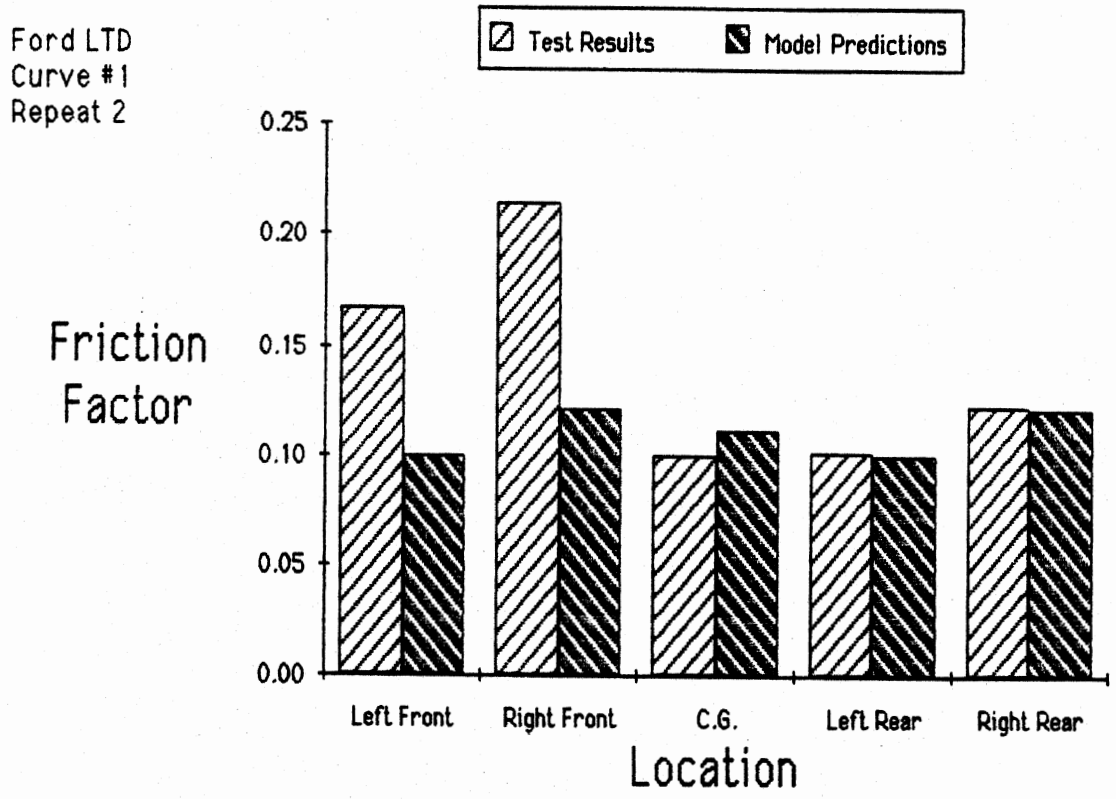

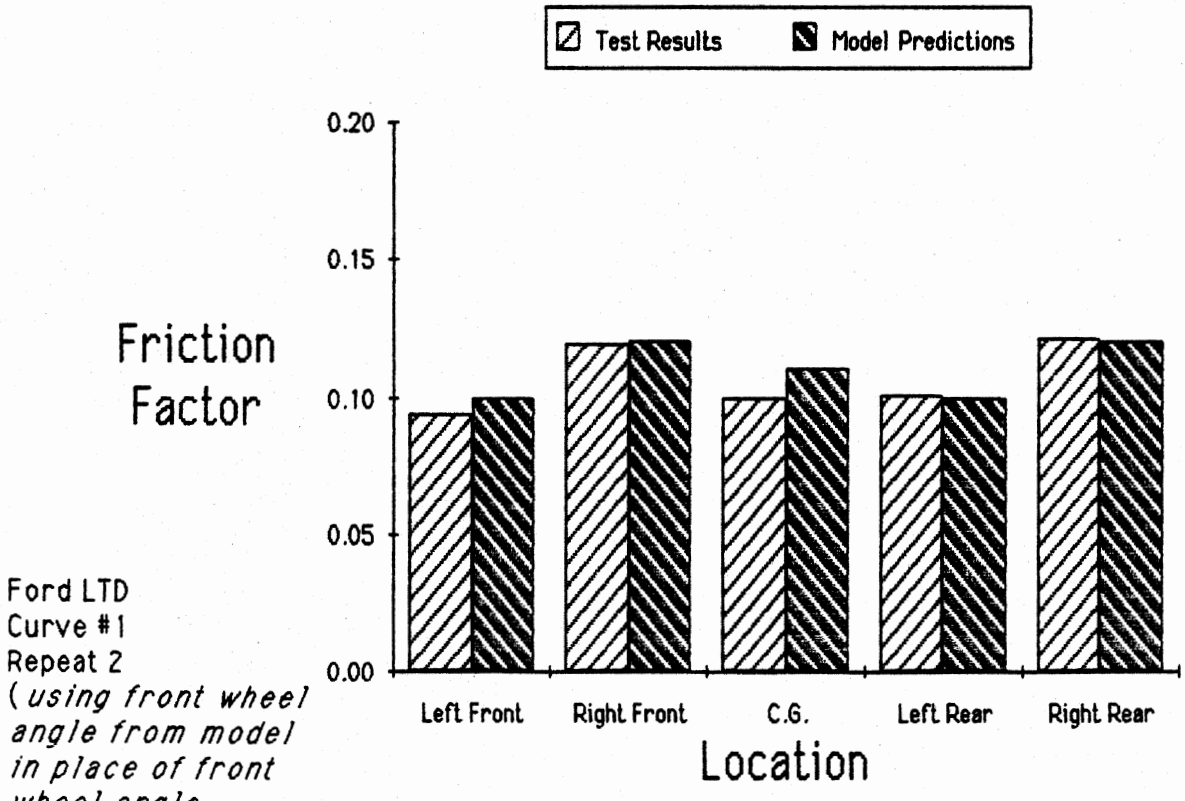

Figure 38. Friction factor comparisons; vehicle B

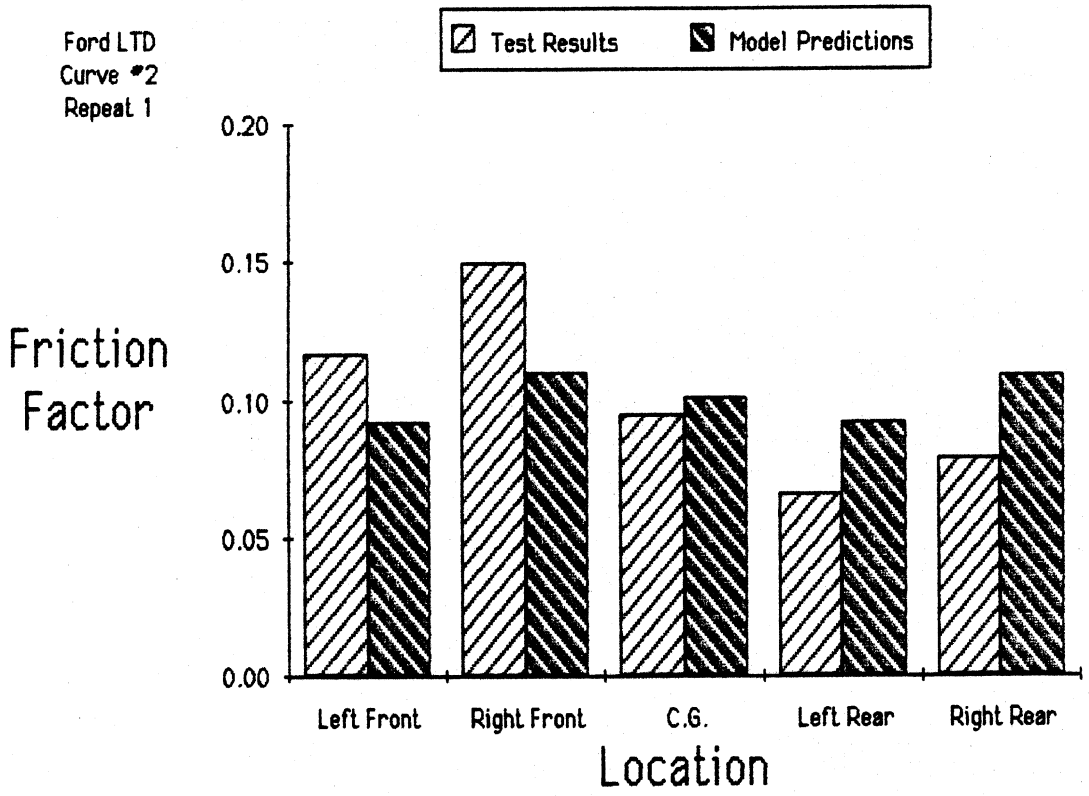

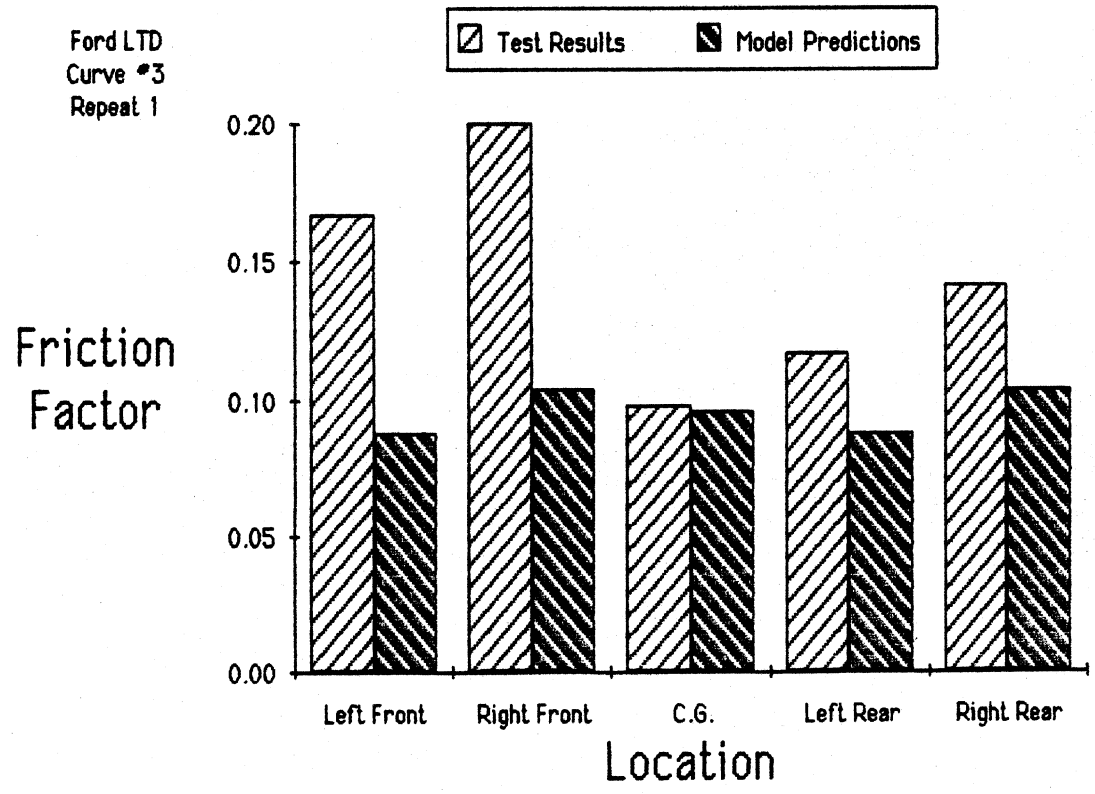

Figure 39. Friction factor comparisons; vehicle B

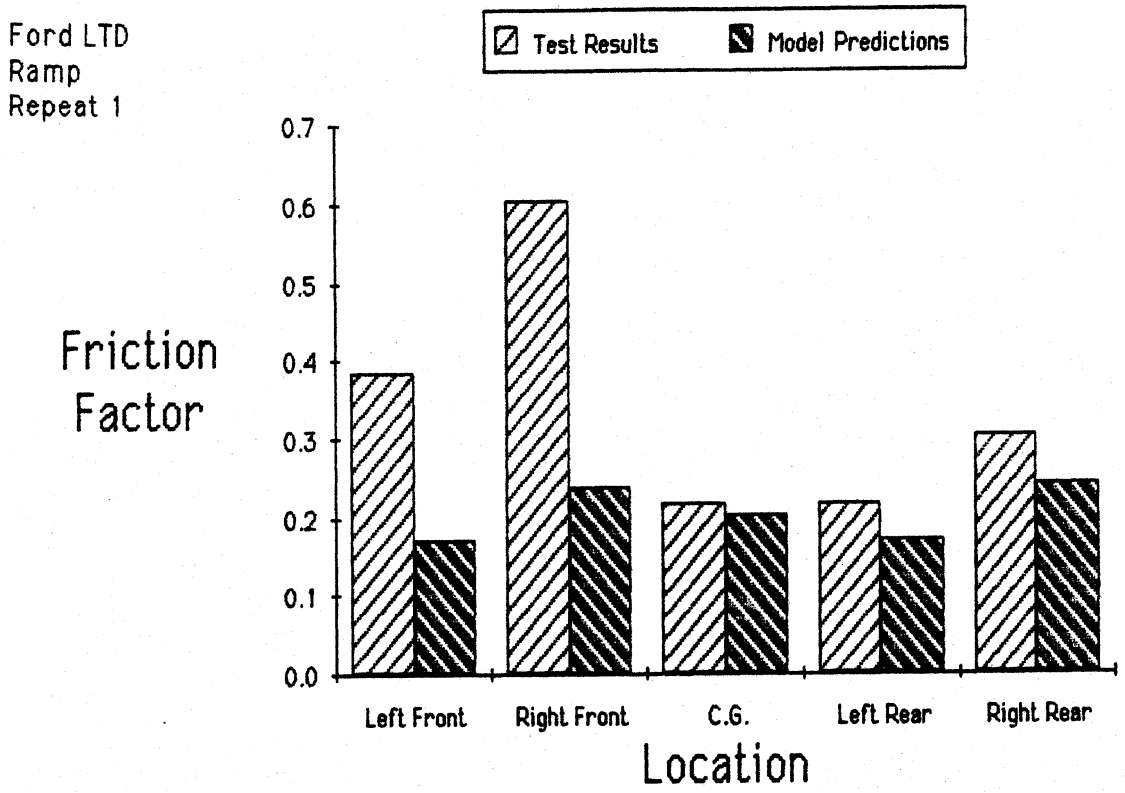

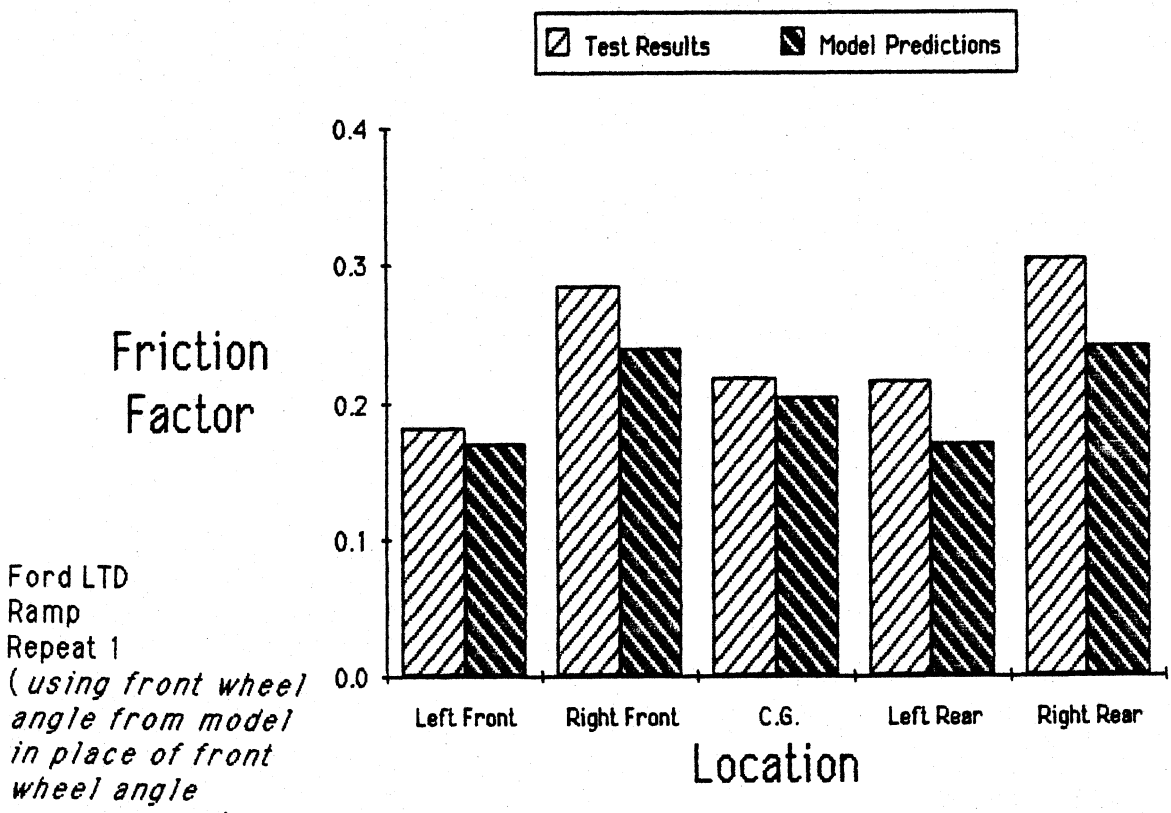

Figure 40. Friction factor comparisons; vehicle B

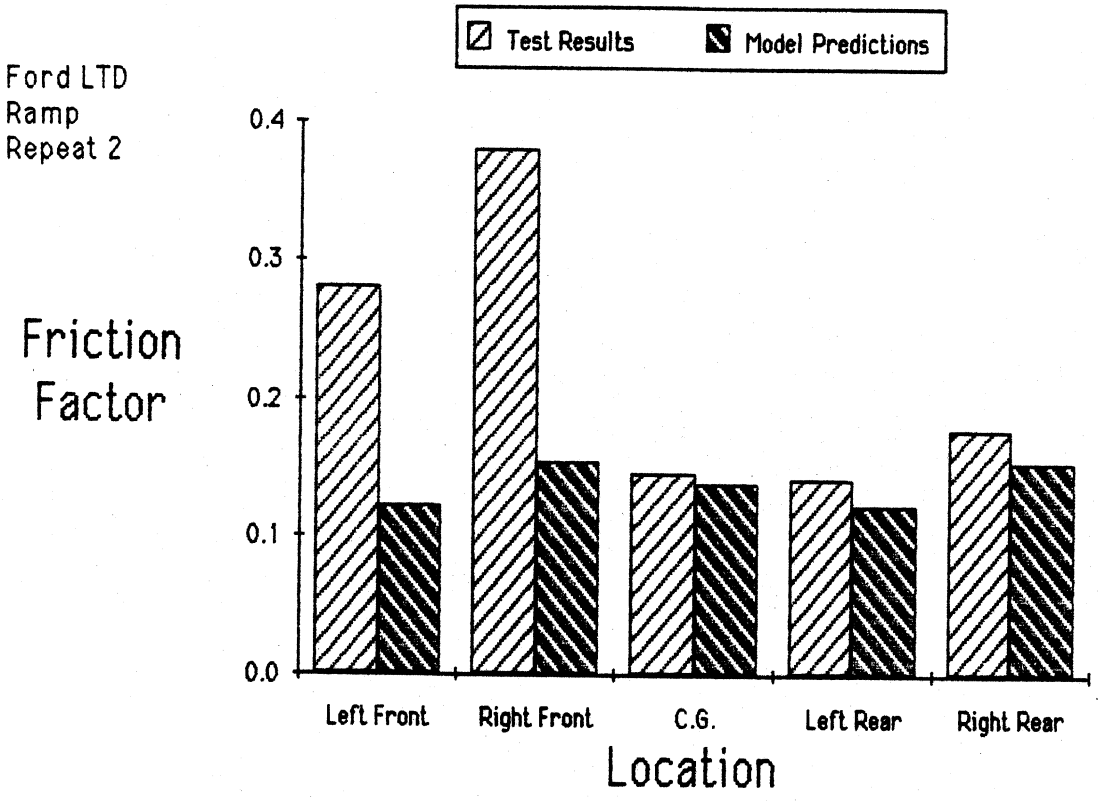

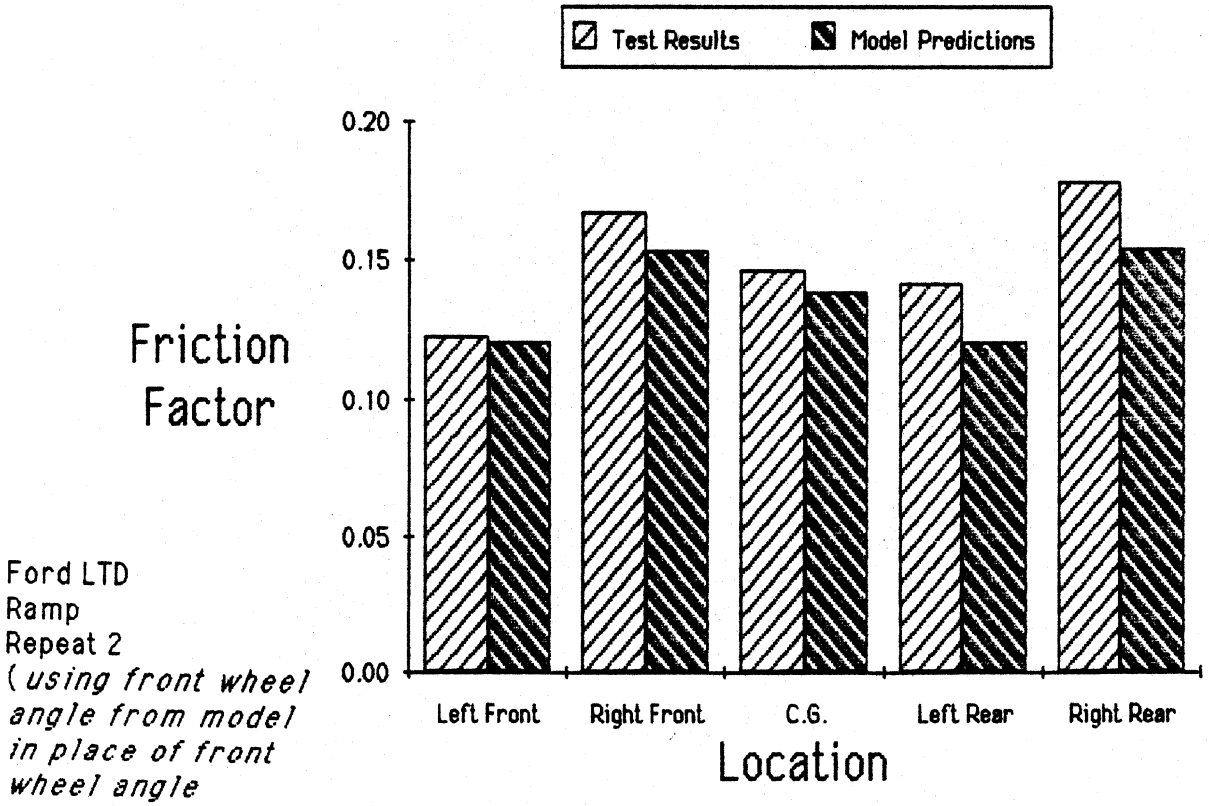

Ford LTD
Ramp
Repeat 2
(*using front wheel angle from model in place of front wheel angle measurement*)

Figure 41. Friction factor comparisons; vehicle B

time history format, rather than as summary charts used for the steady turning comparisons, because of the time varying nature of the test maneuvers.

The model results seen in Figures 43 through 45 were obtained by running the Phase 4 model under driver control (closed-loop) [6] along a superelevated curve having the same geometry as curve 1. Following a steady turning condition, the driver model performs an obstacle avoidance maneuver starting from the outside lane (turning left, as in figure 42). Figure 43 corresponds to the tractor - semitrailer; figure 44 to passenger car A; and figure 45 to passenger car B.

In the actual vehicle tests the driver was allowed to move from the initial travel lane to the adjoining lane with complete freedom. No path or coned course was specified in performing the lane-to-lane movement. In the computer simulation, a path for the driver model to follow during the lane to lane movement must be specified. The path used in the simulation calculations was a simple 12-ft (3.7 m) offset to the inside of the 1273 ft (388 m) radius curve and then back again, varying in a linear fashion over a forward travel distance of approximately 100 to 150 ft (30 to 45 m). See figure 42. Two runs for each vehicle were made with the Phase 4 model to produce the results seen in this section. The second run in each case was a repeat of the first run with a path adjustment of the lane change to better match the observed test results. In general, the level of agreement in these comparisons is very reasonable. All comparisons seen here were made for curve 1.

Each of the figure pages contains a direct comparison of test data (top chart) with its corresponding Phase 4 prediction (bottom chart). In some of the comparisons the simulation results show the lane change being performed somewhat before or after that seen in the test result. The time skew is not important and is only due to where along the curve the simulation lane change occurs. Also, the beginning of the simulation calculations (time=0) has the vehicle starting from a horizontal plane position and driving on to a 6.7 percent superelevated curve over a distance of 200 feet (61 m). The starting position for the test vehicle was an inclined tangent of variable superelevation. Accordingly, the first few seconds of simulation predictions will be different from the test measurements, particularly in roll response.

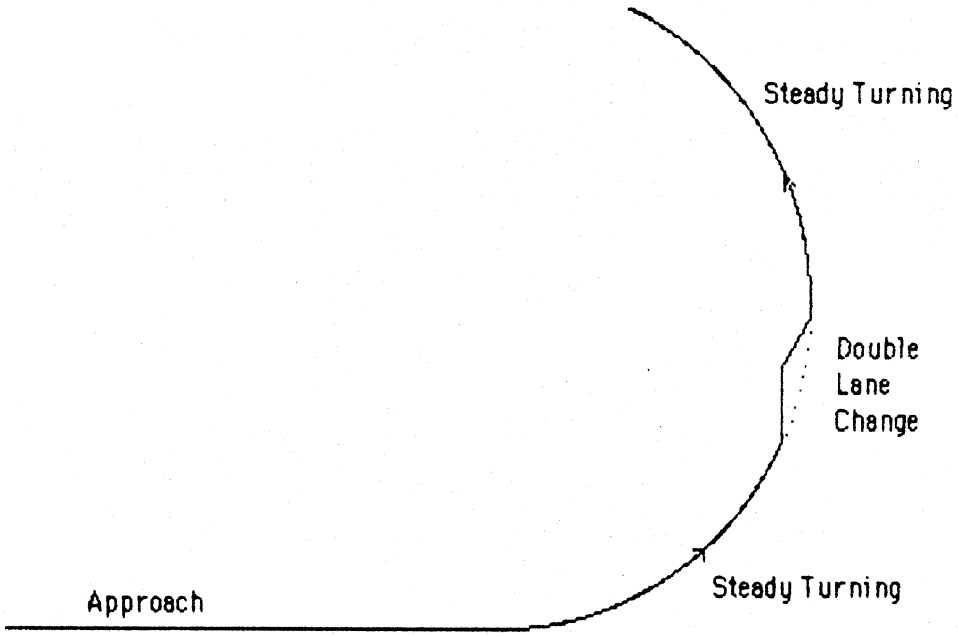

Figure 42. Obstacle avoidance (double lane change) maneuver

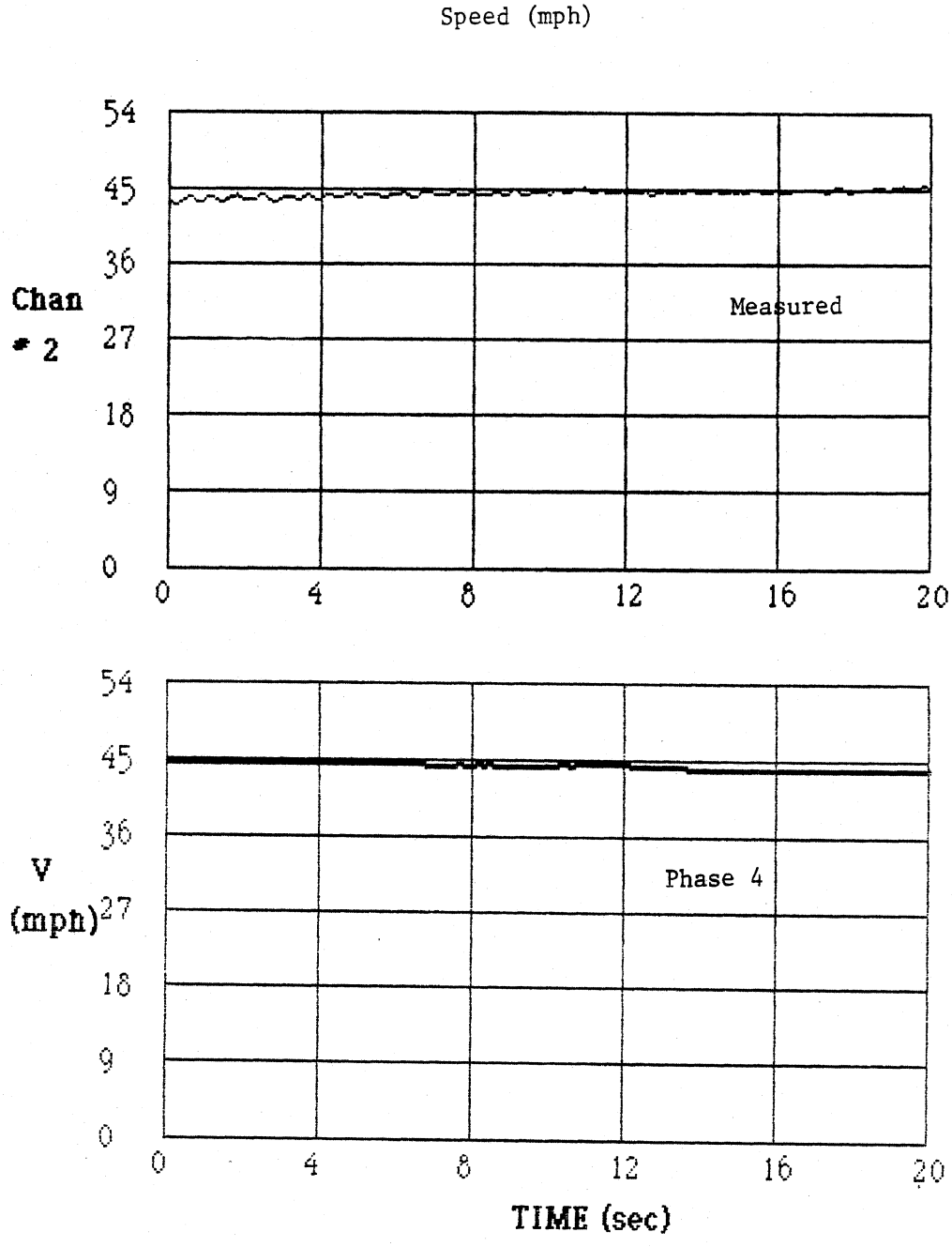

Figure 43. Phase 4 model/test comparison; obstacle avoidance maneuver; vehicle C.

Lateral Acceleration (g's)

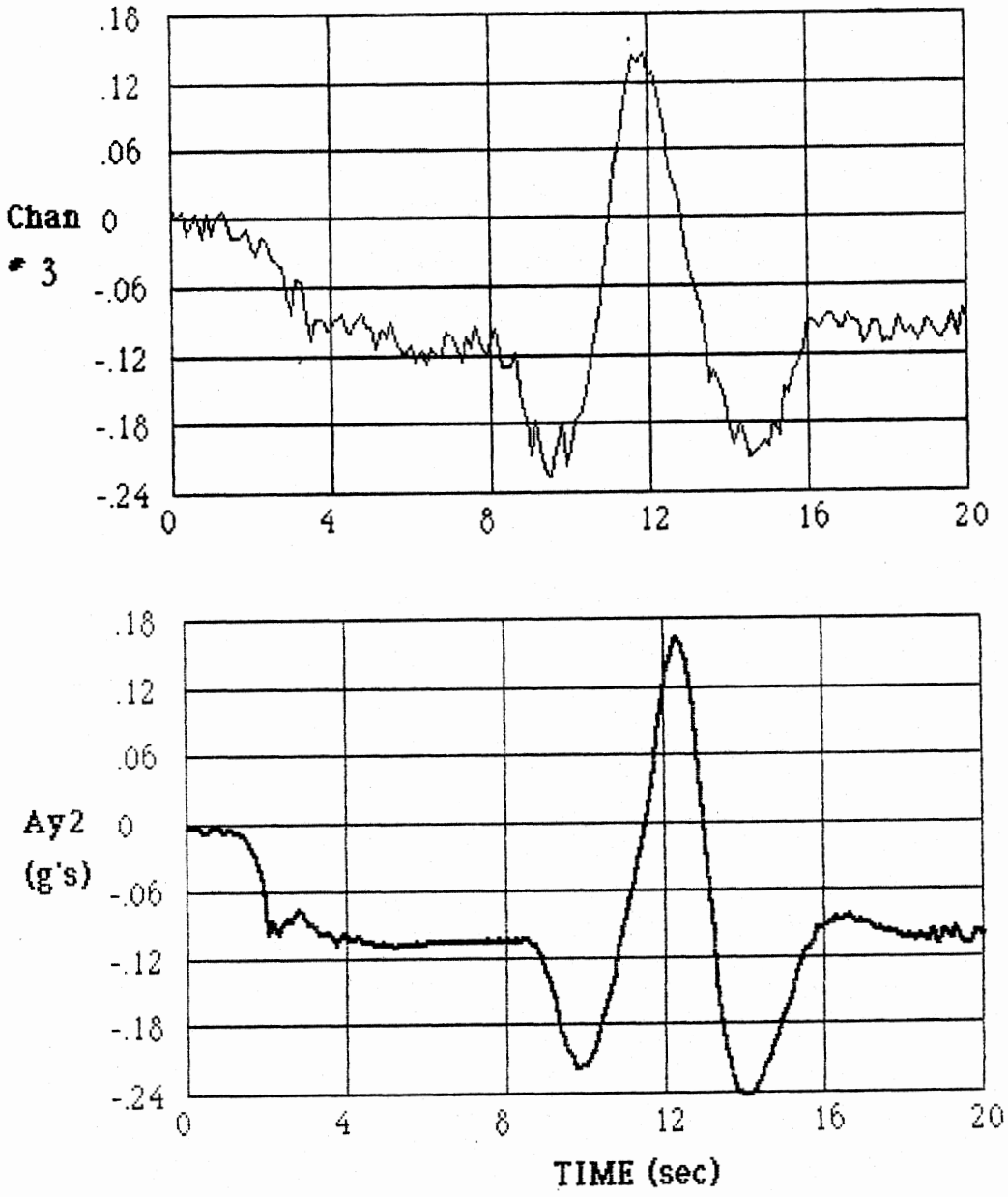

Figure 43 (cont)

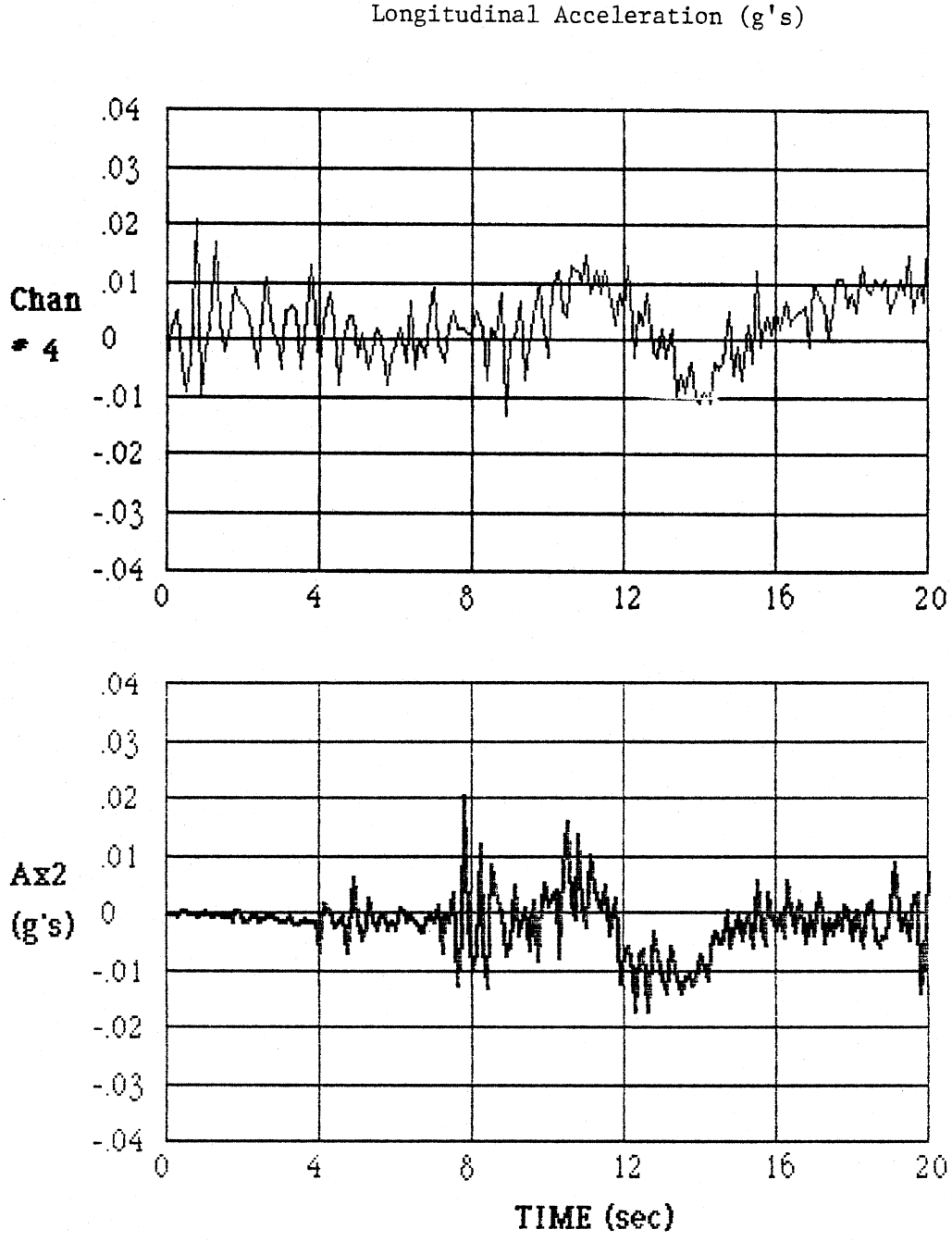

Figure 43 (cont)

Trailer Yaw Rate (deg/s)

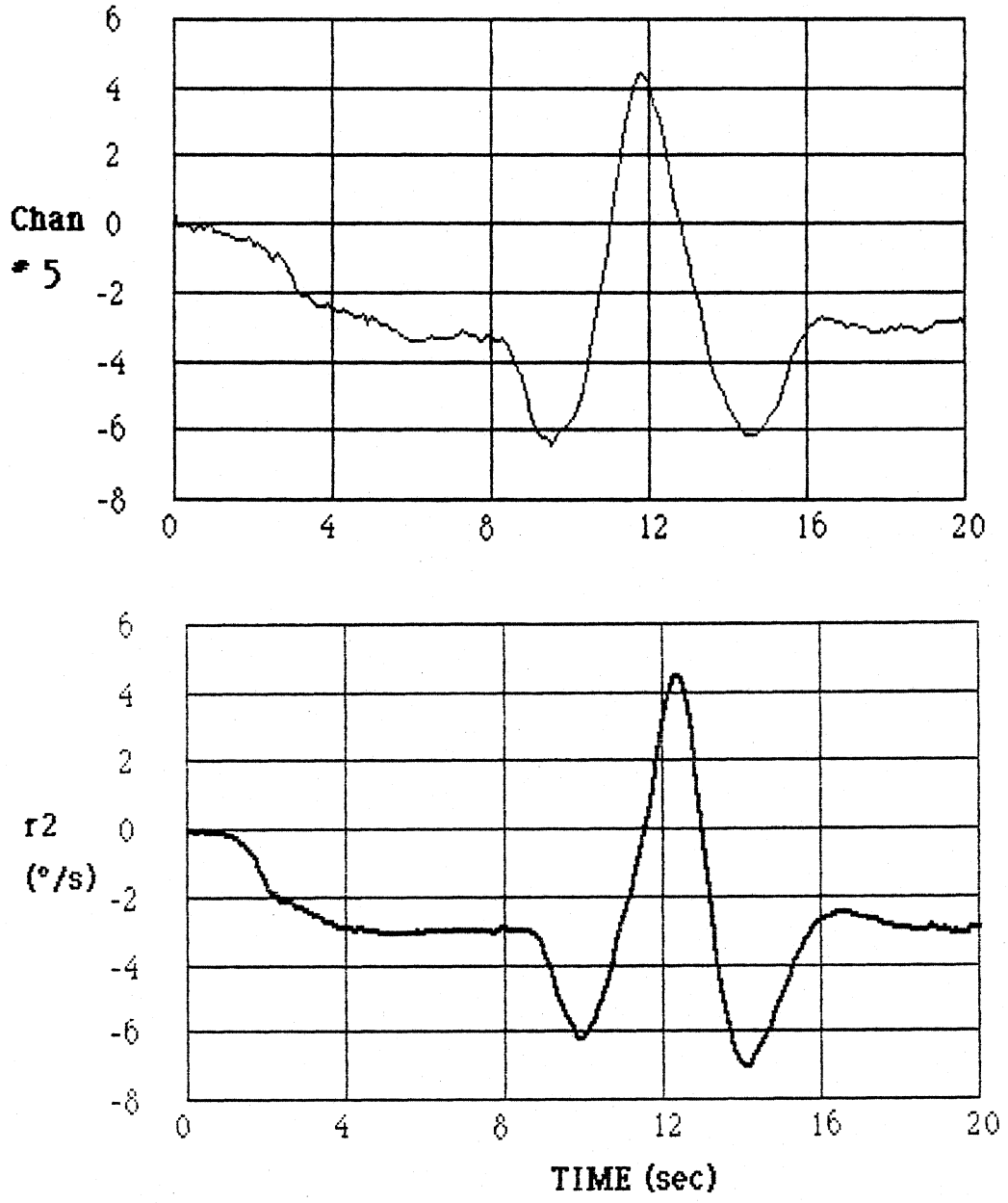

Figure 43 (cont)

Trailer Roll Angle (deg)

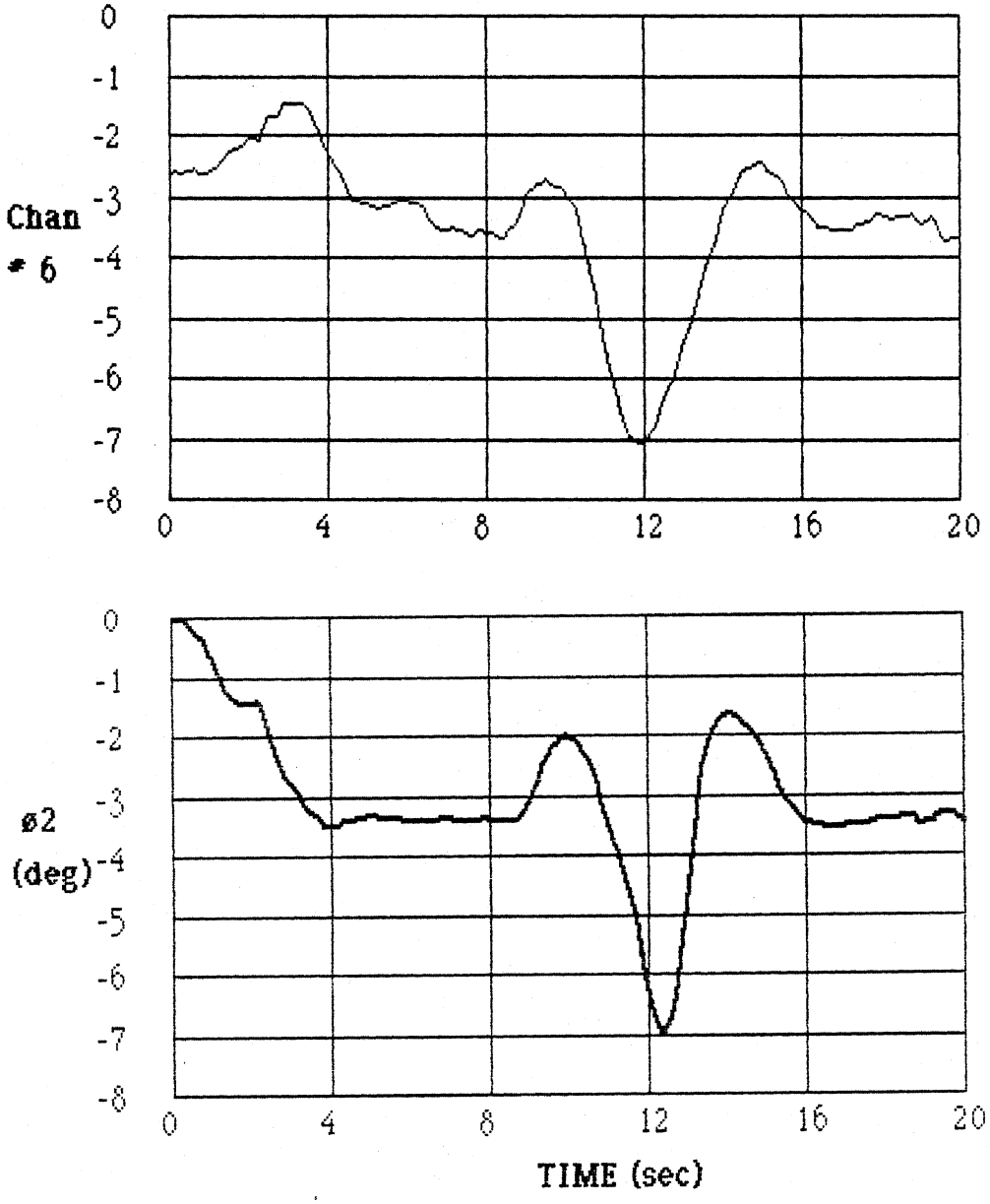

Figure 43 (cont)

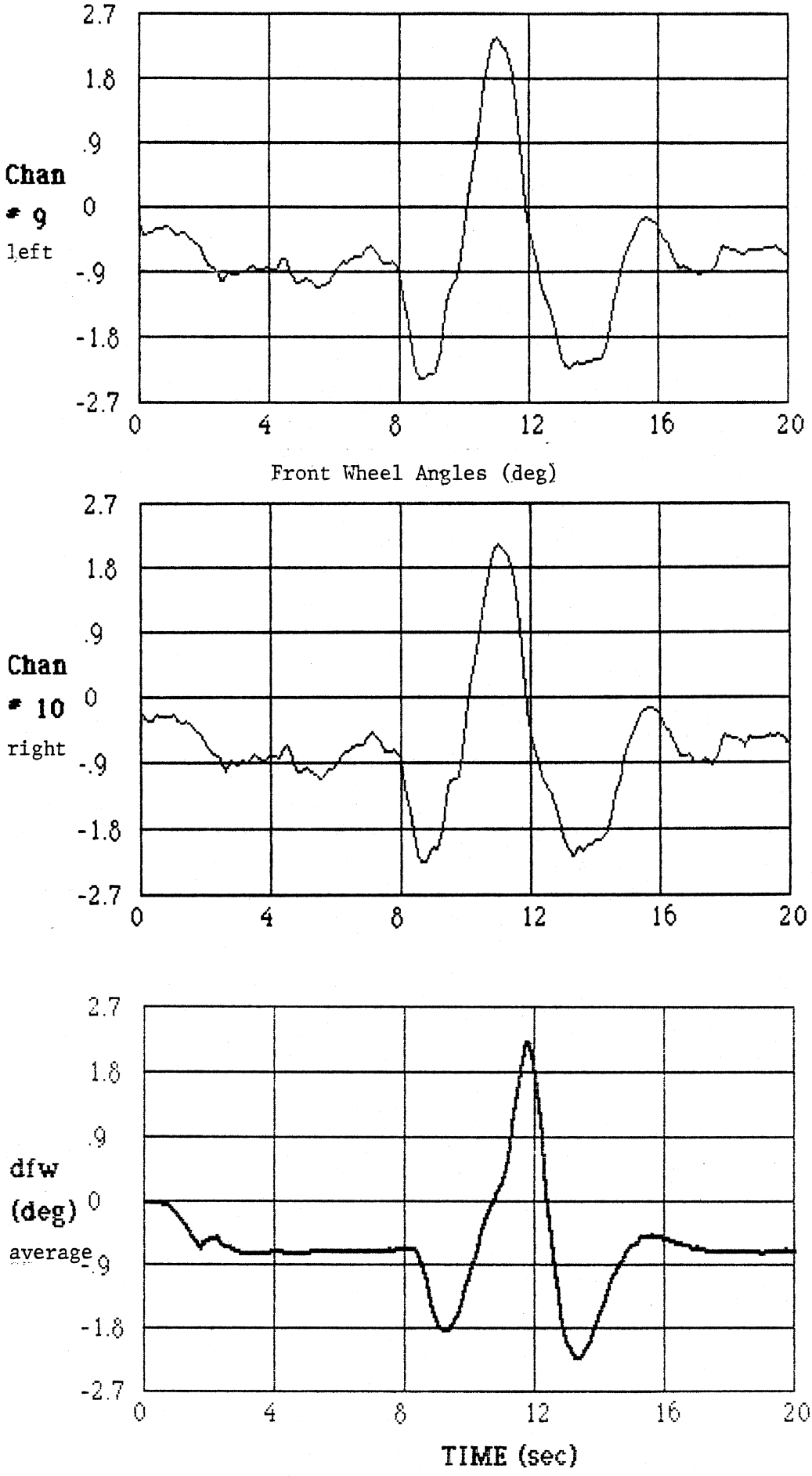

Figure 43 (cont)

Articulation Angle (deg)

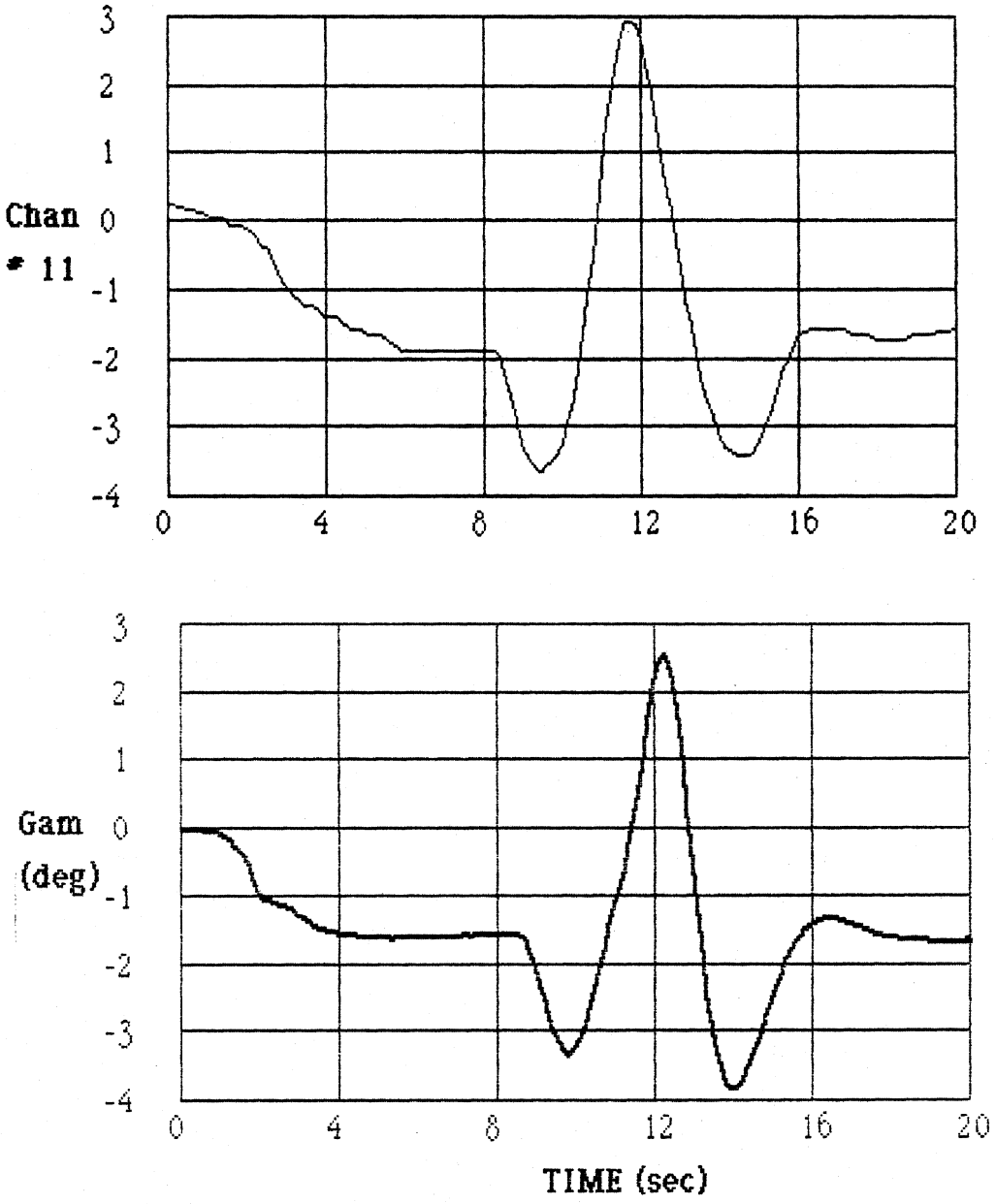

Figure 43 (cont)

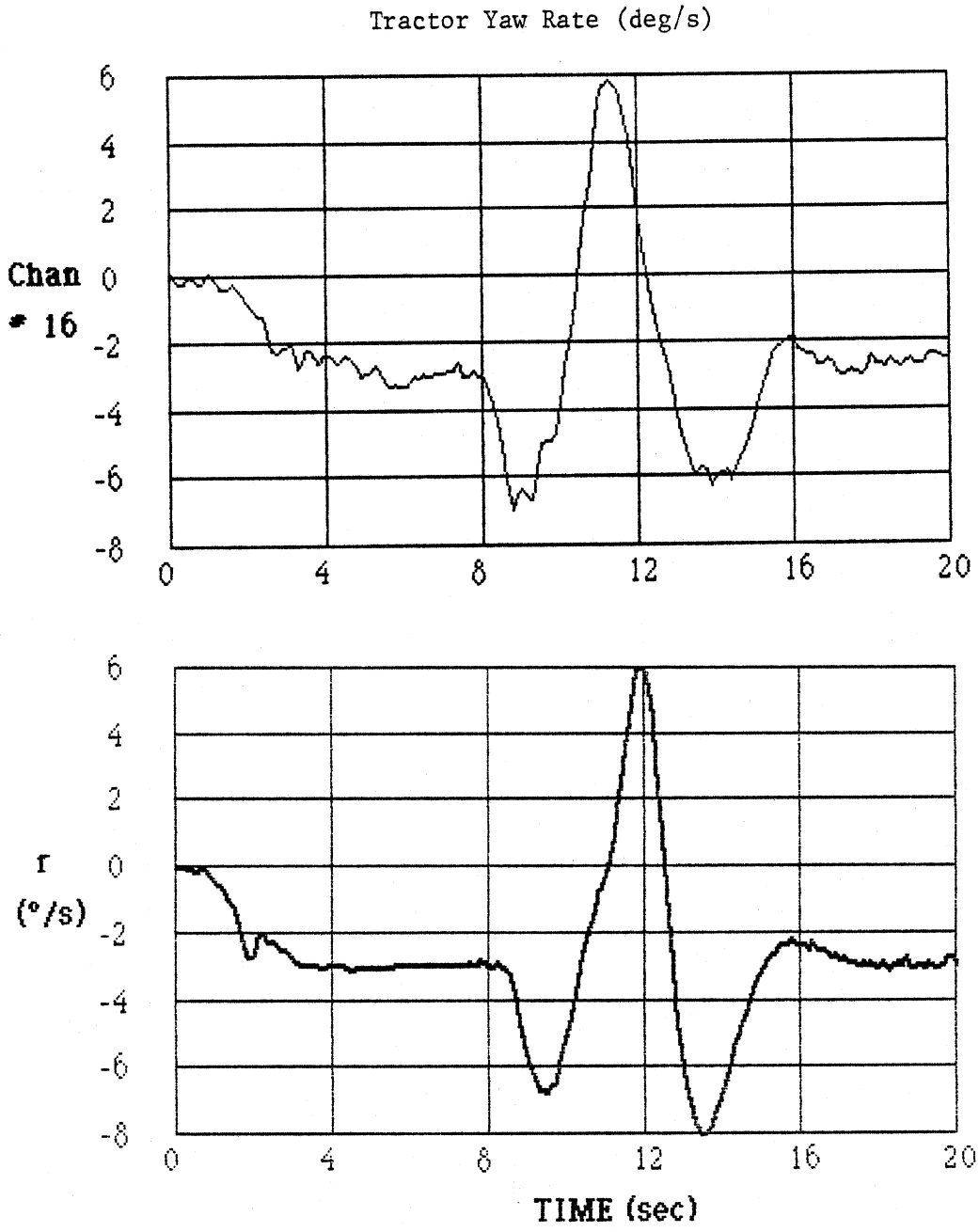

Figure 43 (cont)

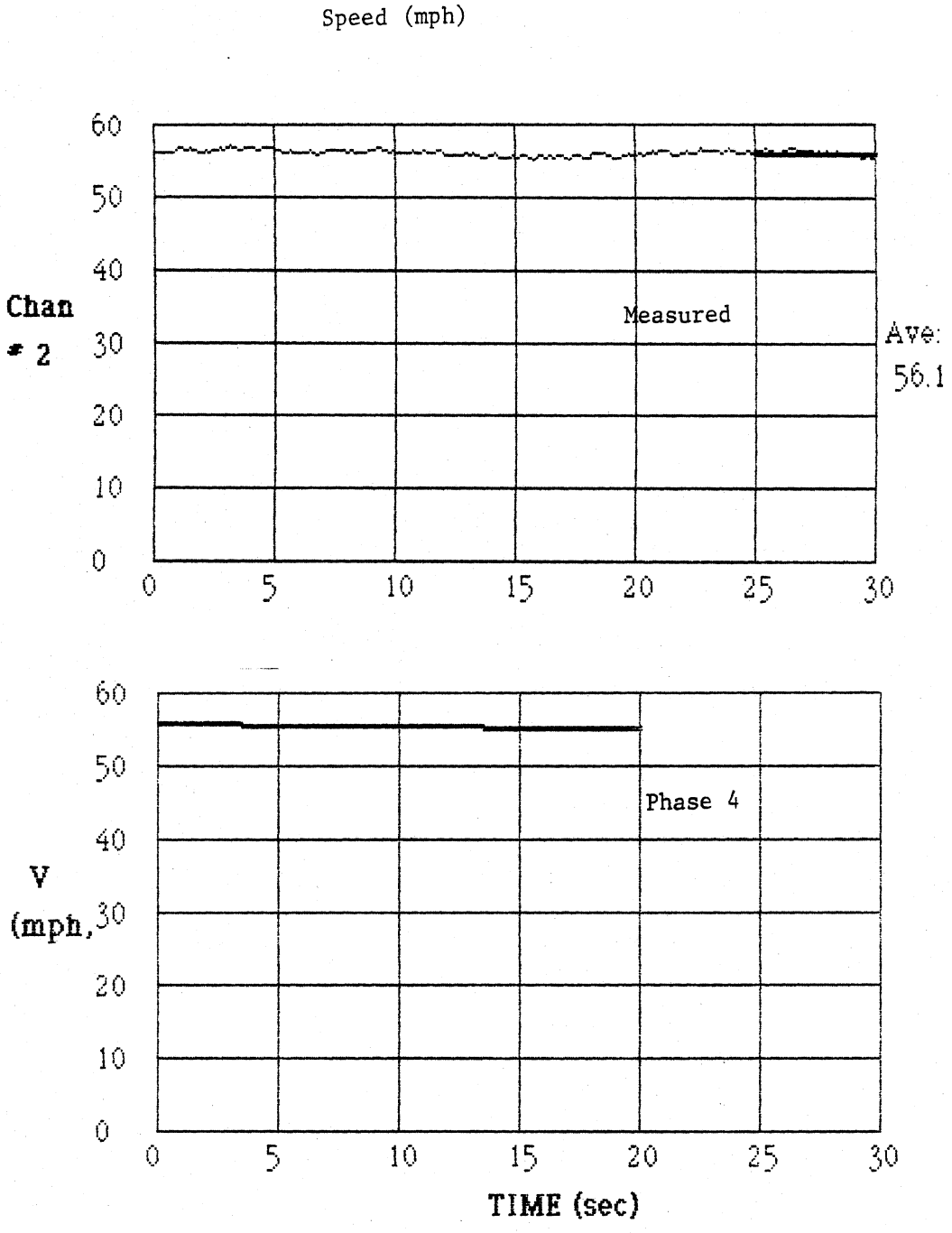

Figure 44. Phase 4 model/test comparisons; obstacle avoidance maneuver; vehicle A.

Lateral Acceleration (g's)

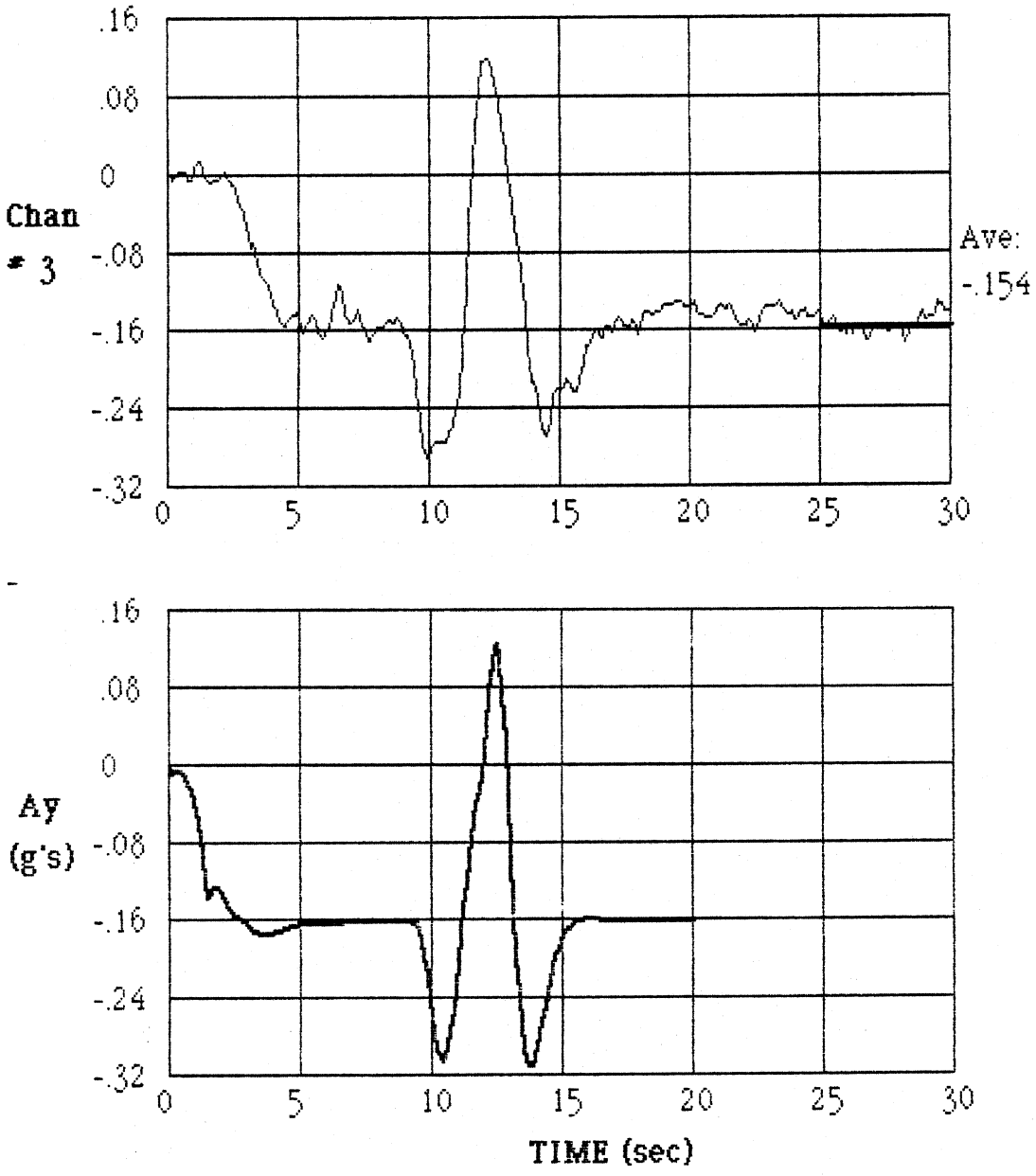

Figure 44 (cont)

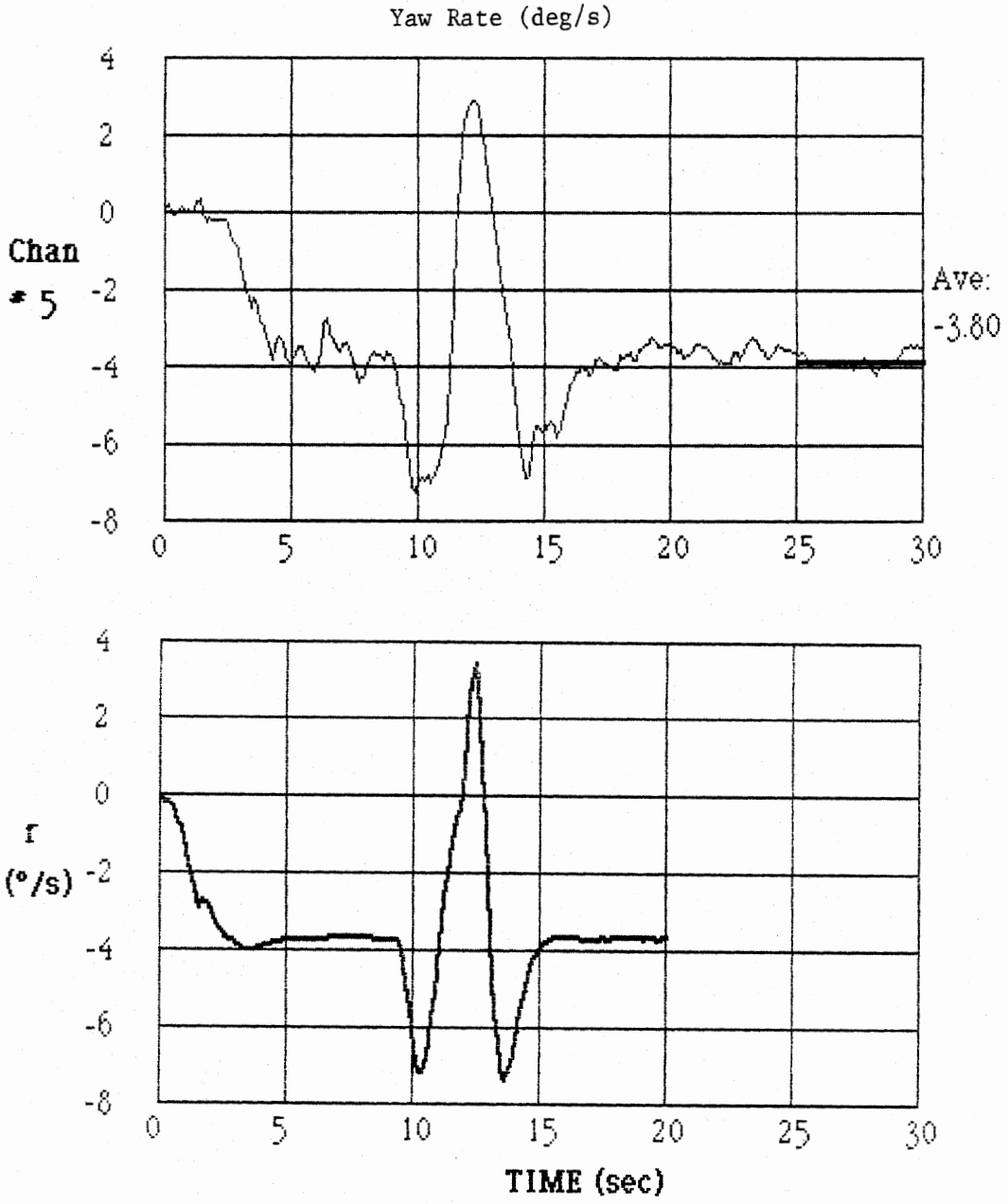

Figure 44 (cont)

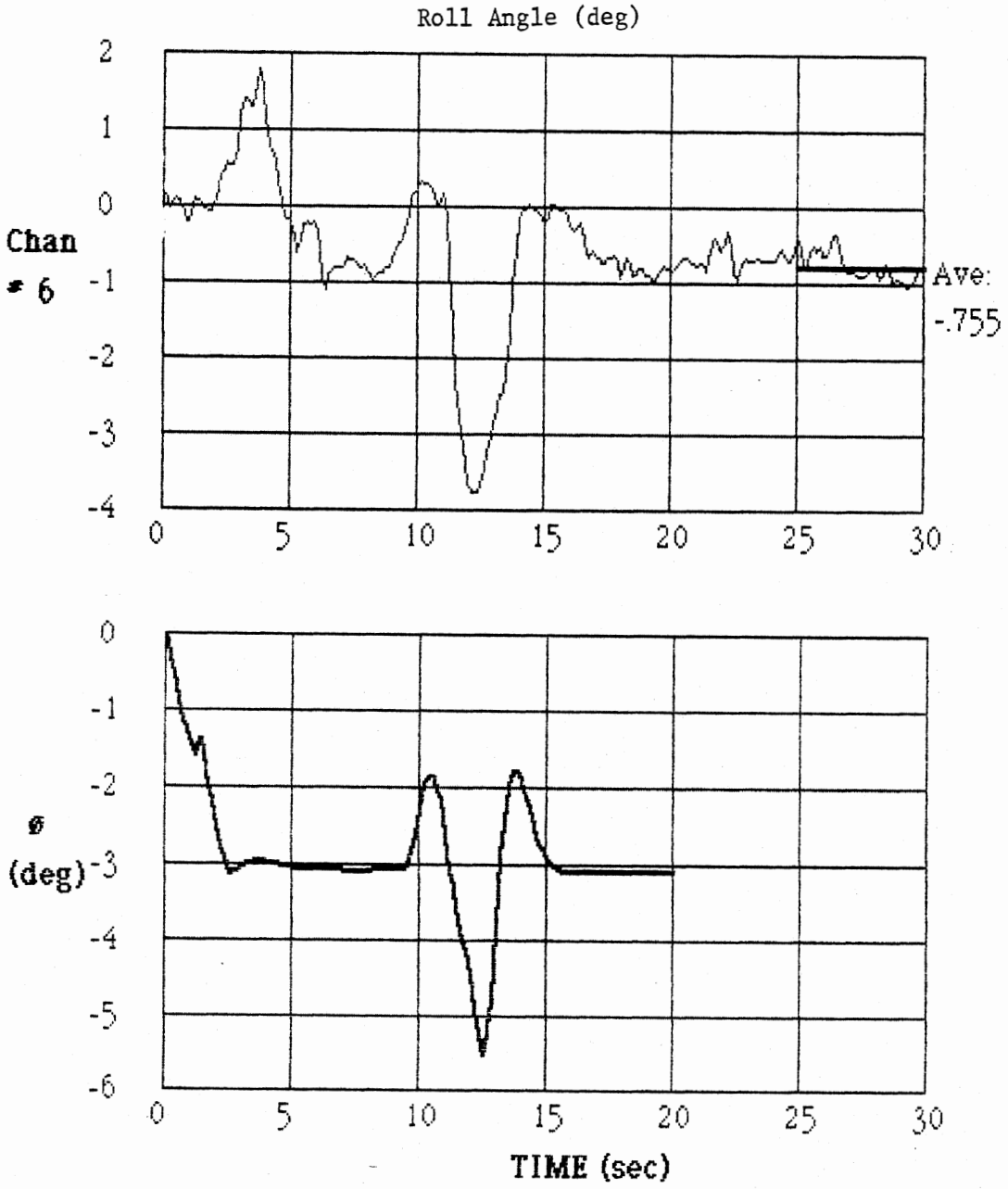

Figure 44 (cont)

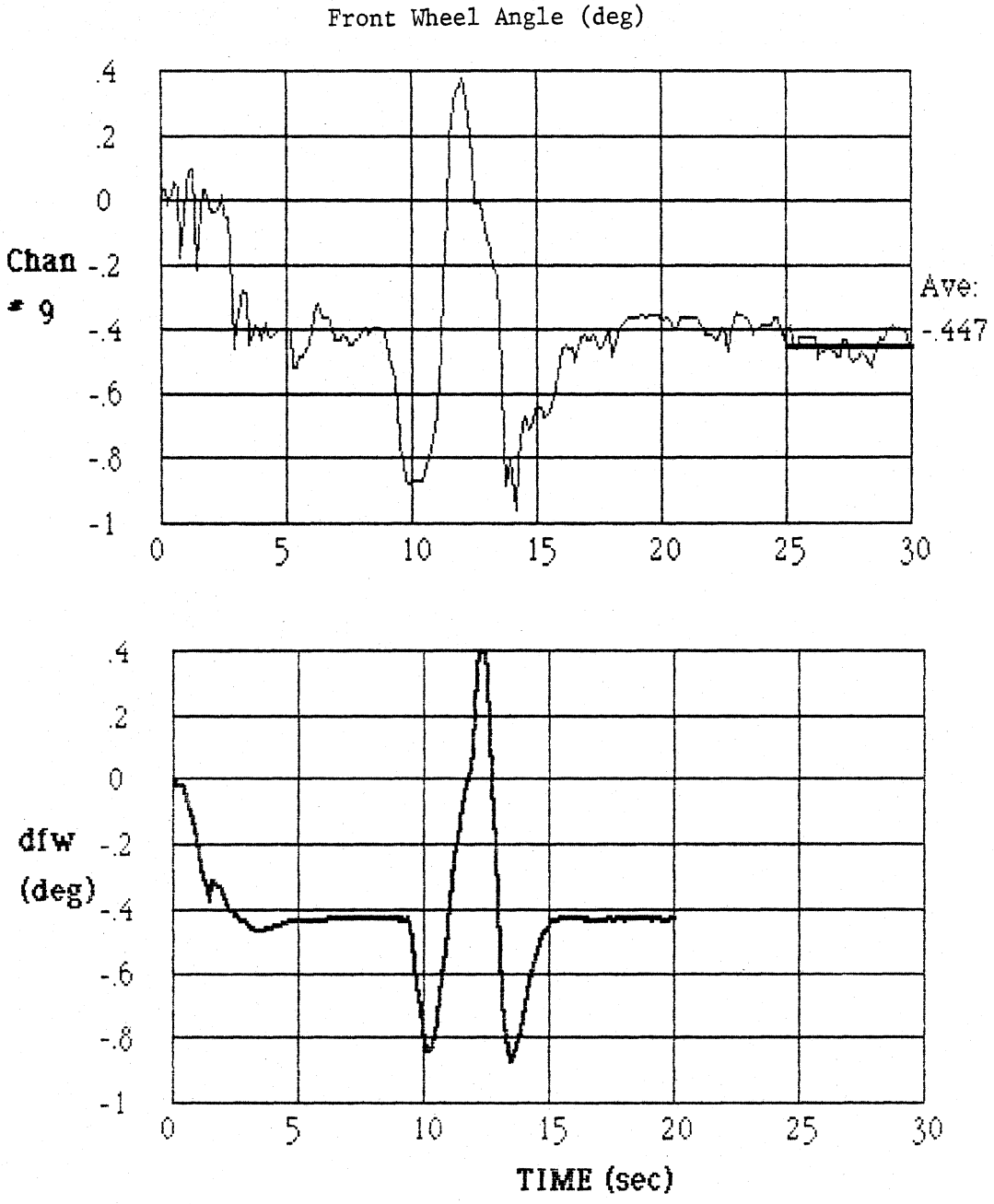

Figure 44 (cont)

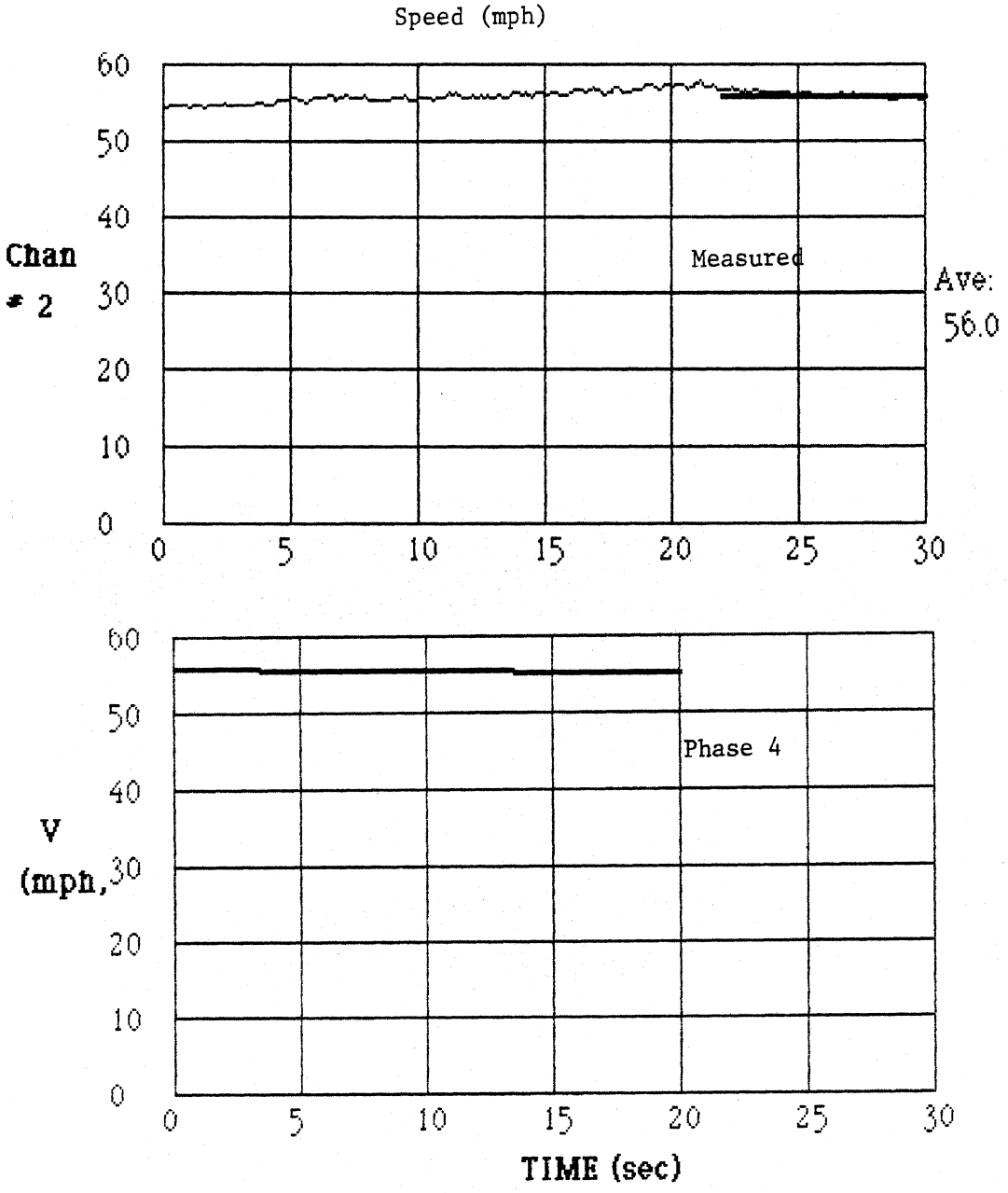

Figure 45. Phase 4 model/test comparisons; obstacle avoidance maneuver; vehicle B.

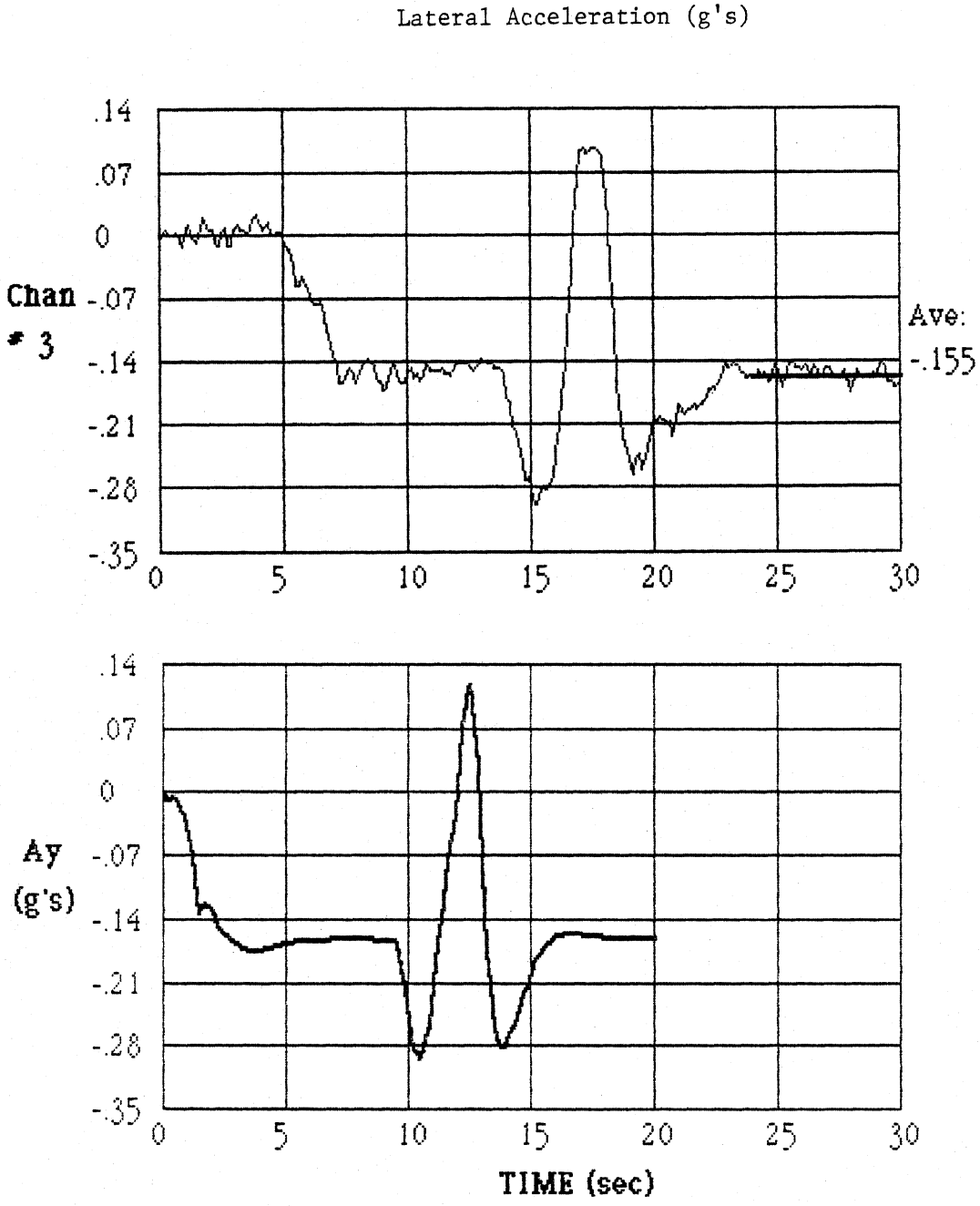

Figure 45 (cont)

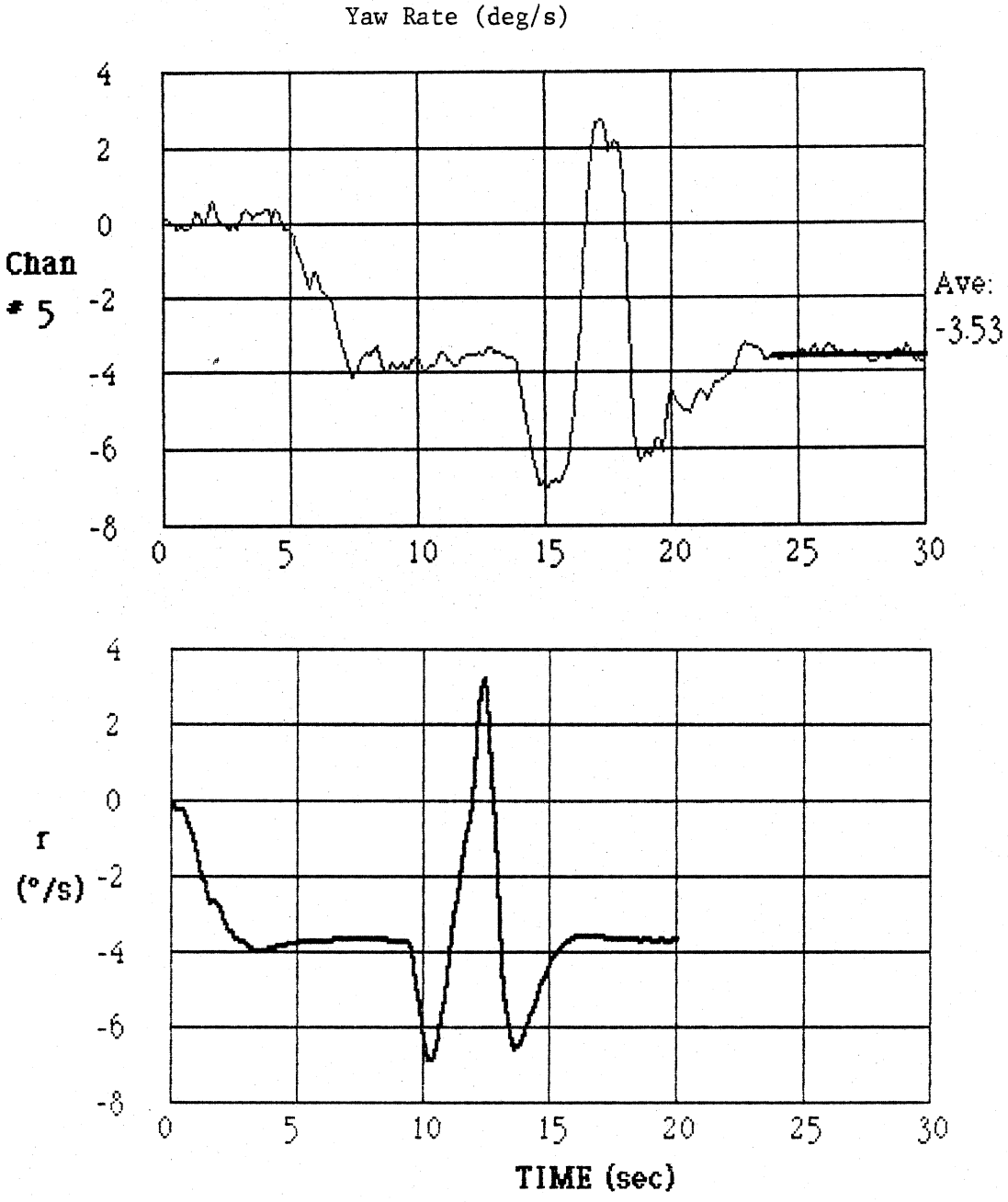

Figure 45 (cont)

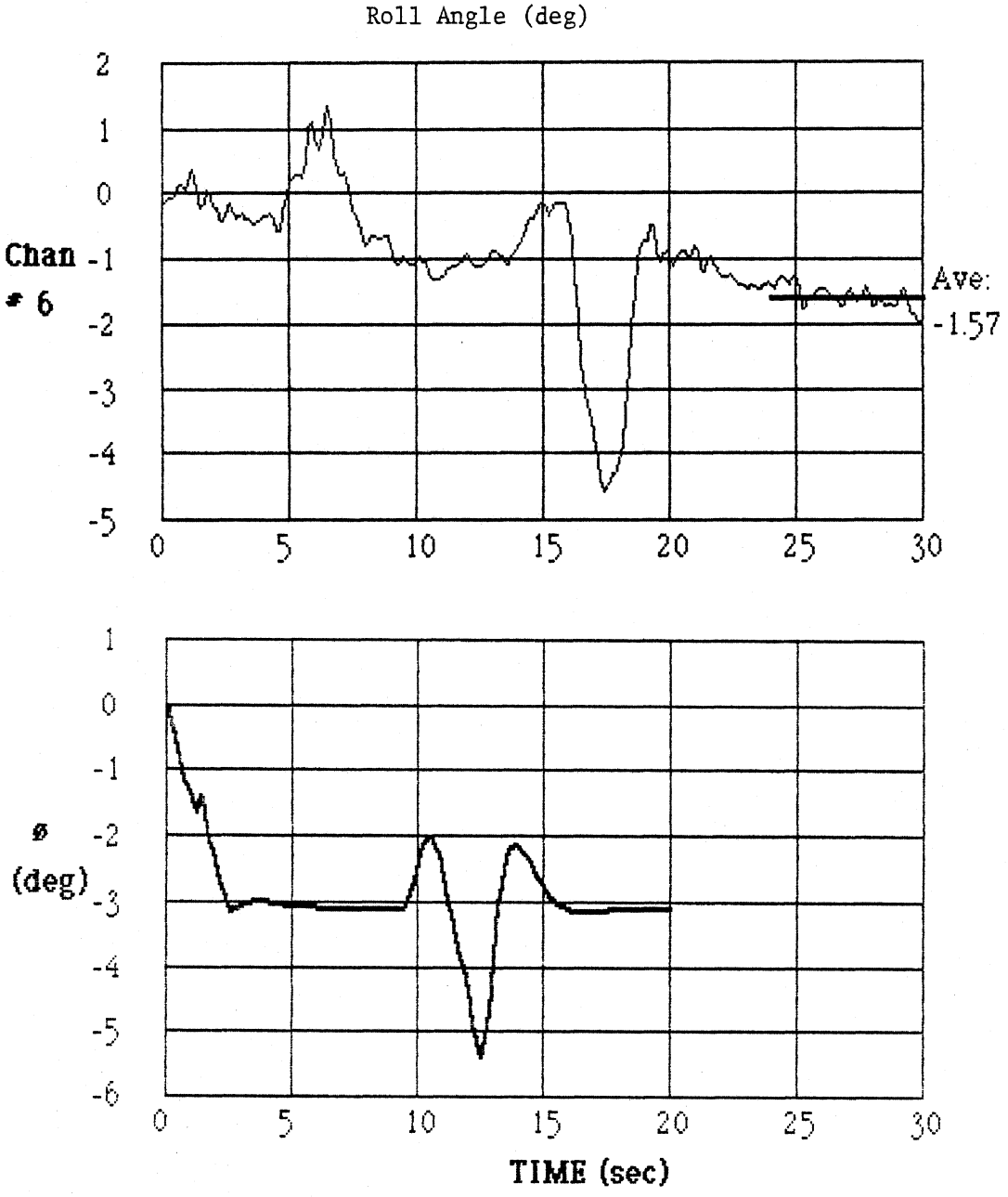

Figure 45 (cont)

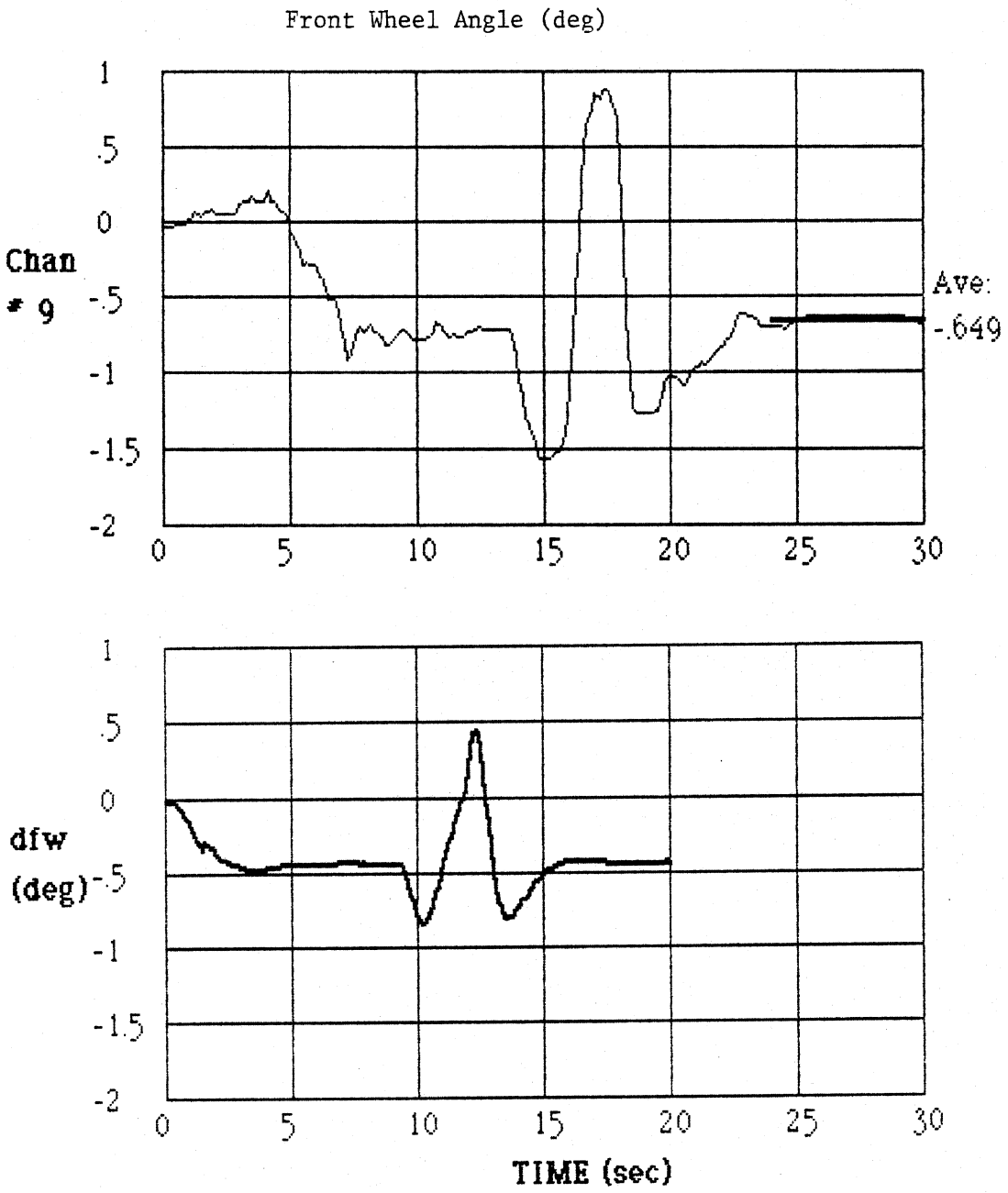

Figure 45 (cont)

Also, roll and steering gain discrepancies that were observed in the steady turning comparisons will, in general, also appear in these data as well. For example, the measured steering responses for passenger car B seen in figure 45 (obstacle avoidance maneuver), disagree to about the same extent in gain as that observed in the steady turning comparisons. Overall, the level of agreement seen in these comparisons is quite good.

5.3 Braking / Accelerating Comparisons

The example comparisons seen in Figures 46 through 48 are for braking and accelerating along a superelevated curve. Figure 46 corresponds to the tractor - semitrailer; figure 47 to passenger car A; and figure 48 to passenger car B. Curve 1 is the site at which the test results seen here were collected. The simulation runs are similar to the ones performed for the obstacle avoidance maneuvers except that braking and acceleration levels, similar to those seen in the test data, were selected. Curve negotiation (without a lane-to-lane movement) is provided by the driver model. Again, the general quality of most responses predicted by the simulation agree with the vehicle measurements. The steering predictions are more variable, partly because of more active steering behavior by the driver in the tractor-semitrailer tests, and partly because of strong bounce-steer interactions seen in the vehicle A measurement. The steering angle transducer was mounted on vehicle A in such a manner that significant vertical movement of the sprung mass (as occurs during braking) would produce a negative steering indication. Hence, the "unusual" (not actual) steering measurement seen occurring during deceleration in the vehicle A data. The braking / accelerating runs also suggest that the model representation has too little understeer. This observation can be seen in the degree to which steering levels differ prior to and following braking. A vehicle with little or no understeer requires approximately the same amount of steering to track a given radius at different speeds (similar to what is observed in the simulation). The test data, however, display greater variations in steering requirements as the vehicle speeds change. Aside from this, the majority of comparisons are very favorable and suggest that the Phase 4 model can be used to accurately represent nominal driver / vehicle responses along superelevated highway curves.

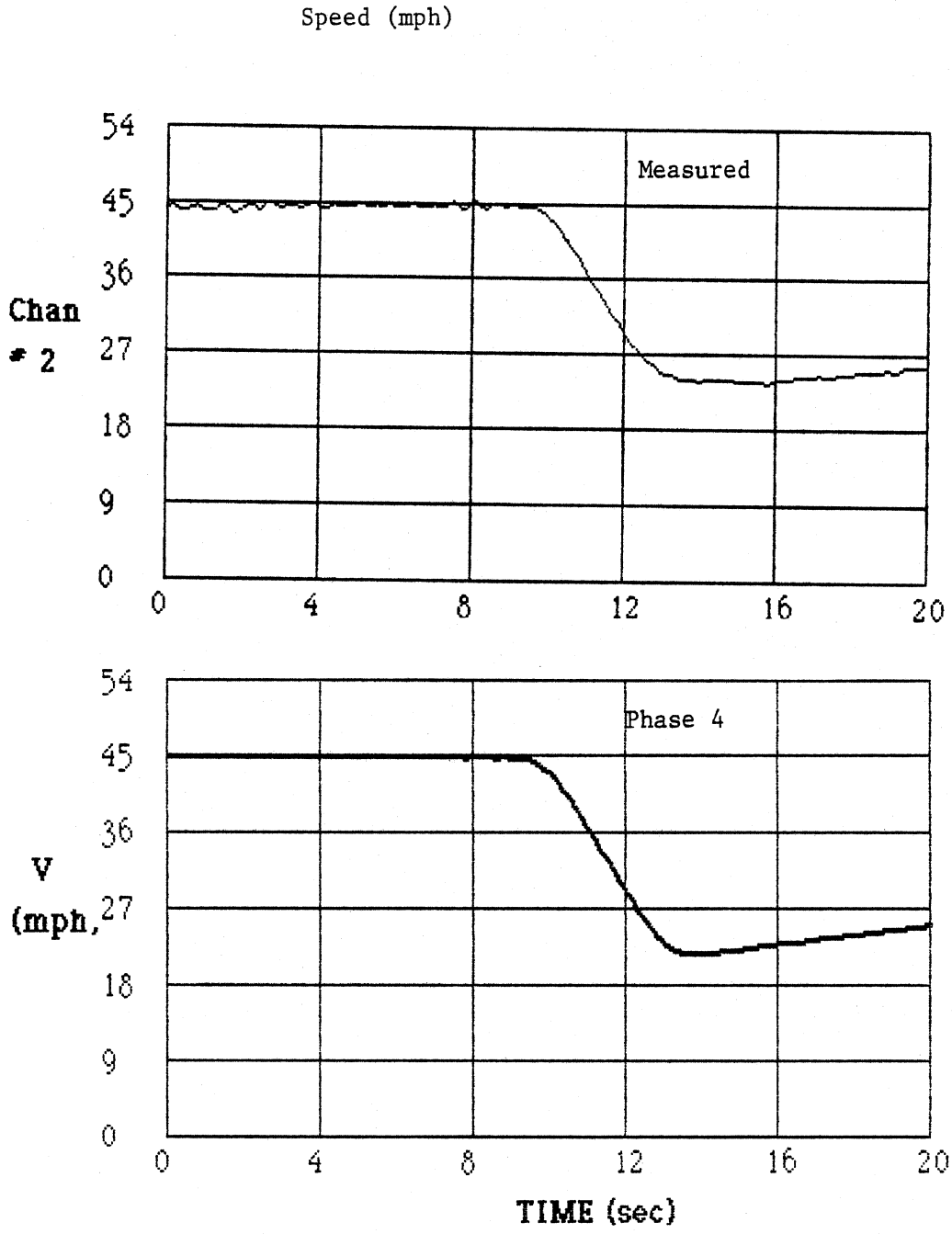

Figure 46. Phase 4 model/test comparisons; braking/accelerating maneuver; vehicle C.

Lateral Acceleration (g's)

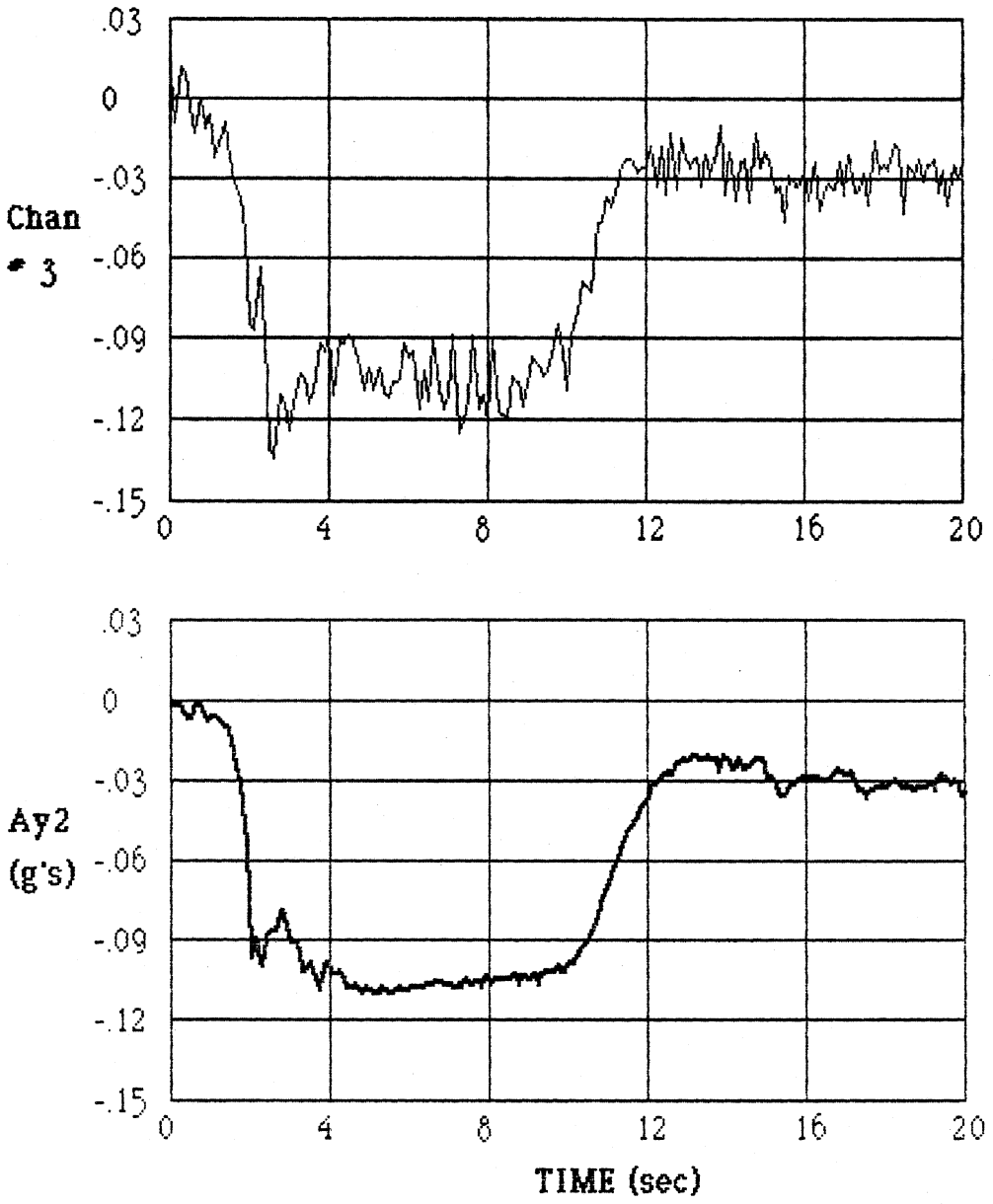

Figure 46 (cont)

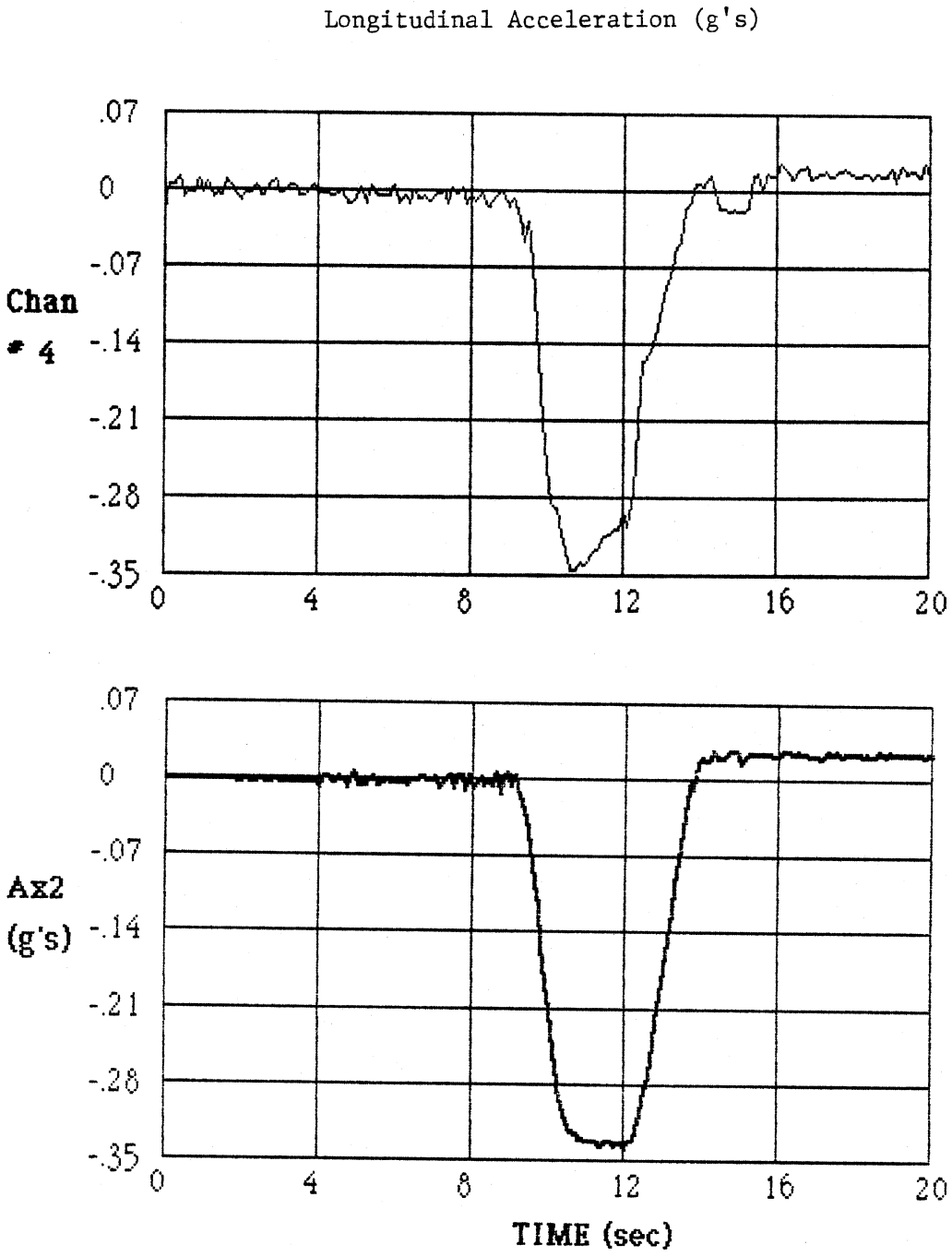

Figure 46 (cont)

Trailer Yaw Rate (deg/s)

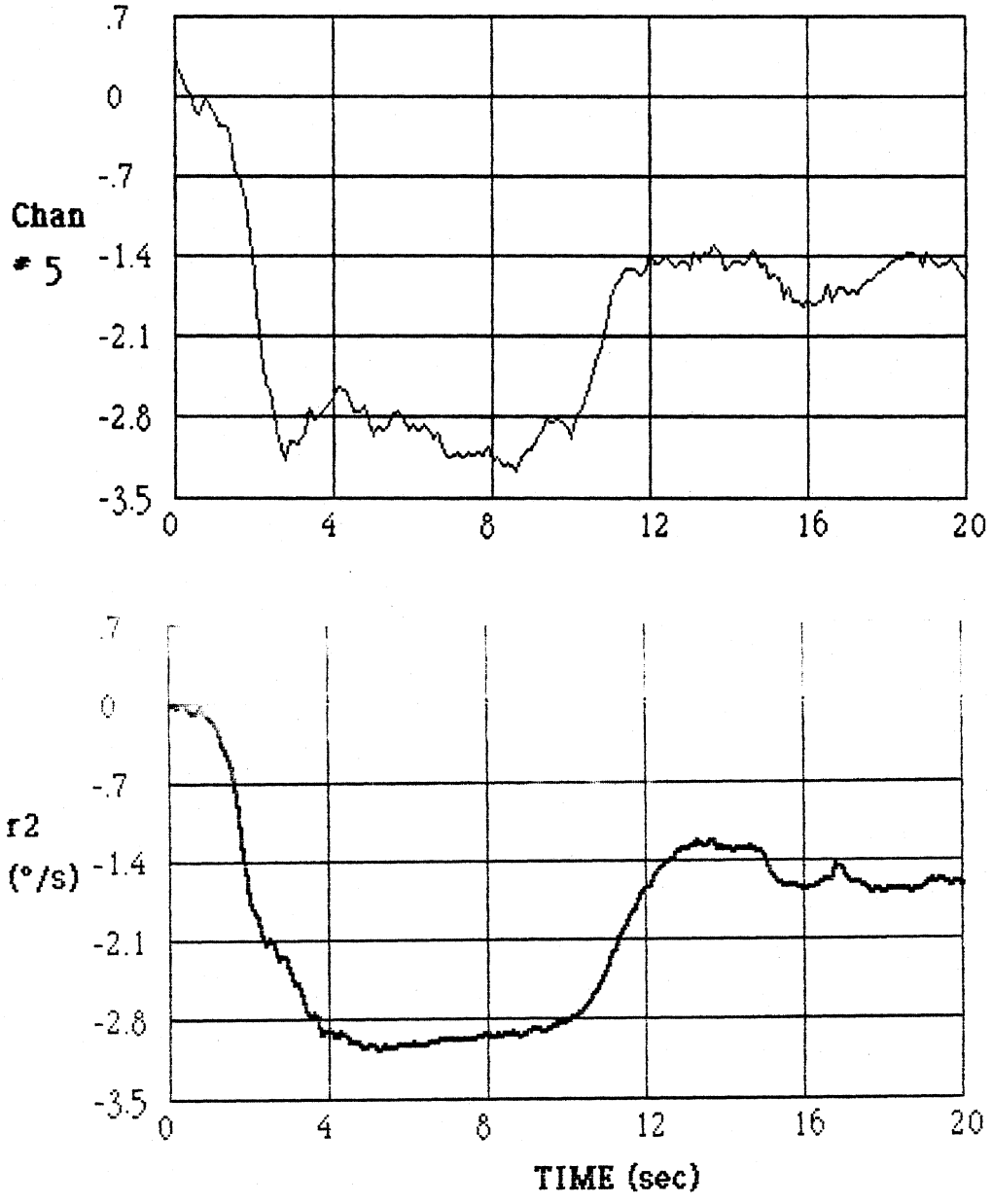

Figure 46 (cont)

Trailer Roll Angle (deg)

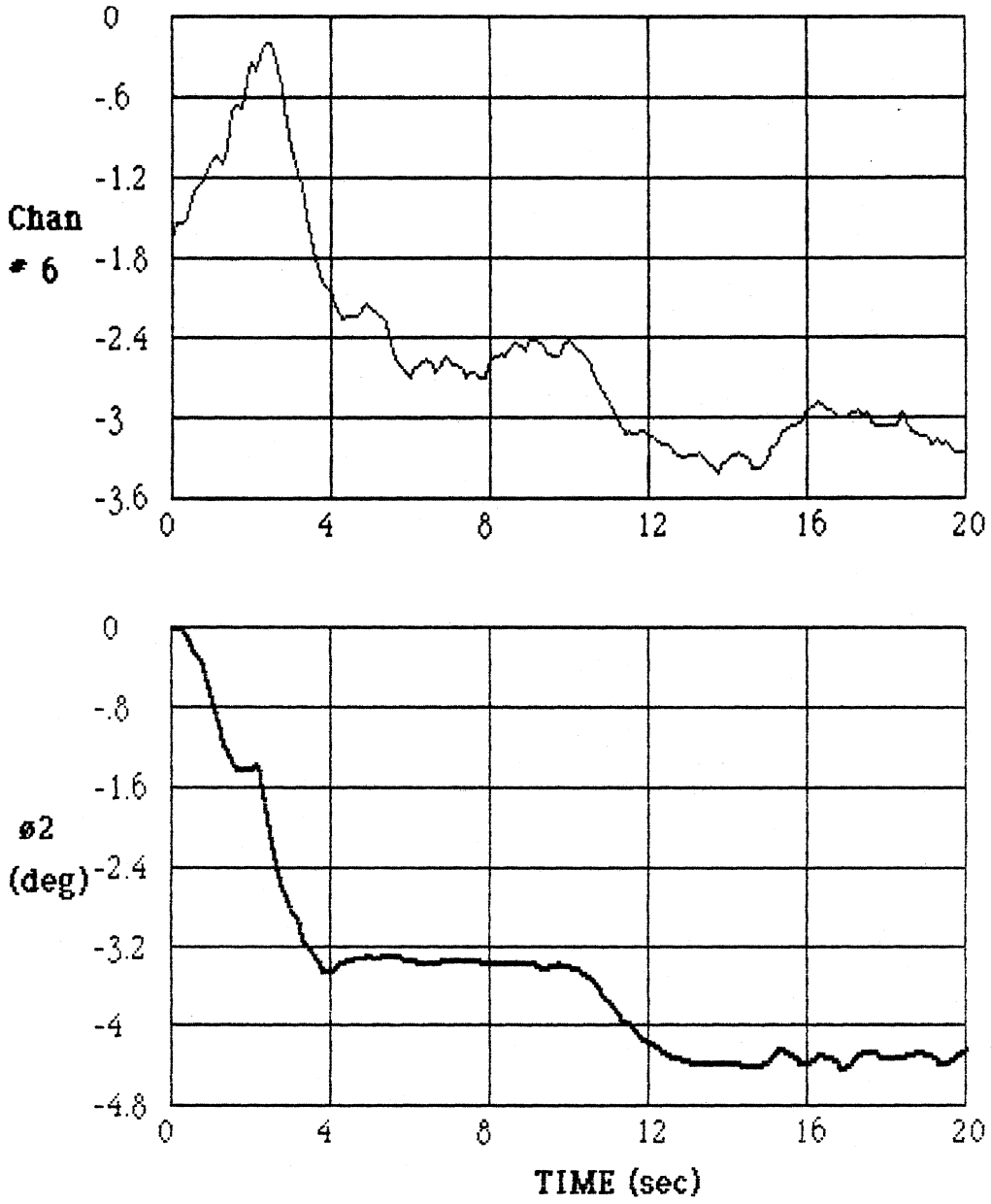

Figure 46 (cont)

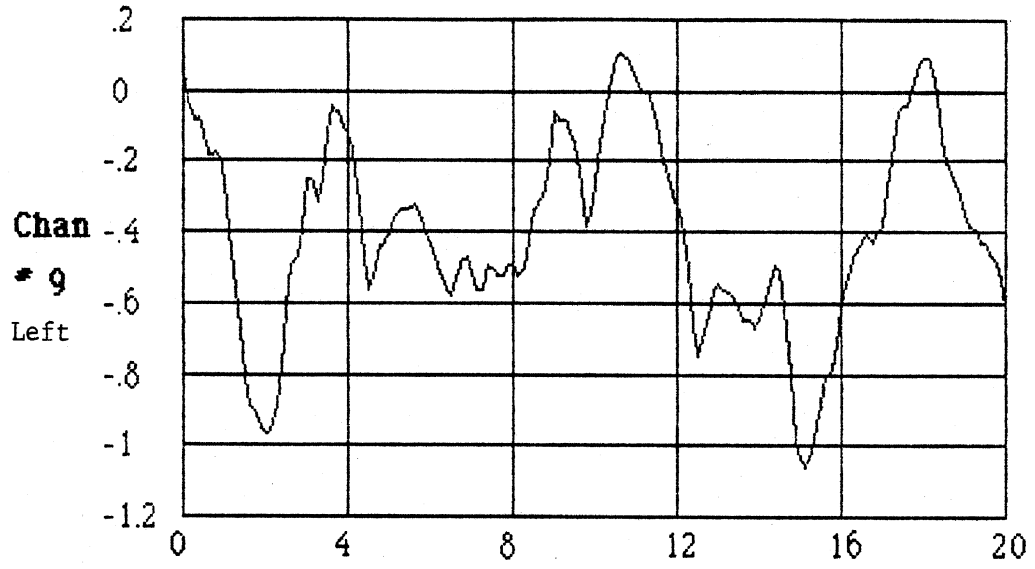

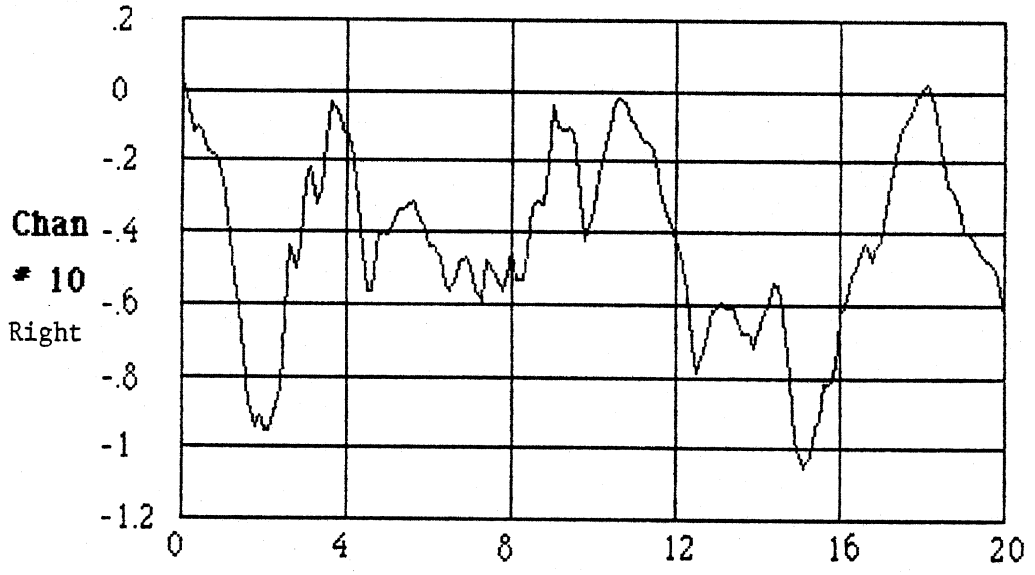

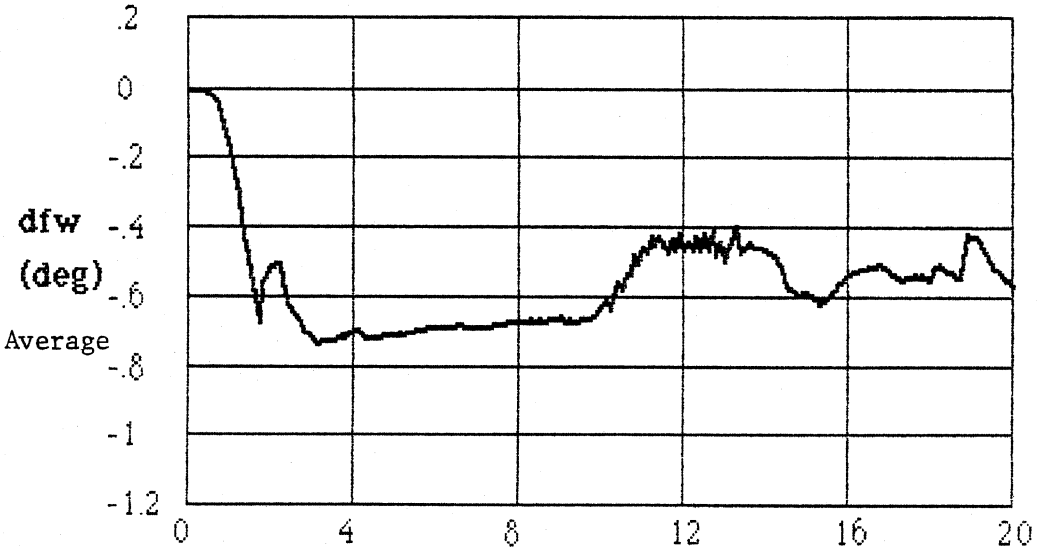

Figure 46 (cont)

Articulation Angle (deg)

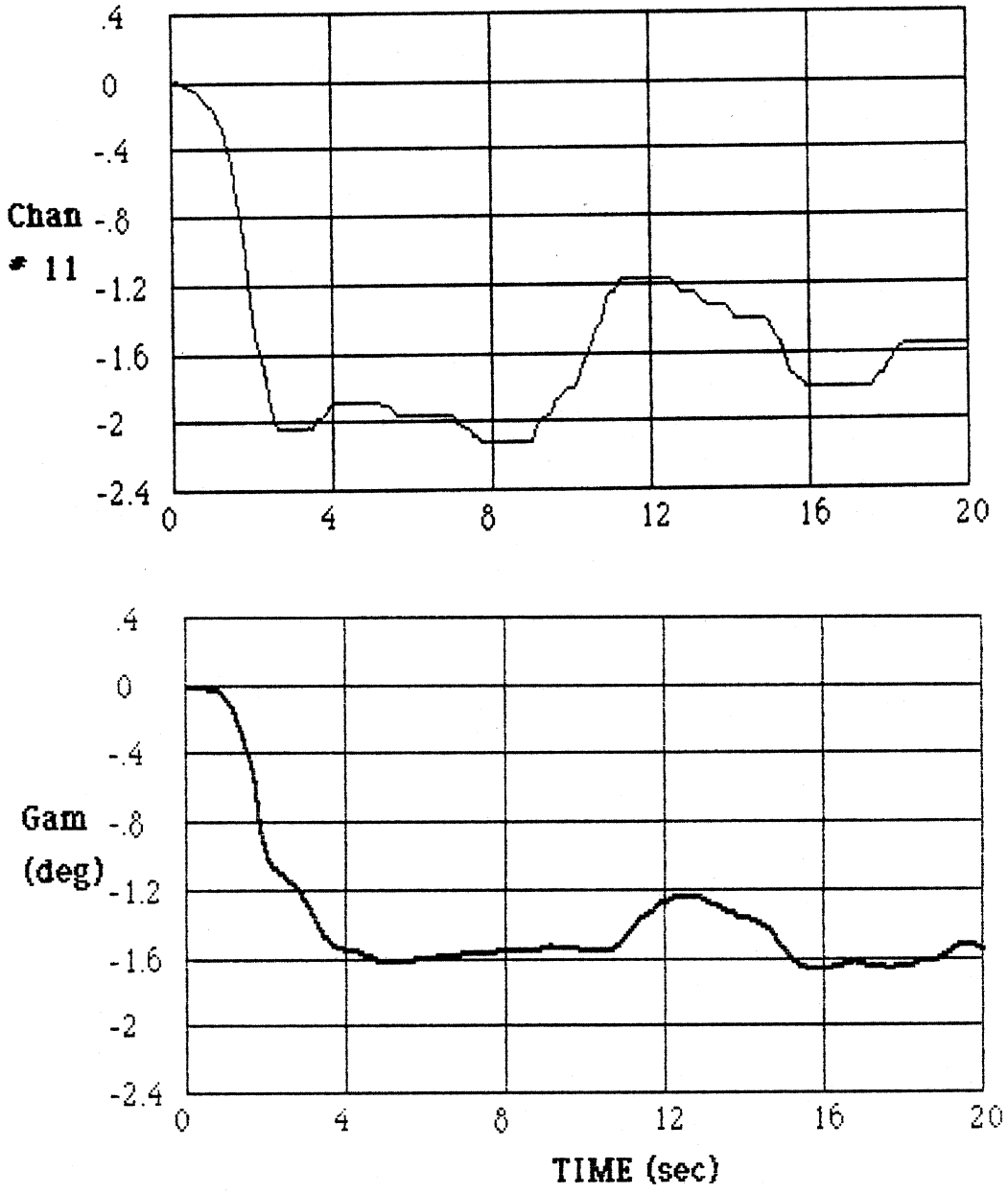

Figure 46 (cont)

Tractor Yaw Rate (deg/s)

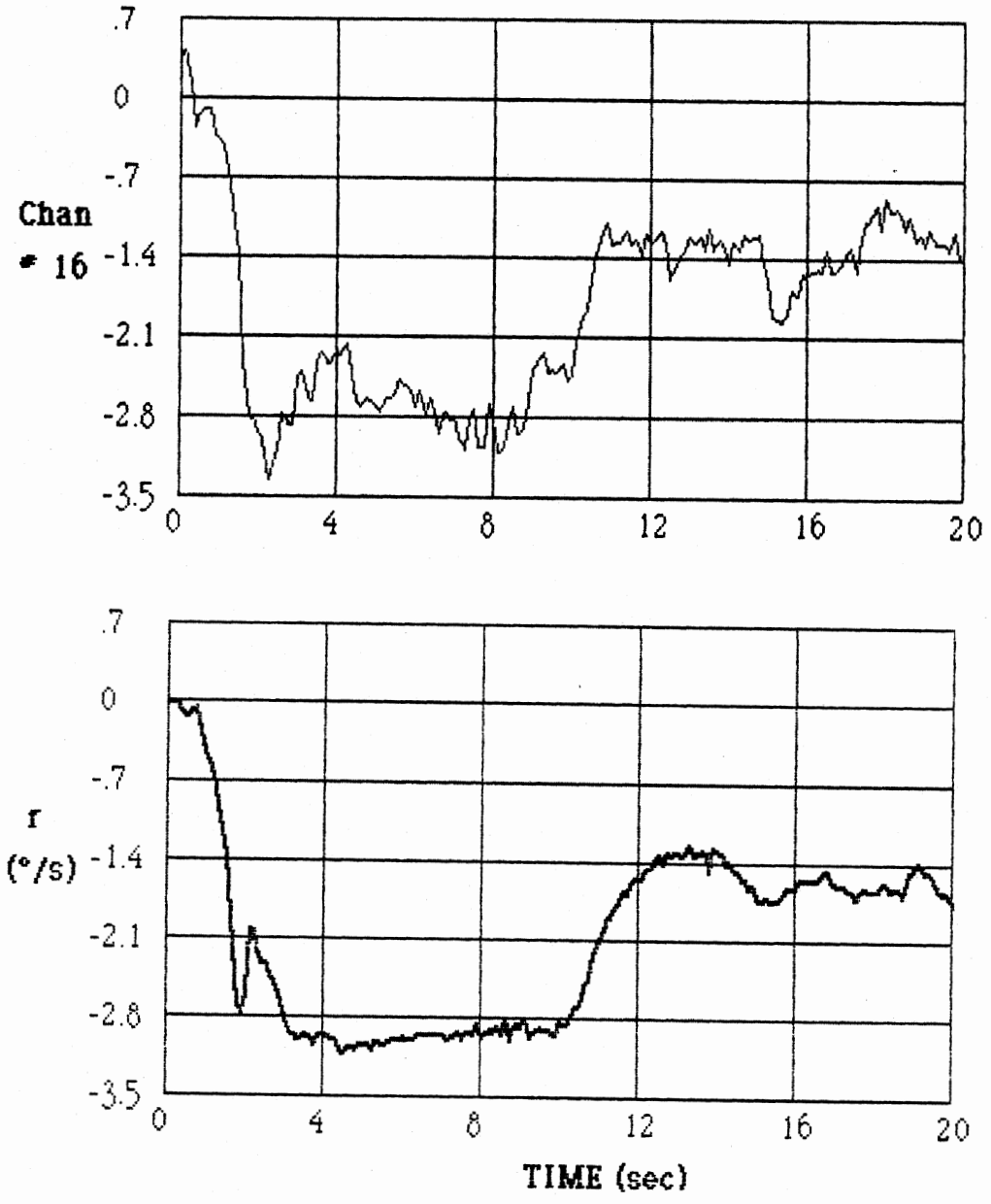

Figure 46 (cont)

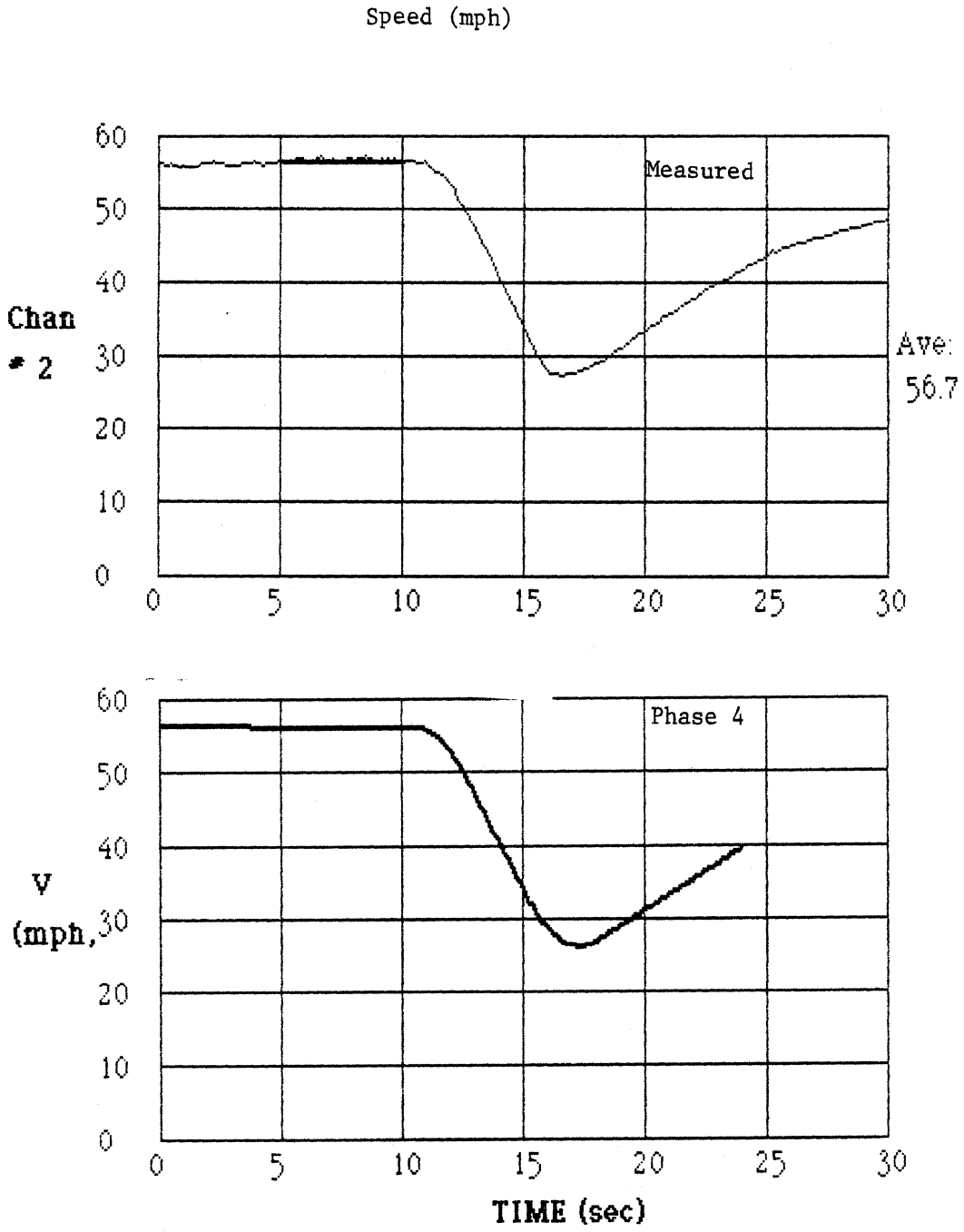

Figure 47. Phase 4 model/test comparisons; braking/accelerating maneuver; vehicle A.

Lateral Acceleration (g's)

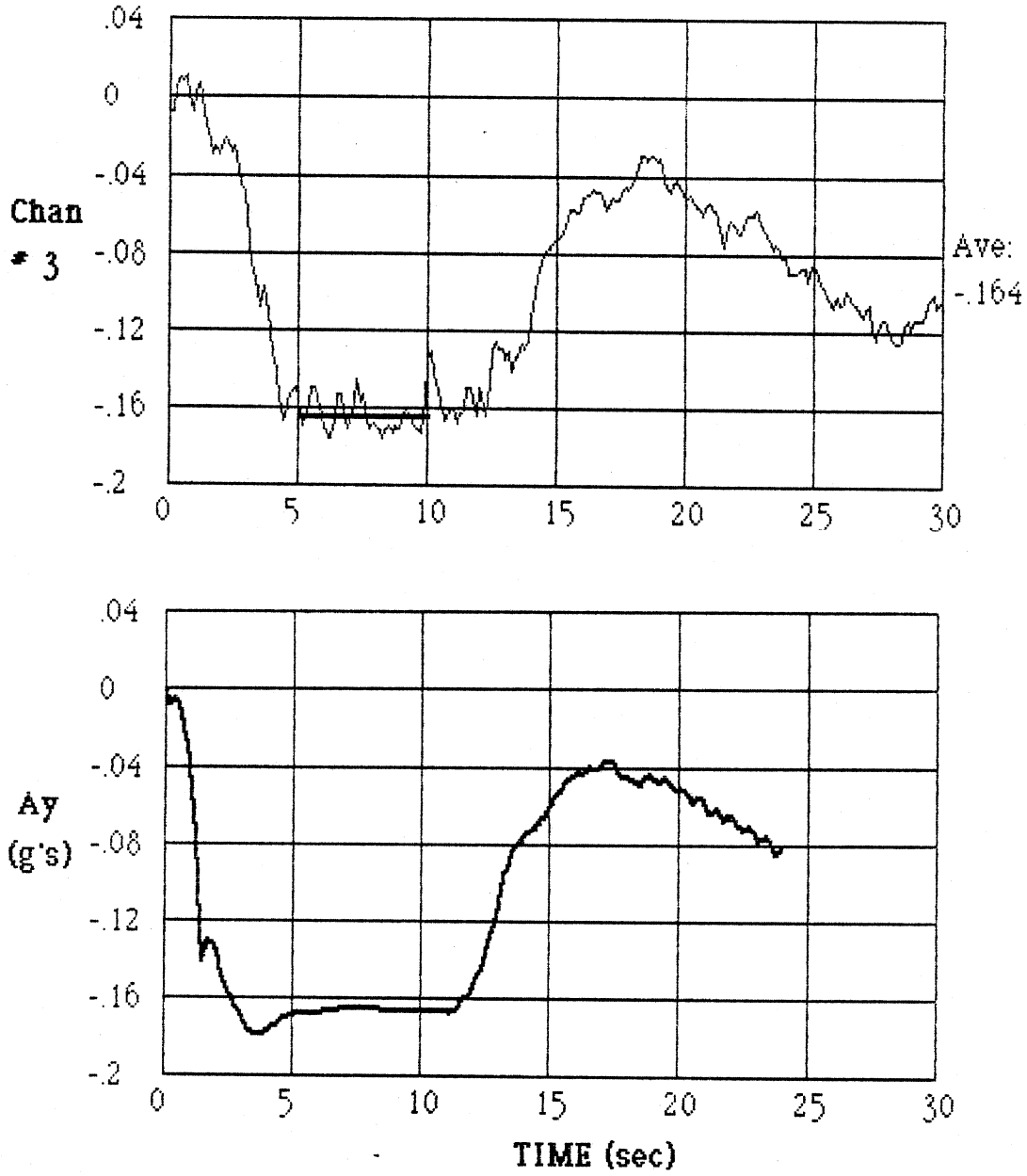

Figure 47 (cont)

Longitudinal Acceleration (g's)

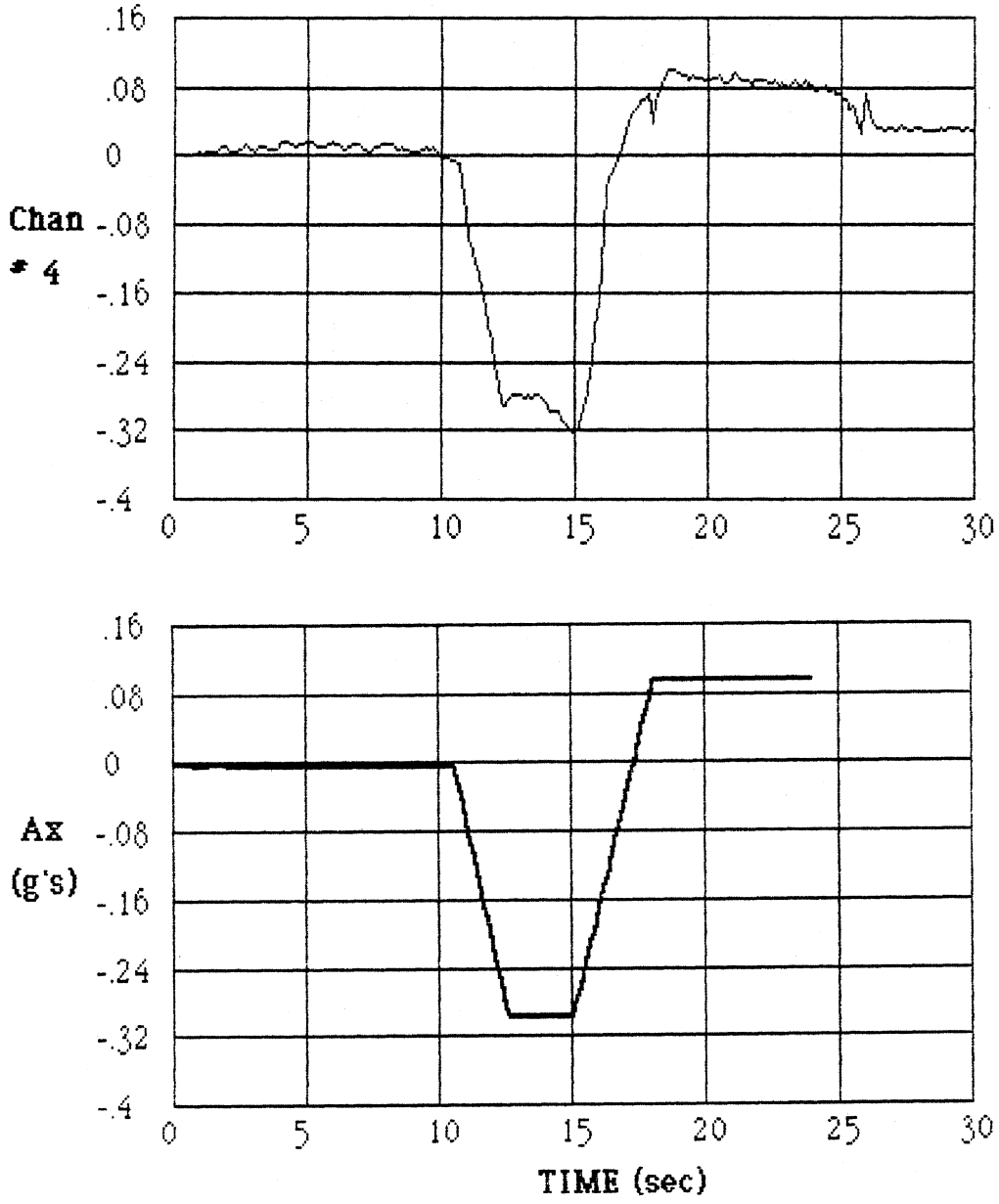

Figure 47 (cont)

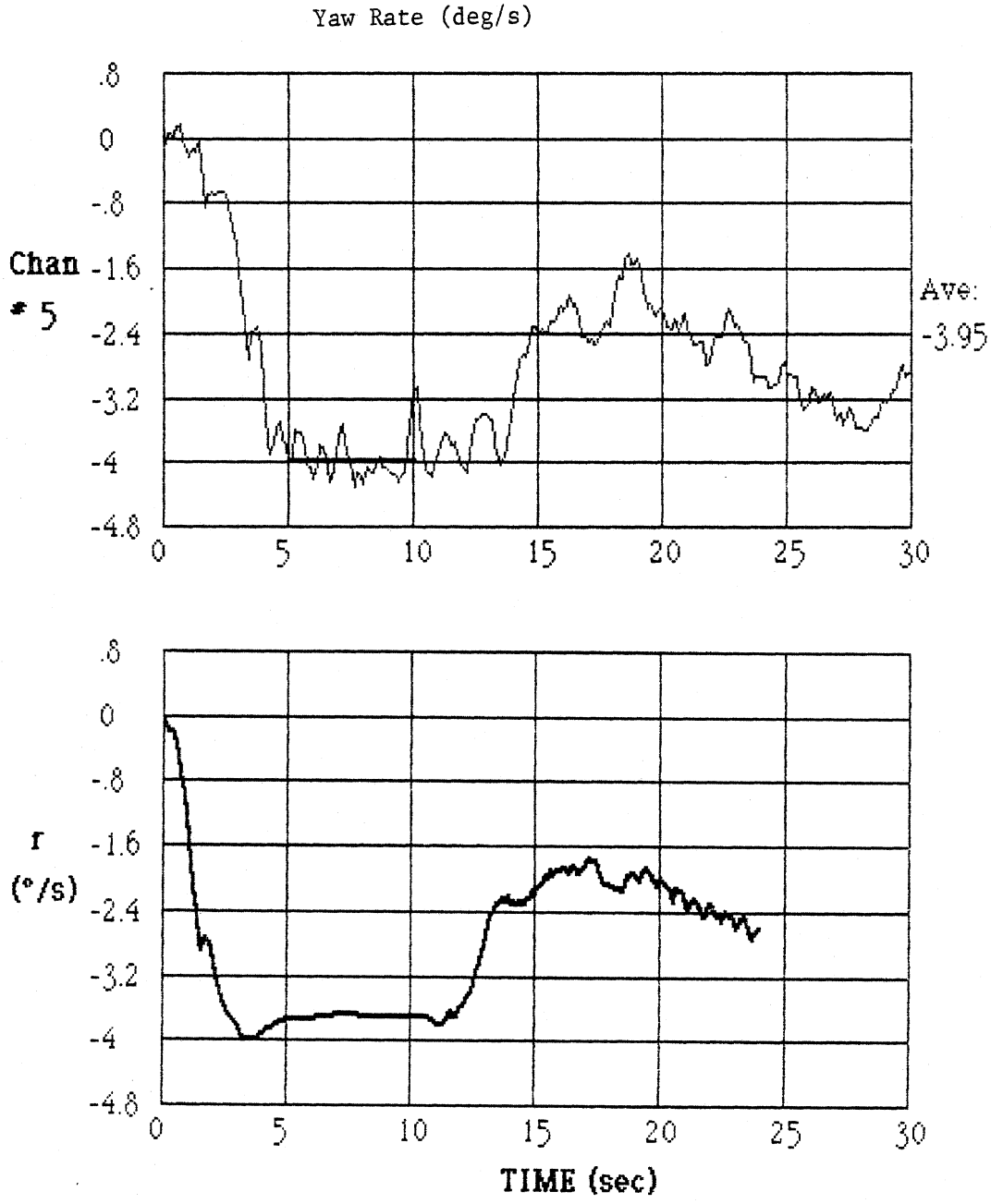

Figure 47 (cont)

Roll Angle (deg)

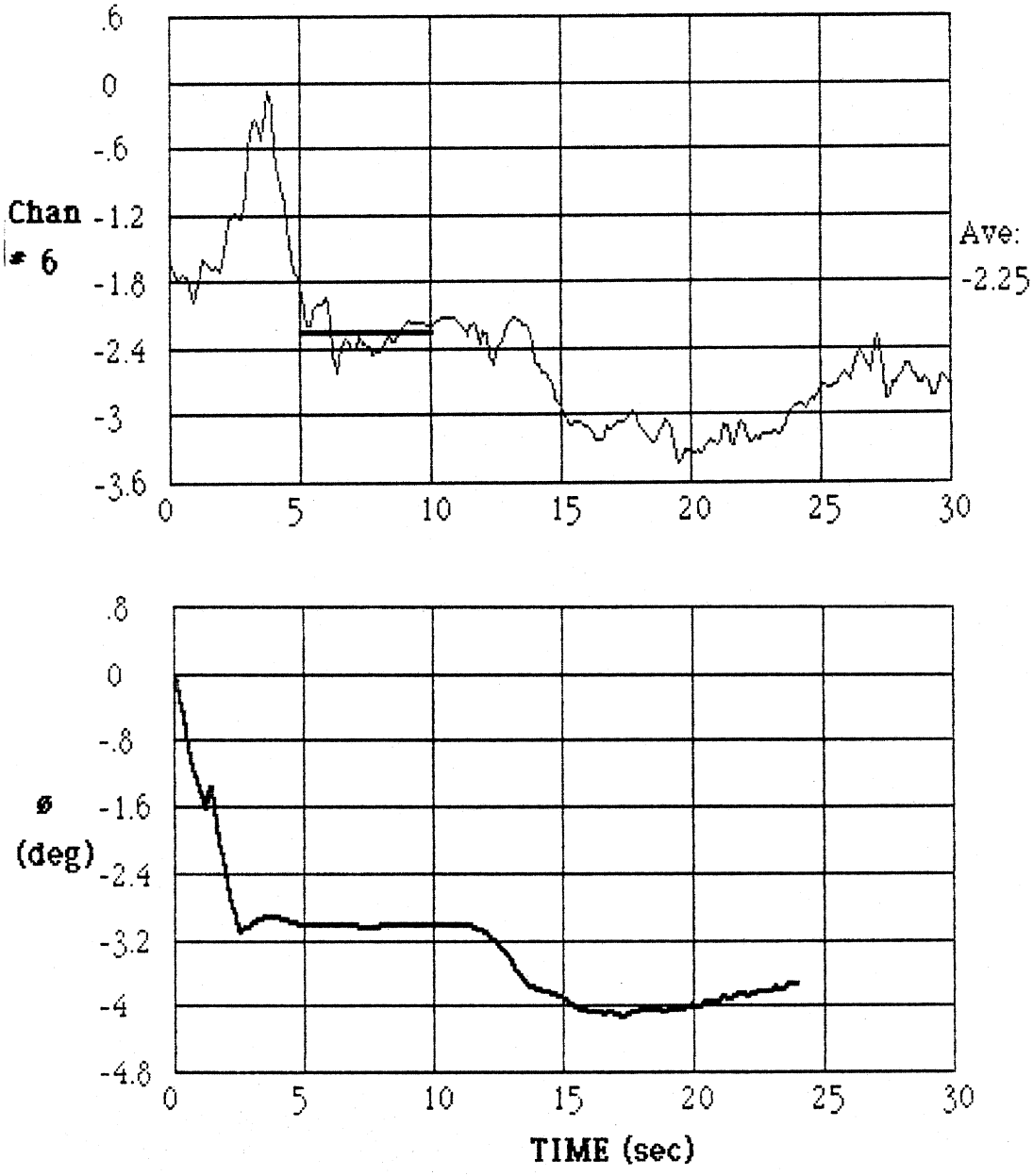

Figure 47 (cont)

Front Wheel Angle (deg)

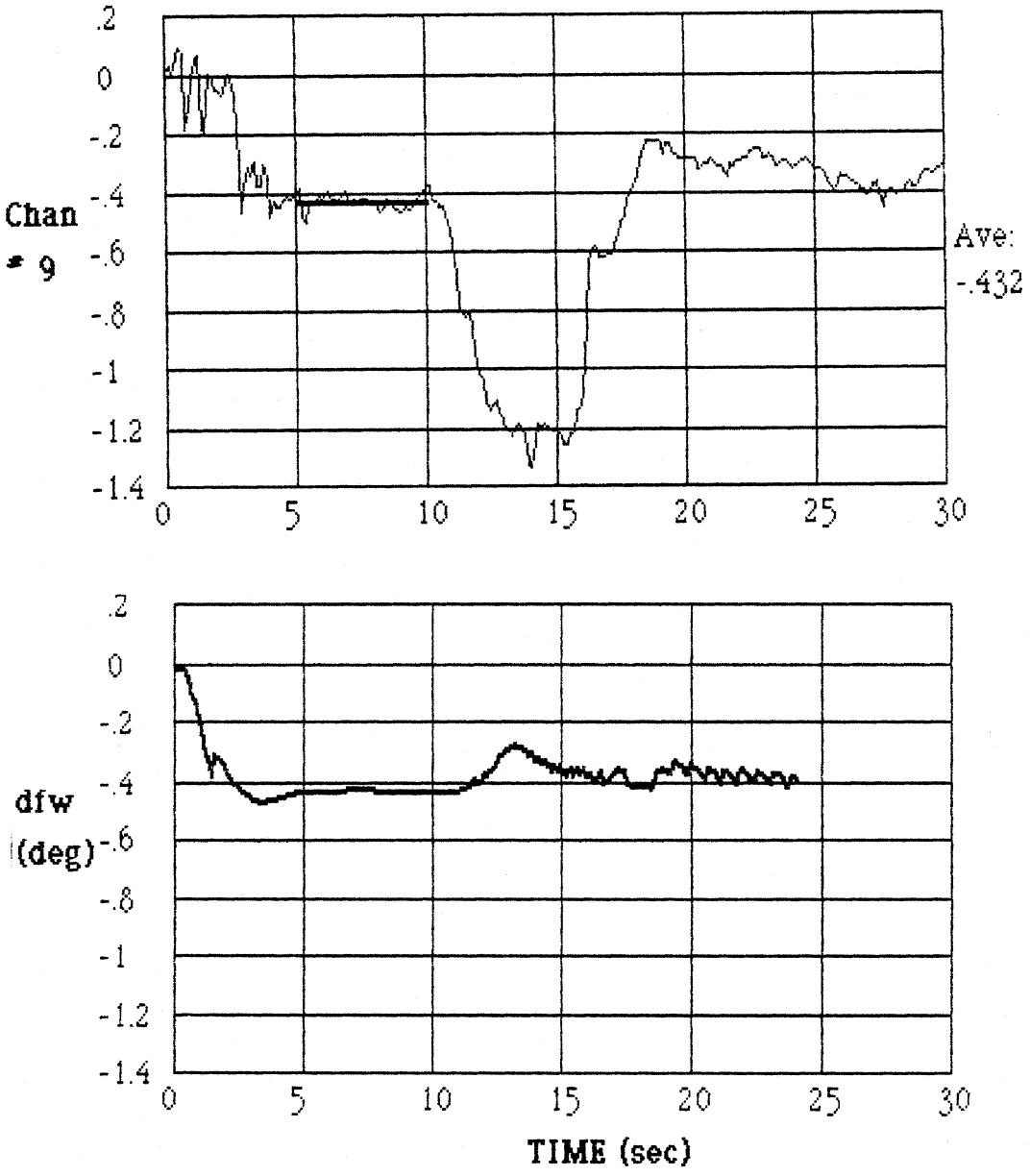

Figure 47 (cont)

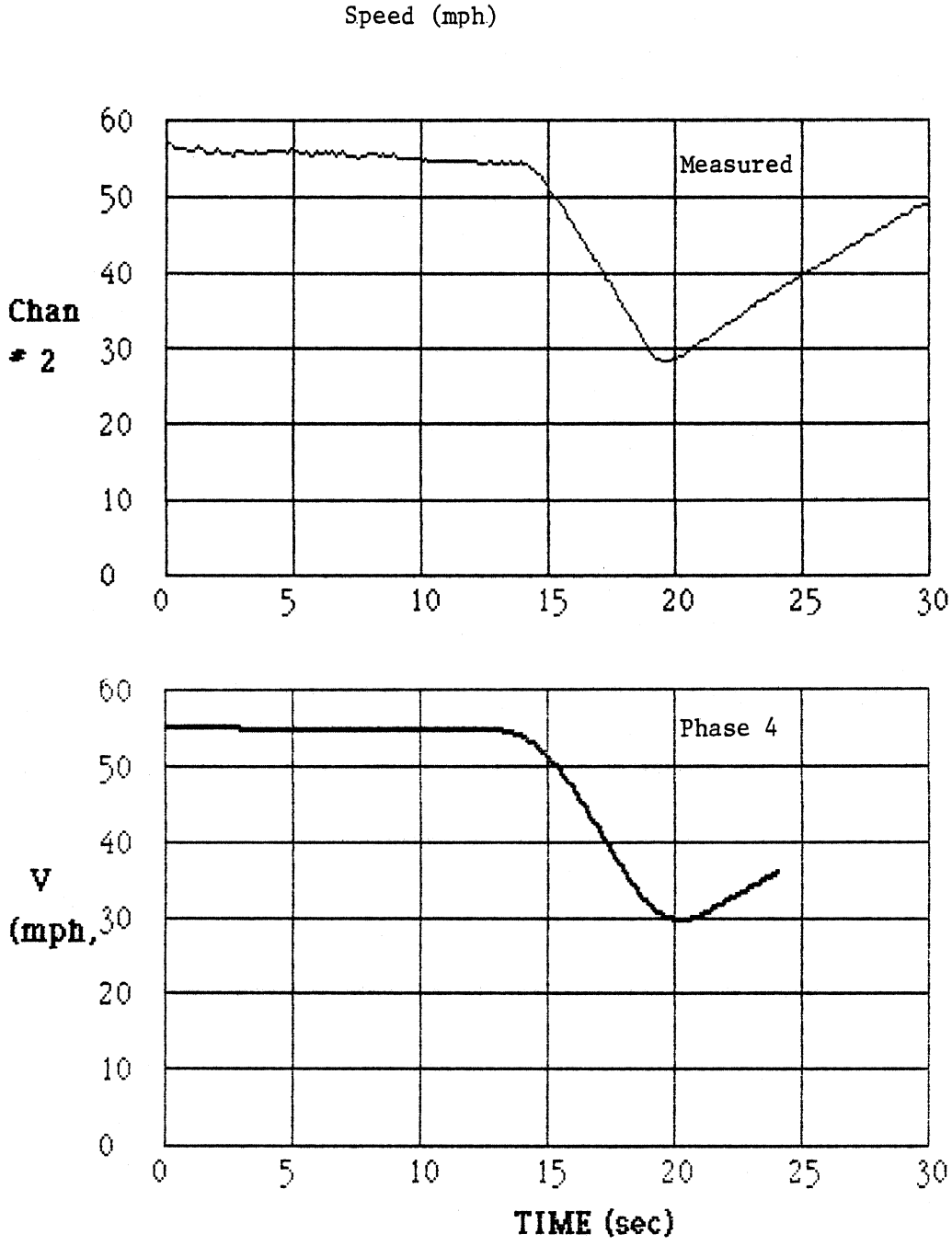

Figure 48. Phase 4 model/test comparisons; braking/accelerating maneuver; vehicle B.

Lateral Acceleration (g's)

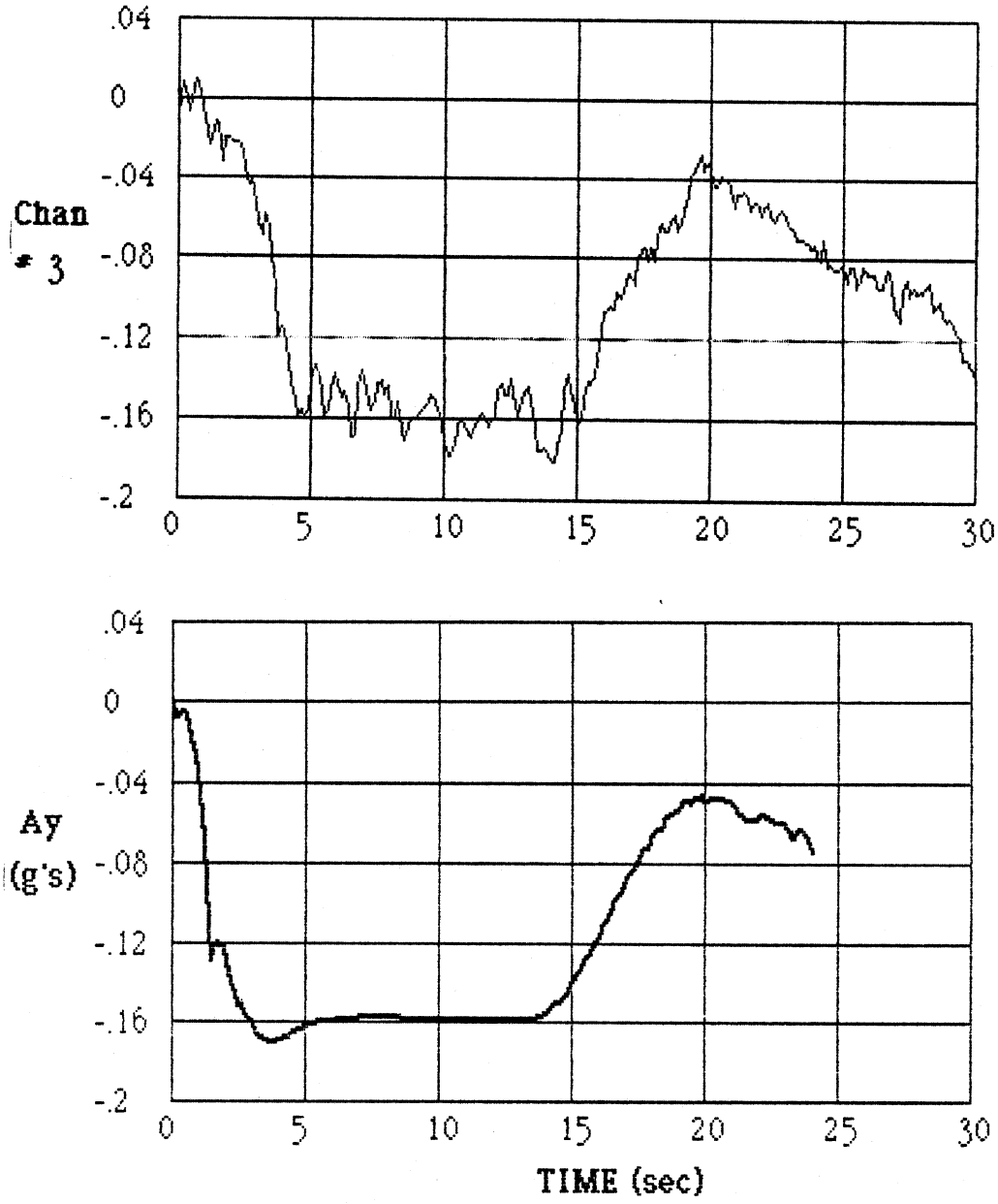

Figure 48 (cont)

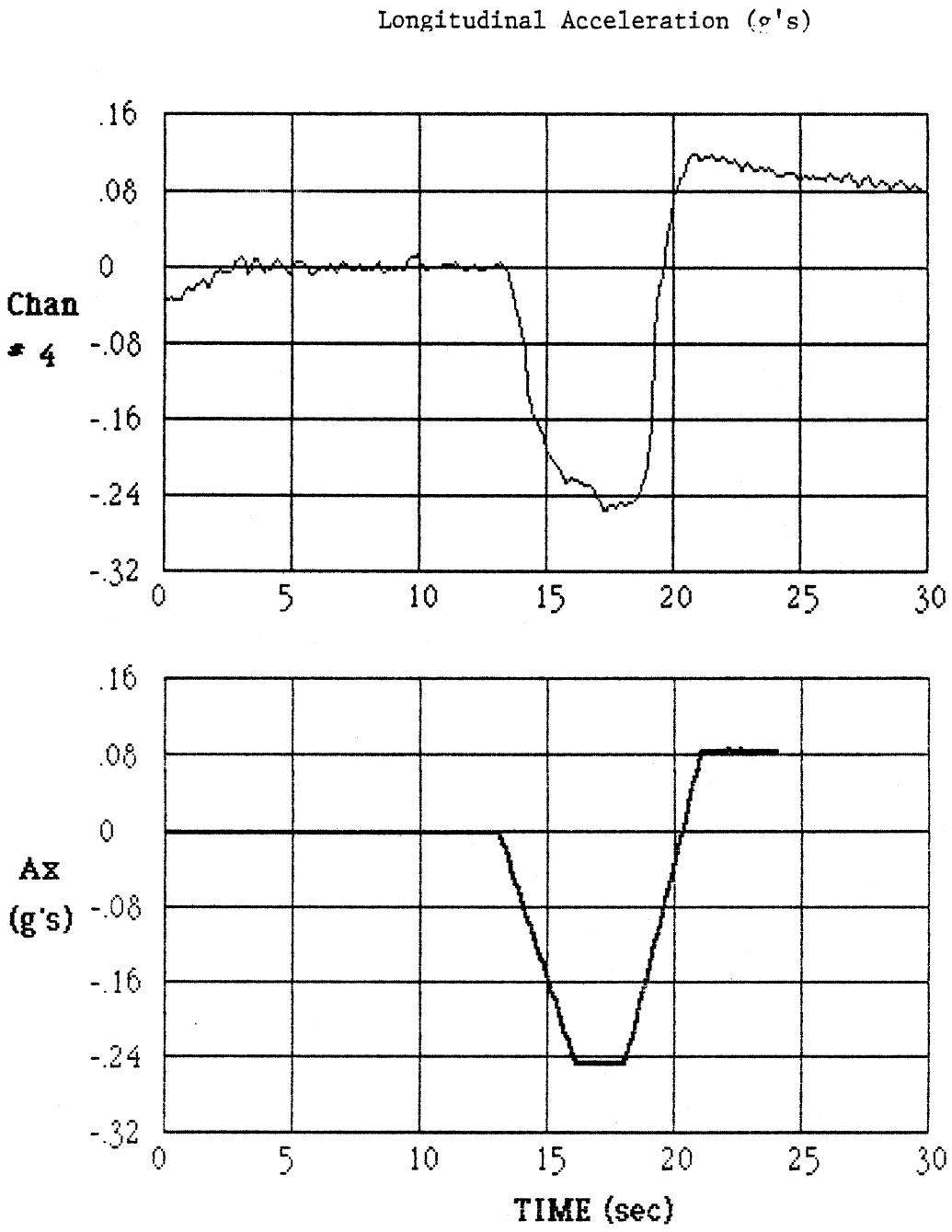

Figure 48 (cont)

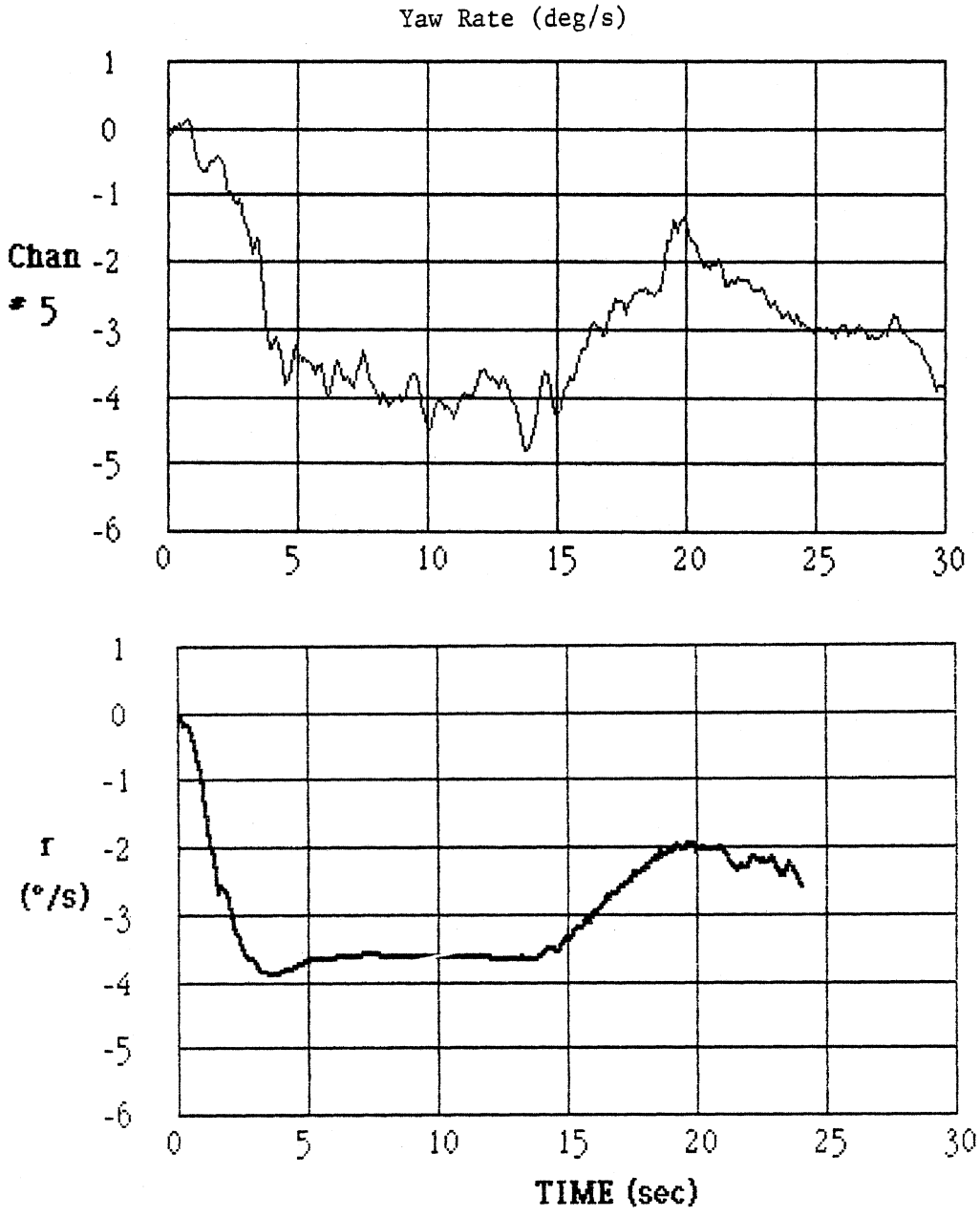

Figure 48 (cont)

Roll Angle (deg)

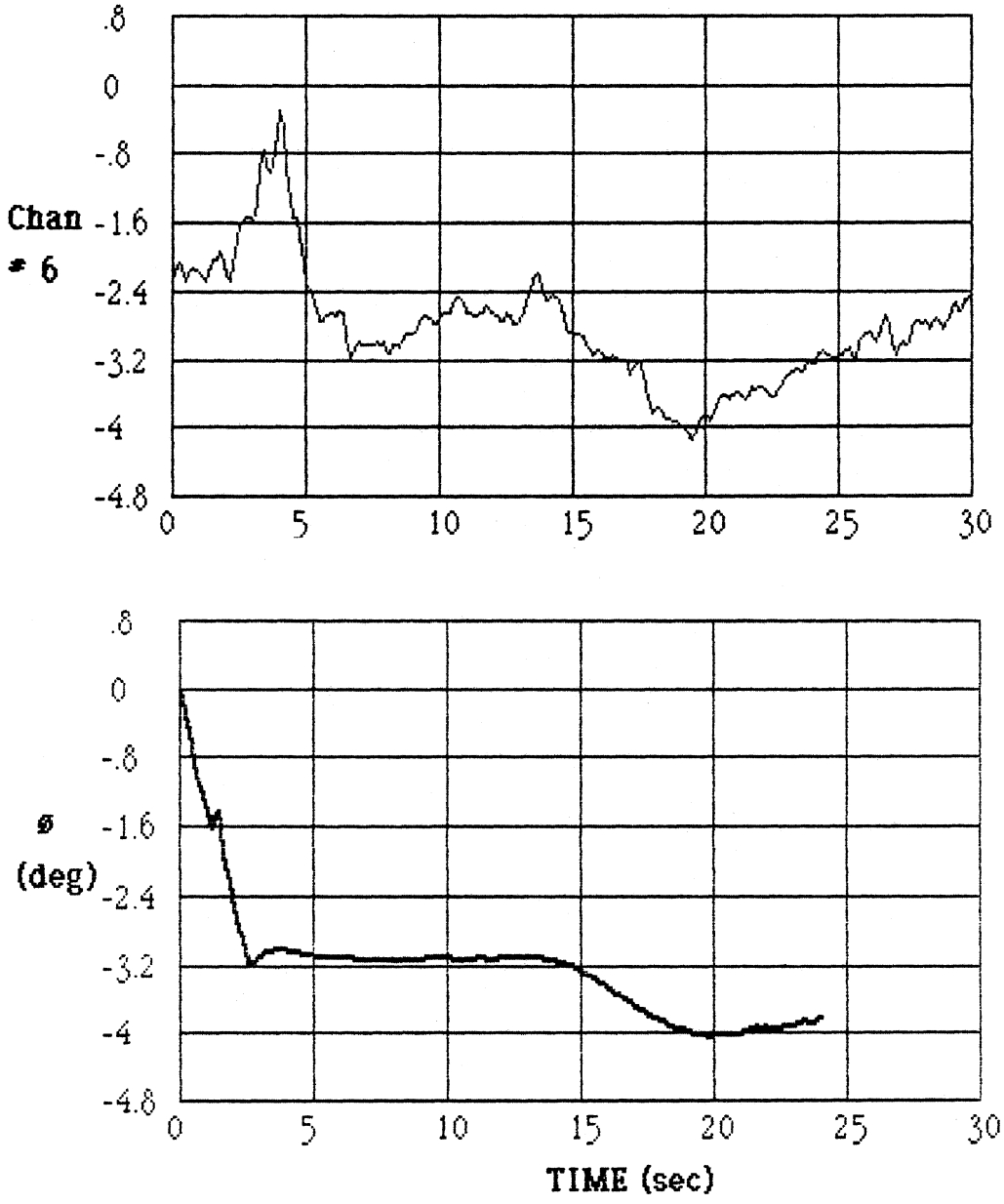

Figure 48 (cont)

Front Wheel Angle (deg)

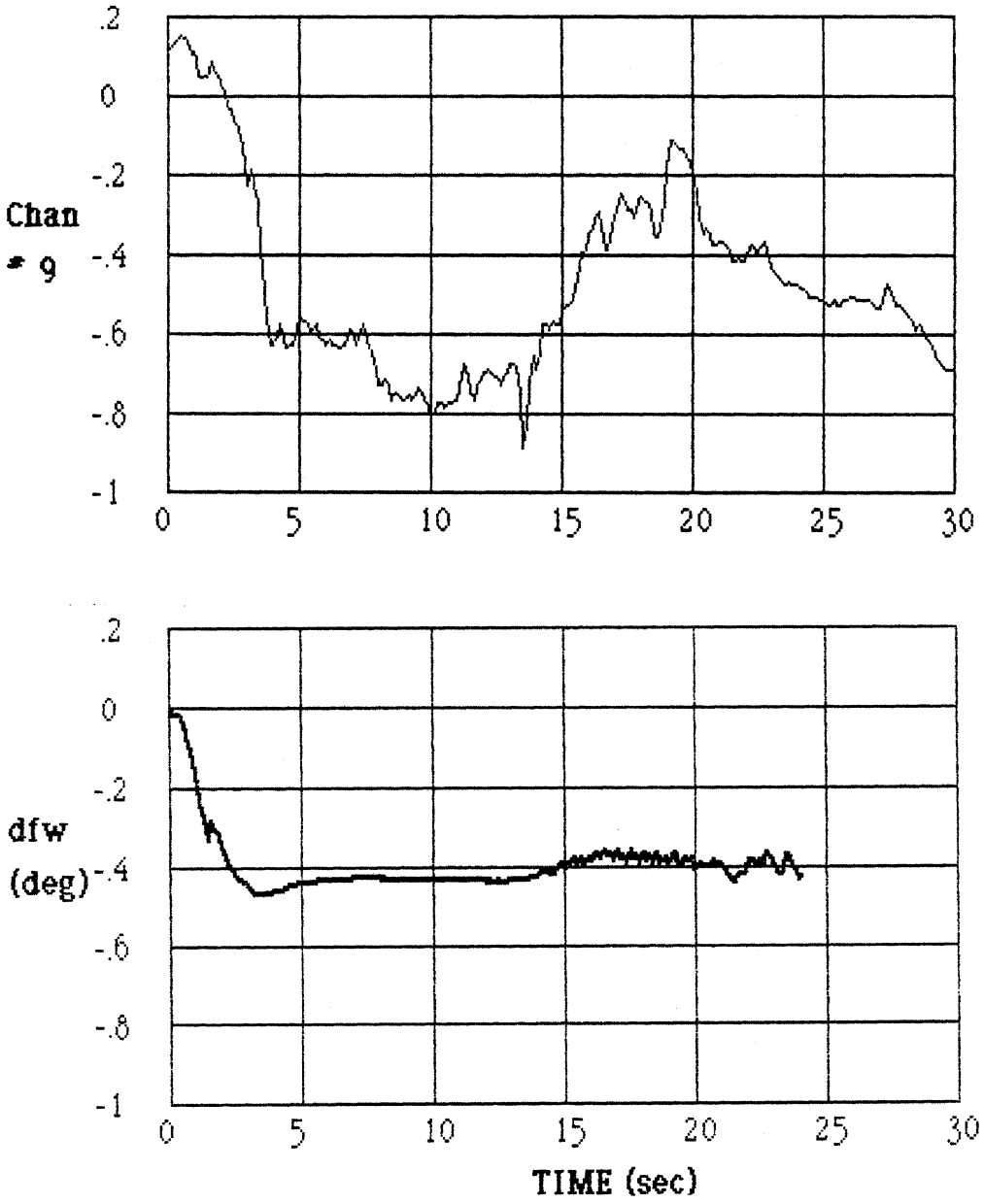

Figure 48 (cont)

5.4 Conclusions Regarding Model Validation

The basic findings concerning model validation as seen here in the comparisons between vehicle measurements and model predictions are:

* General agreement exists between the predictions of vehicle response provided by the steady-turning vehicle models and measurements of actual vehicles under similar operating conditions.

* Comparisons between test results and the Phase 4 model for transient obstacle avoidance and braking / accelerating maneuvers performed along superelvated curves also were shown to exhibit very good agreement.

* Identification of relatively small friction factors at individual wheel locations through processing of normal vehicle response measurements is highly sensitive to the accuracy of those response measurements. The enhanced sensitivity is due to the dependence of each friction factor value on four or more different measured quantities. Therefore, unless all of the contributing measurements are fairly accurate, the expectation of obtaining an accurate estimate for the particular friction factor is diminished. (This matter is addressed further in the next chapter when sensitivities of friction factor values deriving from possible measurement errors are examined.)

* As a consequence of the above observations, use of the steady turning models to predict or estimate individual wheel friction factor values is viewed as more reliable and preferable to currently existing methods of direct measurement. This of course assumes that reasonable or representative estimates of vehicle parameters are used in the models.

Chapter 6

SENSITIVITY ANALYSES

The material contained in this chapter presents results of several sensitivity analyses conducted with the steady turning and Phase 4 models. The general thrust of most of these analyses is directed at the influence that various vehicle and highway gemetric parameters may have in influencing friction factor demand or distribution on a vehicle. A passenger car and a five-axle tractor-semitrailer were used as representative, or baseline, vehicles in the parameter variation studies. The baseline parameter sets used in these analyses correspond to passenger car A and the five-axle tractor-semitrailer test vehicles. The principal difference between the data sets used here and those used for comparisons seen in chapter 5 was vehicle speed. Most of the analyses in this chapter were performed at a baseline speed of approximately 56 mph (90 km/h) (selected from one of the test runs for vehicle A at curve 1). The baseline curve geometry corresponds to that of curve 1 (1273 ft (388 m) radius; 6.7 percent superelevation).

Sections 6.1 and 6.2 present parameter variation studies performed with the steady turning models for the baseline passenger car and tractor-semitrailer. Section 6.3 shows results of a similar study for obstacle avoidance maneuvers using these same vehicles and the Phase 4 model. Steady turning and obstacle avoidance maneuvers performed under low friction conditions are examined in section 6.4 . Section 6.5 discusses basic relationships between friction factors and vehicle response variables and how errors in vehicle measurements can affect estimates of friction factor values. Lastly, section 6.6 examines driver steering requirements and observed behavior during traversal of superelevated curves.

6.1 Passenger Car Parameter Variations

The results seen in this section illustrate the effects upon individual wheel friction factor values and basic vehicle response variables which can be

expected by varying different vehicle and highway geometric parameters. The size of each parameter variation was selected to be representative of possible parameter changes that can occur. For example varying a vehicle's tire cornering stiffness by 50 percent or more would be unreasonable and not representative of likely occurrences in the vehicle population. Variations of 25 percent, however, can occur due to inflation pressure changes and wear-related phenomena. This type of rationale was used for selecting the parameter variations appearing in this study.

The baseline condition for passenger car A corresponds to curve site 1 and a travel speed of 56.7 mph (91 km/h). Figures 49 through 54 present results for friction factor variations resulting from various changes in vehicle and highway parameters. For example, the top portion of figure 49 shows the influence of varying curve radius by 10 percent. Friction factor values are seen to increase and decrease from the baseline condition, for each wheel location and the equivalent point-mass (c.g.) value, in response to the curve radius changes. Likewise the lower portion of figure 49 illustrate similar results due to changes in highway superelevation rate (8.7, 6.7, and 4.7 percent). For all of the results seen in this section, only one parameter variation at a time away from the baseline condition is being performed. Figure 50 illustrates the effect that changes in speed and highway grade have upon altering friction factor levels. As seen in figures 49 and 50, and which should be expected based upon a point-mass analysis, the friction factor values are significantly affected by curvature, superelevation and speed, but very little by highway grade. Moreover, the degree of friction factor variations seen in figure 49 for each of the wheel locations is more or less the same amount exhibited by the point mass value. That is, no particular wheel location is seen changing by a disproportionate amount in comparison to the point-mass value. As such, these results suggest that a point-mass formulation provides not only a reasonably accurate prediction of the values of the individual wheel friction factors for passenger cars, but also, the degree to which they can be expected to respond to variations in highway geometry.

Examination of figures 51 through 54, which apply to vehicle-related parameter variations, shows that variations in most vehicle parameters have

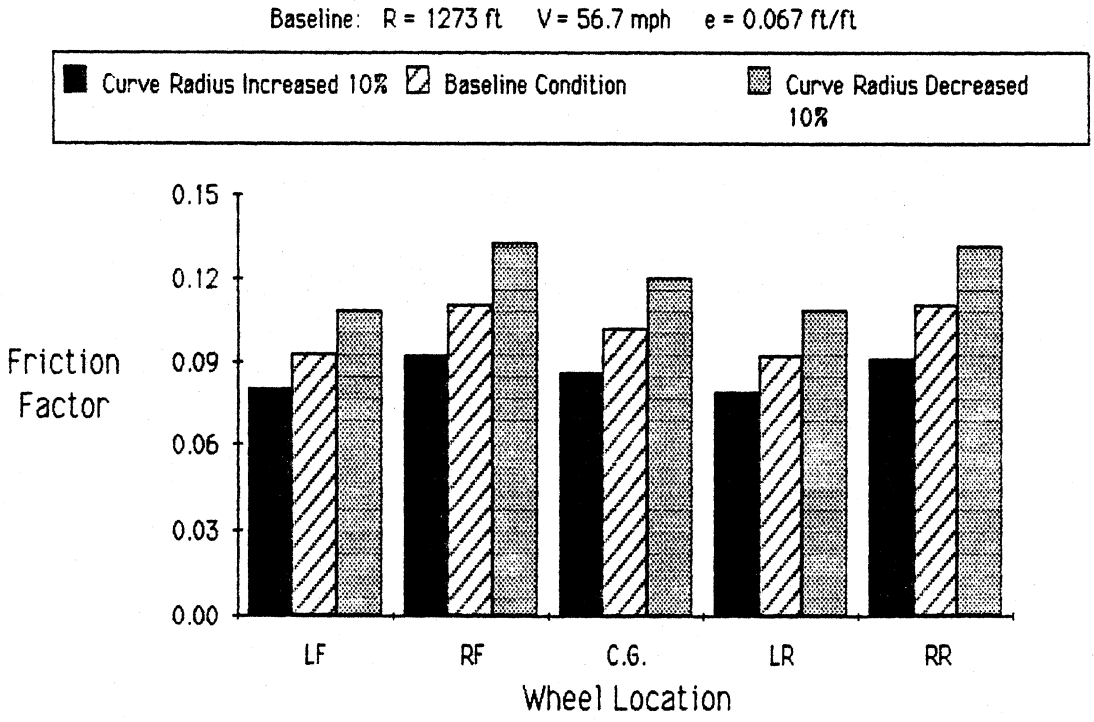

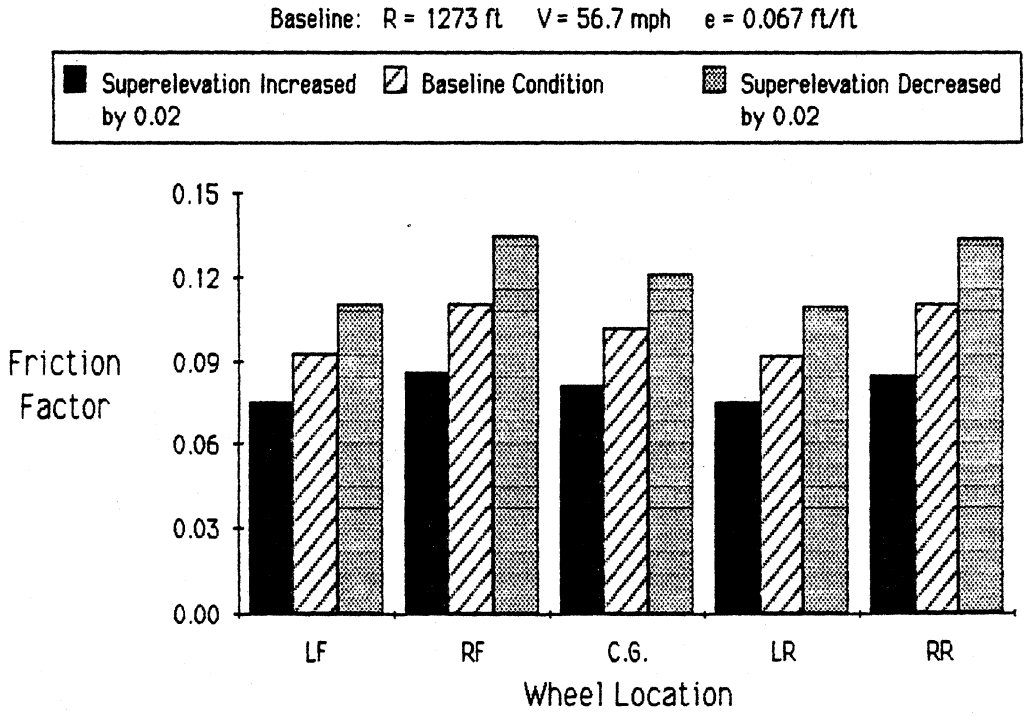

Figure 49. Passenger car parameter variations.

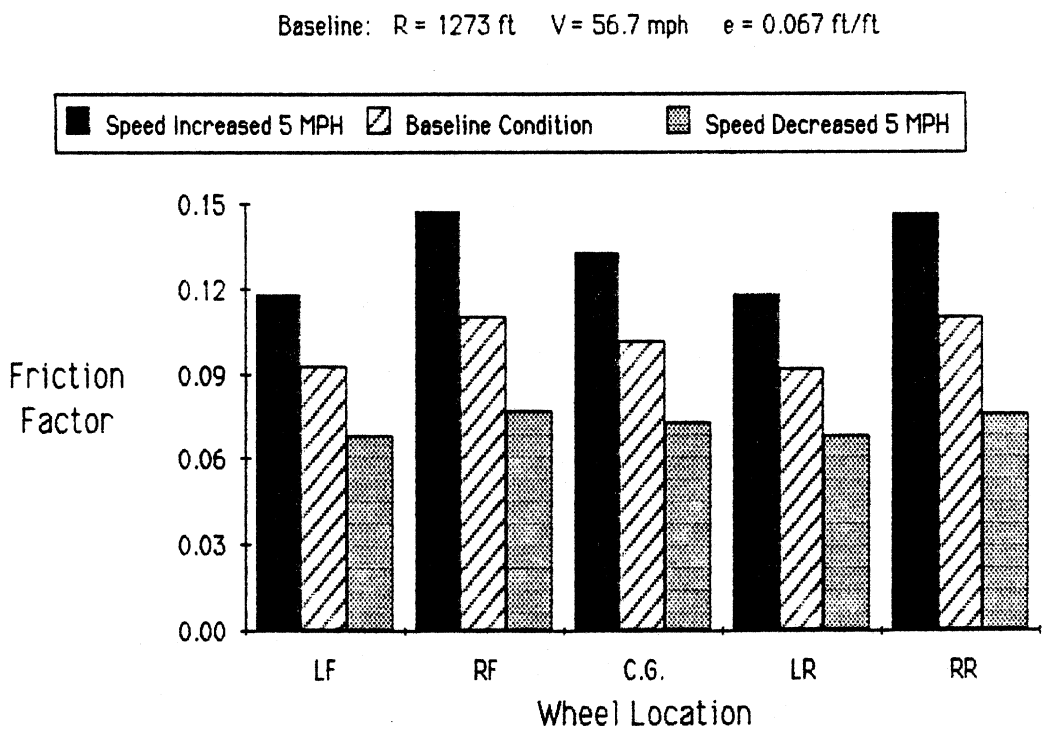

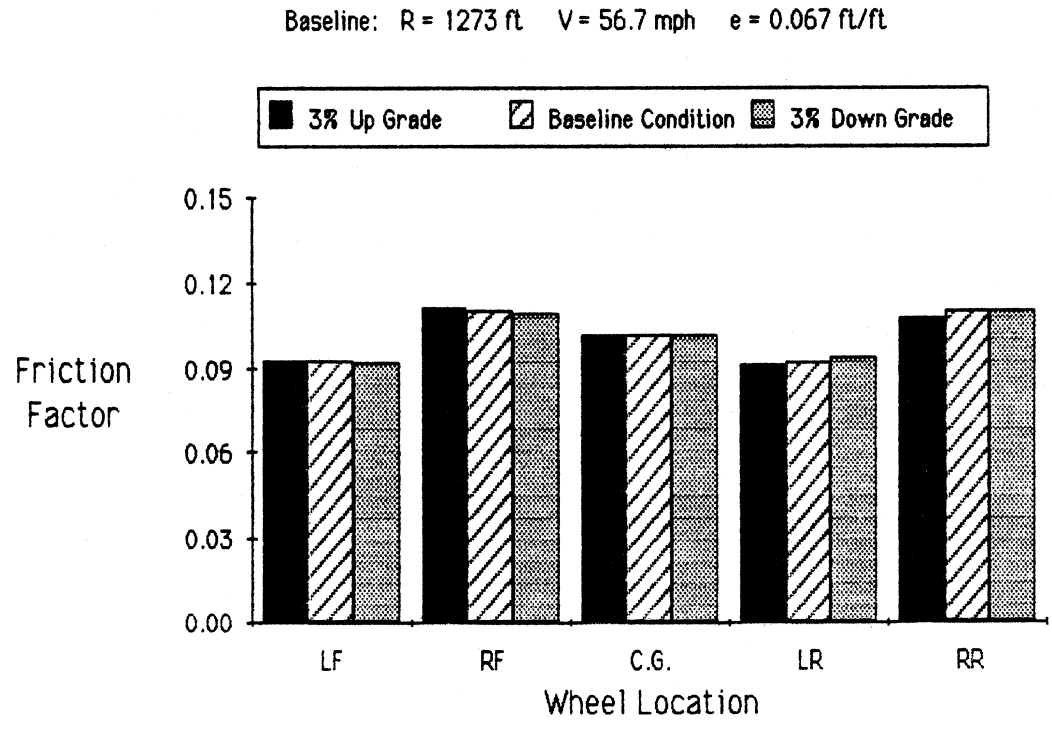

Figure 50. Passenger car parameter variations.

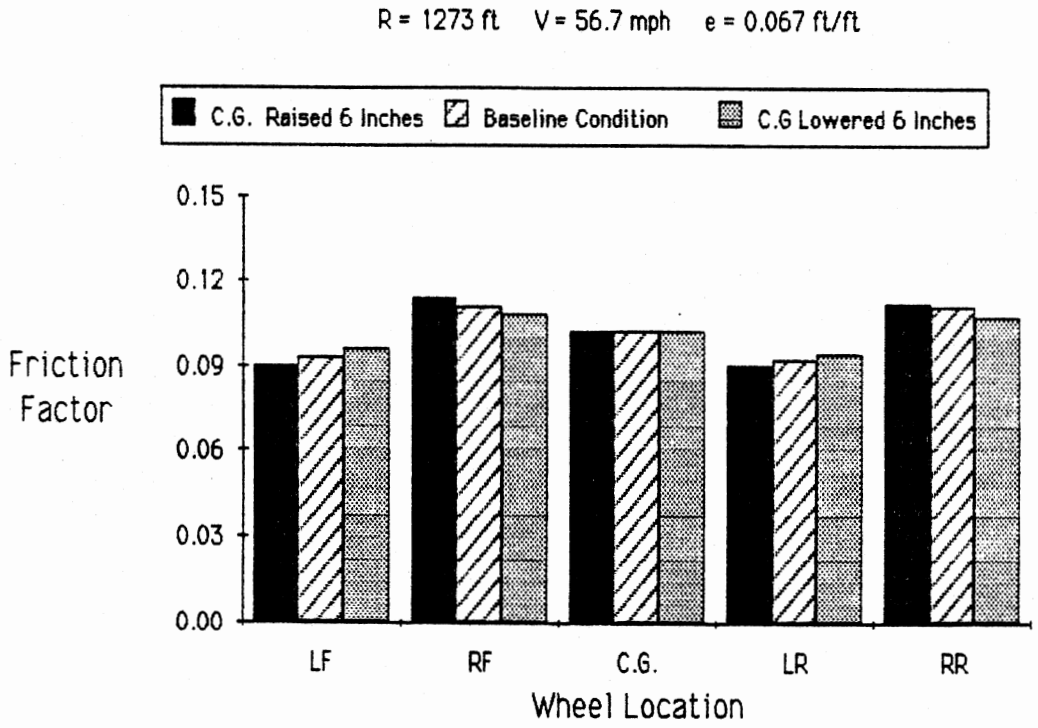

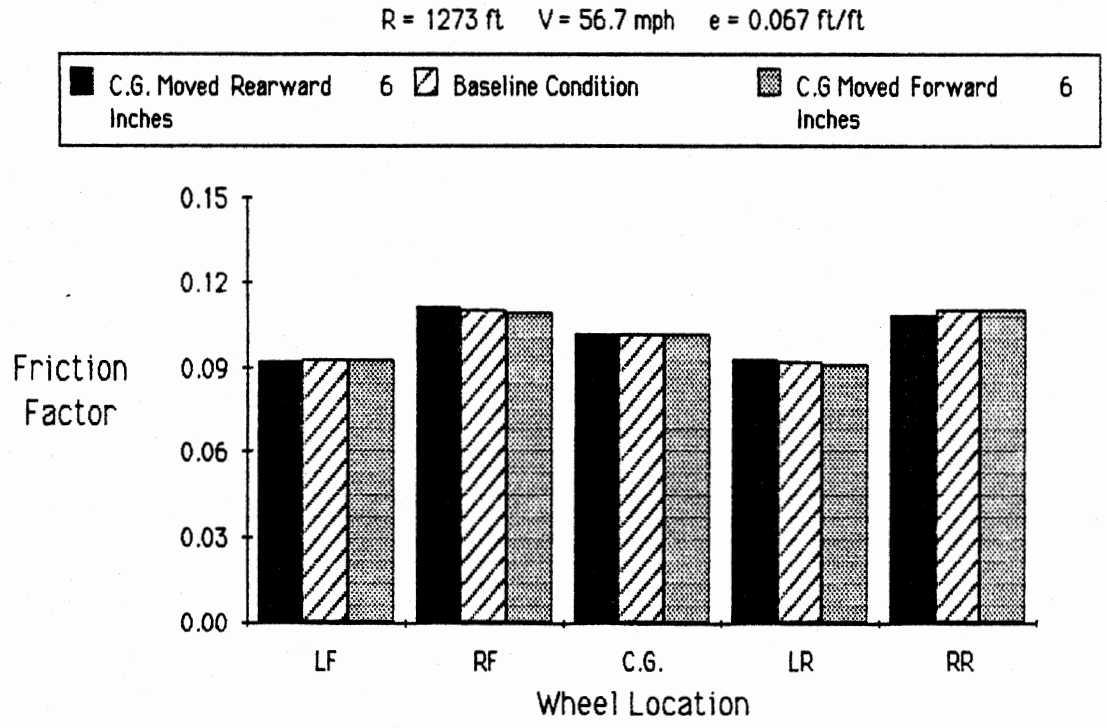

Figure 51. Passenger car parameter variations.

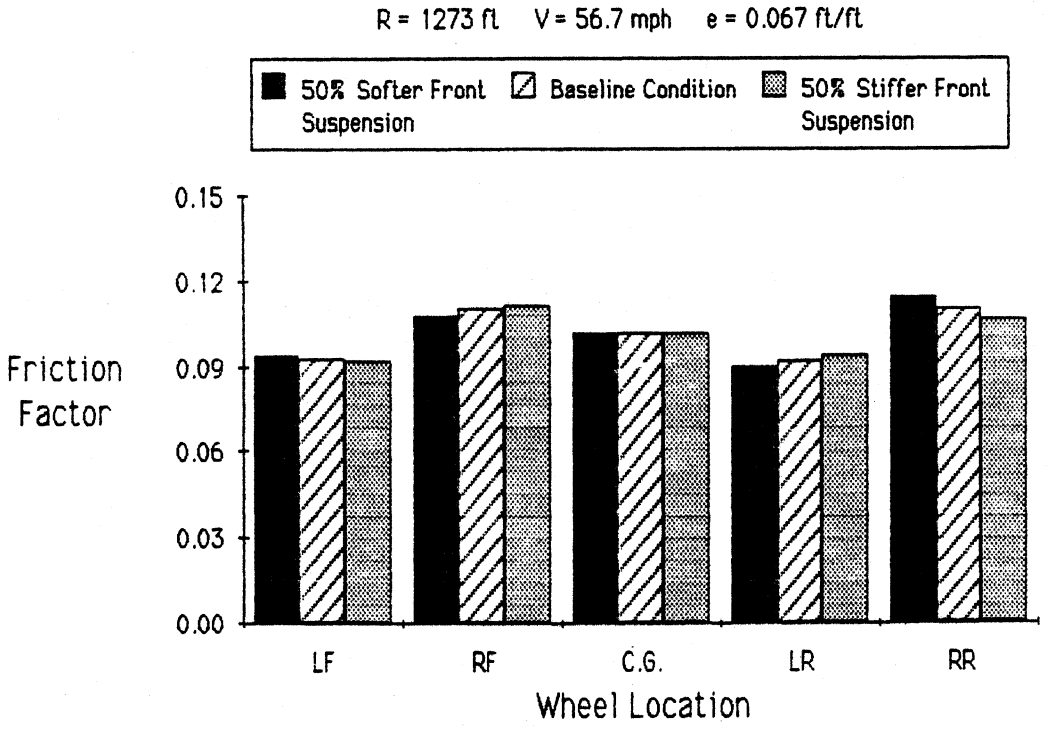

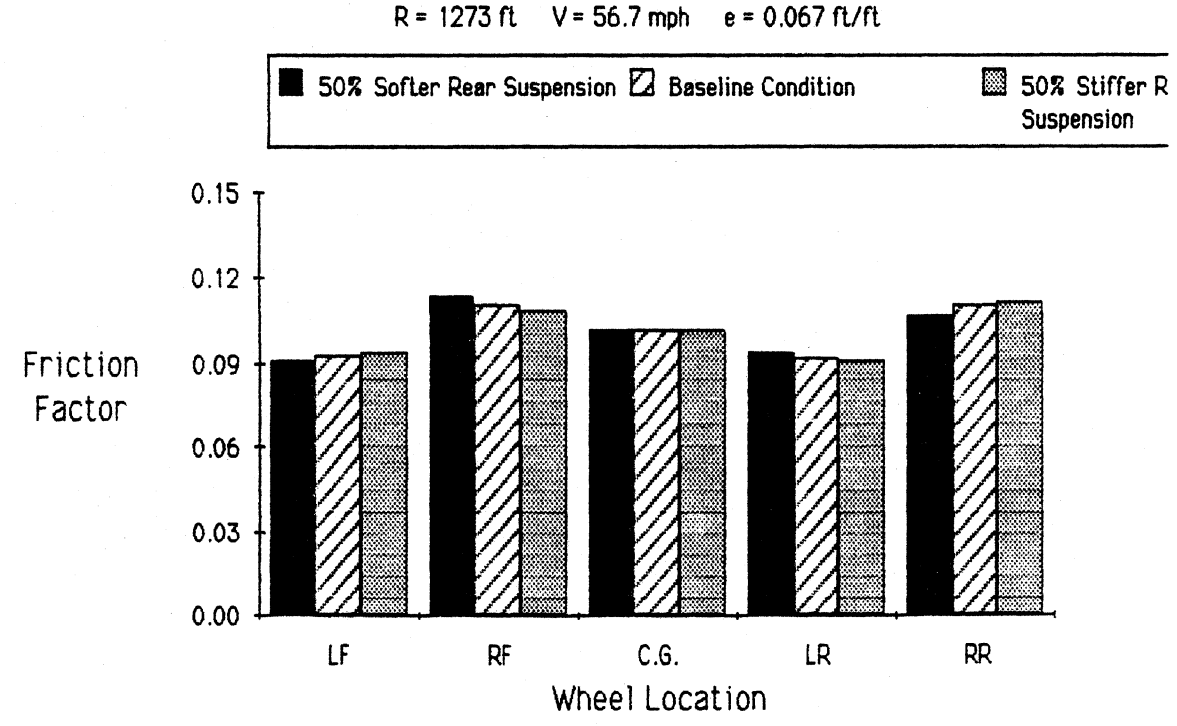

Figure 52. Passenger car parameter variations.

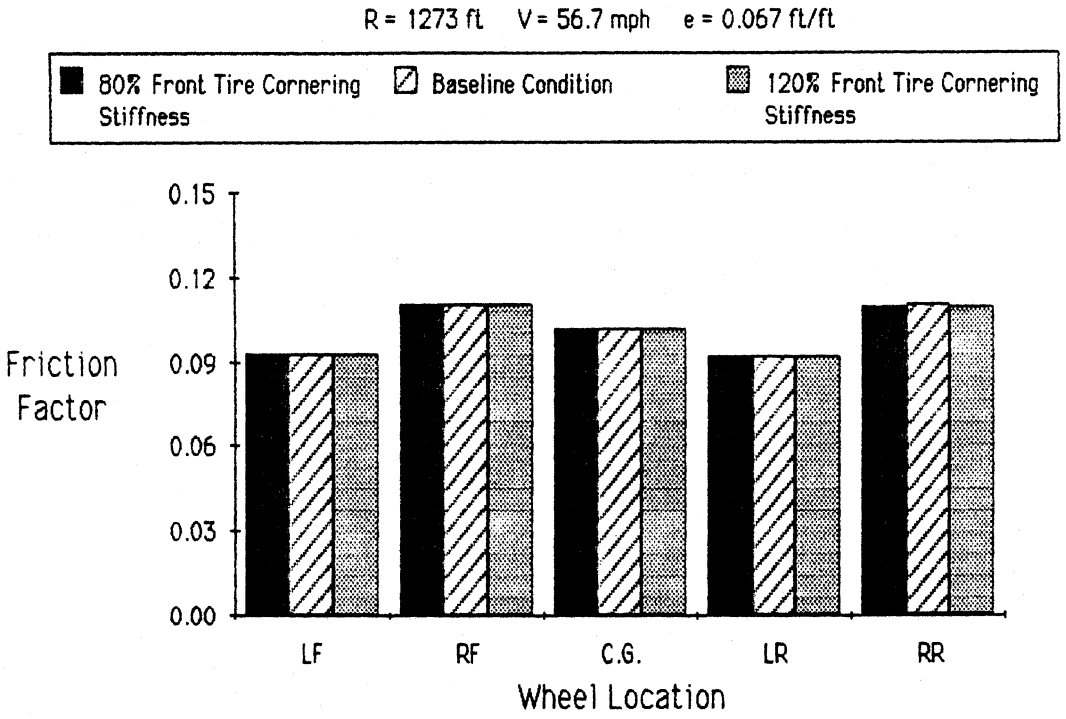

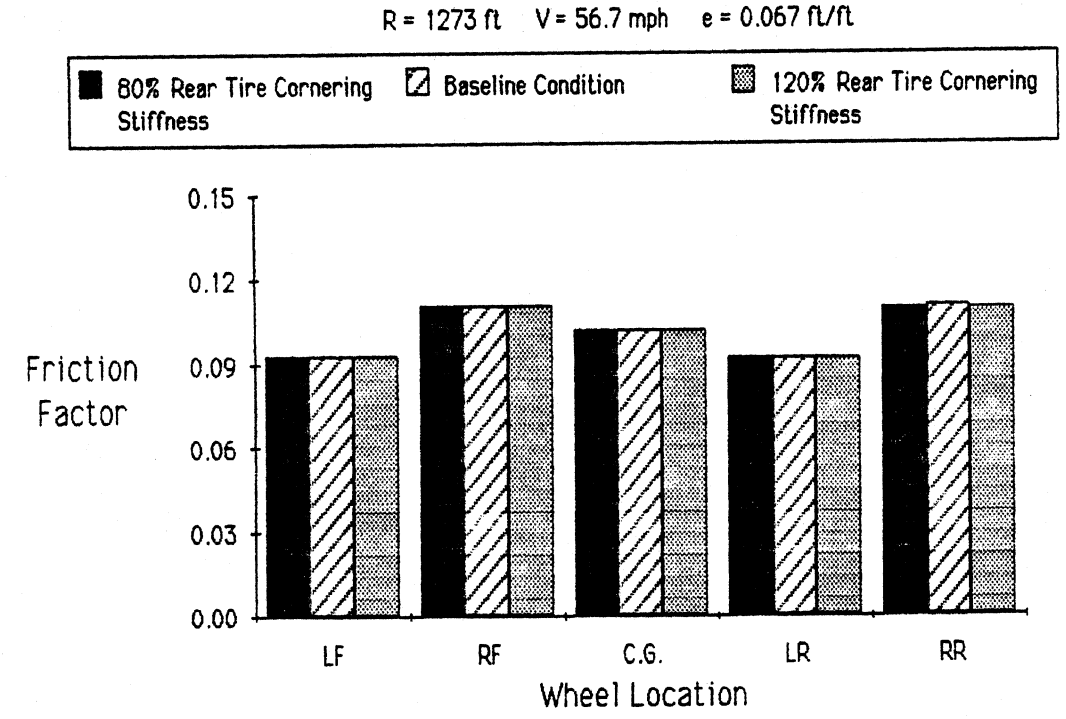

Figure 53. Passenger car parameter variations.

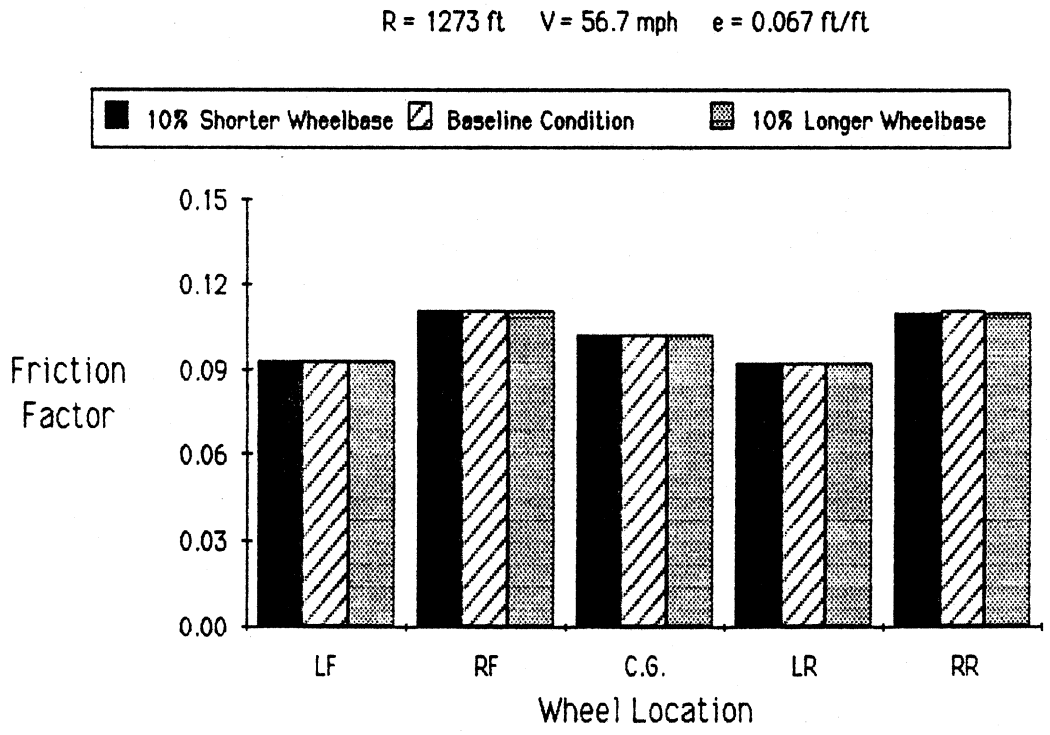

Figure 54. Passenger car parameter variations.

little or no effect upon modifying friction factor values for a representative passenger car. Less than 5 percent variations are seen here occurring for variations in center of gravity height, figure 51, and variations in suspension properties, figure 52. Interestingly, tire cornering stiffness variations, figure 53, have no influence whatsoever upon friction factor values. The overall insensitivity of friction factor values to variations in passenger car properties is of course beneficial to the highway designer. Provided that a reasonable representation of the vehicle is employed, modest changes in vehicle properties (as perhaps represented by the bulk of the passenger car vehicle population) should have little or no impact upon the friction factor values occurring in the basic design. Hence, a particular curve design, based upon a mid-size Chevrolet, should apply equally to Chevettes and Cadillacs.

The next set of figures, 55 through 63, show results of three basic vehicle responses predicted by the steady turning model for the same set of parametric variations just considered. Instead of examining friction factor changes, as seen in figures 49 through 54, the corresponding vehicle responses are seen. Such plots are very useful in explaining how changes in vehicle or highway geometry affect basic vehicle behavior. Figure 55 illustrates how changes in curve radius affects three vehicle response variables: required front wheel steer angle, roll angle, and vehicle sideslip angle (angle between the vehicle heading and the velocity vector of the mass center). For example, smaller curve radii require larger steer angles and produce roll angles further away from the road plane (the "roll angle" of the baseline road plane is 3.8 degrees). Also, tighter turning requires additional sideslip response.

These vehicle response plots are useful in explaining why and how vehicles respond to different parameter variations during steady turning motion, even though their friction factor values may vary by only small amounts or not at all. For example, significant changes in tire cornering stiffnesses were seen to have no effect upon friction factor values in figure 53. However, examination of figure 63 shows that significant changes do occur in the basic response of the vehicle for the corresponding tire variations. In particular, different front wheel steer angles are required for front tire cornering stiffness variations, while front wheel steer angle changes and

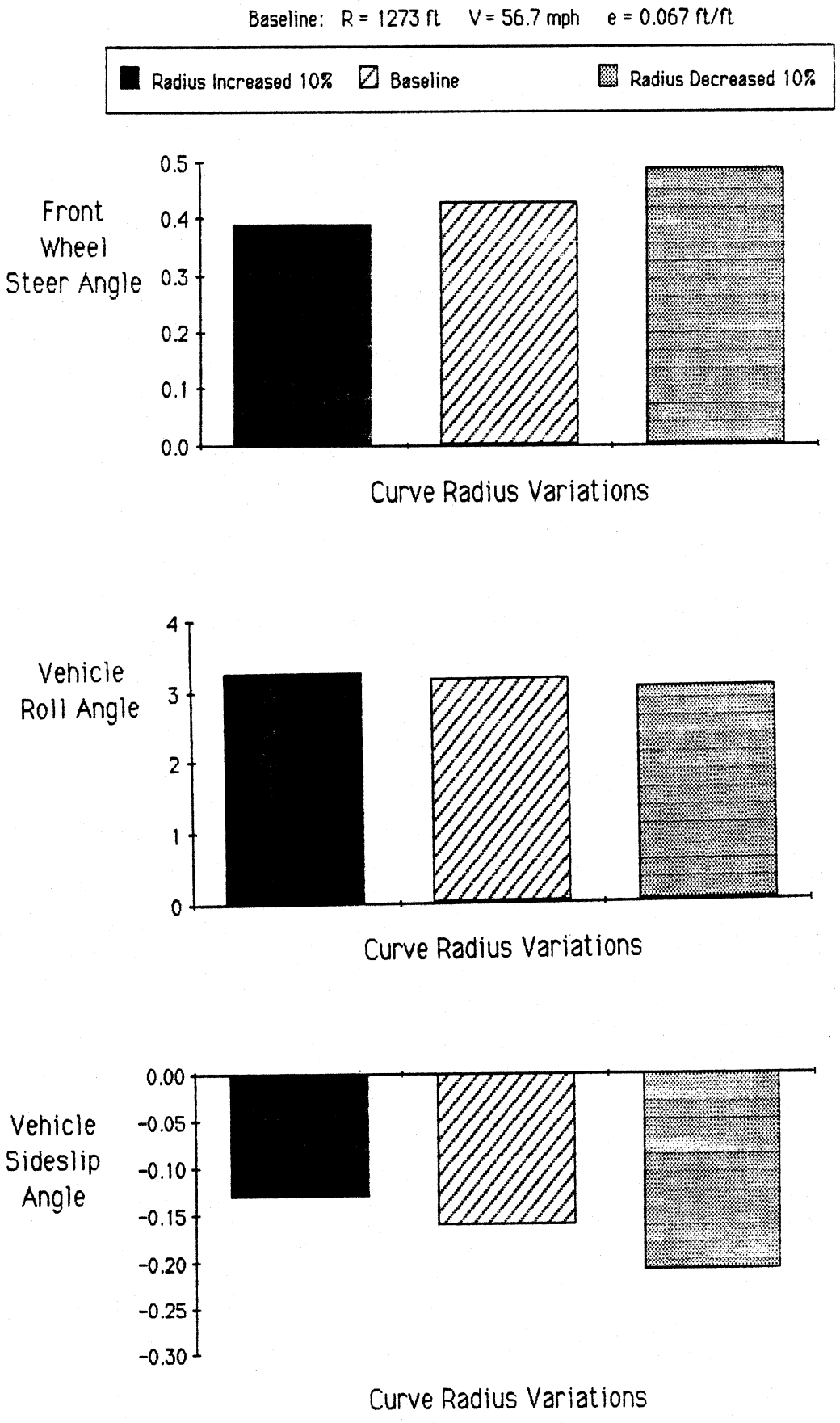

Figure 55. Passenger car response variables.

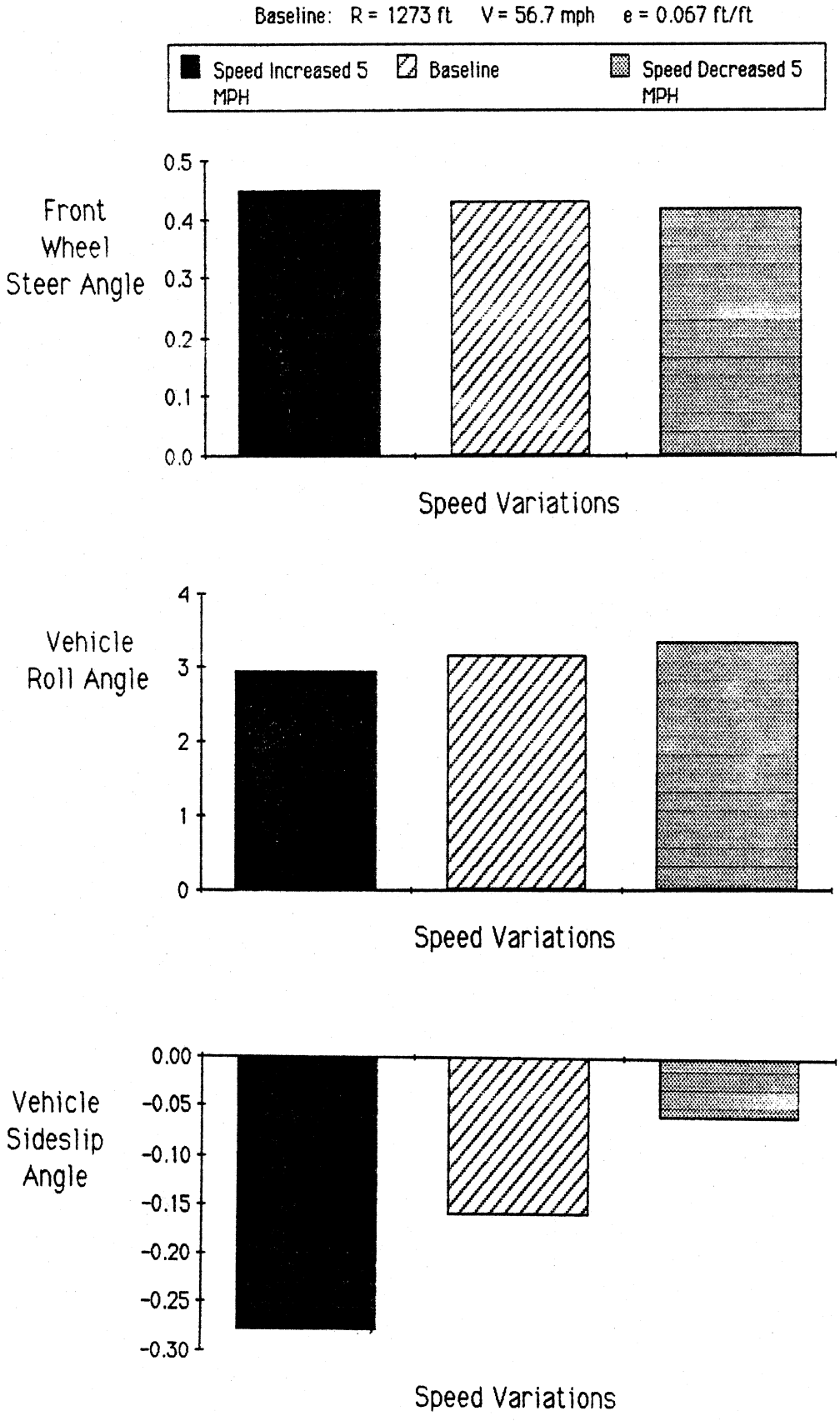

Figure 56. Passenger car response variables.

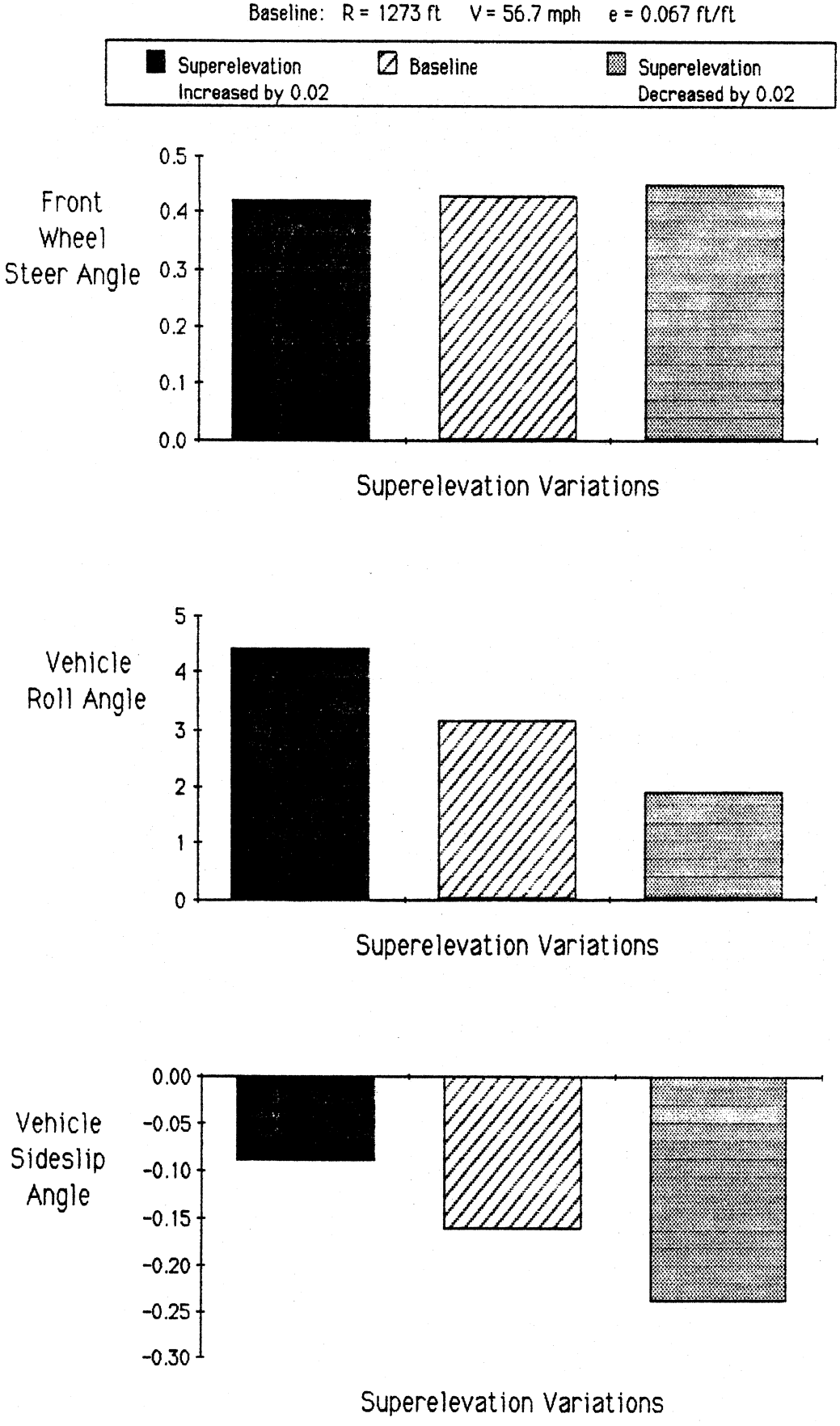

Figure 57. Passenger car response variables.

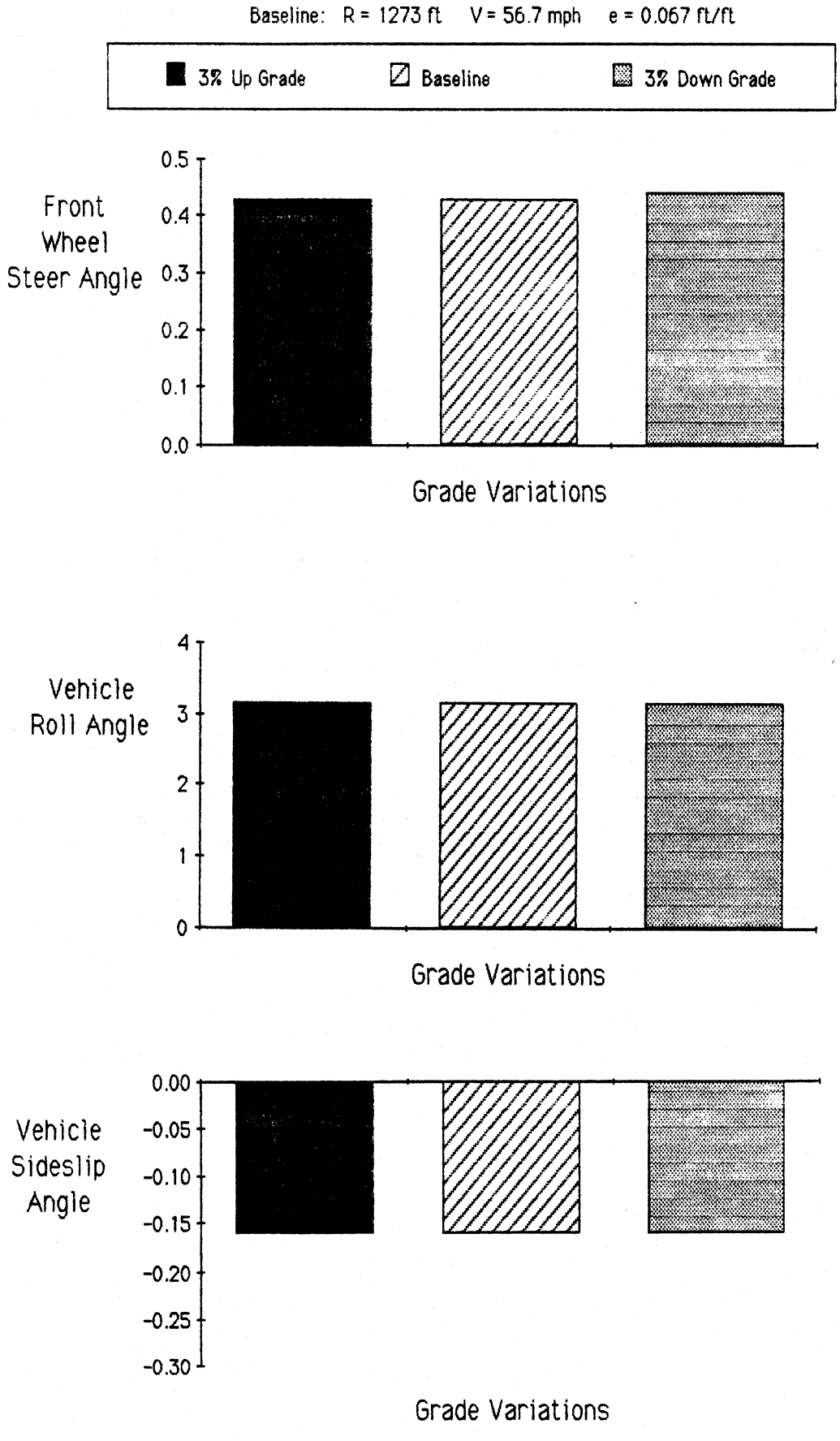

Figure 58. Passenger car response variables.

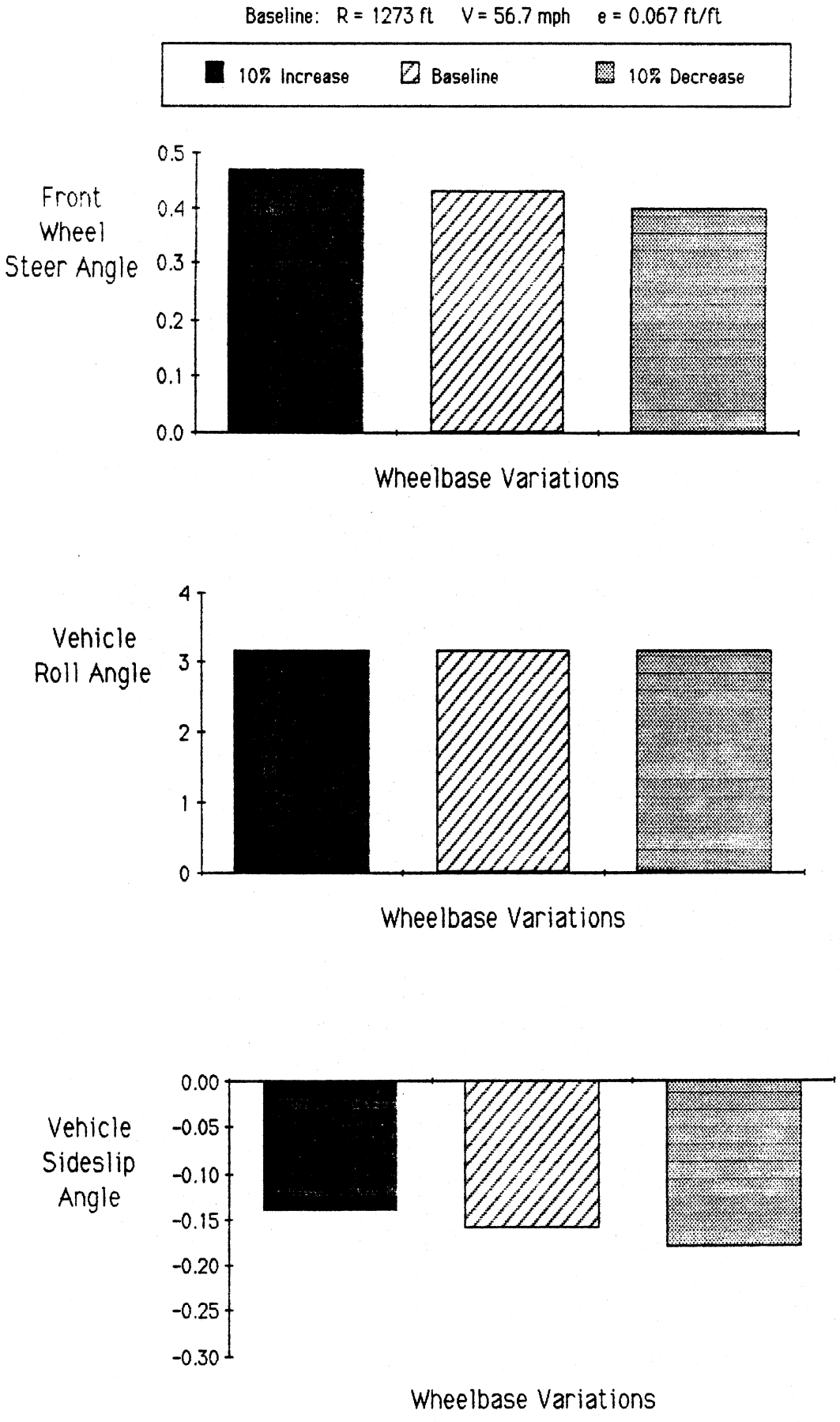

Figure 59. Passenger car response variables.

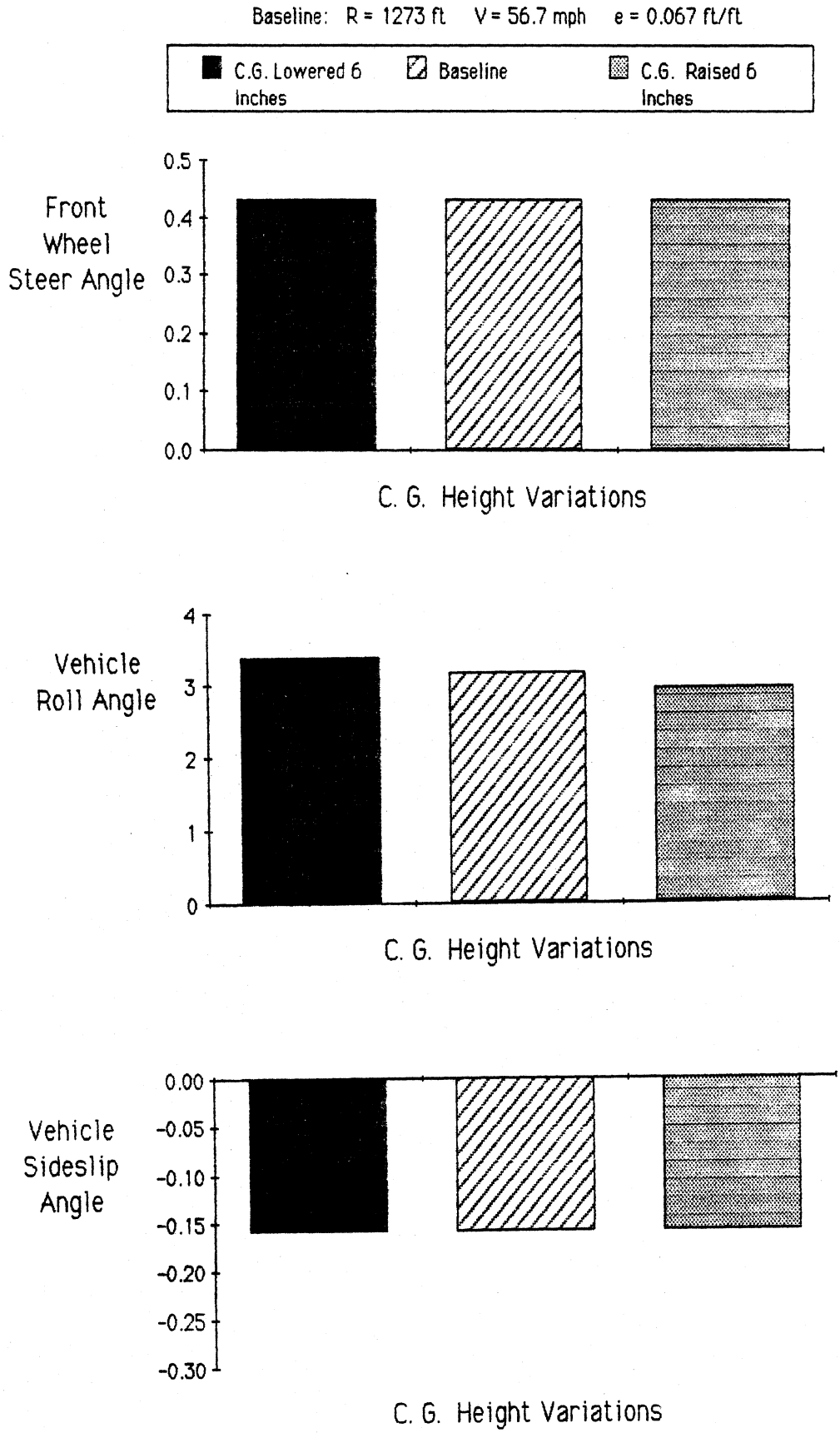

Figure 60. Passenger car response variables.

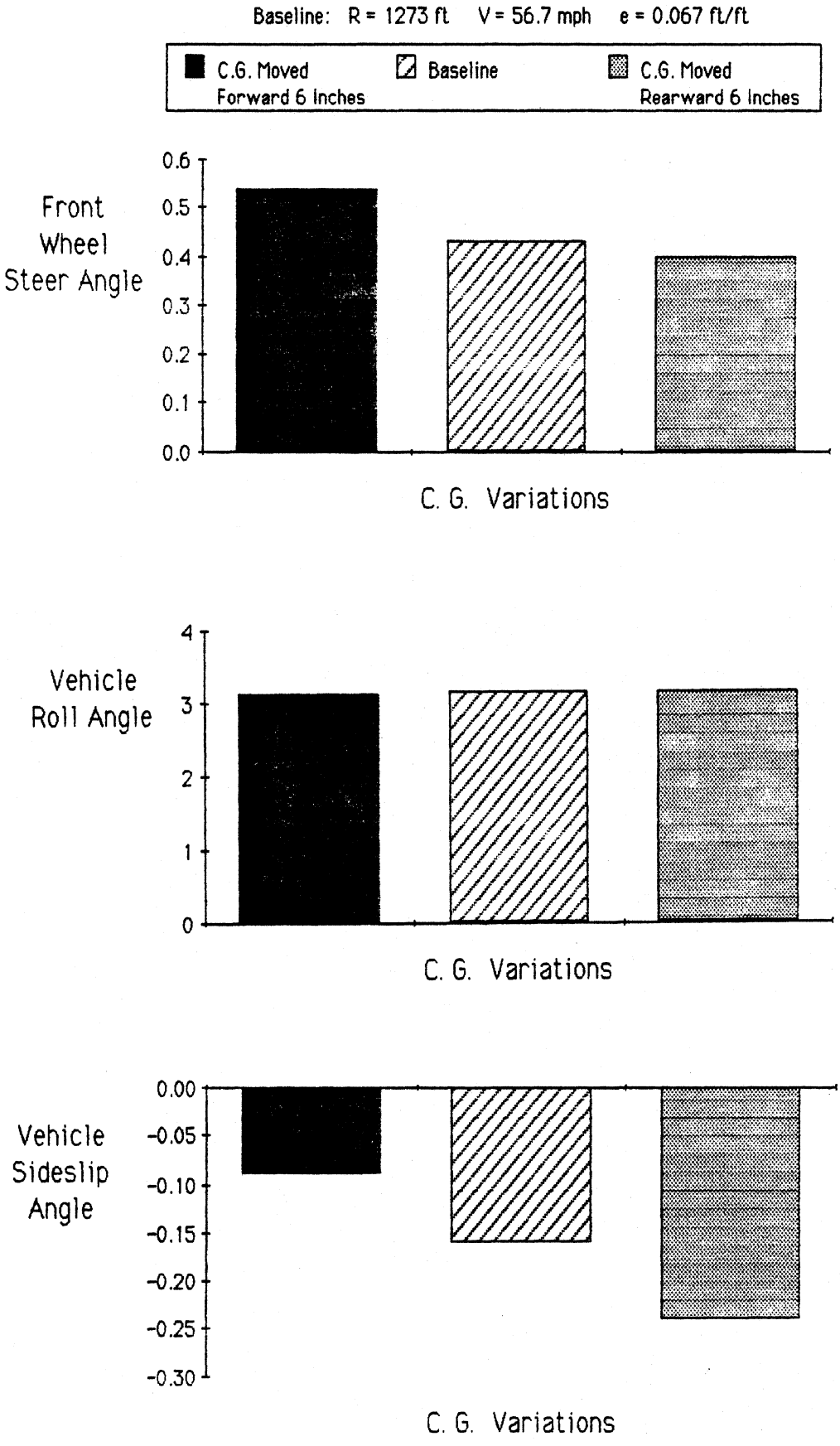

Figure 61. Passenger car response variables.

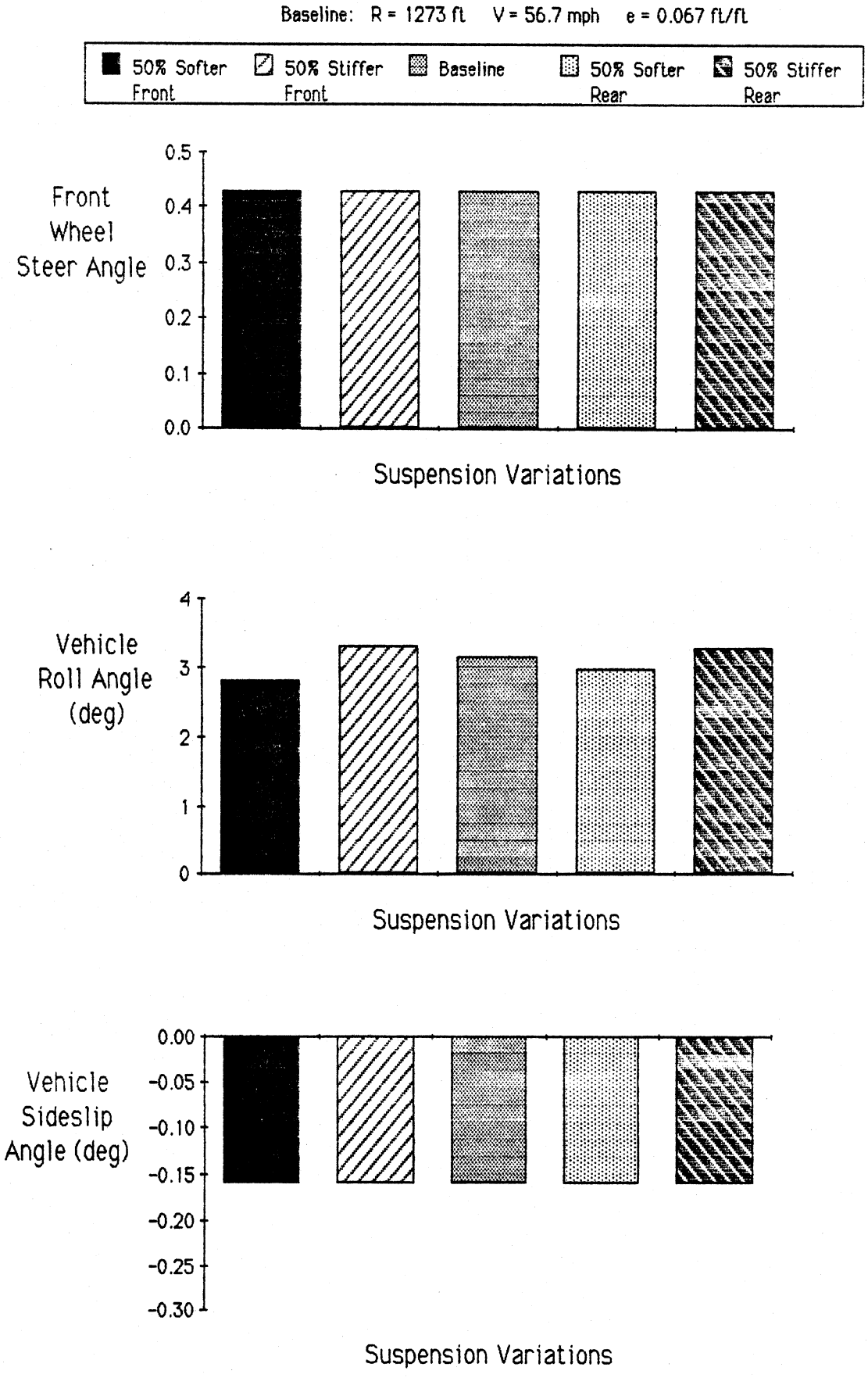

Figure 62. Passenger car response variables.

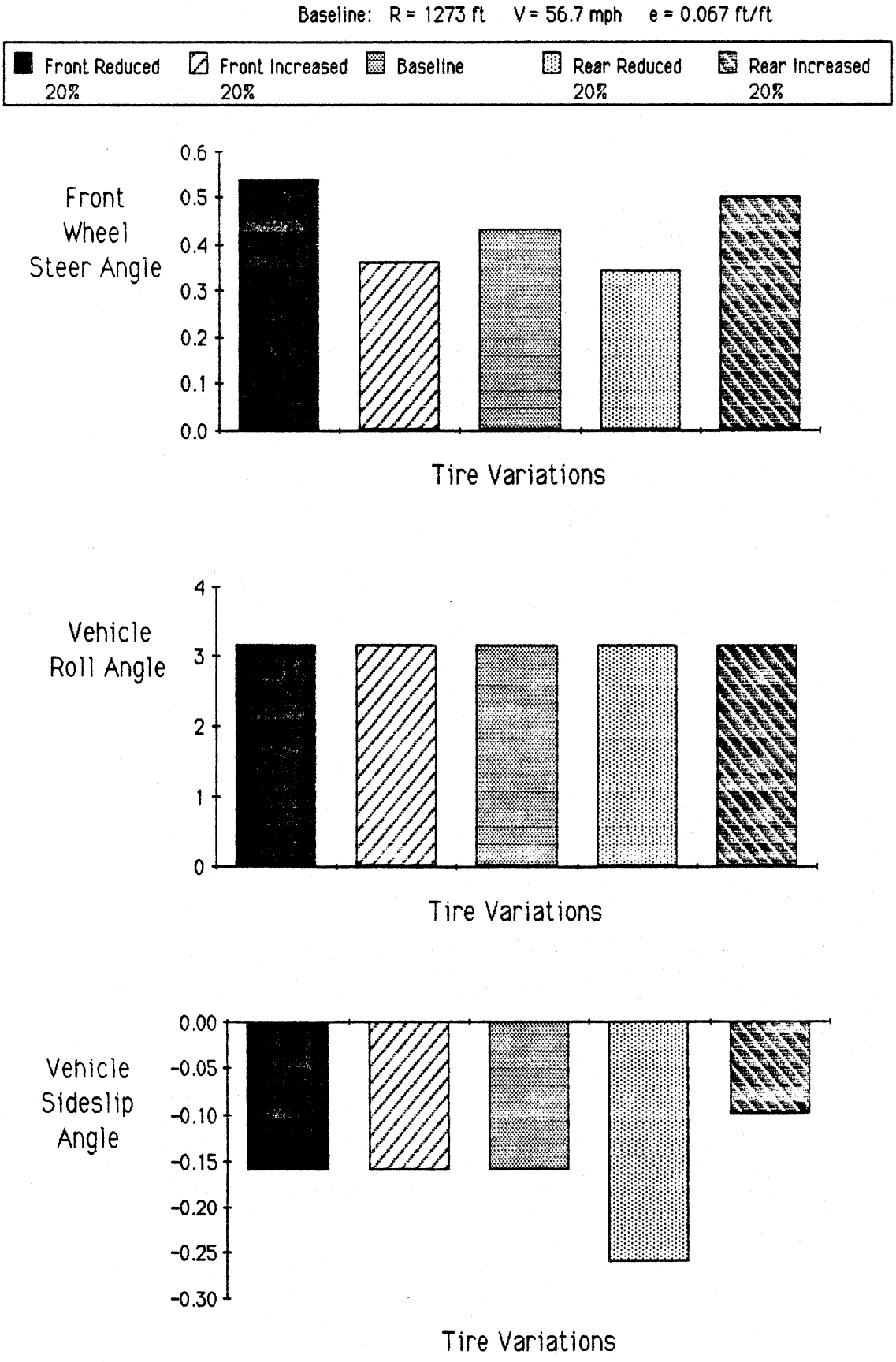

Figure 63. Passenger car response variables.

sideslip response changes both occur for similar rear tire variations. This simply tells us that the vehicle is "trimmed" to a new attitude in response to tire variations such as these, but that no change in lateral or vertical tire forces occur.

Similar interpretations can be applied to figures 56 through 62 for understanding how vehicles respond to the remaining parameter variations. Most of these are fairly straightforward. For example, highway grade changes, figure 58, have no discernable effect upon the directional vehicle responses. Changes in mass center height and suspension properties, figures 60 and 62, only influence the roll response, whereas fore/aft changes in mass center primarily affect the required steer angle and sideslip response, figure 61. Variations in vehicle speed and highway superelevation, figures 56 and 57, probably have the greatest overall influence on the vehicle responses seen here. Lastly, vehicle wheelbase variations, figure 59, produce modest changes in required steer angles and small variations in sideslip response.

6.2 Tractor-Semitrailer Parameter Variations

The material presented in this section for the baseline tractor-semitrailer closely parallels that seen in the previous section for the passenger car. The principal difference here is that the baseline speed of the tractor-semitrailer, 47.6 mph (76 km/h), correponds to one of the test runs used at curve site 1. The reason for selecting a speed corresponding to one of the test conditions is so that sensitivities seen here can be related to the test data results seen elsewhere throughout the report. Figures 64 through 72 show baseline friction factor values and their response to changes in various highway and vehicle parameters. The odd numbered wheel locations on these plots correspond to the outside, or more heavily loaded, wheels. (For example, wheel location number 1 corresponds to the outside front wheel, etc.) The "c.g." location corresponds to the semitrailer mass center and is the equivalent point-mass value. As seen in figures 64 and 65, changes in the highway curvature, superelevation, and vehicle speed produce significant changes in the tractor-semitrailer friction factors - similar to those observed in the passenger car. However, unlike the passenger car, a point-mass formulation is not at all appropriate for predicting friction factor

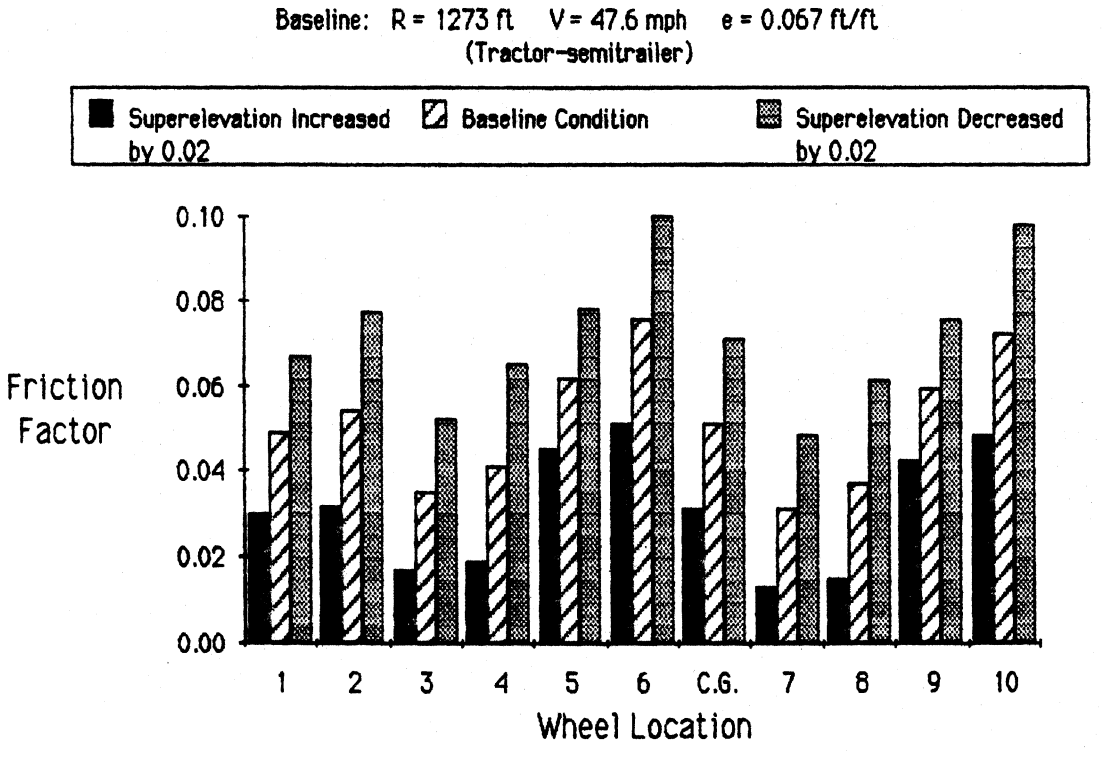

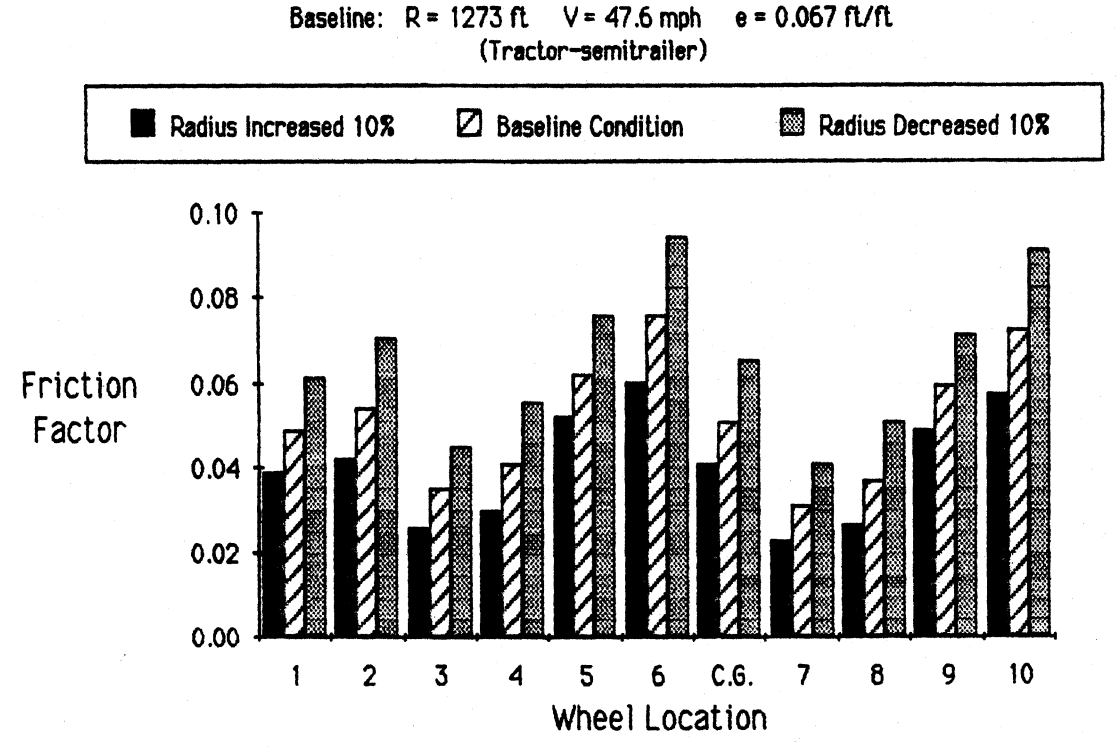

Figure 64. Tractor-semitrailer parameter variations.

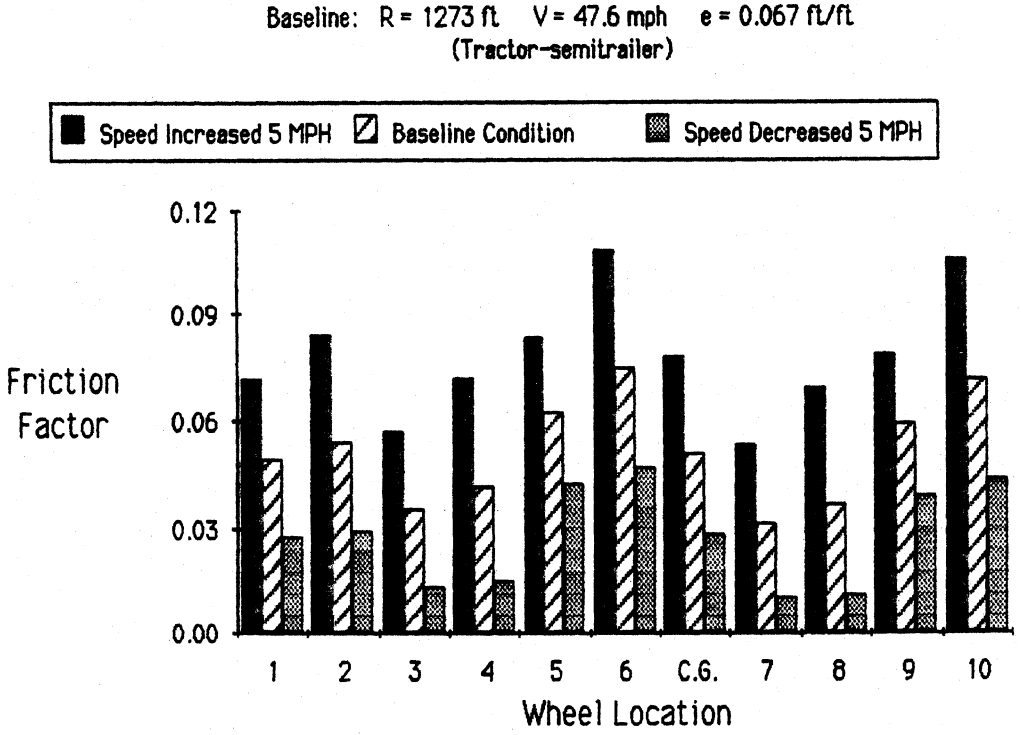

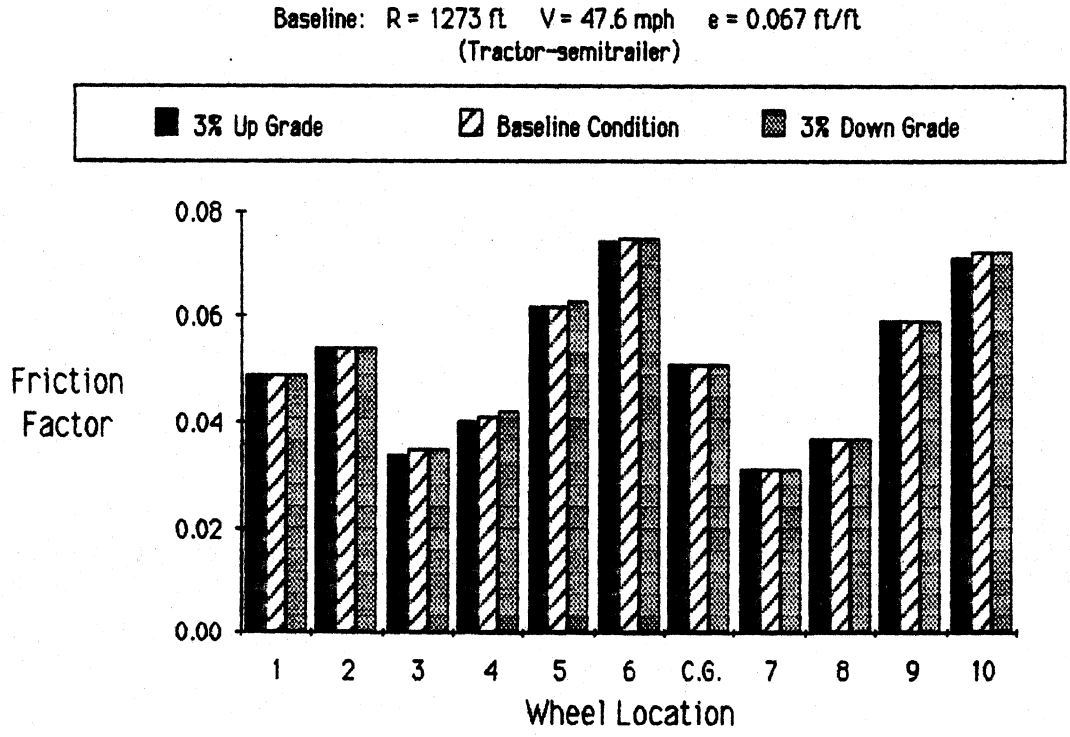

Figure 65. Tractor-semitrailer parameter variations.

values at the various wheel locations of the tractor-semitrailer. In fact, variations in friction factor levels occurring from wheel-to-wheel (because of the commercial vehicle properties discussed in chapter 2) are seen to equal or exceed those variations due to speed, curvature, and superelevation effects considered here. The question of whether the point-mass value (which is essentially a weighted average of the individual wheel friction factors) is an appropriate value to use when designing a highway curve for commercial vehicles, is deferred until section 6.4 .

Figures 65 through 68 show that highway grade, fore/aft and vertical payload movements, and suspension changes do not significantly affect the individual wheel friction factors. Further, front tire cornering stiffness variations and tractor fifth wheel movements likewise play no important role. However, tire cornering stiffness variations at the rear suspensions of the tractor and semitrailer, figure 69, do have modest influences, but only at their respective wheel locations. Wheelbase variations seen in figure 70 have no noticeable effect.

Figure 71 compares friction factor values for the loaded baseline tractor-semitrailer with those predicted for the same vehicle but carrying no payload. Similar comparisons are also seen for a higher operating speed of 60 mph (96 km/h). The results show that at both speeds the empty vehicle configuration displays greater dispersion in its friction factor profile than does the loaded vehicle and that the amount of wheel-to-wheel variation in the friction factors also increases with speed.

Finally, in figure 72, results from running the loaded baseline vehicle at 47, 60, and 70 mph (75, 96, 112 km/h) are shown. The strong influence of forward speed as a determinant of required friction is clearly illustrated in this chart. Not only are the absolute values of friction factors dramatically affected by speed, but so also is the degree of dispersion, or amount of wheel-to-wheel variation.

Figures 73 through 78 (and figures G-1 to G-8 of appendix G) present the corresponding vehicle responses resulting from the same parameter variations just considered in the friction factor plots. Each figure is comprised of

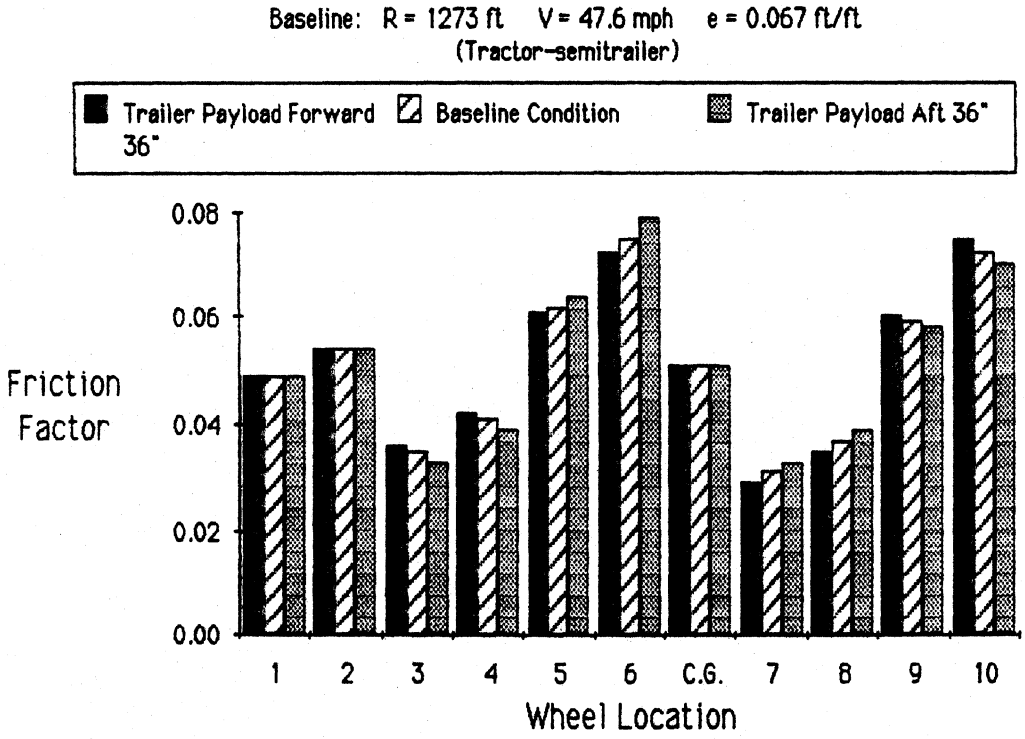

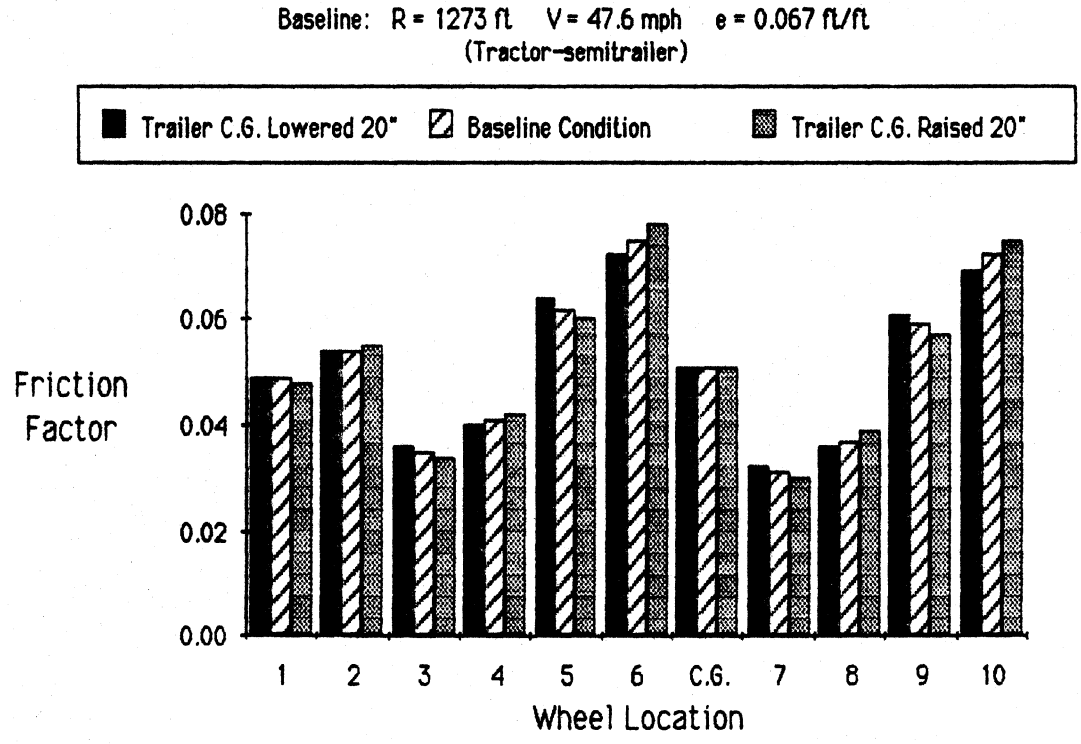

Figure 66. Tractor-semitrailer parameter variations.

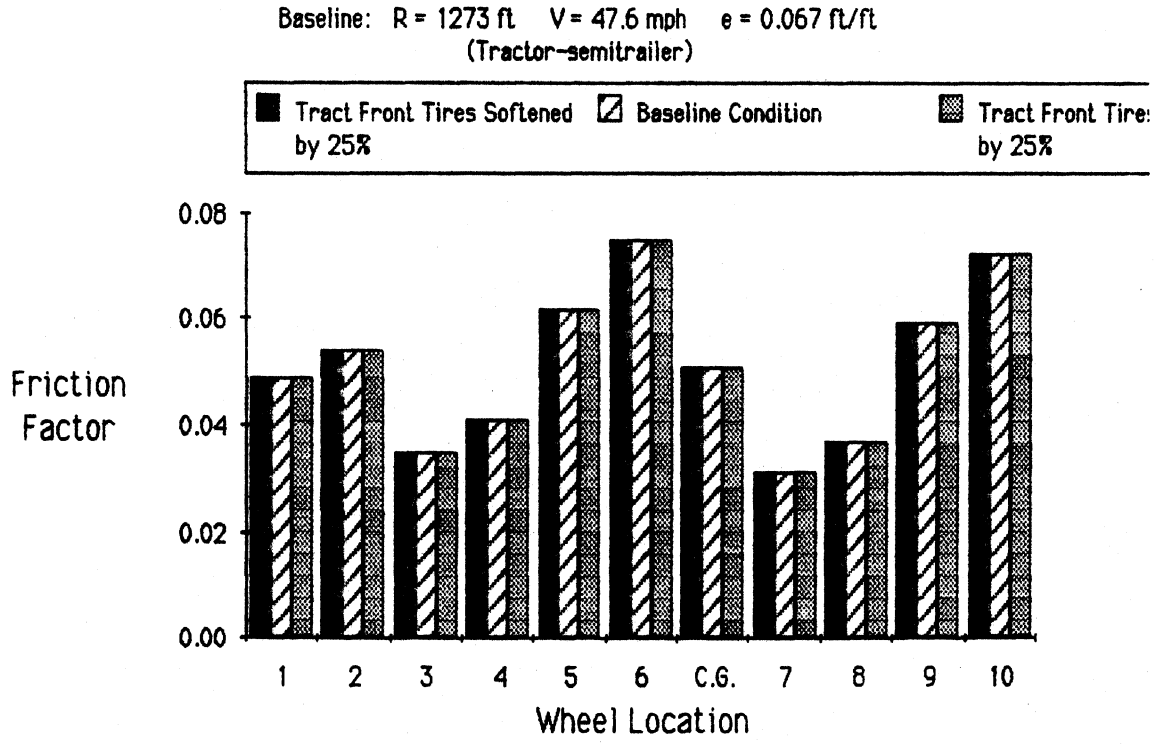

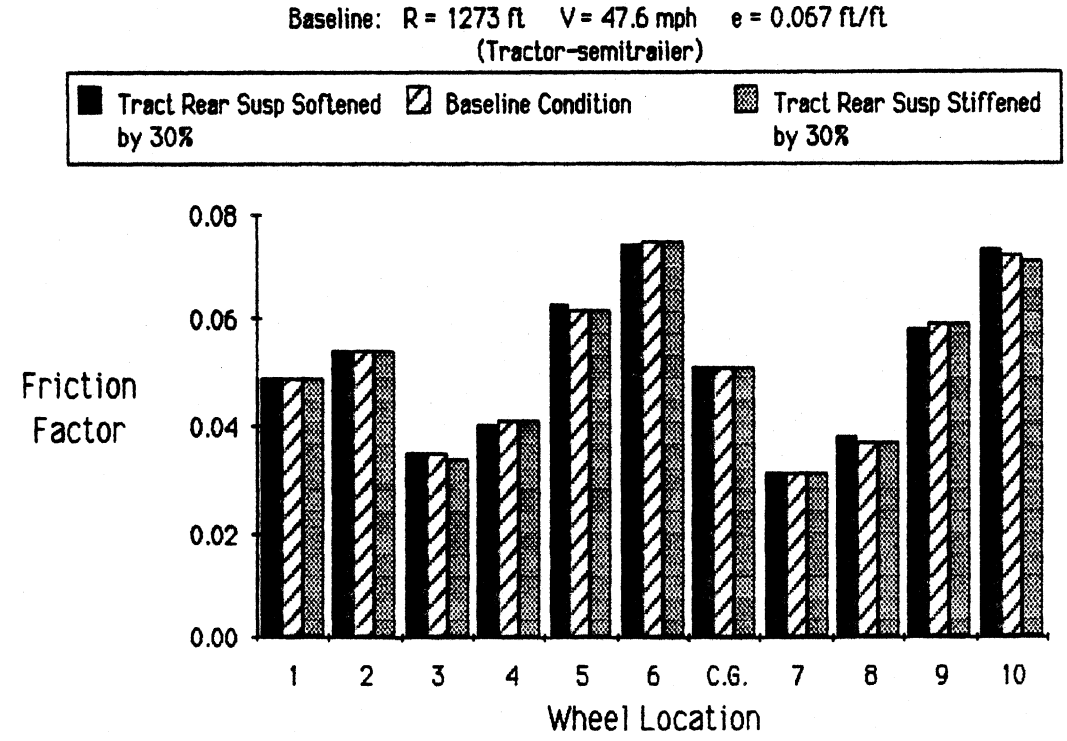

Figure 67. Tractor-semitrailer parameter variations.

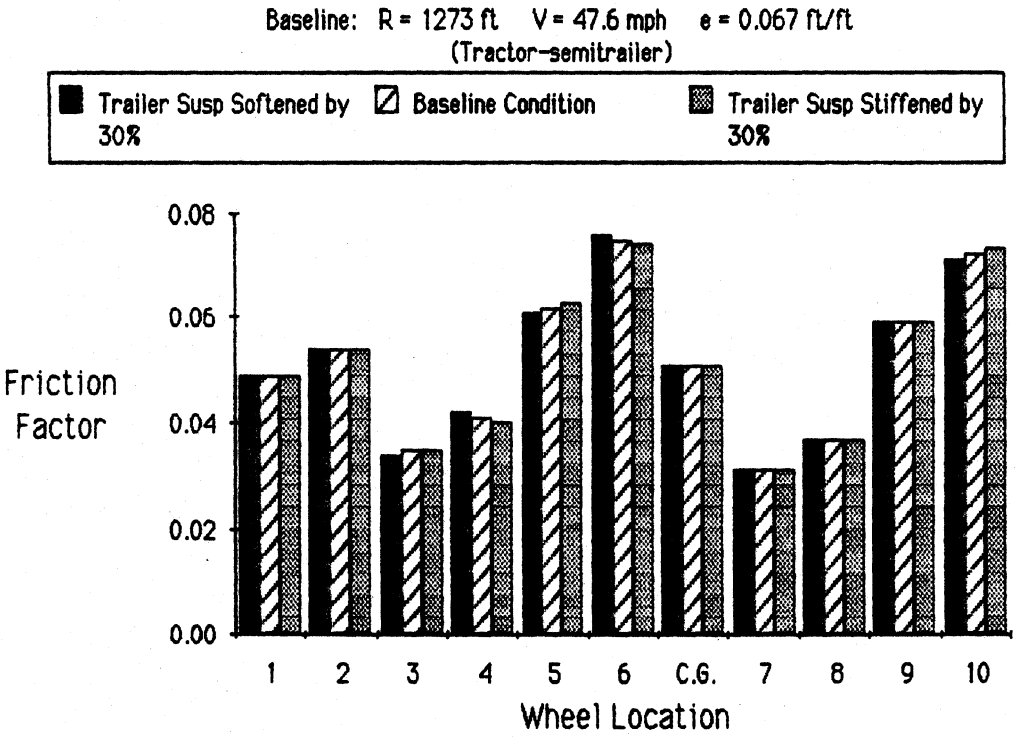

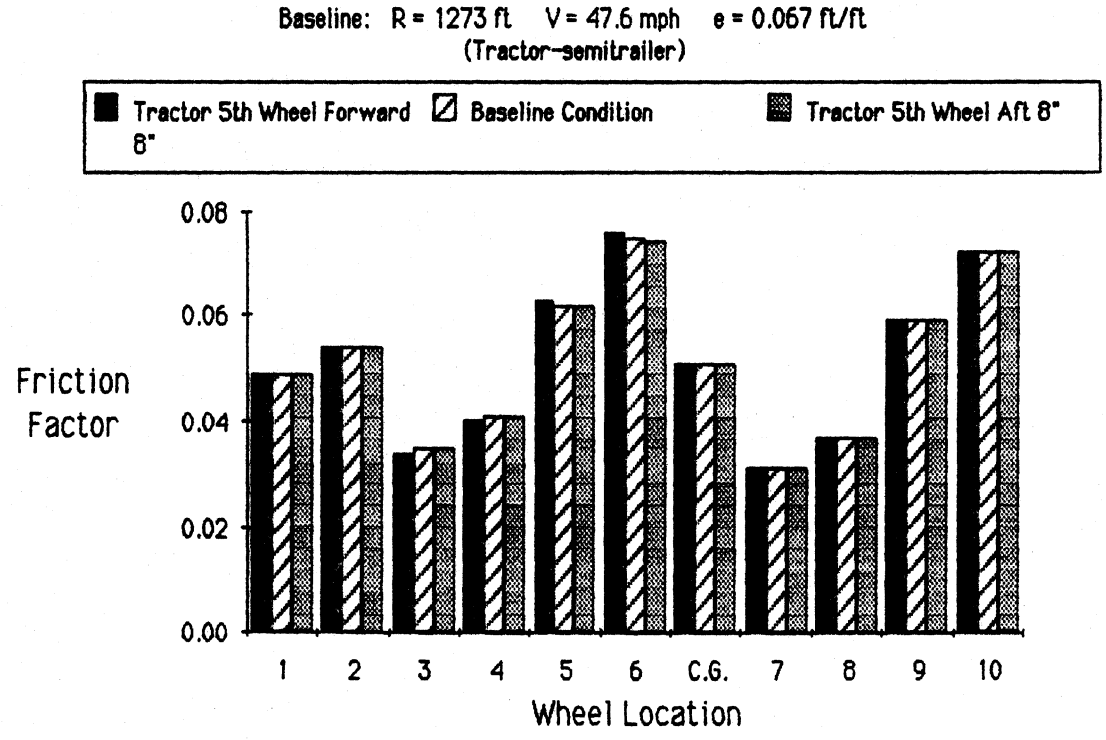

Figure 68. Tractor-semitrailer parameter variations.

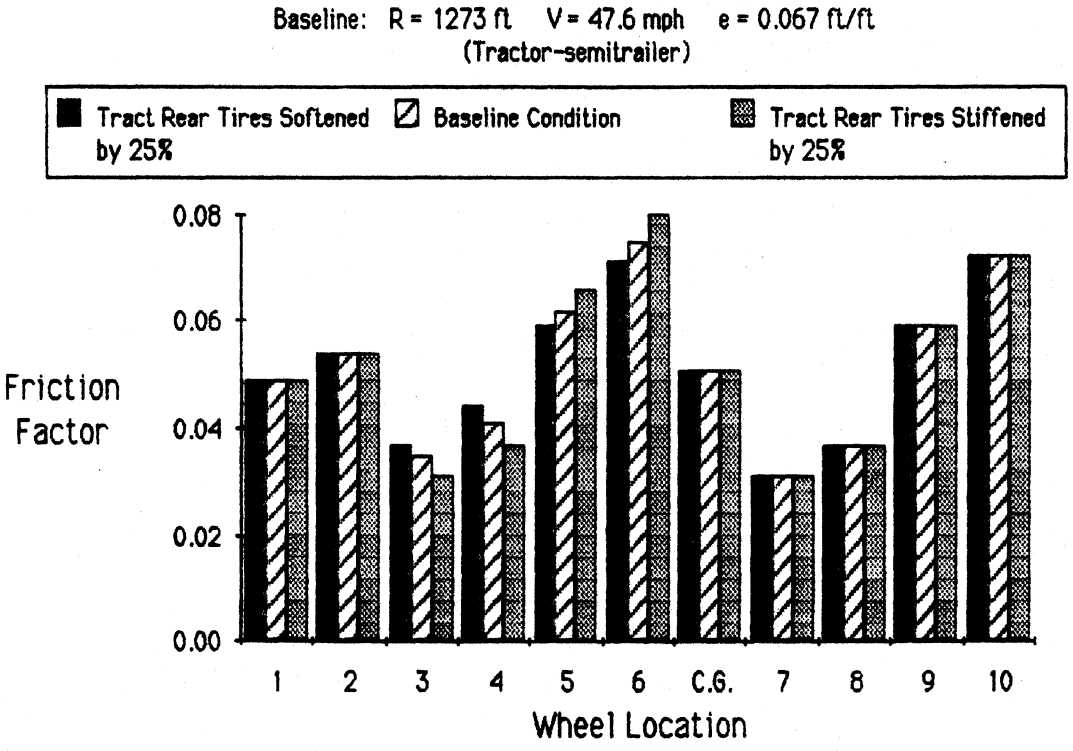

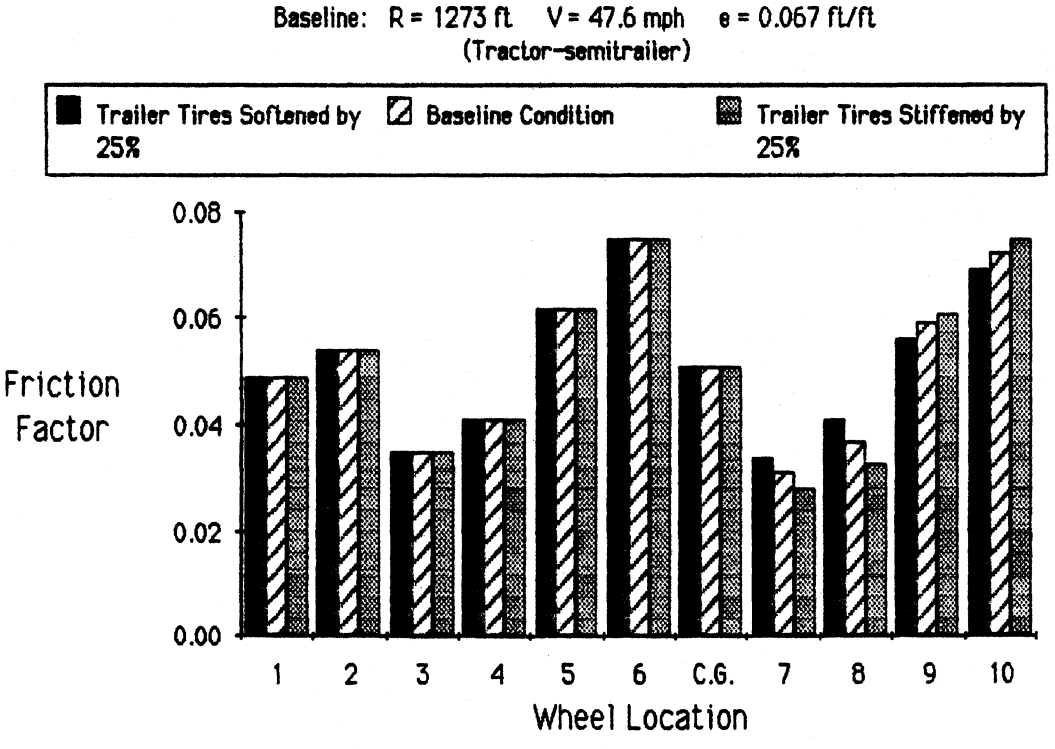

Figure 69. Tractor-semitrailer parameter variations.

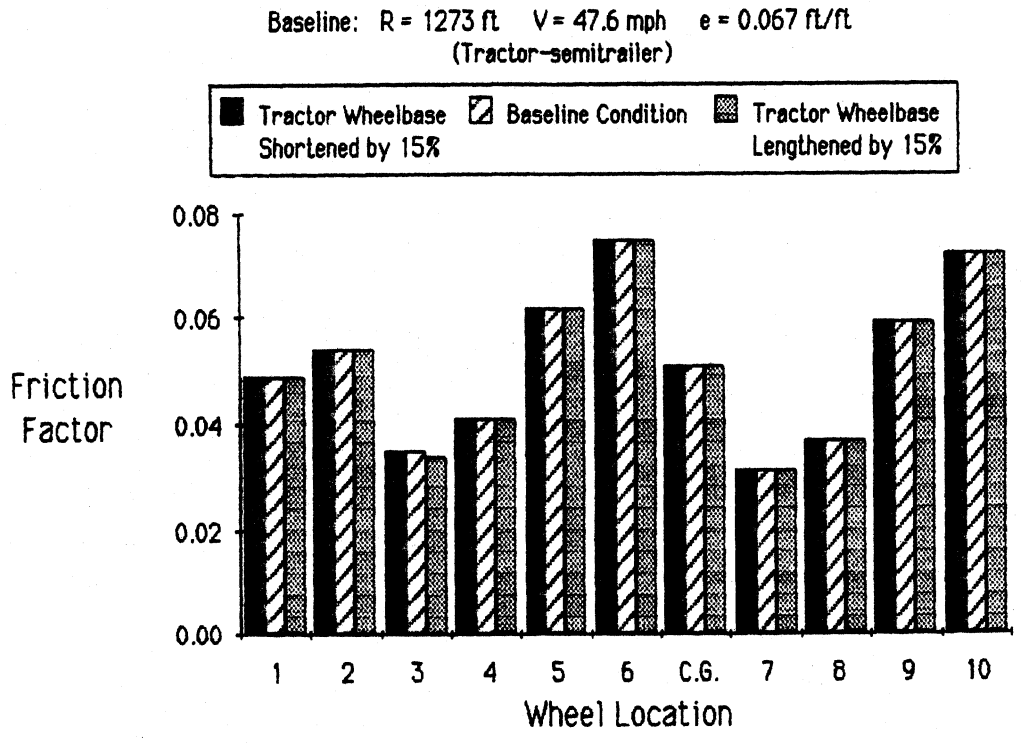

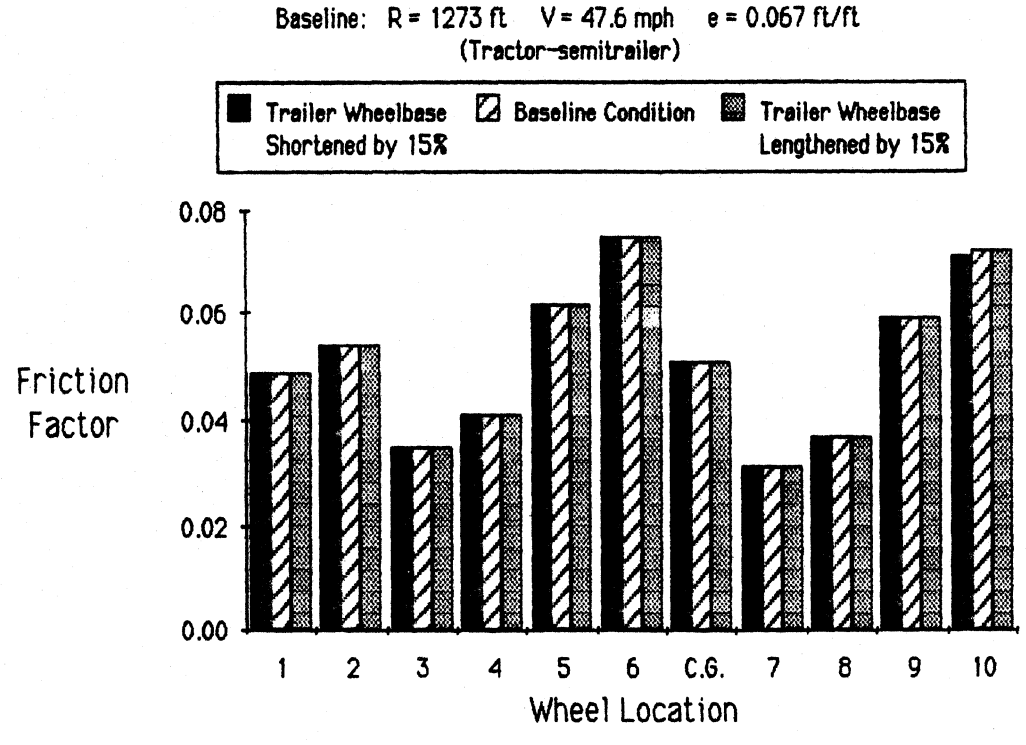

Figure 70. Tractor-semitrailer parameter variations.

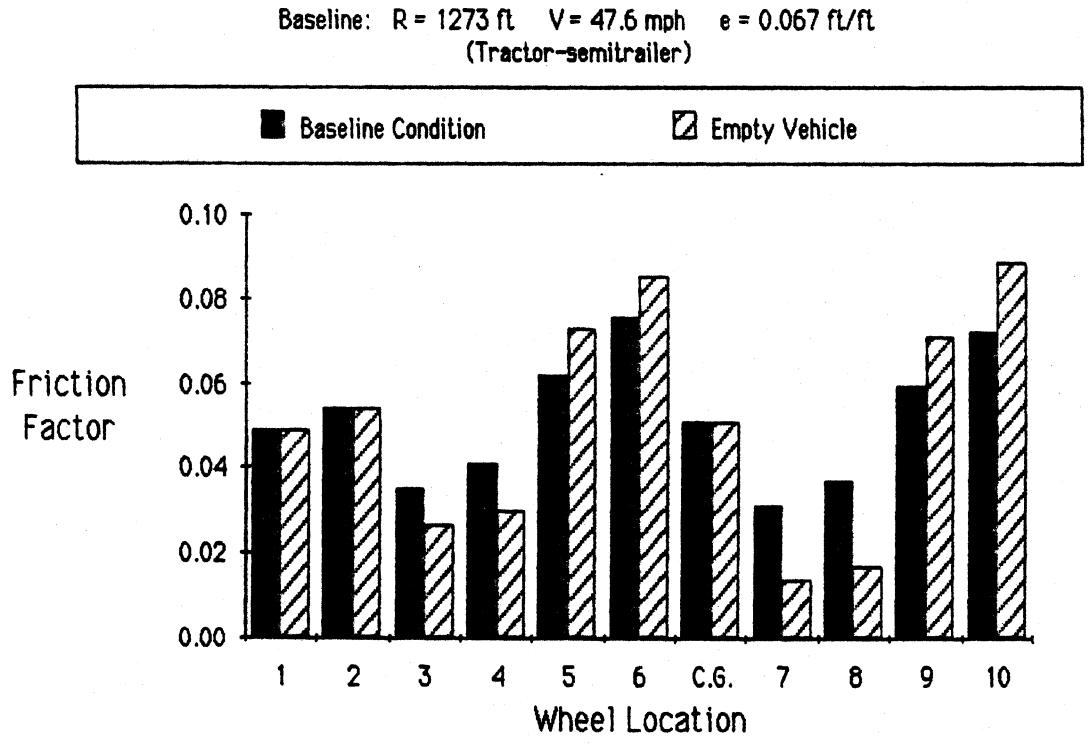

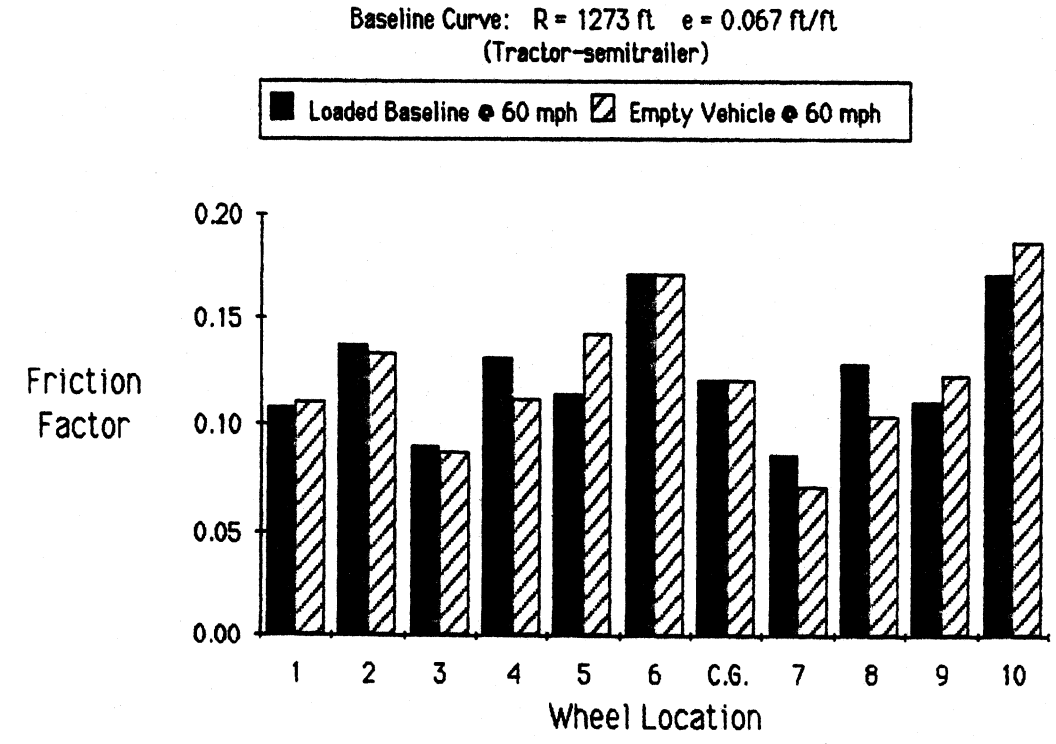

Figure 71. Tractor-semitrailer parameter variations.

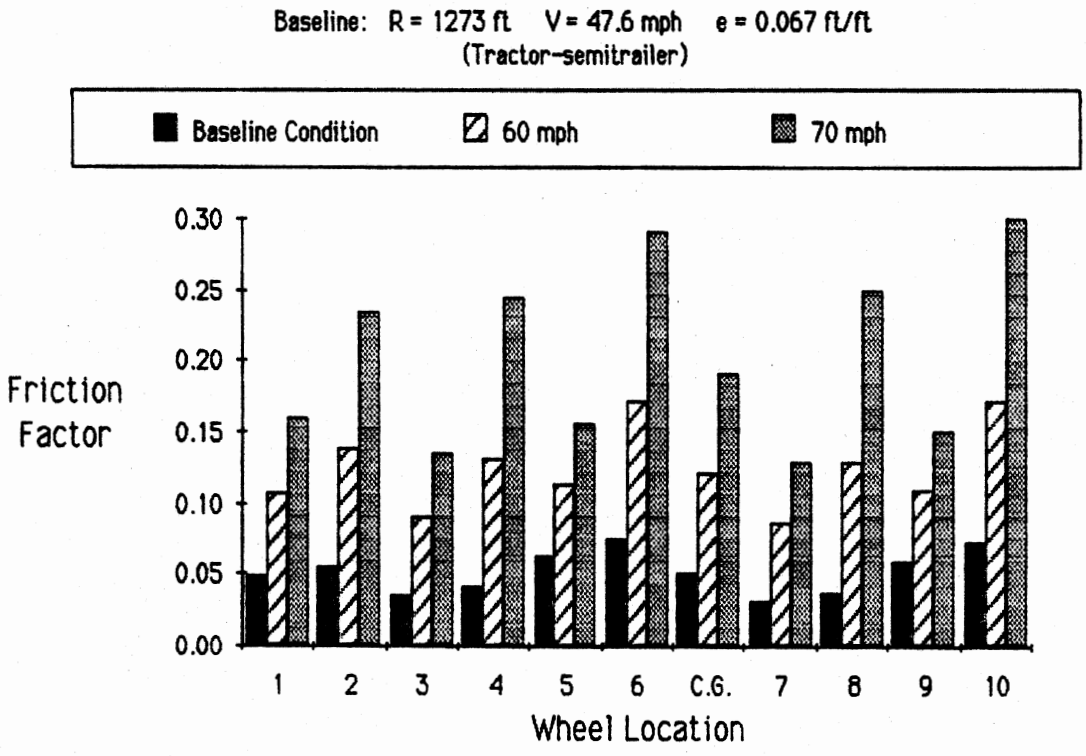

Figure 72. Tractor-semitrailer parameter variations.

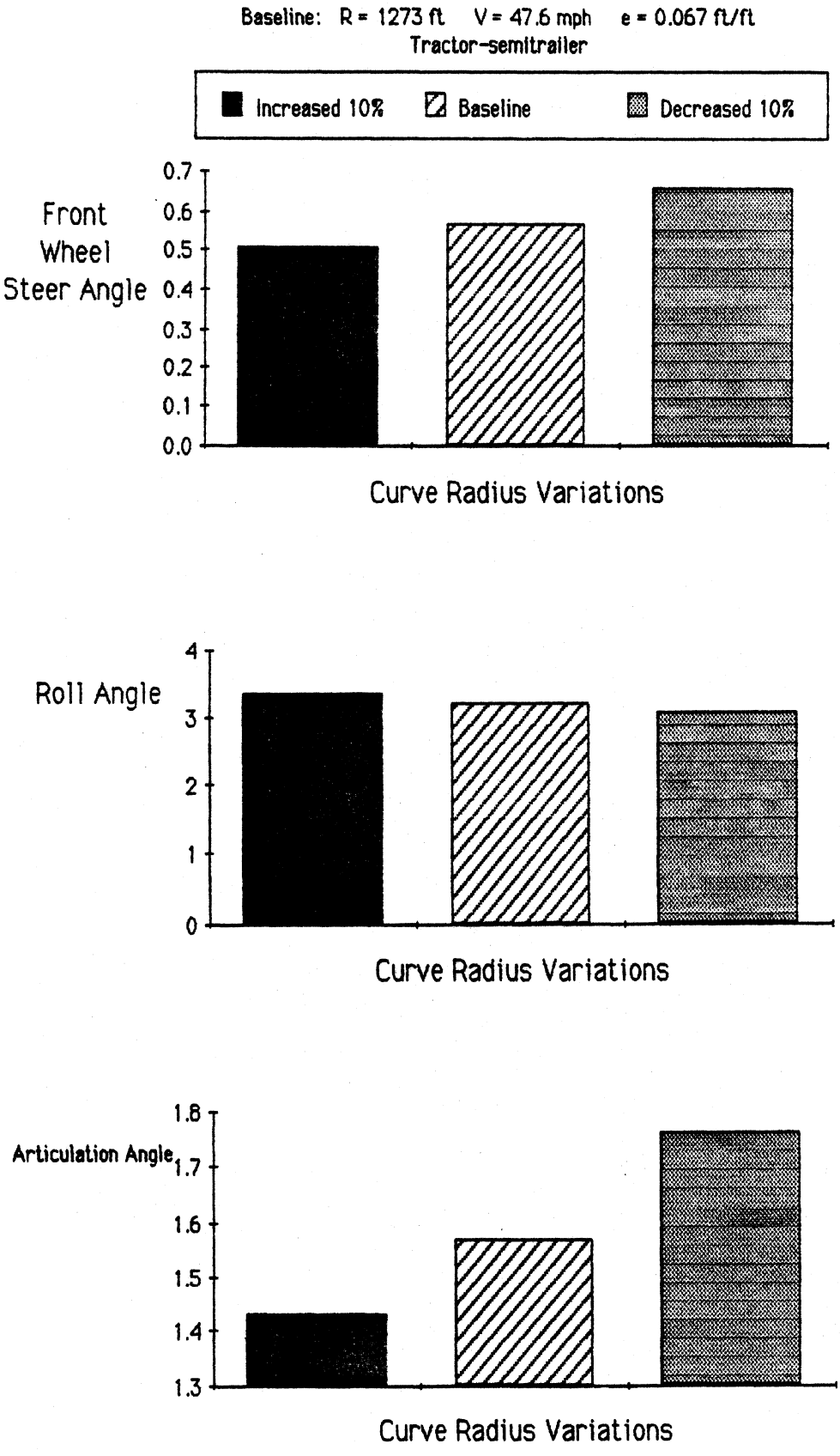

Figure 73. Tractor-semitrailer response variables.

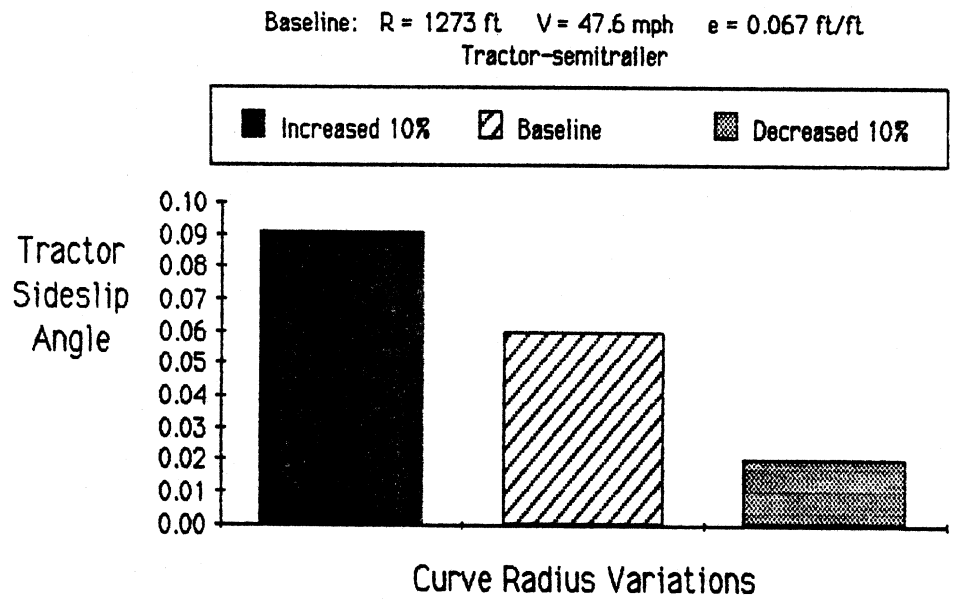

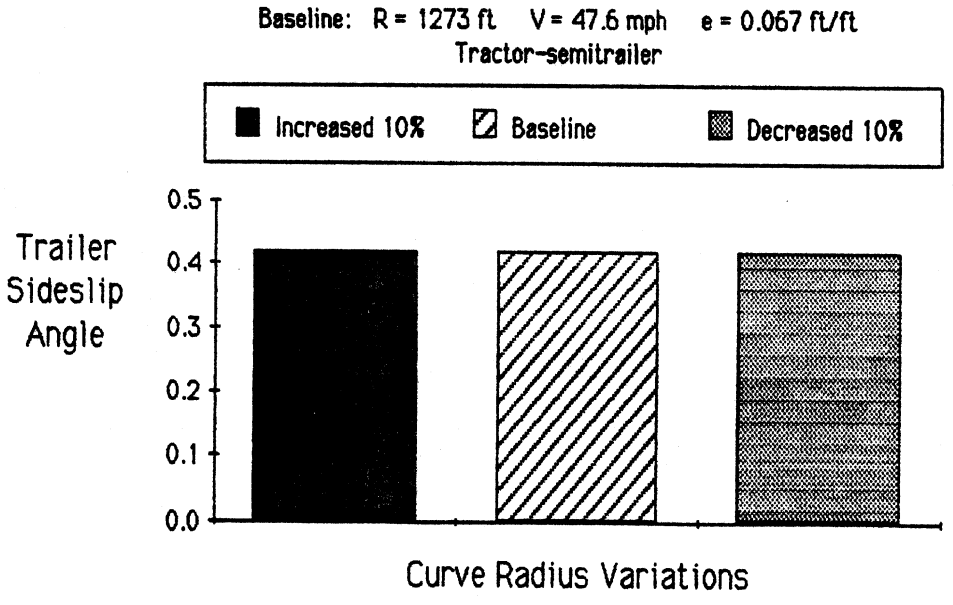

Figure 73 (cont)

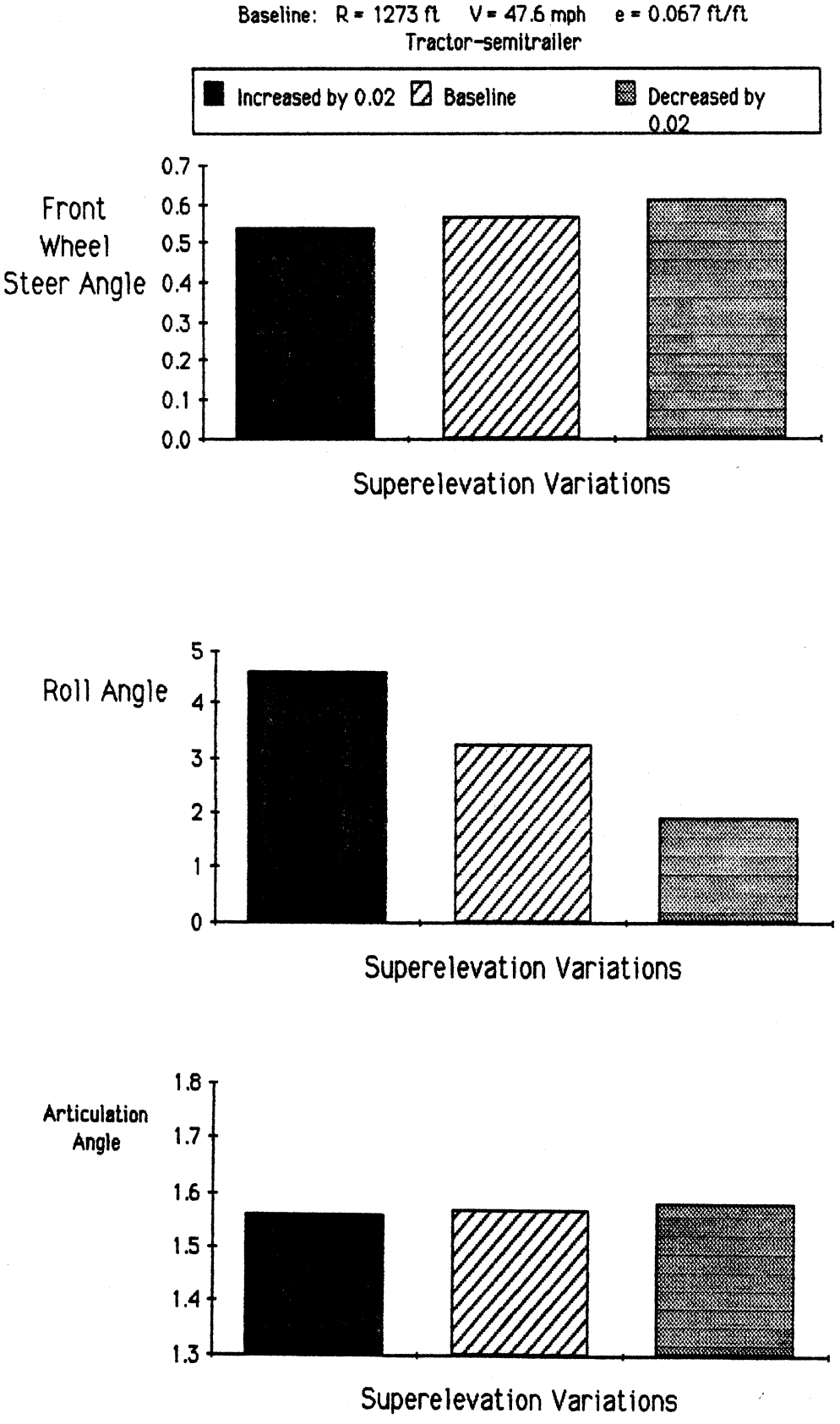

Figure 74. Tractor-semitrailer response variables.

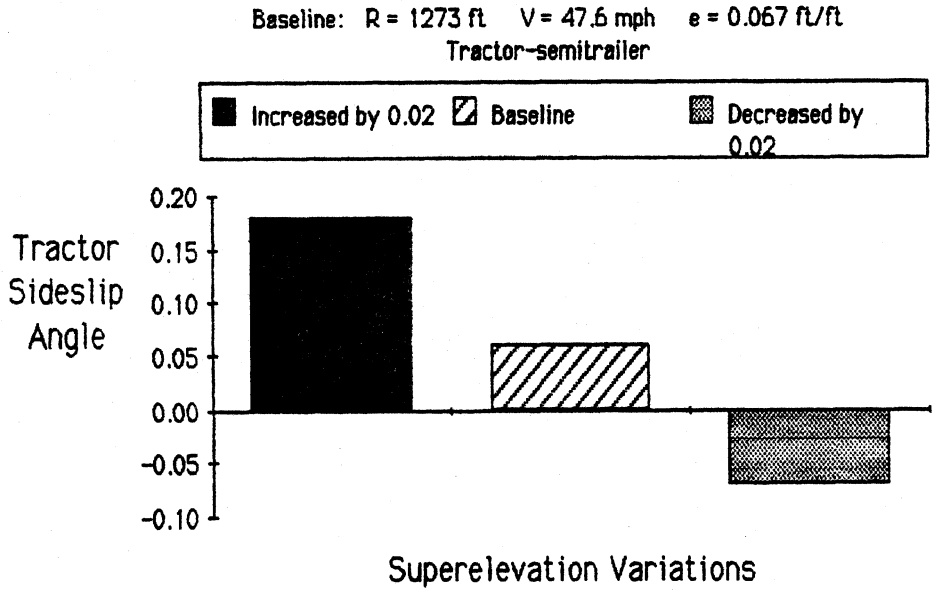

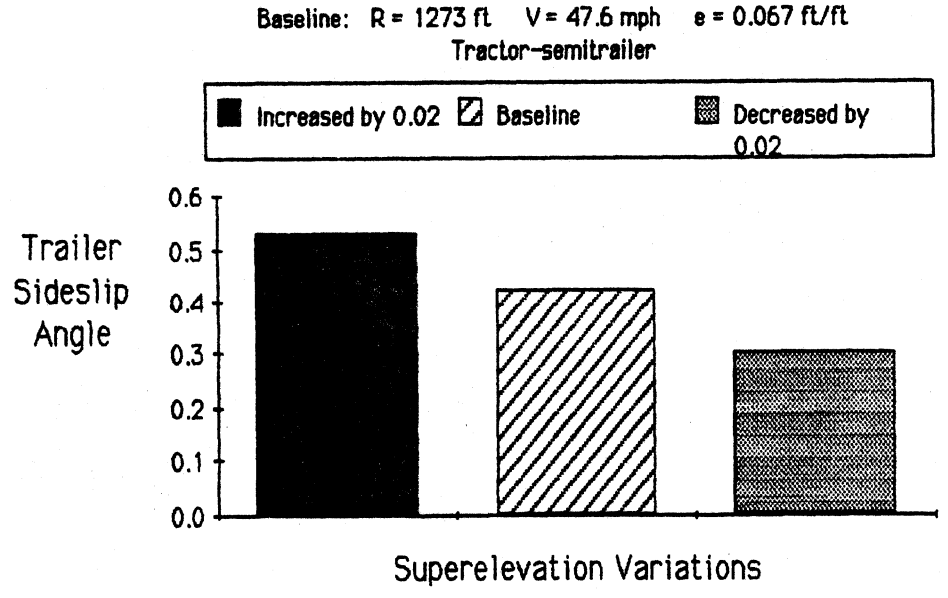

Figure 74 (cont)

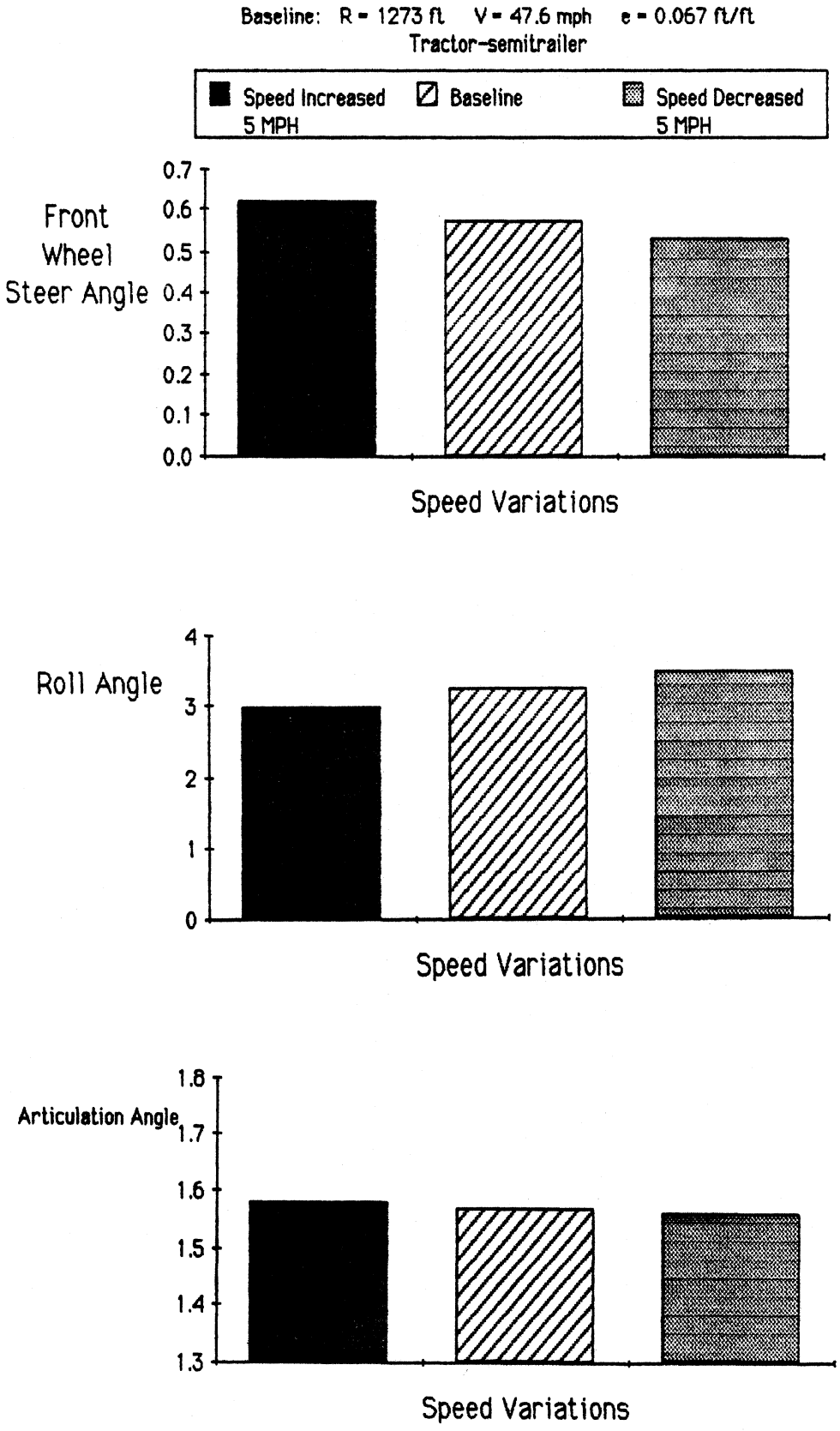

Figure 75. Tractor-semitrailer response variables.

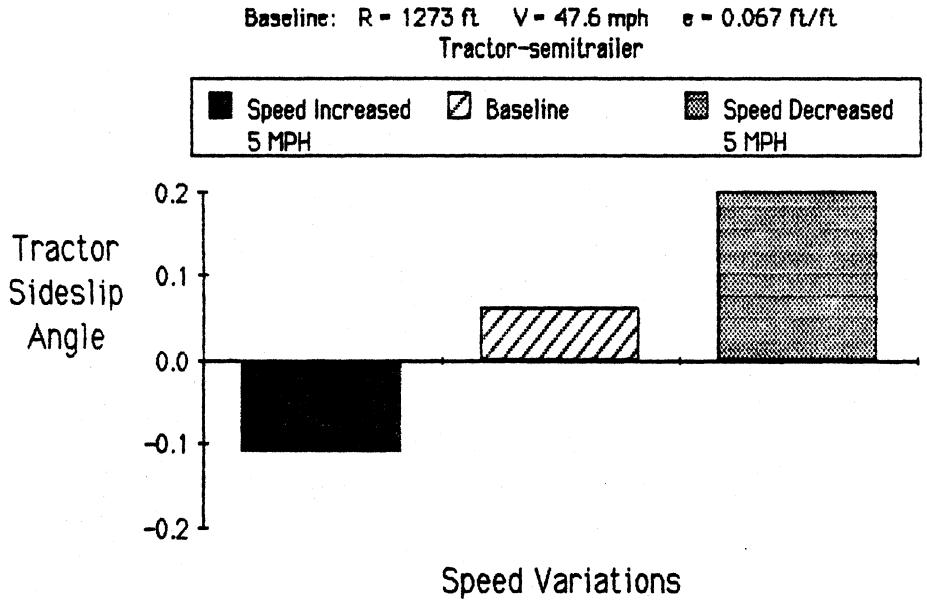

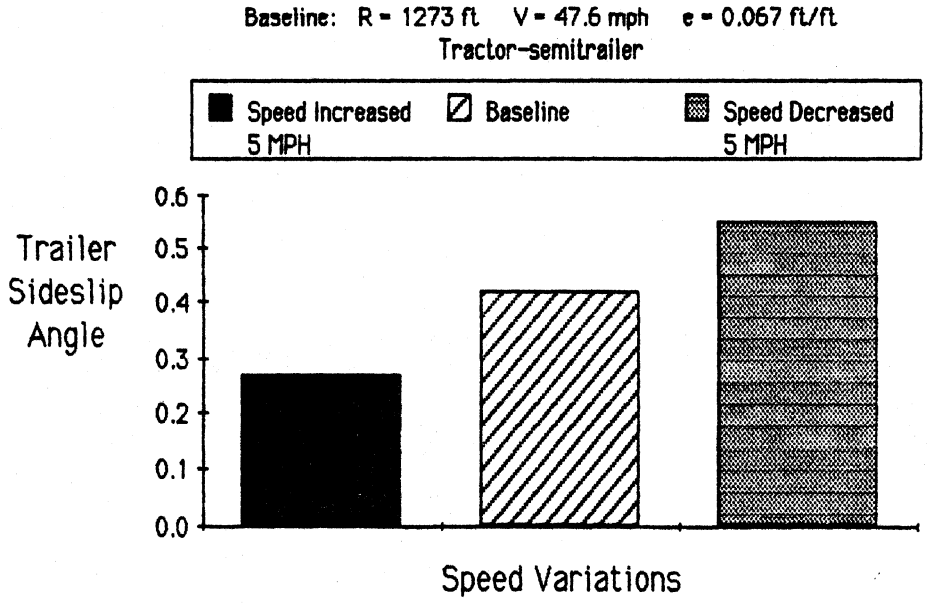

Figure 75 (cont)

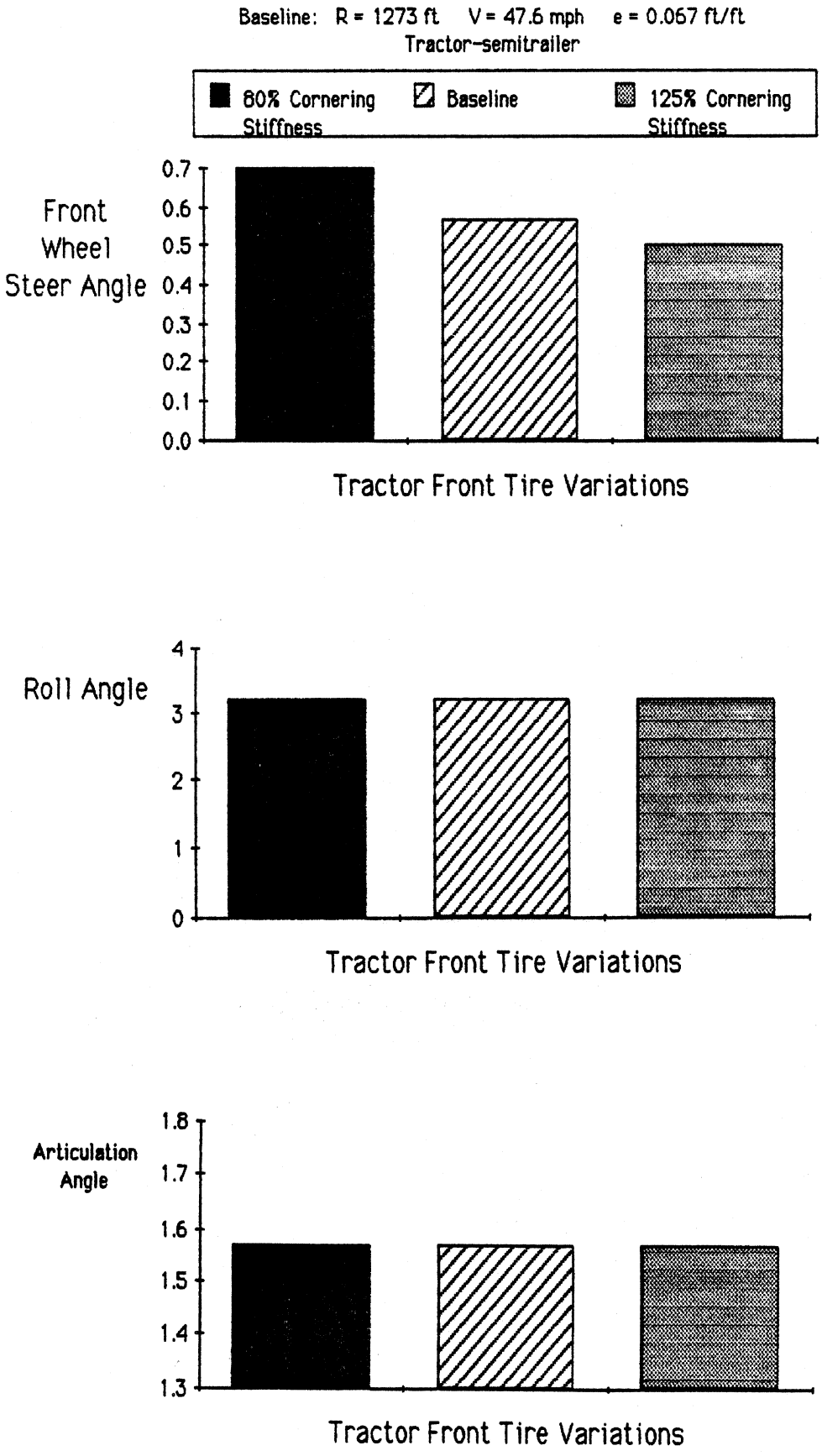

Figure 76. Tractor-semitrailer response variables.

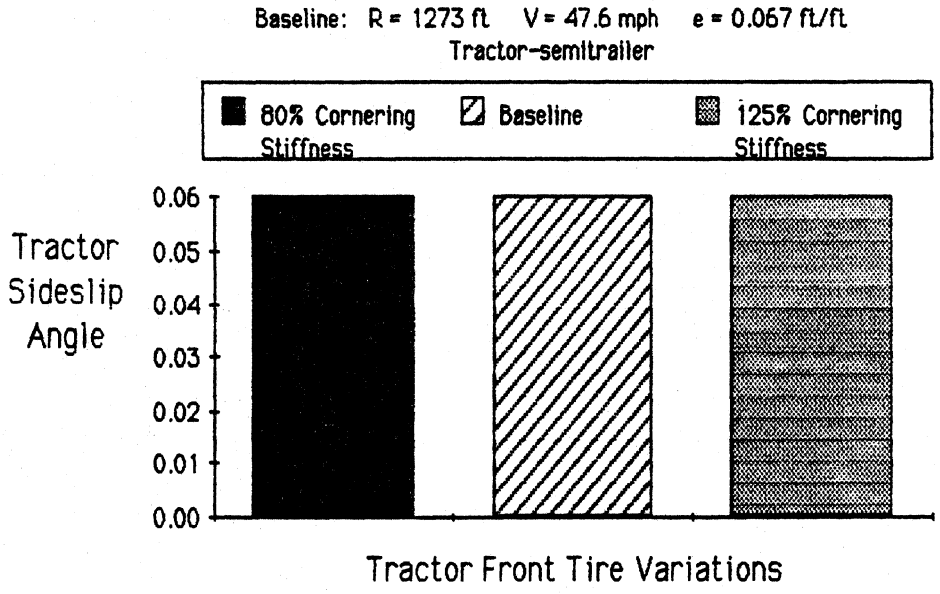

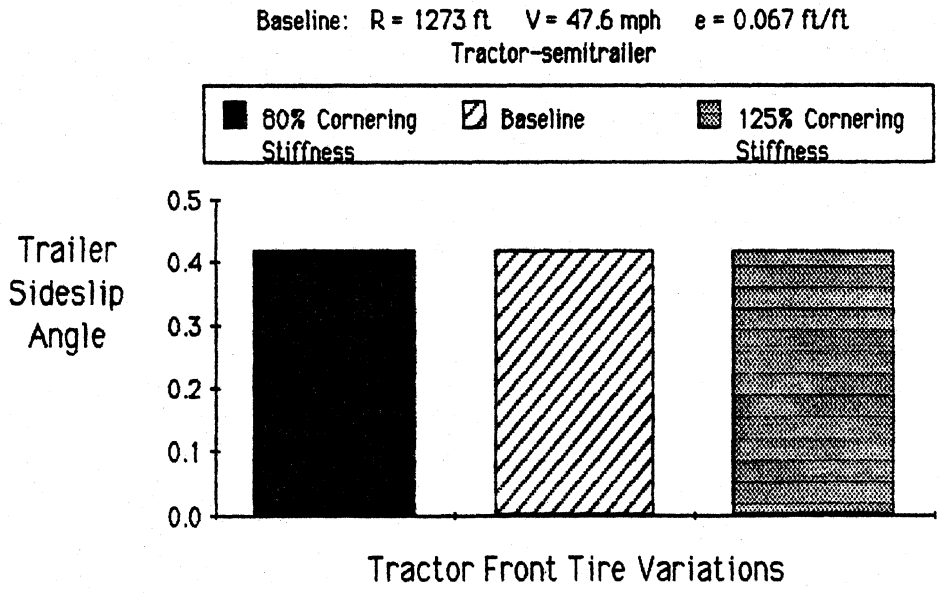

Figure 76 (cont)

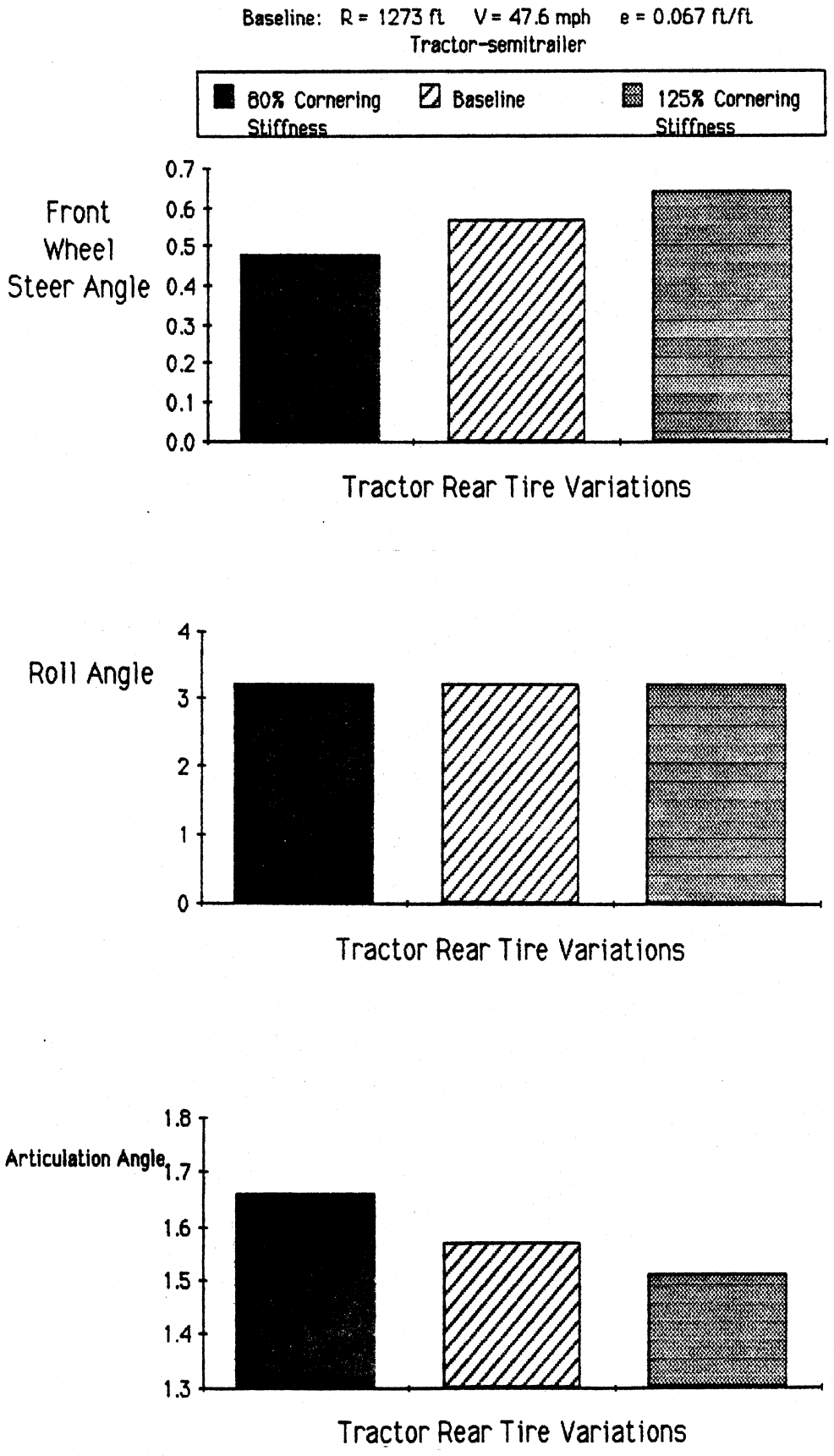

Figure 77. Tractor-semitrailer response variables.

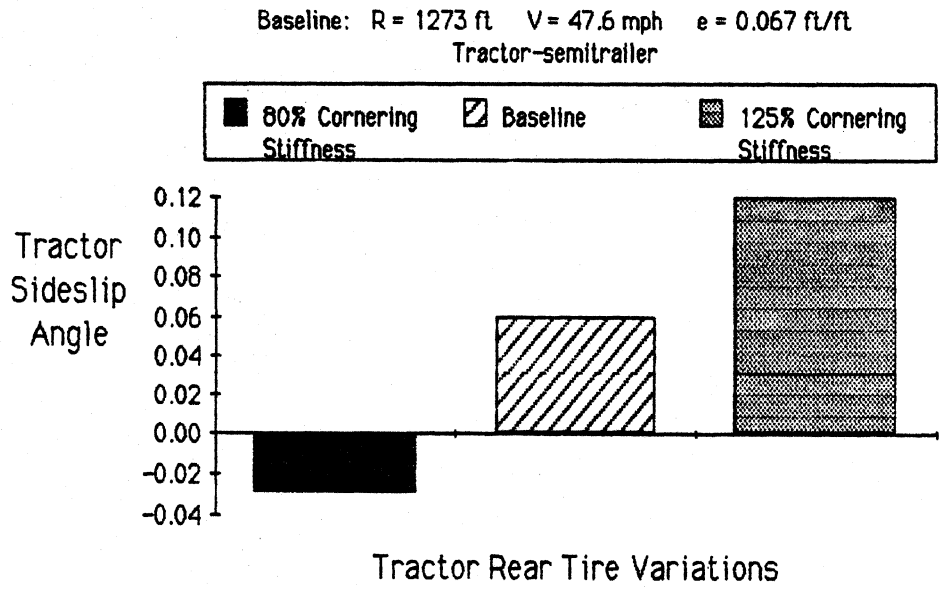

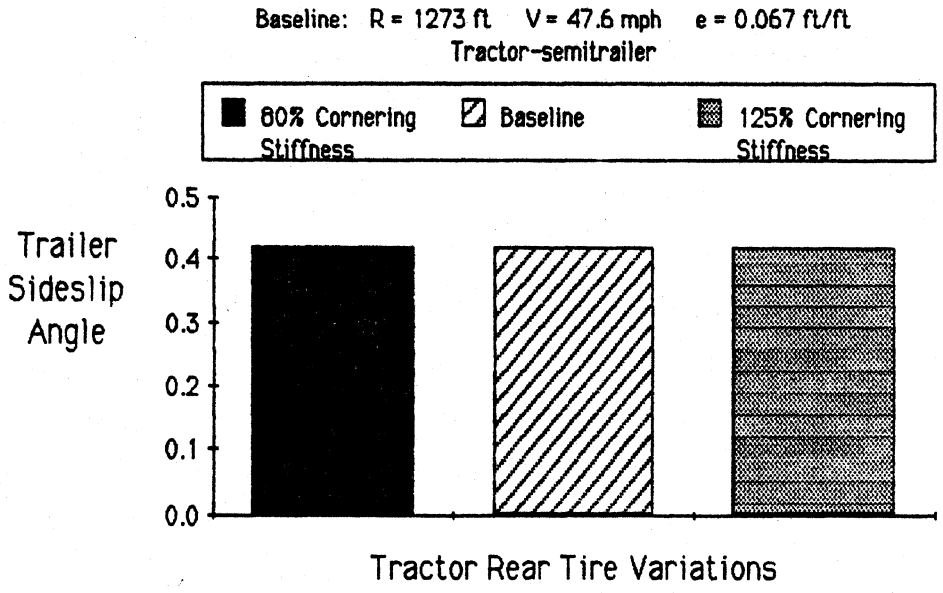

Figure 77 (cont)

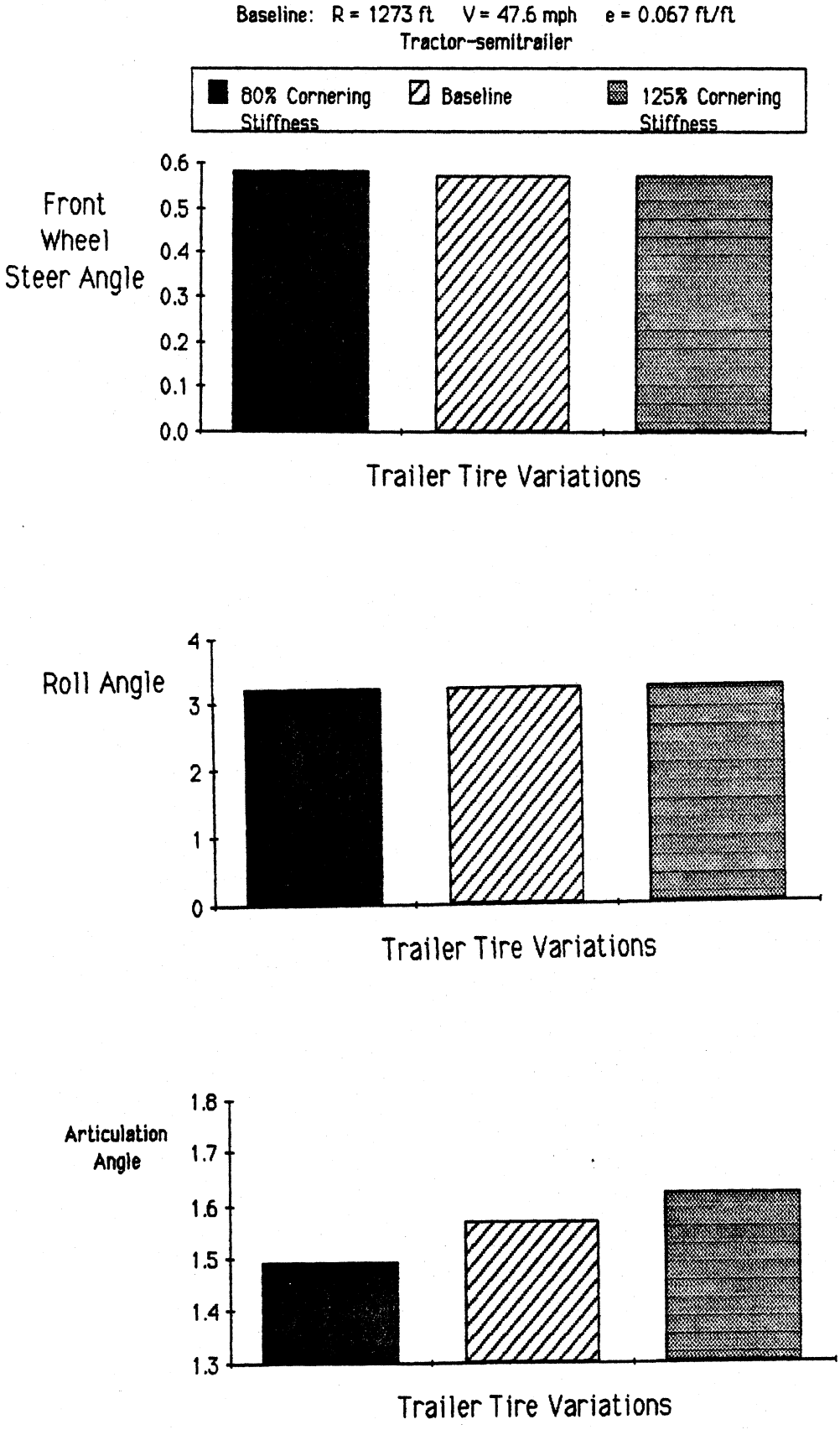

Figure 78. Tractor-semitrailer response variables.

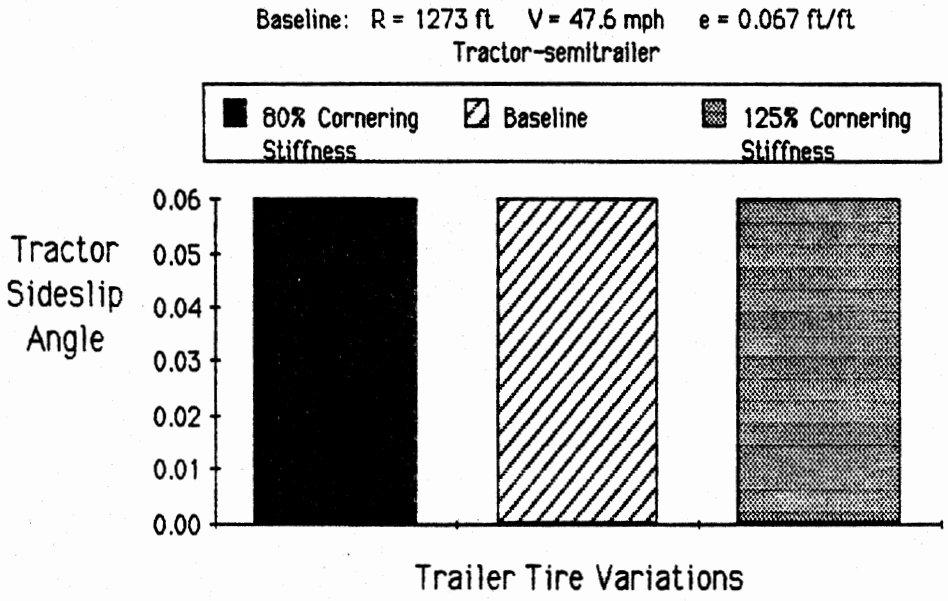

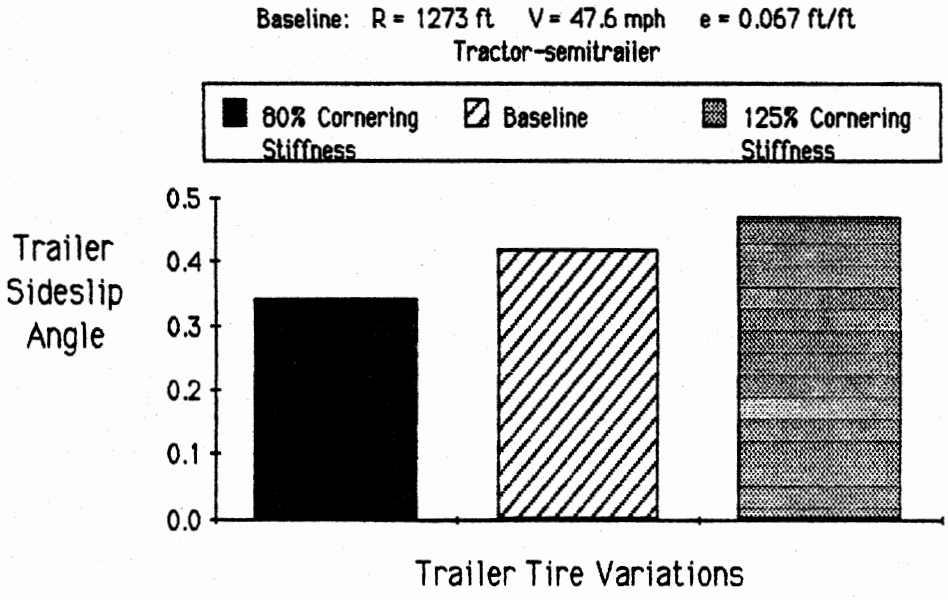

Figure 78 (cont)

five different vehicle response variables and are grouped according to a single parameter variation. For example, figure 73 illustrates the required tractor steer angle, tractor-semitrailer roll angle, articulation angle, tractor and semitrailer sideslip angles resulting from 10 percent changes in curve radii. Use of these vehicle response plots, in combination with the corresponding friction factor plots just examined, permit an understanding of how a vehicle can exhibit little or no change in friction factors despite significant variations of certain vehicle properties. As in the case of the passenger car, tire cornering stiffness variations produce little or no change in individual wheel friction factor values. However, figures 77 and 78 suggest that significant changes do occur in the vehicle response or "trim" condition as a result of these tire variations. Figure 76 shows that tractor steer angle alone is the vehicle response to a change in tractor front tire cornering stiffness. Changes in tractor rear tire properties, figure 77, result in a different tractor steer angle, articulation angle, and tractor sideslip response. And lastly, semitrailer tire variations seen in figure 78 only influence articulation angle and semitrailer sideslip response.

As was observed in the passenger car case and is seen here for the tractor-semitrailer, in figures 73 through 75, variations in highway curvature, superelevation, and vehicle speed have the greatest overall influence, not only in friction factor variations, but in terms of vehicle reponse variations as well. Figure 76 again shows highway grade to have no important effect upon the vehicle steady turning response. Variations in tractor-semitrailer suspension properties, figures G-2 and G-3 of appendix G, are seen to influence only the vehicle roll response. Fore/aft movement of the tractor fifth wheel, figure G-4 of appendix G, primarily affects the required tractor steer angle and the tractor/semitrailer sideslip responses. Vertical movement of the semitrailer mass center only influences roll response whereas fore/aft movement of the semitrailer mass center results in significant changes in articulation angle and vehicle sideslip, figures G-5 and G-6 of appendix G. Lastly, wheelbase variations seen in figures G-7 and G-8 of appendix G, show that tractor wheelbase variations influence the required tractor steer angle and its sideslip response, while variations in semitrailer wheelbase result in changes only to articulation angle and semitrailer sideslip response.

6.3 Sensitivity of Peak Friction Factors During Obstacle Avoidance Maneuvers

This section presents a summary of findings related to peak friction factor values occurring during a simulated obstacle avoidance (double-lane-change) maneuver. The Phase 4 model was used to simulate the earlier described lane-to-lane movement using a driver model [6]. The results seen here are for the same baseline passenger car and tractor-semitrailer. Both vehicles perform the same maneuver (same path input) and at the same speed of 56 mph (90 km/h). The curve geometry corresponds to curve site 1 (left turn). After reaching a steady turning condition on the superelevated curve in the outside travel lane, the driver model steers the vehicle to the inside lane (12 ft (3.6 m) laterally), and then back again to the original lane. The lateral lane change displacements occur over a total forward travel distance of approximately 300 ft (91 m). The "severity" of the maneuver would be classified as "moderate" meaning that it is more demanding than a standard passing maneuver, but considerably less demanding than an evasive emergency maneuver.

Figure 79 shows values of peak friction factor produced at each wheel location and the mass center (point-mass value) of the passenger car during the described baseline maneuver. Also shown on the same plot are peak friction factor values corresponding to runs performed with smaller and larger rates of highway superelevation. The results indicate that although the required friction levels are several times those required for simple steady turning on the same curve, the difference in peak friction factor values due to different rates of highway superelevation differ only by the amount of the superelevation.

Figures 80 and 81 present similar plots showing results of speed changes and tire property variations. The influence of forward speed is significant as seen in figure 80; however, the degree of variation at individual wheel locations is more or less comparable to the variation experienced by the mass center (point-mass). In figure 81, variations in tire properties are considered. The results indicate that peak friction factor values depend only weakly on the lateral effectiveness of the vehicle's tires.

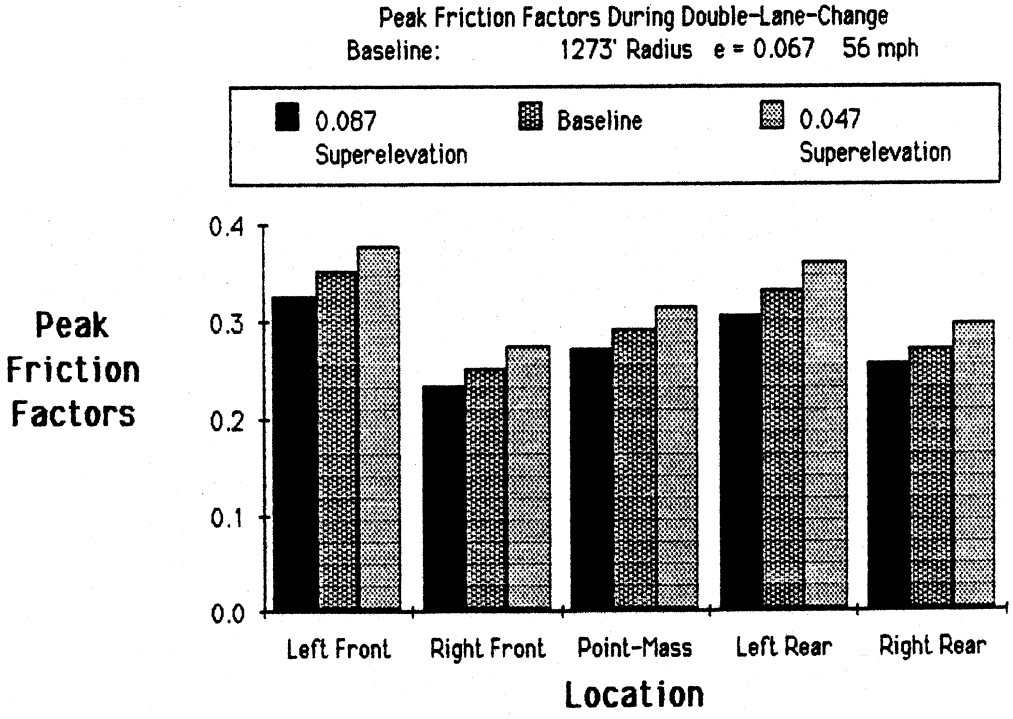

Figure 79. Peak friction factors occurring during obstacle avoidance maneuver; passenger car.

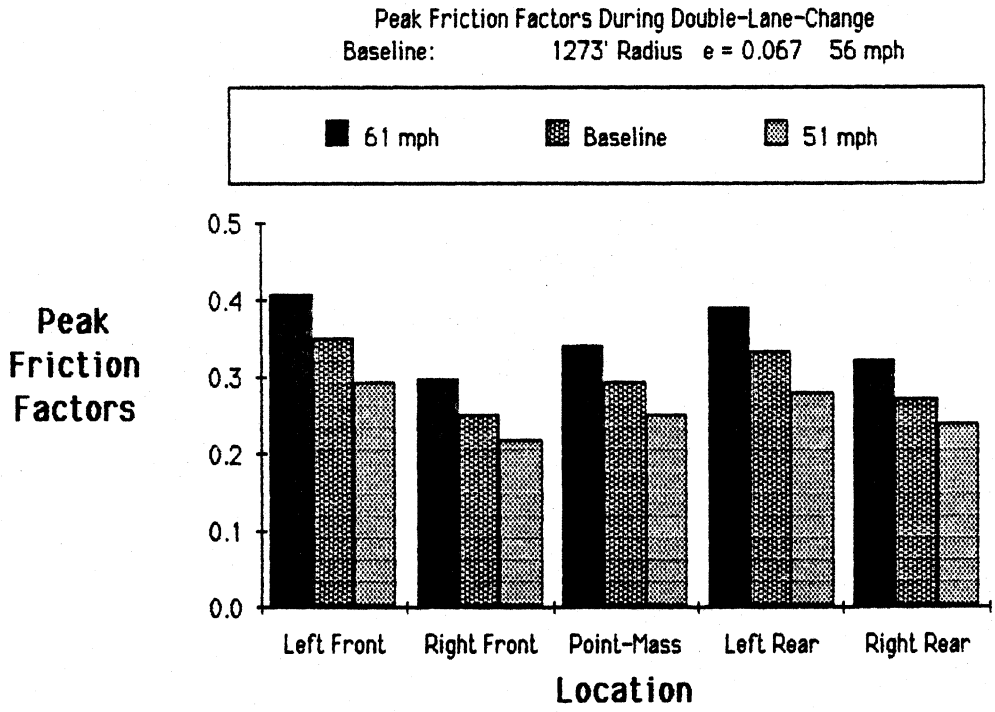

Figure 80. Peak friction factors occurring during obstacle avoidance maneuver; passenger car.

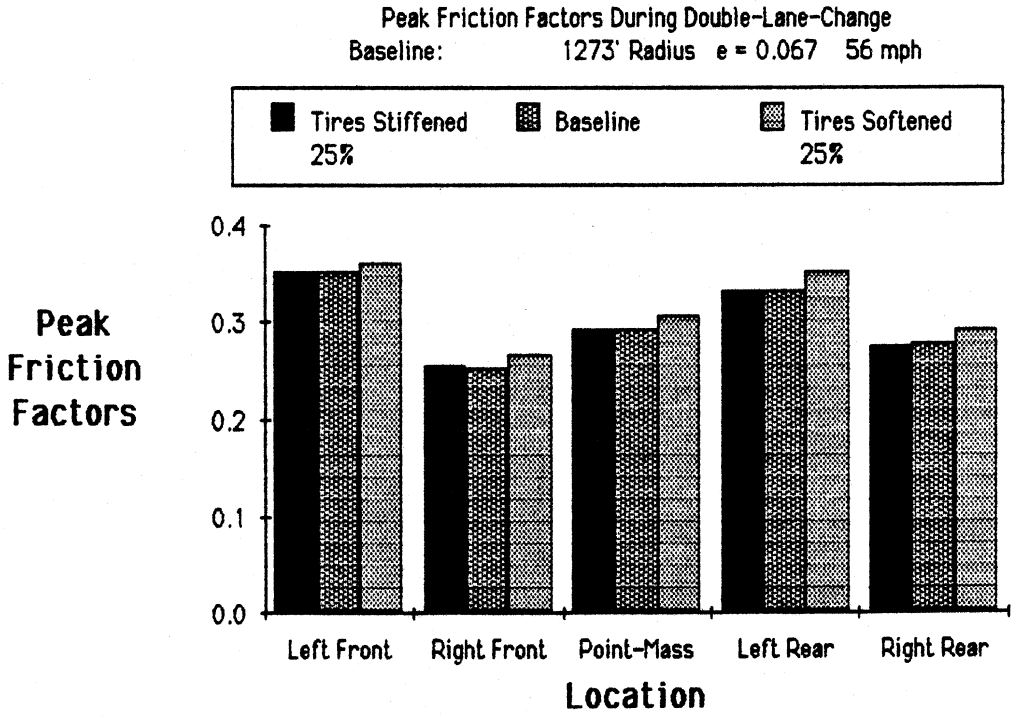

Figure 81. Peak friction factors occurring during obstacle avoidance maneuver; passenger car.

Lastly, figure 82 compares peak friction demand for individual wheel locations of the baseline passenger car during the obstacle avoidance maneuver with steady turning friction factor requirements at the same wheel locations. The plot shows that peak friction demands exceed steady turning friction requirements by factors of 2.5 to 3.5 depending upon the wheel location. The peak friction factor values also exhibit far greater variation from wheel-to-wheel than do the steady turning friction factor values. Section 6.4 will examine, by gradually reducing the level of the available tire/road friction, the minimum friction level requirement of the tire/road surface such that this particular obstacle avoidance maneuver can still be performed in a stable manner.

Figures 83 through 86 show a set of similar plots for the baseline tractor-semitrailer (the odd numbered wheel locations in these figures refer to the left side or inside wheels). The same basic findings apply to the tractor-semitrailer vehicle with the mild exception of figure 85. The influence of tire property variations seen in this figure is somewhat stronger than that seen for the passenger car. The sensitivity differences observed here are primarily attributable to the previously noted differences in vertical load sensitivities of truck tires and passenger car tires. Finally, figure 86 compares peak friction factor values experienced by the tractor-semitrailer during the obstacle avoidance maneuver with friction factor values required for steady turning on the same curve. As in the passenger car case, the peak values exceed the steady turning values by factors of 2.5 to 3.5 depending upon the wheel location. However, unlike the passenger car results, the tractor-semitrailer exhibits significant wheel-to-wheel variations in friction factors for steady turning as well as for peak friction factor values in the obstacle avoidance maneuver. The largest peak friction factor value observed for the tractor-semitrailer, 0.39, is at wheel location 9 (rearmost inside wheel), while the maximum value seen for the passenger car is 0.36 at the left front (inside) wheel location.

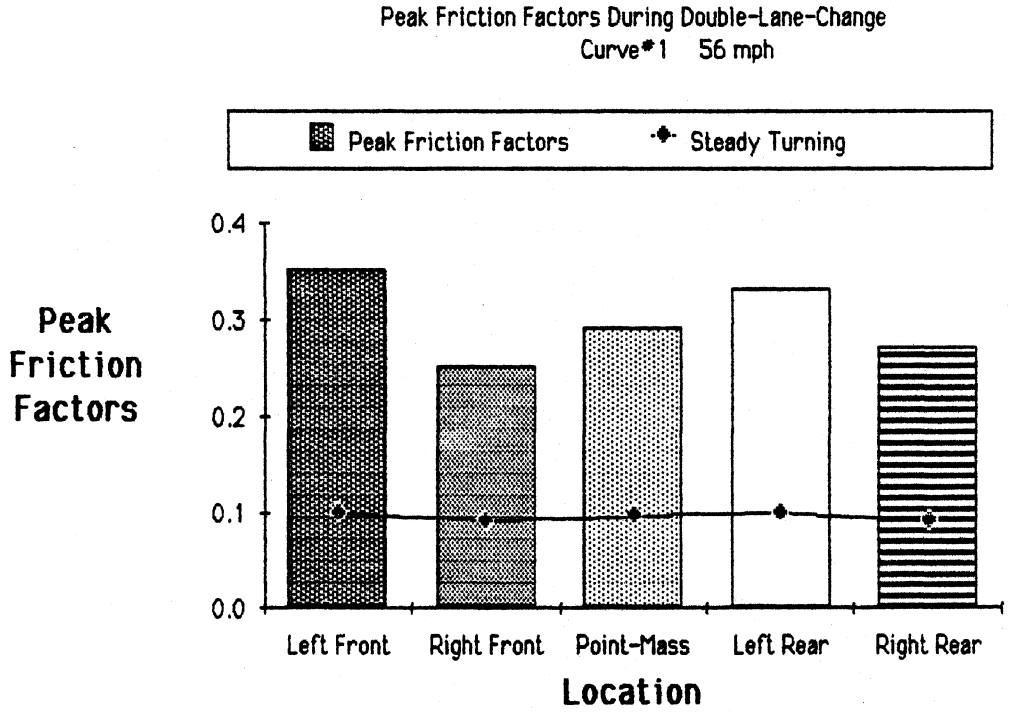

Figure 82. Peak friction factor comparison; obstacle avoidance maneuver vs steady turning maneuver; passenger car.

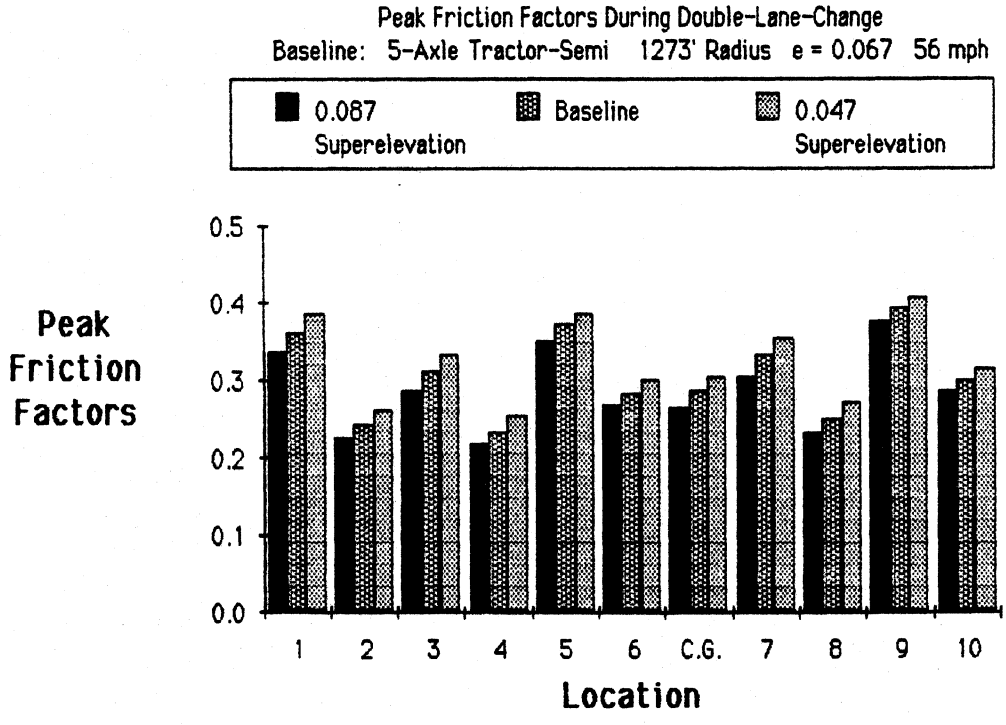

Figure 83. Peak friction factors occurring during obstacle avoidance maneuver; tractor-semitrailer.

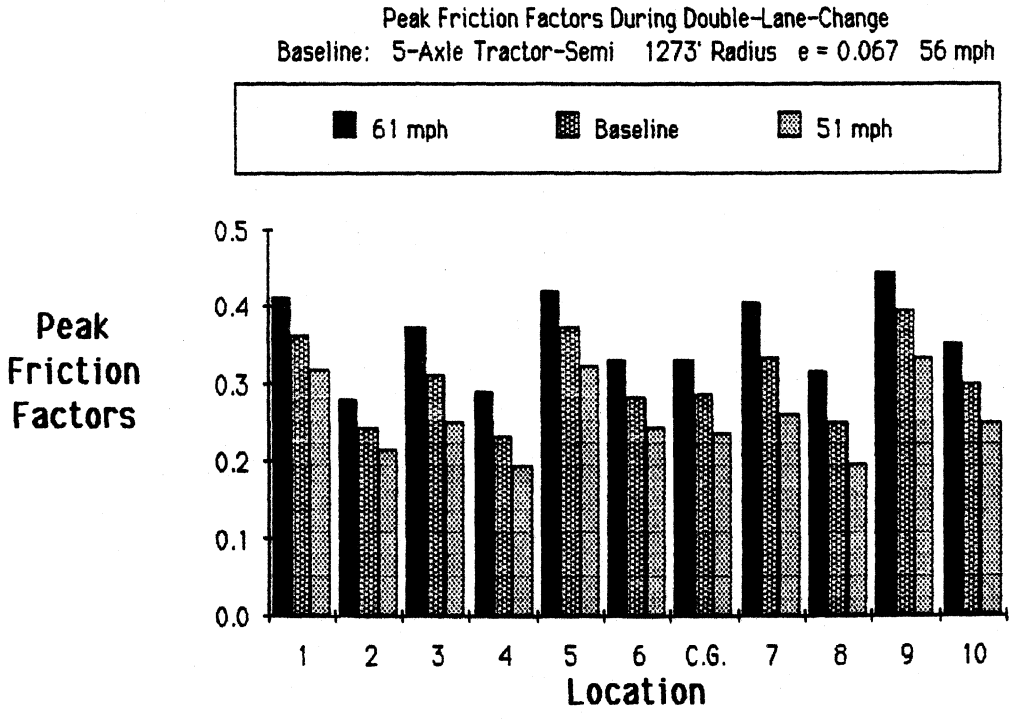

Figure 84. Peak friction factors occurring during obstacle avoidance maneuver; tractor-semitrailer.

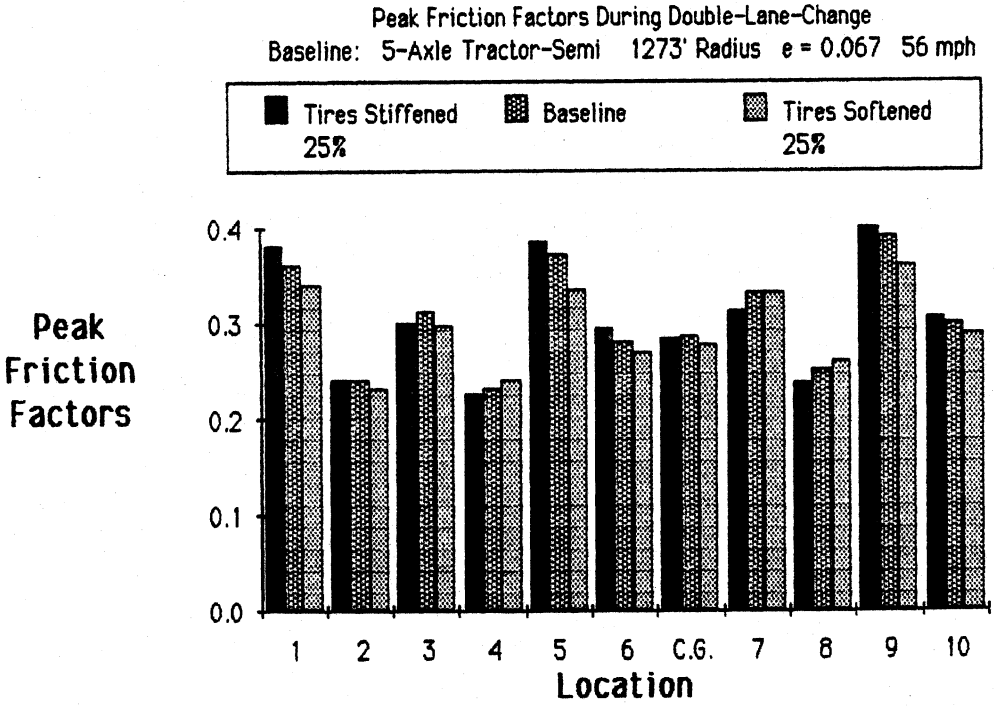

Figure 85. Peak friction factors occurring during obstacle avoidance maneuver; tractor-semitrailer.

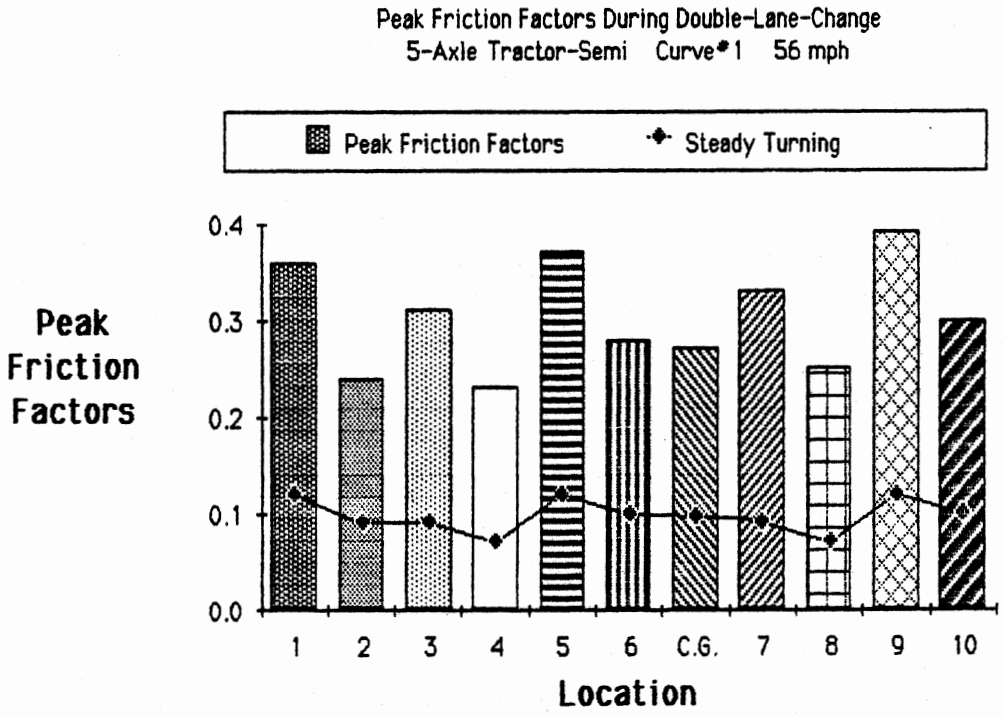

Figure 86. Peak friction factor comparison; obstacle avoidance maneuver vs steady turning maneuver; tractor-semitrailer.

6.4 Steady Turning and Obstacle Avoidance Maneuvers Under Low Friction Conditions

This section presents results of a brief study which examined how low friction conditions may influence observations which heretofore assumed that the demanded or required friction at each wheel location was available during steady turning and obstacle avoidance maneuvers. In this section simulation runs identical to those just conducted were performed under low friction conditions. The level of maximum tire/road friction was now lowered to various values in the vicinity of the point-mass friction recorded during the high friction runs. The purpose of this study was to examine how wheel-to-wheel variations in friction factor values might influence the directional stability of the driver/vehicle system under these extreme conditions. In general, the results show that as long as the maximum tire/road surface friction level is at least as great as the point-mass (c.g.) value observed during the high friction conditions, the same vehicle maneuver can be performed in a stable manner.

Figure 87 summarizes the results for the steady turning maneuver under low friction conditions. This figure indicates that steady turning runs performed on surfaces having maximum friction levels below a certain value resulted in uncontrollable vehicle behavior. The minimum friction level needed to guarantee stable curve negotiation for the passenger car under these conditions was approximately equal to the point-mass friction factor value. For the tractor-semitrailer, the necessary friction level was approximately 10 percent greater than that required for the passenger car. Even though certain tires may saturate for short periods of time under these friction conditions, the driver/vehicle systems are still able to perform the steady turning maneuver with no unusual vehicle or driver steering behavior. For friction levels below the point-mass value, the nature of the instability that does occur is, first, a slow and gradual loss of path control with the vehicle plowing to the outside of the turn. This is later followed by a "spin-out" or loss of directional control, as the driver increases the steering angle attempting to regain the path as seen in figure 88.

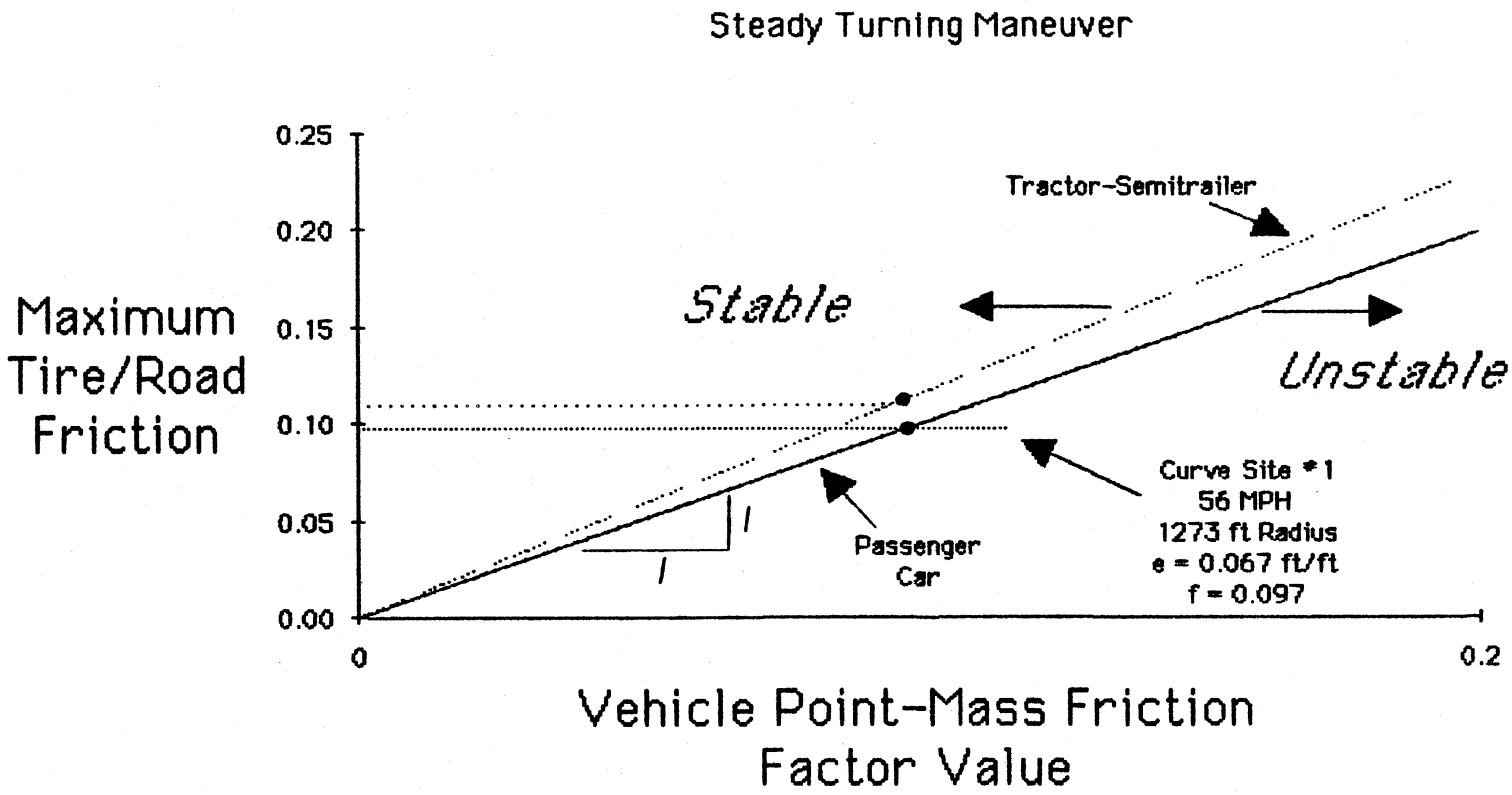

Figure 87. Tire/road friction necessary for stable operation under low friction conditions; steady turning maneuver.

tire/road friction < point-mass value

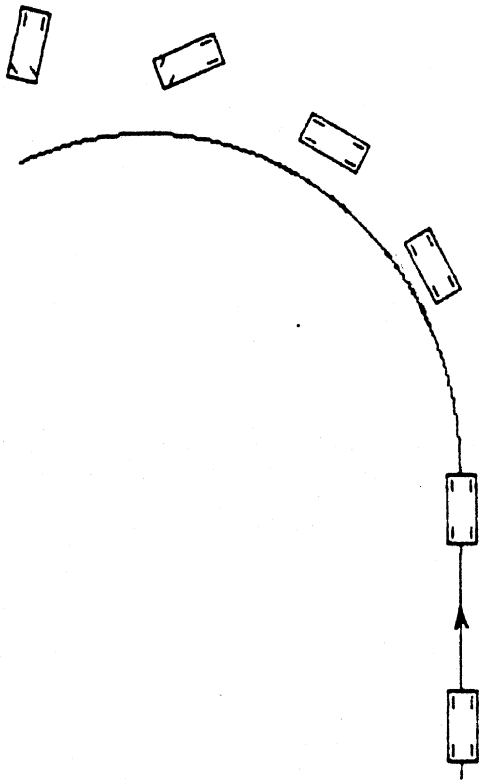

Figure 88. Loss of directional control experienced by passenger car under low friction conditions.

Figure 89 summarizes the results of the low friction obstacle avoidance maneuvers. As observed for the steady turning maneuver, the results show that if the tire/road friction coupling is at least as great as the peak friction factor value experienced by the mass-center during the high friction runs, the vehicle maneuver can be performed in a stable and near normal manner. Again, even though several tires undergo short periods of lateral force saturation during the maneuver, the driver/vehicle systems were able to perform the maneuver very similarly to that seen in the high friction cases. For cases in which the tire/road friction coupling is slightly less than the minimum value, the vehicles exhibited different forms of directional and path instability. The passenger car, for example, begins the turn to the inside lane but is unable to recover its directional stability and continues spinning in the same direction. During the spin, the vehicle mass center moves first to the inside lane, and then back across both lanes to the outside of the curve. The tractor-semitrailer experienced loss of lateral path control during return to the initial travel lane. Although the vehicle did not jackknife, it did overshoot its return to the initial lane by a considerable extent (toward the outside of the curve) and would have encountered a guard rail or steep side slope under most actual highway circumstances.

6.5 Analytical Friction Factor Expressions

From the equations for the steady turning models contained in appendices A and B, symbolic expressions can be formed which relate the friction factor values to the various model parameters and vehicle response variables. Unfortunately, most of these expressions can be quite complex in their complete form. Normally, very little insight is gained by examining such complicated formulas. However, the simplest of these friction factor expressions occur for the two-axle model and are presented here to illustrate the nature of the parametric relationships. Equations (8) through (11) show the friction factor expressions corresponding to the left front, right front, left rear, and right rear wheel locations, respectively, of a passenger car:

$$ff_l = C_{af}(v/V + d_f/R - d_{FW}) \,/\, \{ N_{sf}/2 + [d_f(p - p_r) + z]K_f - (\phi - e)K_f/(2TT_f) + C_{af}(v/V + d_f/R - d_{FW})z_f/TT_f \} \quad (8)$$

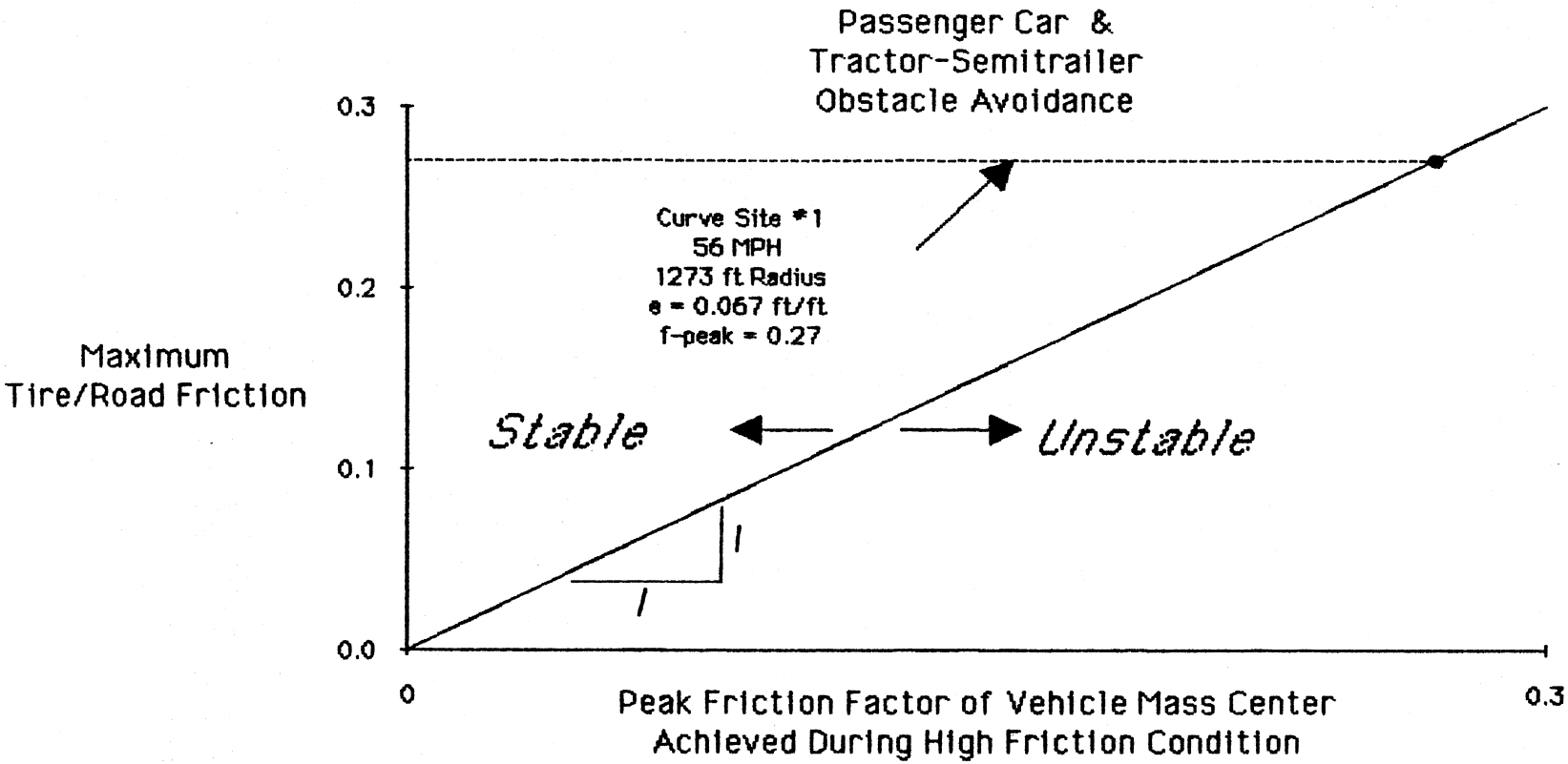

Figure 89. Tire/road friction necessary for stable operation under low friction conditions; obstacle avoidance maneuver.

$$ff_2 = C_{af}(v/V + d_f/R - d_{FW}) / \{ N_{sf}/2 + [d_f(p - p_r) + z]K_f + (\phi - e)K_f/(2TT_f) - C_{af}(v/V + d_f/R - d_{FW})z_f/TT_f \} \quad (9)$$

$$ff_3 = C_{ar}(v/V - d_r/R) / \{ N_{sr}/2 + [-d_r(p - p_r) + z]K_r - (\phi - e)K_r/(2TT_r) + C_{ar}(v/V - d_r/R)z_r/TT_r \} \quad (10)$$

$$ff_4 = C_{ar}(v/V - d_r/R) / \{ N_{sr}/2 + [-d_r(p - p_r) + z]K_r + (\phi - e)K_r/(2TT_r) - C_{ar}(v/V - d_r/R)z_r/TT_r \} \quad (11)$$

The parameters appearing in these expressions are defined in table 5. Since each of these expressions is simply the ratio of lateral tire force, F_y, to vertical tire force, F_z, the numerator and denominator expressions are simply lateral and vertical tire forces expressed in terms of the model parameters and response variables. Equations 8 and 9 show that front tire lateral forces depend upon sideslip velocity, vehicle speed, path curvature, and front wheel steer angle. Rear tire lateral forces depend upon the same vehicle reponses except front wheel steer angle. Since steady turning motion along most highway curve designs produces little load transfer on a vehicle in a fore/aft direction and only modest amounts side to side, the denominator expression for vertical tire load is primarily dominated by the static tire load term. Accordingly, a first order examination of the friction factor sensitivities under the assumed operating conditions should focus on lateral tire force production, or the quantities appearing in the numerator of the above equations. The numerator terms show that variations in friction factor values can be expressed directly in terms of variations in vehicle sideslip, path curvature, or steer angle.

Table 5. Parameter and variable definitions

C_{af}	front tire cornering stiffness (<0)
C_{ar}	rear tire cornering stiffness (<0)
d_f	distance from front axle to vehicle mass center
d_r	distance from rear axle to vehicle mass center
e	highway superelevation
K_f	front suspension stiffness
K_r	rear suspension stiffness
N_{sf}	front static axle load
N_{sr}	rear static axle load
p	vehicle sprung mass pitch angle relative to the horizontal plane normal to the gravity vector
p_r	highway grade
T_F	front suspension spread
T_R	rear suspension spread
TT_f	front tire track
TT_r	rear tire track
R	highway curve radius
v	vehicle lateral sideslip velocity at the body mass center
V	vehicle speed
z	vehicle sprung mass displacement normal to the road surface (relative to the static reference condition)
z_f	height above ground of front suspension roll center
z_r	height above ground of rear suspension roll center
d_{FW}	vehicle front wheel steer angle
ϕ	vehicle sprung mass roll angle relative to the horizontal plane normal to the gravity vector

The above observations can be used to illustrate how errors in experimental estimates of friction factors can occur and how to identify the sources of measurement most responsible. Since the methodology used in this project for determining friction factor values relied on measuring vehicle response quantities, and then deriving the friction factor estimates from expressions similar to those seen above, measurement errors can be analyzed in this same vein. The quantities v/V, R, and d_{FW} were some of the quantities

measured during a typical vehicle steady turning test. If a measurement error occurs in one of these quantities, the influence of the error on the friction factor value will not only be determined by how large the measurement error is, but also by the manner in which it appears in the above expressions. For example, equation (8) shows the term d_f/R appearing in the numerator. If d_f happens to be a very small quantity, significant measurement errors in R can be endured and not adversely affect the estimate of the friction factor.

Reference to chapter 5 and curve 1 for passenger car A shows that the term v/V (sideslip angle) is about 0.15 degrees, d_f/R is about (4/1273)57.3 or 0.2 degrees, and d_{FW} is approximately 0.4 degrees. Therefore, a similar percentage error in each of these quantities would mean that errors in front wheel steer, d_{FW}, would have approximately 2.5 times an adverse effect that the same percentage error would have in sideslip angle, or, twice the effect of a similar percentage error in path curvature. Generally, this type of error is normally associated with transducer gain errors and is usually less common than the other major source of measurement error: zero data offsets. Measurement offset errors tend to affect the measurements in approximately the same manner as described above, provided that each of the transducer / instrumentation ranges are scaled appropriately for the measured data. Of the three measured quantities noted above, measurement of path radius was generally the most accurate, followed by sideslip angle, and then front steer angle. As a result, errors in steer angle measurements would be identified as the greatest contributor to errors in friction factor estimates, followed by sideslip errors, and then path radius errors.

One way of minimizing the likelihood of error propogation in a methodology such as this one is to reduce the number of measured quantities contributing to the individual wheel friction factors. This can sometimes be accomplished by positioning the sensors at different vehicle locations. For example, positioning the trolley (sideslip transducer) at the fore/aft location of a rear, or nonsteered, wheel provides the tire sidelip angle directly with one measurement, thereby avoiding the additional dependence on the path radius (or yaw rate) measurement. The trolley can also be modified to connect directly to a steered wheel in some cases [8]. This would eliminate the dependence on steer angle and yaw rate.

6.6 Steering Requirements for Superelevated Curves

Several studies in the technical literature [3, 10, 11] tend to reference the needs and steering behavior of drivers during superelvated curve negotiation as reasons for possibly modifying current design practice. One of these items relates to required steering changes of vehicles because of the presence of highway superelevation. The other item is associated with the frequent observation that drivers do not typically employ a constant or fixed steering wheel angle when normally driving a curve. The following sections comment on these issues based upon the experience and observations noted in this project.

6.6.1 Steady Turn Steering Requirements Along Superelevated Curves

Simple steady turning analysis of a two axle vehicle shows that the required steering angle (in degrees), d_{FW}, for following a path of constant radius, R, at constant speed, V, is given by the following expression:

$$d_{FW} = 57.3(WB/R) + K\,V^2/R\,g \qquad (12)$$

where,

WB is the vehicle wheelbase dimension

K is the understeer gradient of the vehicle (degrees/g)

and g is the acceleration of gravity.

The above equation (12) applies to a horizontal road surface containing no superelevation. If the road surface now becomes superelevated an amount, e, the above equation is modified to the following form:

$$d_{FW} = 57.3(WB/R) + K(V^2/R\,g - e) \qquad (13)$$

or,

$$d_{FW} = 57.3(WB/R) + K\,f \qquad (14)$$

where,

$f = (V^2/R\,g - e)$ = the point-mass friction factor

Typical values of understeer gradient, K, for most passenger cars and heavy trucks lie in the range of 1 to 5 degrees/g .

Equation (14) can be used to demonstrate how steer angle requirements change on superelevated curves as speed changes occur. The first term in equation (14), 57.3(WB/R), is the "Ackermann" or zero-speed component of the required steer angle, dependent only upon the vehicle wheelbase and curve radius. This is the steer angle required of a two-axle vehicle to track a path of radius R at zero speed on a road surface containing no superelevation. On a road surface containing superelevation of an amount, e, the required zero-speed steer angle becomes,

$$57.3(WB/R) - K\,e \qquad (15)$$

since, at zero speed, f is equal to -e. Evaluation of equation (15) for curve site 1 [R = 1273 ft (388 m); e = 6.7 percent] and vehicle A [WB = 8.3 ft (2.5 m)] shows that the zero-speed steer angle required for this curve is 0.17 degrees for a vehicle understeer gradient of 3 degrees/g. Even for an understeer gradient as large as 5 degrees/g the required zero-speed steer angle is 0.04 degrees.

For most AASHTO curve designs one finds that, unless a vehicle contains an unusually large amount of understeer, steering reversals are not generally possible, even at zero speed. As such, previous concerns about steering reversal along superelevated highway curves appear puzzling [3]. Certainly, counter steering is required on superelevated tangent sections, and perhaps when superelevated tangents are used as transition sections to superelevated curves, steering reversal conflicts may be an issue. However, once established on a superelevated curve, even at low running speeds, superelevation itself should never be a cause for drivers to employ steering displacements away from the direction of turn during steady turning maneuvers.

6.6.2 Non-Steady Steering Behavior by Drivers on Superelevated Curves

Oscillatory or non-steady steering behavior by typical drivers has been argued by some investigators [1, 10] as a reason for modifying current design practice for horizontal curves. The steady turn data seen in appendix E also reflects this behavior by the driver used in this study, even when attempting to drive each curve in a smooth manner. Examination of figure 90, a representative sample from the time history data of appendix E (curve site 1, vehicle A, repeat 1), shows that the passenger car data exhibits driver steering waveforms which vary by amounts of approximately 5 to 10 percent from a fixed value for most curves. Similar variations in yaw rate and lateral acceleration levels are also seen. This would then imply that the instantaneous vehicle path is exhibiting similar variations in turn radius or curvature.

The tractor-semitrailer data seen in appendix E exhibits significantly larger variations in tractor steer angle (20 to 30 percent) about a constant level. However, the articulation angle (which can be thought of as the steer angle of the semitrailer) is observed to vary by amounts closer to 10 to 15 percent of its steady values. The same is generally true of the semitrailer lateral acceleration and yaw rate signals. This suggests that the tractor-semitrailer, as a whole, is undergoing path curvature variations of 10 to 15 percent, but the driver task in steering the tractor unit (20 to 30 percent variations) through the curve is significantly more burdensome than that observed for the passenger cars.

Given that most drivers do exhibit this non-steady steering behavior along highway curves and that, on average, the variations may be larger than those observed in these tests, the argument for modifying current design policy calls for use of a modified R_{min} (or D_{max}) value in the standard "point-mass" design equation [3]. However, prior to reaching the stage of modifying R_{min}, the value of R_{min} must first be determined on the basis of assumed values for e_{max} and f_{max} and invocation of the design equation:

$$e_{max} + f_{max} = V^2 / R_{min}\ g \qquad (16)$$

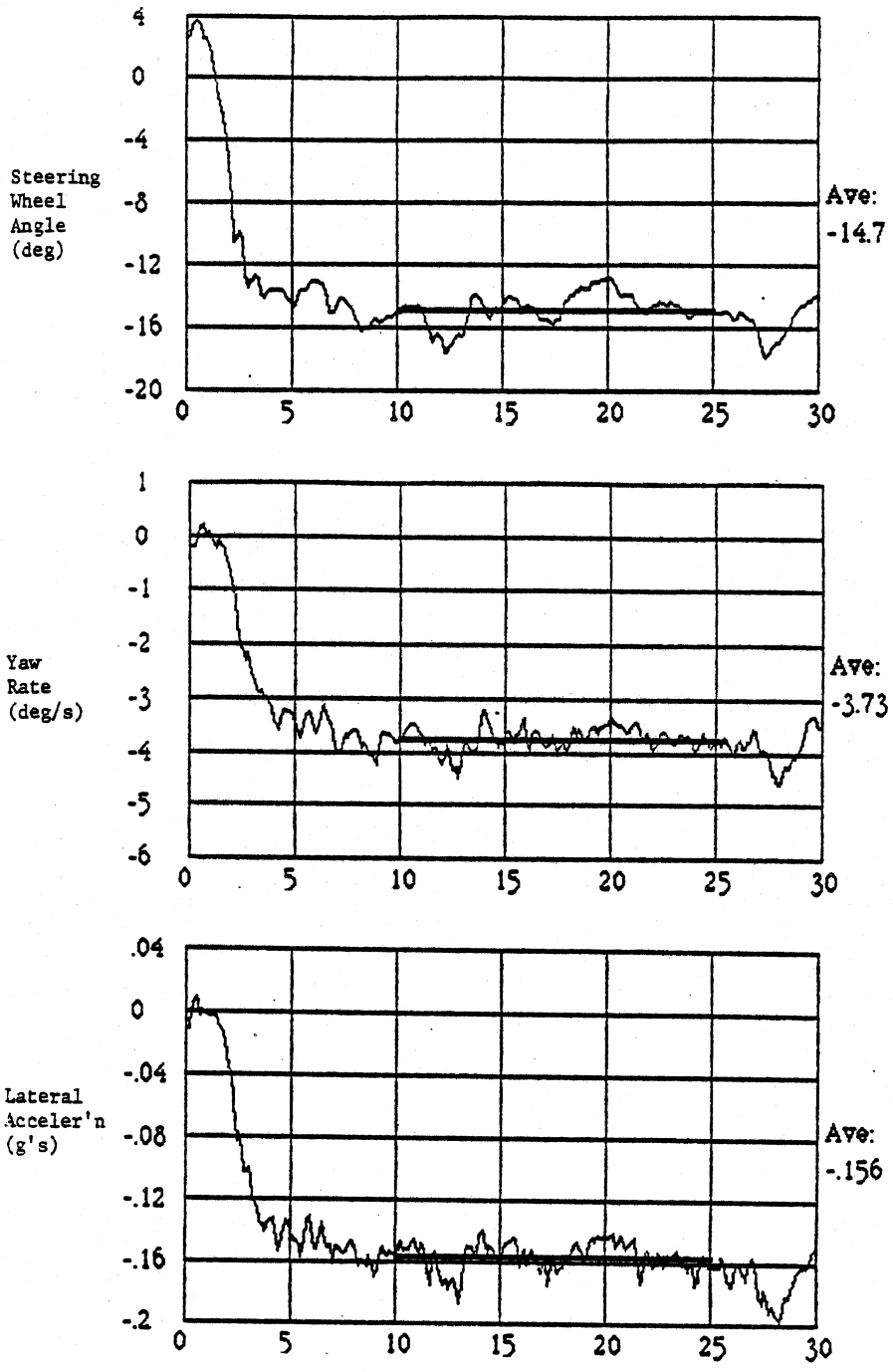

Figure 90. Sample measurement; steady turning; vehicle A.

Familiarity with the process of selecting values for e_{max} and particularly f_{max}, lends some skepticism to arguments that single out R_{min} as a value in need of adjustment. For example, the value of f_{max} normally selected is based upon subjective evaluations or criteria of driver comfort and is usually very conservative (~ 0.12). To assume that this particular value of f_{max} is somehow less susceptible to variation and uncertainty than values of R_{min} seems to require special reasoning.

On the other hand, if the overall intent and purpose of the standard point-mass design equation is to lend simplicity and reasonable accuracy to the process of designing horizontal curves, values of R_{min}, as currently derived from the design equation, seem as reasonable as any alternate values derived from more precise observations of actual vehicle curvature. This is underscored further because of the appearance of e_{max} and f_{max}, two presumably reasonable, though admittedly uncertain, quantities within the same equation. Therefore, unless experimental research shows that actual path curvature variations produced by average drivers operating for extended time periods along superlevated curves is far greater than that observed during the course of this project and some others [1, 11], modification of R_{min} values in the standard design equation does not appear warranted. Horizontal curves of very short duration, or arc length, and subject to "corner cutting," are not viewed as falling within this category. Such cases are perhaps more properly addressed within the general area of transitions.

Chapter 7

RESEARCH FINDINGS AND CURRENT AASHTO DESIGN POLICY

The purpose of this chapter is to discuss the research findings of this project in relationship to current AASHTO design policy. Findings from other recent research studies [1, 2] will also be included to help clarify how similar research performed in each of these studies relate to the work performed here. The chapter discusses topics concerned with the AASHTO horizontal curve design as defined in the "Green Book" [3].

7.1 "Steady Turning" Driver Behavior and Friction Factor Variations

Prior to discussing this topic, certain clarifications are necessary to identify what types of curves and where along the curve the findings of this study and related studies apply. First, the research results contained in this report apply specifically to horizontal curve negotiation after completion of the curve transition. Consequently, driver/vehicle "overshoot" behavior (exceedance of highway curvature at the beginning of a curve) due to transition does not fall within the realm of this study, even though such behavior usually occurs on the horizontal curve shortly after the beginning of the simple curve and is normally a result of the transition. Further, these research results apply primarily to high speed horizontal curves of low to moderate curvature conforming to AASHTO design recommendations. Finally, the term "steady turning" implies a typical degree of oscillatory driver steering behavior superimposed upon a constant steer level. "Steady turning" also refers to the idealized, non-varying steer value when discussing results from the simplified steady-turning model.

Results of the computer analyses and experimental measurements show that modest differences do exist in wheel-to-wheel friction factor values on most vehicles during steady turning conditions. The two primary sources of friction factor variations are: 1) geometric properties of vehicles, and 2) normal driver steering fluctuations during curve negotiation. Consequently, even when drivers are capable of steering a curve in an ideal manner without

mild steering oscillations, wheel-to-wheel friction factor differences would still exist because of the basic vehicle characteristics which set it apart from a "point-mass" object.

A main conclusion is that despite the presence of these wheel-to-wheel friction factor variations, no evidence was found to indicate that the observed friction factor variations would lead to significantly reduced stability margins. Even if the available tire/road friction level was reduced to a value below the demand of the tire having the greatest friction requirement, no vehicle instability would occur. Interestingly, the minimum level of tire/road friction identified for maintaining stability of passenger cars was found to be equal to the "point-mass" design value for the curve. However, the minimum level of friction necessary for maintaining stability of the five axle tractor-semitrailer was approximately 10 percent higher than the point-mass design value. For example, an AASHTO curve with a design speed of 70 mph (f_{max} = 0.10) and an assumed wet road friction level of 0.30, the margin of safety would be 0.20 g's for the passenger car (0.30 - 0.10) and 0.19 g's for the tractor-semitrailer (0.30 -0.11). Accordingly, the safety margins provided by the AASHTO design are seen to be generous for both types of vehicles, even when controlling curve designs are used. Therefore, changes to the standard "point-mass" design equation are not seen as necessary. Again, this conclusion applies to negotiation of horizontal curves well after the PC and does not apply to transition sections or overshoot behavior caused by transitions at the start of a horizontal curve.

Increased margins of safety may appear necessary for high center of gravity heavy trucks operating on lower design speed curves; however, the existing AASHTO policy still provides ample means for reducing side friction demand while also retaining near maximum superelevation rates. Reference to Figure III-8 of the "Green Book" [3] shows that if curvature values 20 percent less than the controlling curvature (D_{max}) are used, f values are reduced by 30 percent and the superelevation rate remains at nearly e_{max}. Consequently, strong control over side friction demands are provided within the existing AAHSTO design policy and is easily effected by modest changes in curve radius. This flexible means of retaining increased superelevation rates while

significantly reducing friction factor requirements is seen as a strong feature of the AASHTO design policy and is discussed further in section 7.2 .

Experimental measurements performed for the two passenger cars and the tractor-semitrailer vehicle showed that mild driver steering oscillations did occur for each vehicle during curve negotiation. The passenger car tests exhibited about 5 to 10 percent variations about the ideal value and the tractor-semitrailer tests exhibited about 10 to 15 percent variations. These measurements and observations apply to curve negotiation well after the PC during "steady" turning conditions. Findings of other researchers, [1], have experimentally observed (through photographic analyses) that actual drivers at different horizontal curve sites often achieve instantaneous path radii which are less than the curve radius design.

The same researchers also found that on many of the same curve sites nearly half of all drivers did not achieve path curvatures as severe as the highway curve design. This latter finding is understandable on curves of short length where "corner cutting" is frequently used by drivers to lower lateral acceleration. However, on curves of greater length where vehicles must remain within the confines of a single lane for an extended period of time, minimum (or "critical" [1]) vehicle path radii greater than the curve design radius would not seem to be physically possible.

Nevertheless, the same study revealed that for certain small sub-samples of the total observations, the "critical path radius" (or momentary minimum path radius achieved during a curve traversal) could be significantly less than the curve radius design value. Most "critical path radii" values occurred shortly after the PC and during the entry to the horizontal curve itself. However, this type of extreme overshoot behavior was not generally observed once the vehicle was established on the curve. This distinction is important to keep in mind in order to relate and resolve any apparent differences in findings between this study and those reported in [1]. Basically, the findings regarding the extreme "critical path radii" reported in [1] are viewed as quite reasonable given that they apply to a momentary phenomena induced by transition sections and extremes of driver behavior. However, rather than modify existing AASHTO horizontal curve design practice

to accomodate imperfect transition sections or extreme driver behavior, this report is in general agreement with the recommendations of [1], to encourage (a) less use of controlling curve designs, where possible, and (b) spiral transitions in place of tangent transition sections. In short, the high friction factor values reported in [1] are seen as a transition design "problem" which can best be handled by use of spiral transitions. These two recommendations are discussed further in sections 7.2 and 7.3 .

7.2 Larger Radii Horizontal Curves

The findings of this study support use of the point-mass concept as a simple means, not only for use in designing horizontal curves, but also for understanding the implications of changes in curve design. In particular, the discussion in this section uses the "point-mass" concept in considering the safety margins resulting from employing larger radii whenever possible. Larger radii for horizontal curves can result from either (1) less use of minimum, or near minimum, radii curves as determined by the AASHTO policy, or (2) the choice of a longer R_{min} (i.e., smaller D_{max}) as the control limit for a given highway.

How might a longer R_{min} be determined? To answer this question, suppose that a highway designer wished to allow for the 10% higher level of minimum friction needed for the stability of heavy trucks. A straightforward approach to provide an additional margin of safety for these vehicles would be to reduce f_{max} (as used in the AASHTO policy) by 10 percent. For example, assume that the design speed is 70 mph (112 km/h) and e_{max} is to be 0.08. For 70 mph (112 km/h), the AASHTO policy [3] lists f_{max} as 0.10 which would be reduced to 0.09 to provide a safety margin for trucks. For f = 0.09, e = 0.08, and V = 70 mph, the "point-mass" equation (in the form $R = V^2/(15(e+f))$) yields a radius, R_{min}, equal to 1922 feet (586 m). If f had been 0.10, e+f would have been 0.18 and R_{min} would equal 1815 feet (553 m). In this situation, a 10 percent decrease in f_{max} results in a 6 percent increase in R_{min}.

In general, the following equation illustrates the relationship between small changes in e_{max} or f_{max} and R_{min}.

$$dR/R_{min} = -(de + df)/(e_{max} + f_{max}) \qquad (17)$$

where dR is the change in R_{min} caused by changing either e_{max} or f_{max}
df is a small change in side friction factor
de is a small change in superelevation
e_{max} is the original e_{max}
f_{max} is the original f_{max}

For cases in which de = 0 (superelevation is fixed), the ratio $df/(e_{max}+f_{max})$ is equal to the fractional change in radius (dR/R_{min}) resulting from a small change in side friction. The greatest influences of percentage changes in f_{max} occur when e_{max} is small and f_{max} is large. (Larger f_{max}'s correspond to lower velocities in the AASHTO policy [3].) In the preceding example, e_{max} and f_{max} were nearly equal so that a 10% change in f_{max} produced approximately a 5% change in R_{min}.

7.3 Spiral Transitions

The use of spiral transitions is recommended and supported by AASHTO design for several reasons: (a) spiral paths are close to actual paths typically selected by drivers during transition driving, (b) spirals provide a desirable means for arranging superelevation runoff, (c) spirals provide a convenient method for widening pavements, and (d) the aesthetic appearance of the highway curve employing spiral transitions is considered more pleasing to the eye. In addition to these reasons, three other significant reasons should be noted. First, the spiral transition is a point-by-point application of the "point-mass" design formula during the transition process. Thus, as curve radius varies continuously (in proportion to the travel distance) as one moves along a spiral, so does the superelevation, thereby causing a smooth and consistent introduction of side friction as the PC of the horizontal curve is reached. Consequently, driver/vehicle systems will not encounter any sudden or abrupt change in lateral acceleration demand along a spiral transition. Furthermore, if the superelevation runoff during the spiral transition is consistent with AASHTO superelevation policy for horizontal curves, drivers will feel more comfortable moving from curve to curve because of retention of the point-mass formula throughout the highway system. Therefore, if drivers

are expected to become "calibrated" to "point-mass" physics along horizontal curves, the same "calibration," (or driver expectations), should be used for transition sections as well.

The second additional reason for using spiral transitions relates primarily to the findings by other researchers [1, 4] concerning driver/vehicle "overshoot" behavior when entering horizontal curves. In general, most findings show that severe "overshoot" behavior is significantly reduced or eliminated when spiral transitions are used. Computer simulation results within this study and several others [1, 2, 4] also support the field study observations conducted in [1] showing significantly lower vehicle path overshoot behavior when spirals are used as transition sections. Thus, spiral transitions are a direct and powerful means for reducing most driver/vehicle overshoot behavior and particularly the extreme values of "critical path radius" that can occur [1].

Finally, use of spiral transitions eliminate the need for drivers to counter-steer (opposite to the direction of turn) as is required when tangents are used as transition sections. Because current AASHTO design policy for tangent transitions recommends 50 - 100 percent (60 - 80 percent preferrable) of the superelevation runoff to occur on the tangent, two adverse features are introduced. First, highway design should be consistent with driver expectations of vehicle control. Normally, vehicles are steered by drivers to move in the direction of the steering displacement. On a transition tangent where superelevation is continually increasing, drivers must steer away from the direction of the approaching curve to counteract the effects of superelevation, particularly in traffic where drifting or spiraling across traffic lanes is not possible. Highway design which conflicts with this inherent driver understanding may cause temporary confusion on the part of some drivers leading to unnecessary steering actions. Also, the presence of tangents and associated countersteering requires the vehicle to adapt more quickly to the correct highway curvature once the beginning of the curve is reached. This would typically cause "overshoot" behavior to occur for most driver/vehicle systems as they entered the first portion of the horizontal curve. Consequently, the use of spiral transitions, in place of tangents, eliminates both of these adverse possibilities. By introducing superelevation

along a spiral in accordance with AASHTO design policy, drivers will steer smoothly in the direction of the approaching turn, even if constrained to one traffic lane, and also avoid the need to make sharp path curvature corrections near the PC.

7.4 Roll Stability Margins for Heavy Trucks

Heavy trucks with high centers of gravity may roll over at levels of lateral acceleration that approach those given in the AASHTO design policy for low-speed urban streets [2]. Furthermore, heavy trucks may experience roll stability problems on low-speed interchange ramps that are designed to requirements that are slightly below AASHTO recommendations [3]. The existing AASHTO policy does not consider and properly address the special roll stability concerns applicable to heavy trucks.

The lateral acceleration needed for curve negotiation comes from both e and f. The portion of this lateral acceleration that is due to f causes the vehicle to roll to the outside of the turn. In the case of heavy trucks, the amount of lateral acceleration that will cause the vehicle to roll over is referred to as the "rollover threshold." Rollover thresholds for heavily laden trucks range from 0.24 to 0.34 g [2]. These rollover thresholds can be viewed as the level of side friction that will cause rollover. Since the rollover thresholds for heavy trucks are considerably lower than the expected level of tire/road friction, even on wet pavements with worn tires, the safety margin for certain heavy trucks is considerably lower than anticipated in the AASHTO policy. With regard to low-speed interchanges, the designer should be aware of this lack of safety margin. Superelevation needs to be introduced before the PC, preferably through a spiral in order to keep the required f as small as possible throughout the curve. Truck drivers may tend to "overdrive" ramps (that is, travel above the design speed), thereby increasing the required f and challenging the vehicle's rollover threshold. In addition, driver steering/curvature variations, as observed in this study, will cause an increase in the maximum lateral acceleration experienced by the truck. Hence, conservative designs of ramps are especially in order where truck traffic is likely to be heavy.

7.5 Steering Requirements Along Superelevated Curves at Reduced Speed

The "Green Book" [3] currently contains a "misconception" regarding driver steering requirements along superelevated curves when operating at reduced speeds. The misconception, expressed on pages 163 and 164, is that drivers need to apply counter-steering (up the slope) to vehicles when traveling at speeds which cause the "point-mass" friction factor to change polarity and act in a direction toward the center of the turn (down the slope). The simple analysis, (verified by both computer simulation and vehicle testing), in chapter 6 (section 6.6.2), shows that most typical vehicles operating on AASHTO curve designs do not require steering reversals to properly track the curve design radius, even at near zero speeds. Although traveling along a superelevated tangent in a straight line does require the described counter-steering behavior, turning motion along a circular superelevated curve does not. The advantage of this to designers is that an increased rate of superelevation does not require reverse steering action to properly track the curve. Consequently, designers can use higher rates of superelevation on AASHTO curves without having to be concerned that low speed vehicles will require steering motion "up the slope" and away from the direction of turn. For example, if a curve designer prefers to use 9 perecnt instead of 8 percent for e_{max} at a particular curve site, concern over driver steering requirements should not be a reason for deciding to use the lower superelevation rate.

Chapter 8

CONCLUSIONS AND RECOMMENDATIONS

The research conducted within this study has led to a number of conclusions and recommendations which are based largely upon findings of computer model predictions and full-scale vehicle test results gathered during the course of the project.

Conclusions

* Steady turning models and vehicle tests have shown that significant differences do exist in wheel-to-wheel friction factor values on most vehicles during steady turning maneuvers along superelevated curves. Passenger cars and other two-axle vehicles exhibit the least wheel-to-wheel variation; commercial vehicles having multiple axle suspensions and elevated mass centers exhibit the greatest dispersion.

* The level of variation in individual wheel friction factors considered and observed in this work indicated there was no significant evidence or finding that vehicles, or driver/vehicle systems, are less stable or otherwise adversly affected by this particular phenomena during steady turning maneuvers along typical superelevated highway curves.

* No substantive evidence regarding friction factor dispersion was identified to conclude that current highway curve design practice, based upon a point-mass formulation, should be modified to accomodate the observed wheel-to-wheel variations. For example, alteration of the standard design equation to account for larger friction factor values derived from an individual wheel analysis, is not seen as necessary. These conclusions

apply to horizontal curve negotiation after completion of the curve transition. Temporary disturbances to driver-vehicle systems during entry in to horizontal curves and due to different curve transition designs were not included in this study.

* Computer analysis of low friction conditions for steady turning maneuvers on superelevated curves suggests that a tire/road friction level approximately equal to the point-mass value is sufficient to permit stable driver/vehicle curve negotiation for passsenger cars. However, for the 5-axle tractor-semitrailer used in this study (and presumably similar commercial vehicles), a minimum friction level approximately 10 percent higher than the point-mass value was generally necessary to guarantee stability for the same maneuver and low friction operating conditions.

* Obstacle avoidance maneuvers simulated along an AASHTO design curve under low friction conditions showed that the minimum tire/road friction level necessary for stable execution of the maneuver is approximately equal to the peak friction value required of a point-mass object undergoing the same maneuver under adequate friction conditions. Therefore, even though certain tires on a vehicle may saturate for short periods of time during a low friction obstacle avoidance maneuver, the driver-vehicle system is able to maintain stability if the minimum tire/road friction level is at least as great as described above. This "rule of thumb" for estimating the minimum friction level needed for such maneuvers applied more or less equally to the passenger car and tractor-semitrailer vehicles used in the study.

* Steady turning computer models developed during the project are viewed as reliable predictors of steady turning vehicle performance along superelevated curves. The models were employed to calculate individual wheel friction factor requirements for steady turning motion of passenger cars and commercial vehicles. The predictions from the steady turning models were shown to

compare favorably with vehicle test data collected during the project and calculations from other comprehensive computer models. Use of these models is recommended for more in-depth analyses of vehicle / highway interactions as part of the highway curve design process.

* Experimental identification and estimation of individual wheel friction factor values was shown to be possible but not highly accurate and repeatable. The methodology employed in this project relied on direct measurement of vehicle responses and derivation of the friction factor values from this information. (Direct measurement of tire forces or wheel loads are not currently possible due to the limited accuracy and signal variability of such transducers that are available.)

* Estimation of individual wheel friction factors through the use of steady turning models and representative vehicle parameters is viewed as sufficiently accurate and reliable for most vehicles. Further experimental validation efforts are not seen as necessary since the sensitivity analyses conducted here failed to identify significant adverse effects attributable to modest variations in wheel-to-wheel friction factor values.

* Concerns occasionally expressed in the technical literature about steering reversal requirements by drivers along superelevated curves during conditions of reduced speed are not supported by the analyses and observations conducted within this project. Rather, steering reversals (up the slope) away from the direction of turn, even at very low speeds, are not viewed as generally possible for the great majority of passenger cars and commercial vehicles. Consequently, highway curve designers can use higher rates of superelevation on AASHTO curves without being concerned that lower speed vehicles may require steering motion "up the slope" and away from the direction of turn.

* Mild oscillatory steering behavior and accompanying path curvature variations during steady turning maneuvers were observed in the test data collected in this study. The magnitude of steering oscillations observed during each curve negotiation, well after completion of the transition, was generally small (see Sections 6.6 and 7.1). Consequently these measurements do not suggest a need to modify existing AASHTO horizontal curve design practice based upon observations of driver-vehicle behavior on curves of fixed radius. Other studies, cited and discussed in Chapter 7, have observed much greater levels of oscillatory driver-vehicle behavior but almost exclusively during entry transitions to horizontal curves.

* The issue of spiral transitions and associated benefits, while not specifically studied or addressed within this project, was frequently encountered during this study. The transitions to each of the curve sites in the test program were not spirals but superelevated tangents, and as such, generally required mild counter-steering and subsequent overshooting of steering responses upon entry into each curve, especially with the tractor - semitrailer. This type of transition design necessitates the above described behavior which runs counter to the more natural driving process of requiring steering displacements in the direction of the anticipated turn. Use of spiral transitions to 1) introduce curvature and superelevation in a manner consistent with driver expectations, and to 2) retain the simple physics of the standard design equation, is supported.

Recommendations

* Recommendations for improving the accuracy and repeatability of the experimental approach used in this work include:

  - use of additional sideslip trolley devices per vehicle

  - improved fore/aft positioning of these devices at or near specific wheel locations

  - use of ground-based roll motion transducers to better estimate side to side vertical load transfer

  - use of optimal (Kalman) filtering techniques during data processing to improve estimates of the measured vehicle responses

* Future vehicle or highway studies considering the use of a sideslip trolley are encouraged to do so based upon the experiences of this project. However, design modifications have been recommended to improve its ruggedness for normal highway travel and to lessen its noise level due to normal road disturbances.

* Preservation of the driver/vehicle test data collected during this project in a standardized format for future reference is recommended. This data could be used as a useful source of representative driver/vehicle responses for further studies of highway curve design.

9.0 REFERENCES

1. Glennon,J.C., Neuman,T.R., and Leisch,J.E. "Safety and Operational Considerations for Design of Rural Highway Curves," Final Report, Federal Highway Administration, Contract No. DOT-FH-11-9575, August 1983.

2. Ervin, R.D. et al., "Impact of Geometric Features at Interchanges," Final Report, Federal Highway Administration, Contract No. DOT-FH61-82-C-00054, August 1985.

3. American Association of State Highway Officials, A Policy on Geometric Design of Highways and Streets, 1984.

4. Segal,D.J. and Banney,T.A. " Evaluation of Horizontal Curve Design," Final Report, Federal Highway Administration, Contract No. DOT-FH-11-8501 (Mod. #7), August 1980.

5. MacAdam,C.C. et al., "A Computerized Model fro Simulating the Braking and Steering Dynamics of Trucks, Tractor-semitrailers, Doubles, and Triples Combinations - Users' Manual - Phase 4," Final Report, MVMA Proj. 1197, Highway Safety Research Inst., Univ. of Mich., Rept. No. UM-HSRI-80-58, September 1980.

6. MacAdam,C.C. "Application of an Optimal Preview Control for Simulation of Closed-Loop Automobile Driving," IEEE Transactions on Systems, Man, and Cyberbetics, Vol. 11, June 1981.

7. "Vehicle Dynamics Terminology - SAE J670," SAE Handbook Supplement, SAE Recommended Practice, June 1978.

8. Little,J. "A Trolley for the Measurement of Vehicle Roll and Slip Angles, and Speed," MIRA Bulletin No. 3, May/June 1970.

9. "Instrumentation of Test Trucks for Measuring Pavement-Vehicle Interactions," Contract No. FH-11-9289, Systems Technology Inc.

10. Glennon,J.C. and Weaver,G.D. "Highway Curve Design for Safe Vehicle Operations," Highway Research Record, 1972.

11. Good.,M.C. "A Review of Empirical Studies of Driver-Vehicle Behaviour on Road Curves," Australian Road Research Board, Dept. of Mech. Enging., University of Melbourne, April 1975.

10.0 SELECTED BIBLIOGRAPHY

1. "Side-Friction Factors in the Design of Highway Curves," NCHRP Research Results Digest, HRB, Digest 55, February 1974.

2. Lamm, R. "Driving Dynamic Considerations: A Comparison of German and American Friction Coefficients for Highway Design," Transportation Research Record 960.

3. Zuk,W. "Instability Analysis of a Vehicle Negotiating a Curve with Downgrade Superelevation," Highway Research Record, HRB, 1972.

4. "Recommended Modification of Superelevation Practice for Long-Radius Curves," NCHRP Research Results Digest, Digest 72, May 1975.

5. Lugner,P. "Investigations into the Steady-State Cornering of a Vehicle on a Banked Curve," ATZ Automobiltechnische Zeitschrift, Vol. 75, No. 8, August 1973.

6. Zador,Z.L. et al. "Superelevation and Roadway Geometry: Deficiency at Crash Sites and on Grades," Presented at the Transportation Research Board Meetings, Washington, D.C., January 1985.

7. Ervin,R.D. et al. "Influence of the Geometric Design of Highway Ramps on the Stability and Control of Heavy Duty Trucks," Presented at the TRB Meeting, Denver, Colorado, August 1985.

8. Good,M.C. "Road Curve Geometry and Driver Behaviour," Australian Road Research Board Report No. 15, May 1978.

9. Bell,N.G. "Horizontal Curve Design on Rural Roads: A Critical Examination," Project Rept. 32 79/80, Dept. of Civil Enging., Portsmouth Polytechnic, June 1980.

10. Literature Review for FHWA Project, "Side Friction for Superelevation on Horizontal Curves," Contract DTFH61-82-C-00019, January 1983.